Elucidating how αvβ3-integrin regulates neuropilin-1's role in tumour angiogenesis in order to improve anti-angiogenic therapy

---

Tim S. Ellison

A thesis submitted for the degree of Doctor of Philosophy (Ph.D.) in Biomolecular Science

University of East Anglia
School of Biological Sciences

September 2015

©This copy of the thesis has been supplied on condition that anyone who consults it is understood to recognise that its copyright rests with the author and that use of any information derived there from must be in accordance with current UK Copyright Law. In addition, any quotation or extract must include full attribution.

Abstract

αvβ3-integrin expression is vastly upregulated in tumour vasculature, and has long been considered a key molecule in promoting tumour angiogenesis. However, its initial promise as a target in anti-angiogenic therapy has wavered since the αvβ3-integrin antagonist cilengitide did not meet its end point in Phase III clinical trials for the treatment of glioblastoma. This failure corresponds with the enhanced tumour growth and angiogenesis observed in β3-integrin-knockout mice, which potentially occurs via a compensatory upregulation of VEGFR2 and enhancement in VEGFR2-neuropilin-1 interactions. Here, I show that tumour growth and angiogenesis are sensitive to neuropilin-1 perturbation even with only a 50% reduction in β3-integrin expression. β3-integrin-heterozygous, but not wild-type, mice show an increased dependence on neuropilin-1 that is not related to changes in neuropilin-1-mediated VEGFR2 function. Rather, the suppression of β3-integrin leads to the activation of a neuropilin-1-dependent endothelial cell migration pathway via a mechanism in which NRP1 is mobilised away from mature focal adhesions following VEGF-stimulation. Concordantly, the simultaneous genetic targeting of both molecules significantly impairs paxillin activation and focal adhesion turnover in endothelial cells, and thus inhibits endothelial cell migration, and tumour growth and angiogenesis, even in established tumours. These findings therefore provide important pre-clinical evidence that pharmacologically targeting both molecules in unison might be an effective anti-angiogenic therapy for patients with advanced cancers.

For Dad and Mum,

who let me be who I am,

but who I strive to become.

Contents

Title Page 1
Abstract 2
Contents 4
List of Figures 8
List of Tables 10
Acknowledgements 11
CHAPTER ONE – Introduction 13
1.1 Preface to the Introduction 13
1.2 The Vascular System 13
1.2.1 Blood vessel function and architecture 14
1.2.1.1 Endothelial cells 16
1.2.1.1 Extracellular matrix 17
1.2.1.1 Pericytes 18
1.3 Blood vessel development/formation 20
1.3.1 Vasculogenesis 20
1.3.2 Angiogenesis 22
1.3.2.1 Mechanisms of Angiogenic sprouting 23
1.3.2.2 The VEGF family and its receptors 28
1.3.2.2.1 VEGF-A 29
1.3.2.2.2 VEGFR2 30
1.4 Angiogenesis in disease 34
1.4.1 Cancer 34
1.3.1.1 Tumour angiogenesis 34
1.3.1.2 Metastasis 39
1.3.1.3 Anti-angiogenic cancer therapy 40
1.5 More Molecular players in angiogenesis 43
1.5.1 Integrins 43
1.5.1.1 Integrins and their ligands 46
1.5.1.2 Integrin activation – ‘inside-out’ signalling 49
1.5.1.3 Integrins and focal adhesion complexes 50
1.5.1.4 Integrin ‘outside-in’ signalling 52
1.5.1.5 Integrin trafficking 53
1.5.1.6 Integrins in angiogenesis 55
1.5.1.6.1 αvβ3-integrin 55
1.5.1.6.1.1 αvβ3-integrin as a pro-angiogenic molecule 56
1.5.1.6.1.2 αvβ3-integrin as an anti-angiogenic molecule 60
1.5.1.6.1.3 Cell-specific functions of αvβ3-integrin 62
1.5.1.6.1.4 Conclusions on αvβ3-integrin 65
1.5.2 Revisiting the integrin adhesome 66
1.5.2.1 Filamin A 71
1.5.2.2 Non-muscle myosin II 72

1.5.2.3 Paxillin 72
1.5.3 Neuropilins 74
1.5.3.1 Structure and isoforms of neuropilins 74
1.5.3.2 The neuropilin ligands 76
1.5.3.3 Neuropilin-1 76
1.5.3.3.1 VEGFR2-dependent roles of neuropilin-1 78
1.5.3.3.2 VEGFR2-independent roles of neuropilin-1 83
1.5.3.3.3 Neuropilin-1 in cancer 88
1.5.3.3.4 Conclusions on neuropilin-1 89
1.6 Research Aims and Objectives 90
CHAPTER TWO – Materials and Methods 91
2.1 Reagents (and antibodies) 91
2.2 Animals 91
2.3 Mouse genotyping 94
2.3.1 PCR genotyping 94
2.3.1.1 β3-integrin-knockout PCR 94
2.3.1.2 β3-integrin-floxed PCR 95
2.3.1.3 NRP1-floxed PCR 96
2.3.1.4 Pdgfb.CreER PCR 96
2.3.1.5 NRP1Δcyto PCR 97
2.3.2 Agarose gel electrophoresis 97
2.4 *In vivo* tumour growth assays 98
2.5 Immunohistochemical analyses 98
2.5.1 Tumour samples 98
2.5.2 Lung samples from metastasis experiment 99
2.6 *Ex vivo* aortic ring assay 100
2.7 *In vivo* metastasis experiment 100
2.7.1 Attempt at luciferase-tagging CMT19TF1 cells 100
2.7.1.1 Lentivirus production in HEK293 cells 100
2.7.1.2 Lentivirus transduction of CMT19TF1 cells 101
2.7.1.3 Reverse transcription PCR to detect luciferase expression 101
2.7.1.4 Bioluminescence imaging 102
2.7.2 *In vivo* metastasis experiment 102
2.8 Mouse tumour endothelial cell isolation 102
2.9 Cell isolation and/or culture 103
2.9.1 Mouse lung microvascular endothelial cell culture 103
2.9.2 Mouse lung microvascular endothelial cell isolation and immortalisation 103
2.9.3 Human umbilical vein endothelial cell culture 104
2.9.4 Other cell culture 104
2.10 Flow cytometry 105
2.11 Western blot analysis 105
2.12 Cell surface biotinylation assay 106
2.13 Immunoprecipitation assays 107
2.14 Adhesion assays 108

2.14.1 Static adhesion 108
2.14.2 Adhesion on various matrix concentrations 109
2.14.3 Cell spreading assay 109
2.15 Migration assays 109
2.15.1 Random migration assay 109
2.15.2 Wound closure assay 110
2.16 Cell fractionation assay 110
2.17 Immunocytochemistry 110
2.18 Mass spectrometry analyses 111
2.19 Focal adhesion enrichment 112
2.20 Focal adhesion tracking 112
2.21 Statistical analysis 113
CHAPTER THREE – Investigating the dual importance of αvβ3-integrin and neuropilin-1 in tumour growth and angiogenesis 114
3.1 Like β3-integrin-knockout mice, β3-integrin-heterozygous mice have significantly increased angiogenesis and tumour growth relative to their wild-type littermates 114
3.2 Tumour growth and angiogenesis in β3-integrin-heterozygous mice are sensitive to endothelial neuropilin-1 depletion 116
3.3 Tumour growth and angiogenesis in β3-integrin-heterozygous mice are sensitive to the loss of neuropilin-1's cytoplasmic tail 119
3.4 Simultaneous depletion of both endothelial β3-integrin and neuropilin-1 blocks pre-established tumour growth and angiogenesis 122
3.5 The investigation of the dual importance of β3-integrin and neuropilin-1 in metastasis was unsuccessful 126
3.6 Discussion 127
CHAPTER FOUR – Investigating how αvβ3-integrin regulates neuropilin-1's VEGFR2-dependent role in endothelial cells 130
4.1 Polyoma-middle-T-antigen immortalised endothelial cells maintain their endothelial identity 130
4.2 VEGFR-2 and neuropilin-1 expression levels are elevated in β3-integrin-heterozygous endothelial cells 130
4.3 VEGFR2 activation and degradation patterns are no different between wild-type and β3-integrin heterozygous endothelial cells with and without neuropilin-1's cytoplasmic tail 132
4.4 Neuropilin-1-regulated VEGFR2 signalling is no different between wild-type and β3-integrin heterozygous endothelial cells with and without neuropilin-1's cytoplasmic tail 135
4.5 Cell surface biotinylation internalisation assays do not reliably measure VEGFR2 trafficking in pMT MLECs, but VEGFR2 surface levels do not appear different in β3-HET ECs with or without NRP1's cytoplasmic tail by flow cytometry 137
4.6 There are no relative differences in neuropilin-1-VEGFR2 interactions between wild-type and β3-heterozygous endothelial cells 140
4.7 Discussion 142

CHAPTER FIVE – Investigating how αvβ3-integrin regulates neuropilin-1's VEGFR2-independent role in endothelial cells 146
5.1 Examining adhesion and cell spreading properties of β3-integrin-wild-type and heterozygous endothelial cells with and without neuropilin-1's cytoplasmic tail 146
5.2 Examining surface levels of integrins in β3-integrin-wild-type and heterozygous endothelial cells with and without neuropilin-1's cytoplasmic tail 147
5.3 VEGF-induced migration in β3-integrin-heterozygous endothelial cells is dependent on neuropilin-1 150
5.4 Neuropilin-1's sub-cellular localisation is proportionally similar between β3-integrin-wild-type and heterozygous endothelial cells 152
5.5 Neuropilin-1's localisation at the ends of actin filaments is altered in stimulated β3-integrin-depleted endothelial cells 152
5.6 β3-integrin and neuropilin-1 co-localise in the same structures, but their interaction is weak 155
5.7 Myosin 9 confirmed to co-associate with neuropilin-1 less in β3-heterozygous endothelial cells 157
5.8 Many of the proteins that are appear differentially associated with NRP1 between β3-wild-type and β3-heterozygous endothelial cells are related to the cytoskeleton 164
5.9 Examining neuropilin-1's associations within the endothelial adhesome . 175
5.10 Neuropilin-1's co-localisation with paxillin-positive focal adhesions is lost upon stimulation with VEGF in only β3-heterozygous endothelial cells 178
5.11 Paxillin activation is sensitive to neuropilin-1 disruption in β3-integrin-heterozygous endothelial cells 181
5.12 Focal adhesion turnover is more sensitive to neuropilin-1 disruption in β3-integrin-heterozygous endothelial cells 181
5.13 Discussion 185
CHAPTER SIX – Final Discussion and Future Work 191
5.1 Final Discussion 191
5.2 Future Work 195
Appendix 199
1. Supplementary Figures 199
2. Publications 203
Abbreviations 228
References 232

List of Figures

Figure 1.1 – Blood vessel architecture 15
Figure 1.2 – Morphological features of blood vessels 19
Figure 1.3 – Blood vessel formation 21
Figure 1.4 – Mechanisms of angiogenesis 27
Figure 1.5 – Structure and signalling of VEGF receptors 33
Figure 1.6 – Tumour angiogenesis 38
Figure 1.7 – Integrin subunits and structure 45
Figure 1.8 – Integrin ligands 48
Figure 1.9 – Integrin inside-out activation 51
Figure 1.10 – Integrin outside-in signalling 54
Figure 1.11 – αvβ3-integrin cross-talk with VEGFR2 59
Figure 1.12 – Classical focal adhesion structures 70
Figure 1.13 – Neuropilin domain organisation 75
Figure 1.14 – Neuropilin-1's VEGFR2-dependent roles 82
Figure 1.15 – Projected model of neuropilin-1's adhesion-dependent role 87
Figure 3.1 – Like β3-integrin-knockout mice, β3-integrin-heterozygous mice have significantly increased angiogenesis and tumour growth relative to their wild-type littermates 115
Figure 3.2 – Tumour growth and angiogenesis in β3-integrin-heterozygous mice are sensitive to endothelial neuropilin-1 depletion 117
Figure 3.3 – Angiogenesis in β3-integrin-heterozygous mice is sensitive to endothelial neuropilin-1 depletion 118
Figure 3.4 – Tumour growth and angiogenesis in β3-integrin-heterozygous mice are sensitive to the loss of neuropilin-1's cytoplasmic tail 120
Figure 3.5 – Angiogenesis in β3-integrin-heterozygous mice is sensitive to the loss of neuropilin-1's cytoplasmic tail 121
Figure 3.6 – Simultaneous depletion of both endothelial β3-integrin and neuropilin-1 blocks pre-initiated microvessel sprouting 124
Figure 3.7 – Simultaneous depletion of both endothelial β3-integrin and neuropilin-1 blocks pre-established tumour growth and angiogenesis 125
Figure 4.1 – Polyoma-middle-T-antigen immortalised endothelial cells maintain their endothelial identity 131
Figure 4.2 – VEGFR-2 and neuropilin-1 expression levels are marginally elevated in β3-integrin-heterozygous endothelial cells 131
Figure 4.3 – VEGFR2 activation and degradation patterns are no different between wild-type and β3-integrin heterozygous endothelial cells with and without neuropilin-1's cytoplasmic tail 134
Figure 4.4 – Neuropilin-1-regulated VEGFR2 signalling via p130Cas and FAK is no different between wild-type and β3-integrin heterozygous endothelial cells with and without neuropilin-1's cytoplasmic tail 136

Figure 4.5 – Cell surface biotinylation internalisation assays do not reliably measure VEGFR2 trafficking in pMT MLECs, but VEGFR2 surface levels do not appear different in β3-HET ECs with or without NRP1's cytoplasmic tail by flow cytometry 139
Figure 4.6 – There are no relative differences in neuropilin-1-VEGFR2 interactions between wild-type and β3-heterozygous endothelial cells 141
Figure 5.1 – Examining adhesion and cell spreading properties of β3-integrin-wild-type and heterozygous endothelial cells with and without neuropilin-1's cytoplasmic tail 148
Figure 5.2 – Examining surface levels of integrins in β3-integrin-wild-type and heterozygous endothelial cells with and without neuropilin-1's cytoplasmic tail 149
Figure 5.3 – VEGF-induced migration in β3-integrin-heterozygous endothelial cells is dependent on neuropilin-1 151
Figure 5.4 – Neuropilin-1's sub-cellular localisation is proportionally similar between β3-integrin-wild-type and heterozygous endothelial cells..... 153
Figure 5.5 – Neuropilin-1's localisation at the ends of actin filaments is altered in stimulated β3-integrin-depleted endothelial cells..... 154
Figure 5.6 – β3-integrin and neuropilin-1 co-localise in the same structures, but their interaction is weak 156
Figure 5.7 – Myosin 9 confirmed to co-associate with neuropilin-1 less in β3-heterozygous endothelial cells..... 163
Figure 5.8 – Quantitative mass spectrometry analysis of neuropilin-1-immunoprecipitated samples highlights differential neuropilin-1 associations between β3-wild-type and β3-heterozygous endothelial cells 171
Figure 5.9 – Quantitative mass spectrometry analysis of neuropilin-1-immunoprecipitated samples highlights differential neuropilin-1 associations between β3-wild-type and β3-heterozygous endothelial cells 172
Figure 5.10 – Examining neuropilin-1's associations within the endothelial adhesome 177
Figure 5.11 – Neuropilin-1's co-localisation with paxillin-positive focal adhesions is lost upon stimulation with VEGF in only β3-heterozygous endothelial cells .. 179
Figure 5.12 – Paxillin activation is sensitive to neuropilin-1 disruption in β3-integrin-heterozygous endothelial cells 183
Figure 5.13 – Focal adhesion turnover is more sensitive to neuropilin-1 disruption in β3-integrin-heterozygous endothelial cells..... 184
Figure 6.1 – Model mechanism..... 194
Appendix Figure 1 – B16F0 tumour growth and angiogenesis in β3-integrin-heterozygous mice are sensitive to endothelial neuropilin-1 depletion 199
Appendix Figure 2 – The investigation of the dual importance of β3-integrin and neuropilin-1 in metastasis was unsuccessful..... 200
Appendix Figure 3 – Neuropilin-1-regulated VEGFR2 signalling via Akt and p38MAPK is no different between wild-type and β3-integrin heterozygous endothelial cells with and without neuropilin-1's cytoplasmic tail..... 201

Appendix Figure 4 – Examining surface levels of integrins in β3-integrin-wild-type and heterozygous endothelial cells with and without neuropilin-1's cytoplasmic tail 202

List of Tables

Table 2.1 – List of primary antibodies 92
Table 2.2 – List of secondary antibodies 94
Table 5.1 – Mass spectrometry results of neuropilin-1-immunoprecipitated β3-WT and β3-HET endothelial cell samples (first experiment) 159
Table 5.2 – Quantitative mass spectrometry results of neuropilin-1-immunoprecipitated β3-WT and β3-HET endothelial cell samples (second experiment) 167
Table 5.3 – Comparison of common hits from mass spectrometry of neuropilin-1-immunoprecipitated β3-WT and β3-HET EC samples between first and second experiments. 170

Acknowledgements

I would like to start by taking this opportunity to express my heartfelt gratitude to my supervisor Dr Stephen Robinson, without whom I would not have been involved in this fantastic project, and may not even be pursuing a career in scientific research. His extreme kindness, generosity, caring attitude, and his willingness to help have made this project an incredibly enjoyable part of my life, and for that I am extremely thankful. He has also been instrumental in boosting my confidence, and his knowledge and diligence are something to strive for. Thank you so much for being a wonderful mentor, Stephen.

My sincerest thanks also go to my secondary supervisors, Dr Jelena Gavrilović and Dr Grant Wheeler, for their support, challenging questions, and advice during my project. Also, thank you Grant for allocating my Master's practical project in Stephen's lab!

Of particular noteworthy mention, I would like to thank Prof Dylan Edwards for his kindness and all of his input into the project in lab meetings and CPG seminars. His knowledge and expertise have been insightful and motivating. I also massively appreciate his generosity in paying for drinks at lab dinners!

A warm thank you goes to Dr Mette Mogensen for giving me the opportunity to gain extensive teaching experience in the teaching labs, which was also financially relieving! And to Dr Paul Thomas for your assistance with bioimaging and for the use of your printer to print this thesis!

I would like to acknowledge all of my fellow lab members, past and present, for their input, friendship, and laughter, over the last few years. Thank you Sally, Salma, Liz, Julie, Christian, Richard, Veronica, Sam, Sophie, Ben, Aleks, Abdullah! Also all of the project/summer students for putting up with me and sharing a good few jokes..

Thank you to all of the labs that make up the CPG group for your participation and friendship. Also thanks to Jasmine Waters and Andy Loveday for their assistance around the lab (and for the bike rides Andy!).

Many thanks to BigC for funding this project and my stipend!

To all of my friends outside of the lab: Thanks for the endless laughter. Special mention goes to my housemates during the PhD (Matt, Ben, Ken, Sophie, James) for their friendships and for putting up with me.

Finally, thank you so much to my family: Mum, Dad, Nick and Grandma. I can't find the words to express how much you all mean to me. Your love, generosity and support over the years are insurmountable. Thank you so much to my lovely Grandma for everything you have done for me over the years. Your contribution to my life and education (and singing lessons!) is massively appreciated. I'm also hugely grateful to you for putting up with me at home whilst writing this thing! Thanks to Nick, for being a wonderful, caring and supportive older brother, and for leading by example. I would like to dedicate this thesis to my amazing parents, John and Sylvia, for everything. I could not ask for better parents. Thank you for always believing in me, for your genorisity, for your fantastic decisions over the years, and your expert parenting. Thanks also for being so understanding whilst I was writing at home. Thanks for all the food and dinners, Mum (even though there was nothing in the fridge that time..), and for the ridiculous number of cups of tea, Dad. You can have 'my chair' back now. 'That will be all'.

1. Introduction

1.1 Preface to the Introduction

The process by which blood vessels form from existing vessels is known as angiogenesis. In cancer, tumours must recruit their own blood supply by angiogenesis in order to grow beyond a certain size and spread (metastasise) around the body. This thesis examines the dual role of two molecules, αvβ3-integrin and neuropilin-1, associated with the cellular drivers of angiogenesis, endothelial cells, to coordinate the process. The results presented aim to promote a discussion on whether the molecules may be used as dual targets in anti-angiogenic therapy to improve cancer prognosis. The following introduction will cover what is already known about the topic and the relevant molecules in detail, starting with a brief overview of the vascular system.

1.2 The Vascular System

In vertebrates, the vascular system, or circulatory system, is an organ system that supports the flow of both blood and lymph fluid throughout the body. To achieve this, there are two distinct components of the vascular system: the cardiovascular system, which circulates blood, and the lymphatic system, which transports lymph [1]. Blood contains plasma, red blood cells (erythrocytes), immune/white blood cells (leukocytes), and platelets, whilst lymph mainly consists of plasma originally derived from the blood, and leukocytes.

In the cardiovascular system, cyclical contractions of the heart pump blood through specialised blood vessels, delivering oxygen, nutrients, hormones and leukocytes to tissues, and removing carbon dioxide and other metabolic waste products from them. The system is a ‘closed loop’, meaning blood never leaves the vessel circuit. Instead, blood is oxygenated at the lungs, and travels through arteries and arterioles to capillary beds, where gases and metabolites are allowed to exchange with those in the surrounding tissues, and blood cells can

leave by extravasation. Deoxygenated blood is then returned to the heart through venules and veins for further circuits around the body.

The lymphatic system, in contrast, is 'open'. It mainly functions as a drainage system, in which plasma that has leaked into the interstitial space surrounding tissues is unidirectionally returned to blood vessels as lymph in lymphatic vessels, via lymph nodes. As its name suggests, lymph contains lymphocytes, and so it is also heavily involved in the immune response.

1.2.1 Blood vessel function and architecture

Blood vessels, although specialised for their environment and physiological function, generally consist of three layers: the *tunica intima*, the *tunica media* and the *tunica adventitia*. The *tunica intima*, the innermost layer in direct contact with the flow of blood in the lumen, is a single sheet of endothelial cells (ECs) which forms a tube and an underlying basement membrane (BM). Vascular mural cells, such as smooth muscle cells (vSMCs) and pericytes, surround the *tunica intima* to help form the *tunica media*, and the outermost *tunica adventitia* is composed of fibrous connective tissue.

Differently sized blood vessels have different compositions of the vessel wall to suit their physiological function. Larger vessels, like arteries and veins, contain elastic layers, and have multiple layers of vSMCs, collagen, elastin and proteoglycans within the tunica media, and an elastic and collagenous tunica adventitia [2]. In smaller vessels, like capillaries, however, the endothelial tube is only sparsely covered in pericytes, and there is no perceptible adventitial layer [3]. A key difference between arteries and veins is that arteries have stronger elastic vessel walls for withstanding high blood pressures, whereas veins contain valves for preventing the backflow of blood under low pressure [2] (**Figure 1.1**).

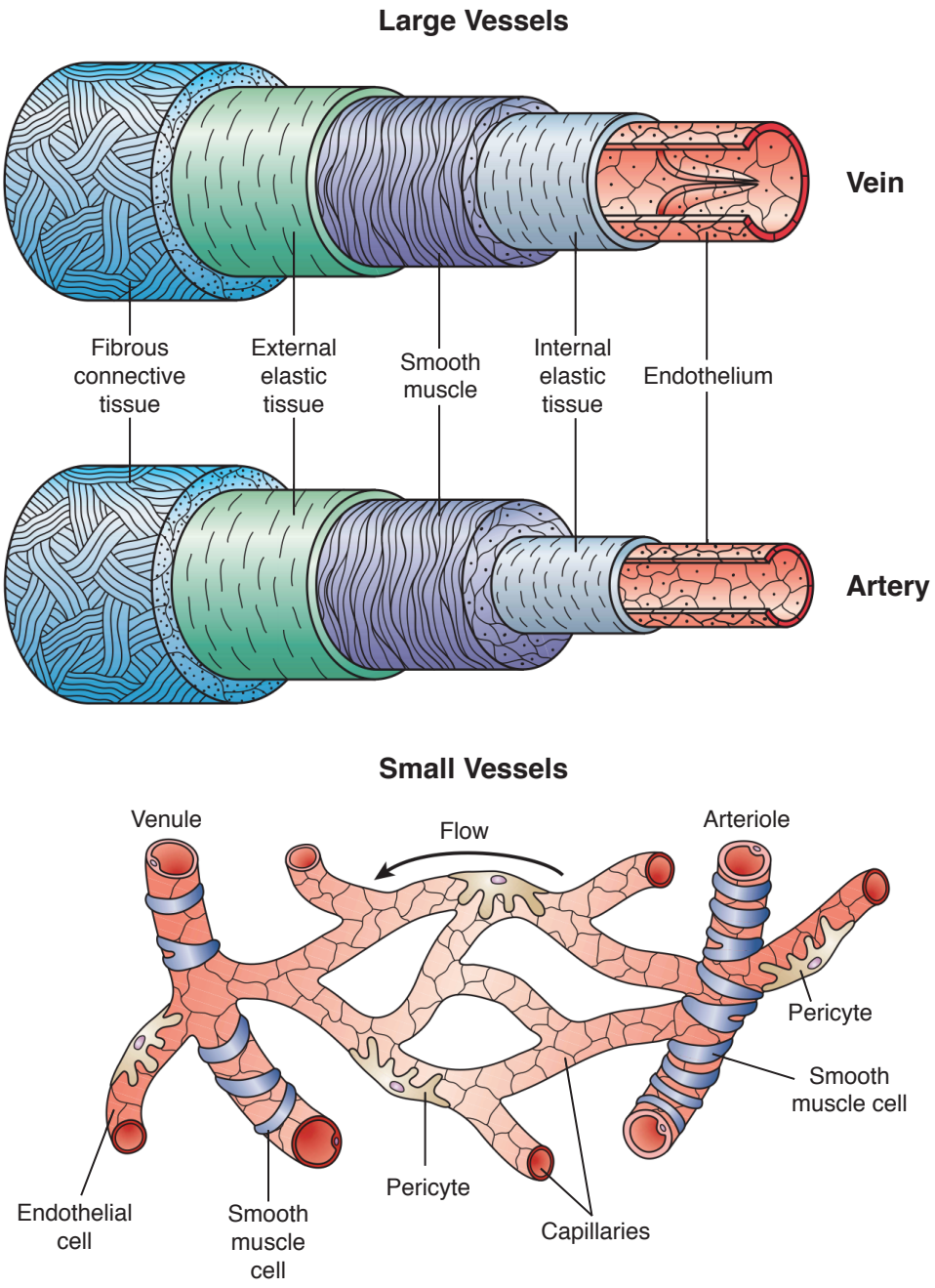

Figure 1.1: Blood vessel architecture. The vascular walls of large vessels (arteries and veins) consists of a *tunica intima*, which comprises a layer of endothelial cells, a basement membrane, and an internal elastic layer; a *tunica media*, composed of multiple layers of vascular smooth muscle cells, collagen, elastin and proteoglycans; and an elastic and collagenous *tunica adventitia*. Arteries have strong elastic walls for withstanding high blood pressures, and veins contain valves for preventing the backflow of blood under low pressure. Smaller vessels have a *tunica intima* without an elastic layer, and a *tunica media* that consists of sparsely covered smooth muscle cells or pericytes in capillaries. Small vessels have no perciptible *tunica adventitia*. Figure adapted from [2].

1.2.1.1 Endothelial cells

The ECs lining blood vessel walls are remarkably heterogeneous themselves, both between tissues and vessels, and even within organs [4] (reviewed in [5,6]). Firstly, at a morphological level, the endothelium can be classified as continuous, fenestrated or discontinuous, according to the physiological requirement of the tissue [2,7] (**Figure 1.2A**). Continuous endothelium is a contiguous layer of cells connected closely to one another by inter-endothelial junctions, and surrounded by an uninterrupted BM. It is found in arteries, veins, and capillaries of the brain, skin, heart, and lung [8]. Fenestrated endothelium is similar, except for the presence of small 80-100 nm-wide openings, called fenestrae, which allow macromolecules to rapidly pass through [2]. This endothelium is therefore characteristic of capillaries in areas involved in filtration or secretion, such as exocrine and endocrine glands, gastric and intestinal mucosa, the choroid plexus, glomeruli, and renal tubules [7]. Discontinuous endothelium has larger fenestrae, which give rise to large gaps in the cells, and a discontinuous or absent BM. It is mainly found in sinusoidal vascular beds, such as those in the liver [7,8].

ECs may also differ in size, shape, orientation relative to the direction of blood flow, the complexity of inter-endothelial junctions, and the presence of plasmalemmal vesicles known as Weibel-Palade bodies [2,9]. For example, microvascular ECs are thinner, more flattened and elongated compared to larger vessels; they also tend to have less complex endothelial junctions and fewer Weibel-Pilade bodies [9]. In normal resting blood vessels, ECs are generally referred to as quiescent 'phalanx' cells due to their resemblance to a close formation of marching soldiers; in this state, ECs are tightly aligned in a monolayer in the direction of blood flow to maintain optimum perfusion [10].

The endothelial intercellular junctions are tight junctions, adherens junctions, and gap junctions, which differ in their junctional protein composition (reviewed in [11,12]). For example, tight junctions contain claudins and occludins, whilst adherens junctions contain cadherins (**Figure 1.2B**). Intercellular junctions mediate adhesion and communication between adjoining ECs to control vascular homeostasis in a way that depends on the permeability requirements of their environment [11]. As an example, whilst adherens junctions are ubiquitous

across all blood vessels, tight junctions are poorly organised in post-capillary venules, where solutes and cells rapidly exchange between blood and tissues, but are highly complex in brain microvasculature to lower the permeability between blood and the nervous system [11,12].

ECs can control vascular homeostasis in many different ways, and they therefore observe considerable functional heterogeneity. As well as being able to perform organ-specific functions like differential permeability highlighted above, ECs control leukocyte homing, diapedesis (leukocyte extravasation), vascular tone (vasoconstriction and vasodilation), coagulation, thrombosis and fibrinolysis, acute inflammation and blood vessel formation [2] (reviewed in [13]).

1.2.1.2 Extracellular Matrix

ECs are adhered to and embedded within an extracellular matrix (ECM), which is organised into two different compartments [14]. The first of these is the BM, which lies in-between the ECs and their supporting mural cells. The BM consists of a network of molecules including collagen type IV, laminins, nidogens, heparan sulfate proteoglycans (HPSGs), such as perlecan, and fibronectin [14,15]. In most normal adult tissues, quiescent ECs mainly adhere to this ECM [14,16]. However, during angiogenesis, when ECs are required to sprout out to form new vessels, enzymes like matrix metalloproteinases (MMPs) can degrade the BM, allowing ECs to invade through, and adhere to, components of a second ECM, the interstitial matrix, until the newly formed vessels mature and regain another BM [14,16]. The interstitial ECM normally mainly contains elastin and fibrillar collagens like collagen type I, but during angiogenesis, fibrin and the glycoproteins fibronectin and vitronectin extravasate into a ‘provisional’ interstitial matrix from blood plasma [16,17].

1.2.1.3 Pericytes

Pericytes, like vSMCs, must associate with nascent blood vessels in order for them to stabilise and mature. These cells share, and co-synthesise, the BM with ECs, although they are on the opposite side of it [18]. Pericyte coverage of the endothelial tube is only partial, and varies between capillaries of different tissues for functional reasons [19]. Pericytes have primary cytoplasmic processes that

run along the length of the tube, and secondary processes that extend out perpendicularly to encircle, or ‘girdle’, the vessel [20]. Where holes arise in the BM separating ECs and pericytes, endothelial-pericyte, or peg-socket, contacts can be made, in which pericyte cytoplasmic fingers are inserted into endothelial invaginations [18]. These peg-socket contacts can contain tight-, gap-, and adherens junctions [19,21]. Additionally, there are further endothelial-pericyte contacts called adhesion plaques, which contain fibronectin deposits [21]. See **Figure 1.2C.**

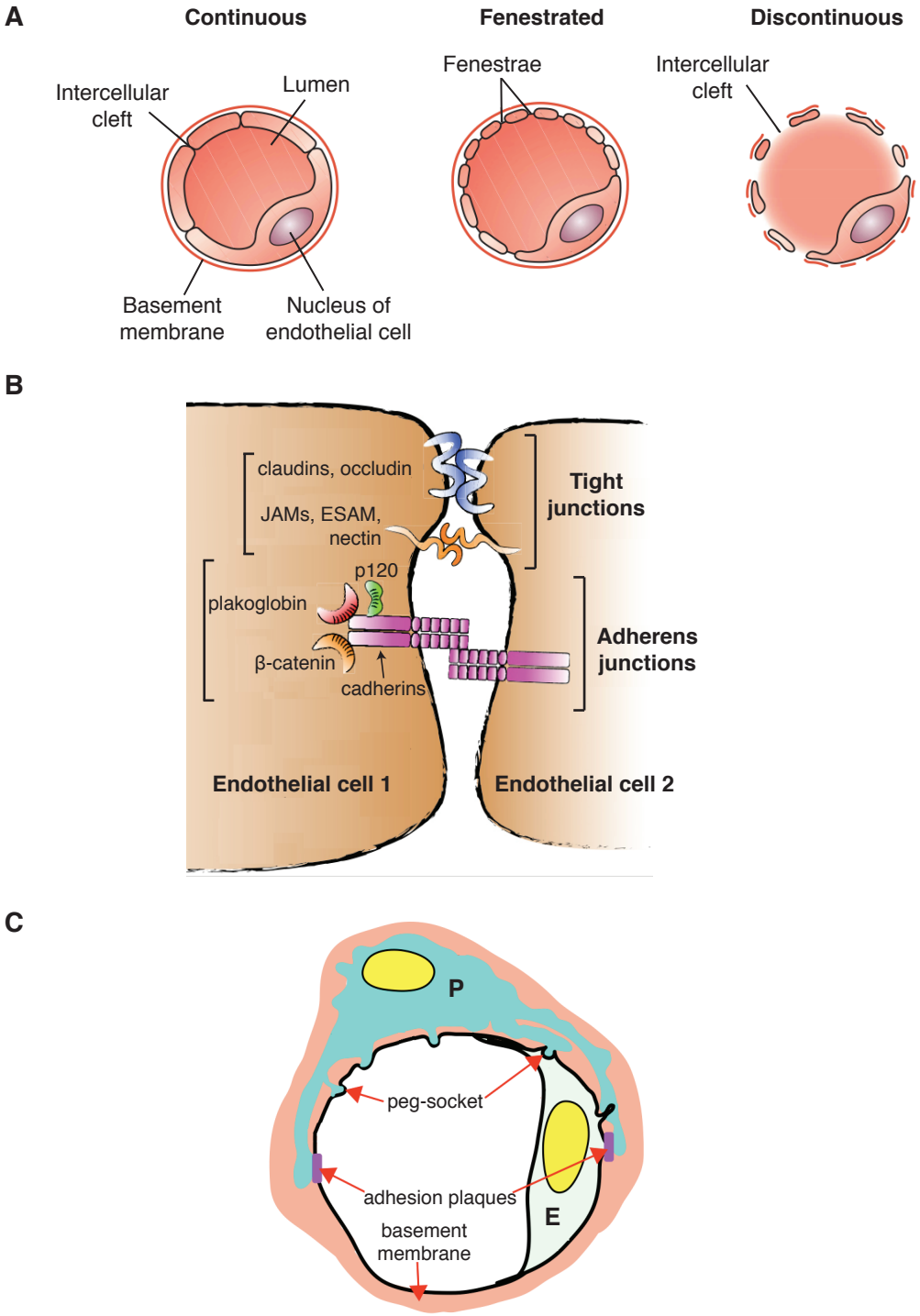

Figure 1.2: Morphological features of blood vessels. A The endothelium of blood vessels can be morphologically classified as continuous, fenestrated, and discontinuous, depending on the physiological requirements of the tissue. Continuous endothelium is a layer of cells connected closely to one another by inter-endothelial junctions, and surrounded by an uninterrupted basement membrane (BM). Fenestrated endothelium additionally contains small 80-100 nm-wide openings, called fenestrae, which allow macromolecules to rapidly pass through. Discontinuous endothelium has larger fenestrae, which give rise to large gaps in the cells, and a discontinuous or absent BM. **B** Inter-endothelial adhesion junctions include tight junctions and adherens junctions, which differ in their protein composition. **C** Pericytes share a BM with, and encircle, endothelial cells in mature blood vessels. Endothelial-pericyte contacts can be made where holes arise in the BM separating ECs and pericytes (peg-sockets), or at adhesion plaques. Figures adapted from [2], [33], and [106].

1.3 Blood vessel development/formation

Blood vessels represent the first 'organ' to form and function during embryogenesis [22]. During a lifespan, blood vessels can form in three main different ways: vasculogenesis, sprouting angiogenesis, and intussusception. Vasculogenesis is the term used to describe how blood vessels form into a primitive network *de novo* from differentiating angioblasts in the developing embryo. After arterial or venous differentiation has been specified, blood vessels can expand and pattern from this vascular 'plexus' by sprouting angiogenesis, or intussusception, the splitting of vessels by interstitial tissue columns entering and partitioning the lumen [23,24]. A final, more controversial method of blood vessel formation is postnatal vasculogenesis, in which bone-marrow-derived cells (BMDCs) and/or endothelial progenitor cells (EPCs) are recruited and incorporated into the endothelial lining [24] (**Figure 1.3**). After branching, nascent vessels can expand their lumens, and recruit mural cells for stabilisation, which themselves can proliferate, migrate, and differentiate to help remodel stronger, more contractile and elastic mature vessels that can control perfusion [25,26]. This constitutes a separate process known as arteriogenesis. Finally, during the patterning process, blood vessels can also be 'pruned' and specialised to meet local tissue demands [26].

1.3.1 Vasculogenesis

The process of vasculogenesis begins extraembryonically in the yolk sac. Here, hemangioblasts, which are mesoderm-derived progenitors of both ECs and hematopoietic cells, form aggregates called 'blood islands' [22]. Cells on the periphery of these aggregates differentiate into angioblasts, which migrate and further differentiate into ECs. These ECs are then able to assemble into the endothelial tubes that ultimately make up the vascular plexus [25].

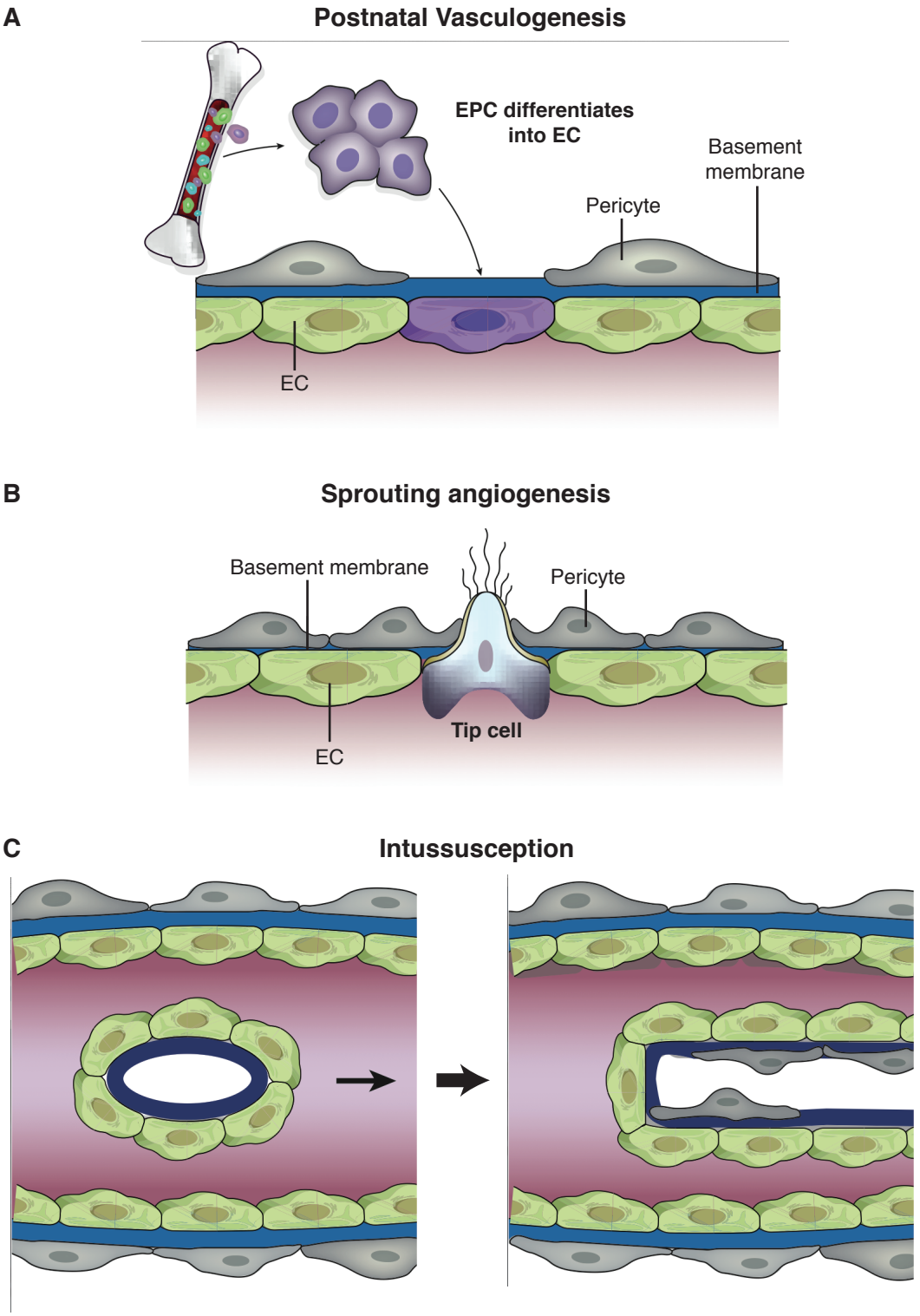

Figure 1.3: Blood vessel formation. Following the *de novo* formation of blood vessels by vasculogenesis in the developing embryo, new blood vessels can form by: **A** postnatal vasculogenesis, the recruitment of endothelial progenitor cells (EPC) that differentiate into endothelial cells (EC); **B** sprouting angiogenesis; and **C** intussusceptive angiogenesis, the splitting of vessels by interstitial tissue columns entering and partitioning the lumen. Figure adapted from [24].

1.3.2 Angiogenesis

Angiogenesis is strictly defined as the formation of blood vessels from pre-existing vasculature, meaning both sprouting angiogenesis and intussusceptive angiogenesis are encompassed by the term. It occurs during embryonic development in order to establish an advanced system of stable vessels after the primitive vascular plexus has formed by vasculogenesis, and subsequently also occurs postnatally to support growing tissues [17]. In adults, where most blood vessels are quiescent, physiological angiogenesis is less common. However, it remains an important process in the uterus and ovary during the menstrual cycle, in the placenta during pregnancy, in skeletal muscle after exercise, and in regenerating tissues following injury [27]. Unfortunately, angiogenesis can become dysregulated and contribute to a range of pathological conditions, including cancer.

Angiogenesis is a complicated process with many stages and molecular 'players' expressed by different cell types. It will be discussed in greater mechanistic detail in the next sub-chapter, but as an overview: Angiogenesis initiates when hypoxic, inflammatory or tumour cells release a plethora of pro-angiogenic growth factors, such as vascular endothelial growth factors (VEGFs), angiopoietin 2 (ANG2), or fibroblast growth factors (FGFs). This tips the balance away from anti-angiogenic factors to turn on the angiogenic 'switch', triggering the removal of pericytes from nearby capillaries and degradation of the BM and ECM by proteases like MMPs. ECs loosen their intercellular junctions, proliferate, and, in response to integrin signalling, migrate onto newly forming and remodelling ECM, guided chemotactically towards the released soluble growth factors. Finally, ECs re-establish their junctions and are covered by new BM and pericytes to form tube-like structures that support blood flow to the original growth factor-releasing cells [24]. Vessels made from ECs that are not covered with pericytes are unstable, and undergo regression [28]. See **Figure 1.4**, which includes molecular players mentioned in the following chapter.

1.3.2.1 Mechanisms of Angiogenic sprouting

To examine the process of sprouting angiogenesis in more detail, each important step, which is not necessarily sequential, has been divided into the following sections below: *i) Hypoxia and growth factor release*; *ii) Pericyte removal and BM degradation*; *iii) EC junction loosening and ECM deposition*; *iv) Endothelial tip cell selection and guidance; v) EC migration and vessel anastomosis*; *vi) Vessel maturation*.

i) Hypoxia and growth factor release:

When tissues grow enough to outstrip their oxygen supply, they are said to become 'hypoxic', and must recruit new blood vessels by angiogenesis to meet their oxygen demand again. Under hypoxia, oxygen sensors called prolyl hydroxylase domains (PHDs) can no longer use oxygen to hydoxylate hypoxia-inducible factors (HIFs), such as HIF-1α, meaning HIFs escape proteasomal degradation and are stabilised [24,29]. HIFs can then bind hypoxia response elements in DNA to induce the expression of genes involved in angiogenesis, such as VEGF, VEGF receptors 1 and 2 (VEGFR1 and VEGFR2), neuropilin-1, ANG2, nitric oxide synthase, transforming growth factor-β (TGFβ), platelet-derived growth factor-BB (PDGF-BB), endothelin-1, interleukin-8, insulin growth factor 2 (IGF2), TIE1, and cyclooxygenase-2 [25] (reviewed in [30]). Hypoxic tissues therefore release growth factors, setting up gradients towards nearby ECs that in response upregulate their own angiogenic growth factors and receptors. Growth factor binding to cell receptors initiates different angiogenesis signalling cascades and responses.

ii) Pericyte removal and BM degradation:

Pericytes, which normally stably interact with ECs and suppress their proliferation via ANG1 (a ligand of the TIE2 endothelial receptor), detach from the vessel wall in response to ANG2, which can antagonise ANG1 through competition [24]. Meanwhile, the BM ECM is degraded by proteinases including MMPs, such as MT-MMP1, and ADAMs (A disintegrin and metalloproteinases), thus liberating the pericytes further [24,29,31].

iii) EC junction loosening and ECM deposition:

In tandem, angiogenic factors also cause EC junctions to loosen. For example, the transmembrane adherens junction protein VE-cadherin, a major regulator of vessel integrity and permeability, loses its adhesive function between ECs partly due to its VEGF-mediated endocytosis [24,31,32] reviewed in [33,34]). Endothelial quiescence is also disrupted by ANG2, which inhibits ANG1-mediated TIE2 clustering in *trans* at cell-cell junctions [24]. As ECs loosen their junctions, blood vessels dilate in response to nitric oxide, and VEGF increases their permeability, allowing ECM proteins like fibrin, fibronectin and vitronectin to extravasate and lay down a provisional interstitial ECM for migrating ECs [16,17,24,25].

iv) Endothelial tip cell selection and guidance:

To direct angiogenic sprouting toward a growth factor stimulus in a coordinated manner, an endothelial 'tip' cell must be selected to lead and guide an emerging sprout [35]. These tip cells are motile; they extend out filopodia in response to guidance cues, allowing them to migrate down the growth factor gradient. Lying adjacent are endothelial 'stalk' cells, which form a vessel lumen and proliferate to elongate the sprout from behind [29]. Tip/stalk cell specification and guidance is mainly regulated by the VEGF, NOTCH, and WNT pathways, as reviewed extensively recently by [24,29,31,36-38], and briefly described below.

ECs compete for the tip position following their upregulation of the NOTCH ligand, Delta-like-ligand 4 (DLL4), partly in response to VEGF activation of VEGFR2 [38-40]. DLL4 binds to NOTCH receptors on neighbouring ECs, causing them to decrease their VEGFR2, VEGFR3, and neuropilin-1 expression, and increase their levels of the VEGF decoy receptor, VEGFR1 [31,38,40]. This signalling specifies these neighbouring cells as the stalk cells, making them less responsive to sprouting signals from VEGF, yet more responsive to the VEGFR1 ligand, placental growth factor (PlGF) [24]. Stalk cells additionally preferentially express another NOTCH ligand, JAGGED1, which heightens the tip/stalk divide by antagonising DLL4-NOTCH activation back on tip cells [41]. Following this initial tip/stalk cell specification, ECs continue to dynamically compete for the tip

position based on the degree of their VEGFR2:VEGFR1 level ratio, meaning tip cells are always best equipped to respond to VEGF and take the lead [38,40].

Tip cells are guided in response to cues from VEGF, ephrins, semaphorins, and Slits, which coordinate filopodial extension [24]. Meanwhile, stalk cells create perfused vessels by establishing the lumen, utilising VEGF, VE-cadherin, CD34, sialomucins, and hedgehog [24]. Stalk cell proliferation, responsible for vessel elongation, is partly mediated by NOTCH-induced WNT signalling through FRIZZLED receptors [24].

v) EC migration and vessel anastomosis:

As ECs are specified, guided and proliferated, they use their adhesion molecules, such as integrins, to adhere to, and migrate through continuously remodelling interstitial ECM. Migration is achieved by ECs propelling themselves forwards whilst constantly assembling and disassembling their adhesions with the surrounding ECM, which is degraded by proteinases and re-scaffolded by extravasating glycoproteins into a more accommodating environment for invasion. As proteinases (MMPs, plasminogen activators, heparinases, chymases etc.), degrade the ECM, growth factors (FGF, VEGF, and insulin growth factor 1 (IGF1)) sequestered within it are mobilised to enhance the angiogenic response [17,24,25].

Sprouting vessels are redundant unless they reconnect with the circulation to maintain blood flow. Tip cells therefore undergo anastomosis with cells from other nearby sprouts to form perfused vessel loops [29]. Anastomosis is facilitated by the accumulation of macrophages, and reaches conclusion when VE-cadherin-containing junctions form, and vessels stabilise and mature (see below) [29,42].

vi) Vessel maturation:

Once nascent blood vessel sprouts anastomose, the network becomes subject to a remodelling process, in which vascular branches either mature or regress to meet the oxygen requirements of the surrounding tissue. In order to become quiescent and functional, vessels must mature by re-establishing endothelial intercellular junctions, forming a new BM, and recruiting stabilising mural cells,

mainly through TGF-β, PDGF-B, and ANG1 signalling, as described below. If vessels do not become perfused, they undergo regression [26].

TGF-β, as well as promoting the recruitment of pericytes by regulating their proliferation, migration, and differentiation from precursor cells, is involved in BM deposition through its induction of the expression of fibronectin and collagens I, IV, and V [26,29,38,43]. BM maturation is further aided by TGF-β due to its signalling inducing the expression of the protease inhibitor plasminogen activator inhibitor-1 (PAI-1), which, along with tissue inhibitors of metalloproteinases (TIMPs), prevents ECM degradation [24,26,29,44].

Aside from TGF-β, mural cell recruitment is controlled by endothelial PDGF-B, which is secreted and subsequently signalled through PDGF receptor-β (PDGFR-β) in mural cells to stimulate their migration and proliferation towards the immature vessel [29,45,46]. The binding of ANG1, expressed on the surfaces of mural cells, to TIE2 receptors on ECs promotes a stable interaction between these cells, and tightens endothelial junctions, as mentioned above (reviewed by [47]). However, ANG1's role in mural cell recruitment is now contentious [38]. EC/mural cell interactions are also enhanced by sphingosine-1-phosphate (S1P), which increases the expression of N-cadherin at this junctional interface, and downregulates endothelial ANG2 [38,48]. S1P further promotes maturation by inhibiting VEGF signalling and stabilising VE-cadherin-containing junctions in ECs [38,49].

Mural cell recruitment and vessel maturation have additionally been shown to be regulated by other pathways, including DLL4/NOTCH [36], ephrins/Eph receptors [50], WNT [51], and integrins [52].

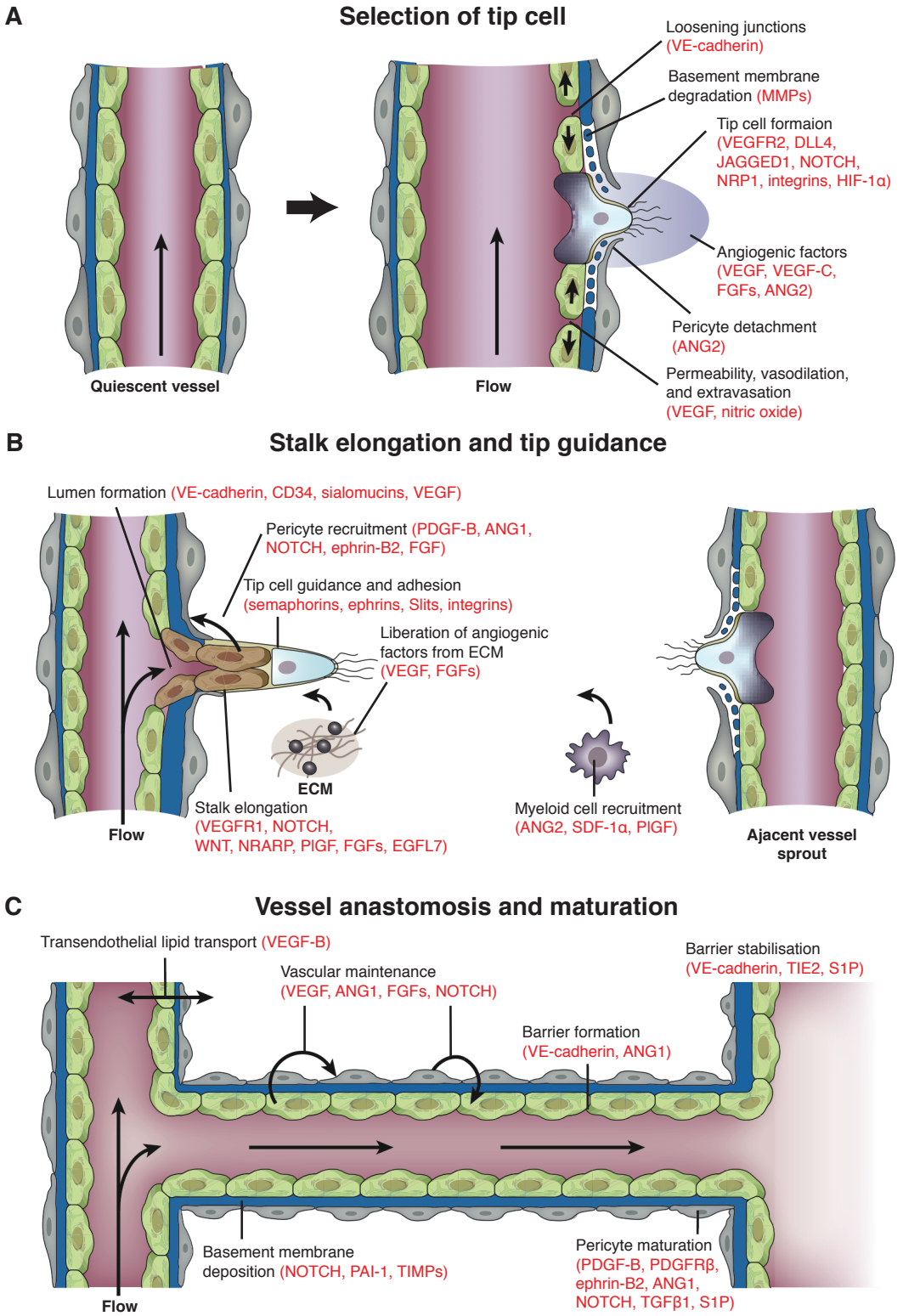

Figure 1.4: Mechanism of angiogenic sprouting. The schematic highlights the stages of angiogenesis, as described in the main text, and includes the key molecular players (in red). **A** The release of local angiogenic factors results in pericyte removal, basement membrane degradation, the loosening of endothelial junctions, increased blood vessel permeability, and the selection of a tip cell. **B** Tip cells are guided in response to environmental cues, whilst the stalk cells behind form a vessel lumen, proliferate and elongate to extend the forming sprouting endothelial cells, which migrate through the remodelling extracellular matrix in an integrin-dependent manner. **C** Sprouting vessels anastomose with other sprouts, and mature by depositing new basement membrane, re-establishing endothelial junctions, and recruiting pericytes. Figure adapted from [24].

1.3.2.2 The VEGF family and its receptors

Of all the pro-angiogenic growth factors released in angiogenesis, VEGFs are seen as the most important, demonstrated by the fact that they are upregulated by up to 30-fold within minutes of the stabilisation of HIFs [17]. VEGFs are dimeric glycoproteins that belong to the PDGF supergene family. In mammals, the family members include VEGF-A, -B, -C, -D, and placental growth factor, each of which shares a common structure that comprises a VEGF homology domain with eight characteristically spaced cysteine residues [53,54]. VEGFs can bind different variants of type III receptor tyrosine kinases, VEGF receptors 1, 2 and 3 (VEGFR1/2/3), causing them to homo- or hetero-dimerise [55,56] (**Figure 1.5A**). VEGFR signalling cascades are activated downstream of this ligand-induced dimerisation by activation of the kinase domain, and can be further regulated by the recruitment of co-receptors, such as neuropilins and integrins [55].

VEGF-A, the major mediator of angiogenesis, signals mainly through VEGFR2, which is upregulated in ECs of angiogenic vessels [57]. VEGFR2 activation leads to EC migration, proliferation, differentiation and survival, as well as vessel sprouting and permeability, through a variety of different signalling pathways [54,58].

VEGF-C binds VEGFR2 weakly, but mainly activates VEGFR3 to also induce tip cell sprouting, although not as efficaciously as VEGF-A [38]. Despite this, VEGFR3 is primarily involved in vasculogenesis and lymphangiogenesis (the lymphatic vessel equivalent of angiogenesis) [24]. VEGF-D also binds both VEGFR2 and VEGFR3, although not the former in mice, and has some angiogenic and lymphangiogenic potential [53].

The role of VEGFR1 in angiogenesis (otherwise known as Flt1 - FMS-like tyrosine kinase) is much less certain. Indeed, its affinity for VEGF-A is higher than that of VEGFR2, yet its kinase activity is much weaker [58]. This has led to the proposal that VEGFR1 acts as a ‘decoy’ for VEGF-A, preventing its more potent activation of angiogenesis via VEGFR2. As described above, this probably explains how stalk cells, which have high levels of VEGFR1, are less responsive

to sprouting signals from VEGF-A. As well as existing in a membrane-anchored form, VEGFR1 can be alternatively spliced to become soluble (sFlt1). In this form, VEGFR1 can similarly inhibit signaling by sequestering free endogenous VEGF-A [24,54,58]. Aside from VEGFR1's disputed role in angiogenesis, it also acts as a receptor for VEGF-B, whose *in vivo* role is poorly defined, and PlGF, which is more associated with arteriogenesis [53].

It is worth noting here that VEGFs are produced by different cells, and function as cytokines not only for ECs, but for various cell types, including EPCs, lymphatic ECs, and mural cells [58]. Given their overwhelmingly dominant role in angiogenesis, I will focus on VEGF-A, and VEGFR2 in this thesis.

1.3.2.2.1 VEGF-A

The dominance of VEGF-A (hitherto, and hereafter referred to as VEGF) in vasculogenesis and angiogenesis is highlighted by the fact that mice lacking a single VEGF allele die at approximately embryonic day (E)9.5 with severe vascular defects [59,60]. VEGF coordinates the angiogenic response in many different contexts by binding its receptors VEGFR1 and VEGFR2, as well as its 'co-receptors' neuropilin-1 (NRP1) and neuropilin-2 (NRP2), to induce EC sprouting, migration, proliferation, survival, and permeability through different mechanisms [53,61]. For example, VEGF can promote EC survival by inducing the expression of the anti-apoptotic proteins Bcl2 and A1 [62], and permeability/vasodilation by inducing the expression of endothelial nitric oxide synthase (eNOS) [63].

Due to alternative splicing and proteolytic processing, there are four main isoforms of VEGF, each denoted by their number of amino acids ($VEGF_{121}$, $VEGF_{165}$, $VEGF_{189}$, and $VEGF_{206}$) [22]. These isoforms differ in their ability to bind HPSGs in the ECM [53]. Because of this, different VEGF isoforms are either soluble ($VEGF_{121}$ and $VEGF_{165}$) or matrix-bound ($VEGF_{189}$ and $VEGF_{206}$), and have identifiable, yet overlapping functions [53]. This balance between the soluble and HPSG-bound isoforms helps maintain the VEGF gradient, which is vital for coordinated vessel sprouting, but also affects VEGFR-integrin/neuropilin engagement and the spatial distribution of VEGFR signalling [22,64-66]. The

most commonly produced VEGF isoforms are $VEGF_{121}$, $VEGF_{165}$, and $VEGF_{189}$, although knockout studies in mice suggest that $VEGF_{165}$ is the most efficacious [53]. Indeed, $VEGF_{165}$, which despite its solubility can bind heparin, has increased signalling potential over the non-heparin binding $VEGF_{121}$, potentially due to its ability to promote NRP1-VEGFR2 complex formation [67-69]. More recently, further VEGF splice variants denoted VEGF-$A_{(xxx)b}$ have been discovered, although they appear to be anti-angiogenic (reviewed in [70]).

Interestingly, there is disparity between the actions of paracrine VEGF on ECs and autocrine VEGF produced by ECs. Whereas paracrine VEGF induces EC sprouting, autocrine VEGF is more involved in maintaining vessel homeostasis [58,71].

1.3.2.2.2 VEGFR2

VEGFR2, also known as KDR (kinase domain receptor) in the human and Flk1 (fetal liver kinase-1) in the mouse, is the main VEGFR in ECs [65]. Like the other VEGFRs, it is made up of seven extracellular immunoglobulin (Ig)-like domains, a transmembrane (TM) domain, a regulatory juxtamembrane domain, an intracellular tyrosine kinase domain, a kinase insert domain, and a carboxy(C)-terminal domain [55]. VEGF binds VEGFR2 at Ig-like domains 2-3 to induce its dimerisation and allow trans/autophosphorylation of intracellular tyrosine (Y) residues, which include Y951, Y1054, Y1059, Y1175 and Y1214 [65]. These phosphorylated tyrosines serve as binding sites for downstream signalling mediators containing SRC homology 2 (SH2) domains. For example, phosphorylation of Y1175, located at the C-terminal domain, results in the recruitment of signalling mediators like phospholipase Cγ (PLCγ), the adapter proteins SHB and SCK, and SHCA and GRB2, which in turn recruit SOS [65]. Various signalling cascades follow to initiate different cellular events involved in the angiogenic response including cell proliferation, migration, survival, and permeability (**Figure 1.5B**) [65].

EC proliferation is mainly induced by VEGF via activation of the RAS/RAF/MEK/ERK (mitogen activated protein kinase (MAPK)) pathway [65,72]. Signals are directed through this pathway via phosphorylated PLCγ, which

hydrolyses phosphatidylinositol bisphosphate (PIP_2) at the membrane to DAG and IP_3. DAG subsequently activates PKC, which is believed to propagate the signal through the MAPK pathway partly via sphingosine kinase (SPK) phosphorylation of RAS [73], but PKC can also feed in independently of RAS [65,74].

The VEGFR2-dependent migration of ECs can be dictated through signalling transducers that bind phosphorylated(p) Y951, Y1175, and Y1214 [65]. For example, pY1175-mediated SHB recruitment results in SRC-dependent SHB phosphorylation [75]. In turn, SHB binds focal adhesion kinase (FAK), resulting in its phosphorylation [65,76]. FAK is then able to influence migration through its role in regulating the turnover of focal adhesions and actin organisation [55]. Another stimulator of migration, Rac, which generates 'ruffles' in the membrane, is activated in response to GAB1-mediated PI3K production of phosphatidylinositol trisphosphate (PIP_3), although GAB1's VEGFR2-binding site is yet to be determined [65,77]. Additionally, pY1214 recruits a NCK/FYN complex, which mediates the activation of migration enhancers Cdc42 and p38MAPK via phosphorylation of PAK2 [78]. Various other inducers of migration are activated through VEGFR2 signalling, including IQGAP1, HSP27, and TSAd [65].

The production of PIP_3 via VEGFR2-activated PI3K also leads to the activation of Akt, which is one of the molecules involved in inhibiting apoptosis and therefore promoting cell survival [65]. VEGFR2's mediation of vessel permeability involves signalling through eNOS, and the phosphorylation or endocytosis of VE-cadherin [32,65,79].

VEGFR2 signalling output can be modulated by clustering, heterodimerisation, phosphatases, its co-receptors, integrins and neuropilins, as described later, and also by its subcellular location. Indeed, although VEGFR-2 was previously thought to exclusively signal at the plasma membrane, it is now known to additionally signal from early or recycling endosomes [80-85]. Moreover, the endocytosis of cell surface receptors like VEGFR2 is widely reported to enhance downstream signalling (e.g. via ERK1/2) and angiogenesis [86,87]. In resting

ECs, a significant proportion of VEGFR2 is stored in intracellular vesicles, but is delivered to the plasma membrane in a SRC-dependent manner upon VEGF stimulation [88]. Meanwhile, VEGF also initiates VEGFR2 membranal internalisation into endosomes, which is regulated by ephrinB2, VE-cadherin, and the phosphatase DEP1 [65,83,85,89-91]. Subsequently, VEGFR2 is either degraded following its ubiquitination, or recycled to the membrane, allowing it to continue signalling. This recycling process is dependent on VEGFR2's interaction with NRP1, and will therefore be discussed in more detail later.

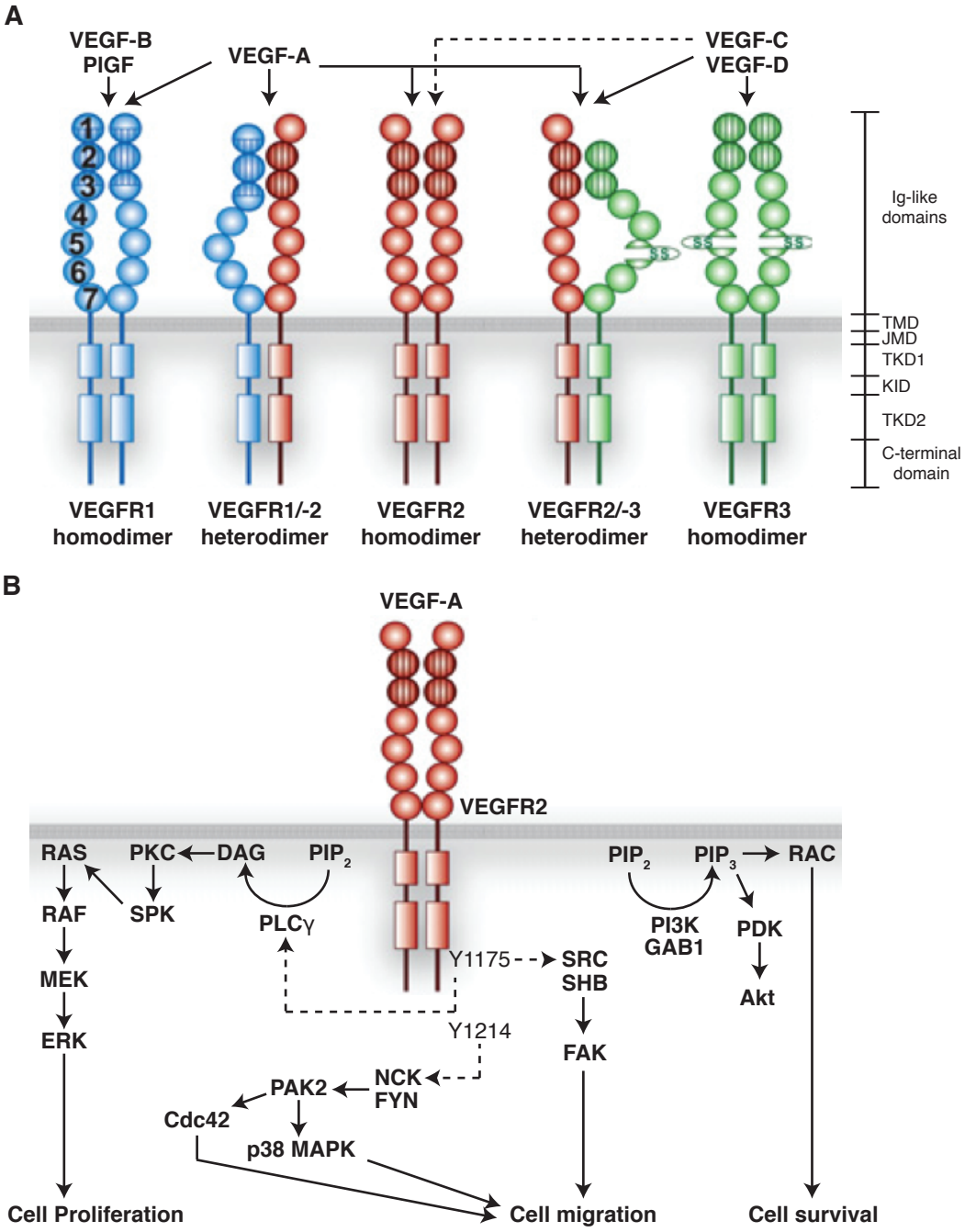

Figure 1.5: Structure and signalling of VEGF receptors. A VEGFs can bind different variants of type III receptor tyrosine kinases, VEGF receptors 1, 2 and 3 (VEGFR1/2/3), causing them to homo- or hetero-dimerise. VEGF-A signals mainly through VEGFR2. VEGF-B and PlGF bind VEGFR1. VEGF-C binds VEGFR2 weakly, but mainly activates VEGFR3, and VEGF-D also binds both VEGFR2 and VEGFR3, although not the former in mice. VEGFRs consist of extracellular immunoglobulin (Ig)-like domains, a transmembrane domain (TMD), a regulatory juxtamembrane domain (JMD), an intracellular tyrosine kinase domain (TKD), a kinase insert domain (KID), and a carboxy(C)-terminal domain. **B** VEGF-A activates VEGFR2, resulting in the phosphorylation of its intracellular tyrosine (Y) residues. For example, Y1175 phosphorylation results in activation of the RAS-RAF-MEK-ERK pathway, and SRC/FAK, to promote cell proliferation and migration, respectively. Y1214 phosphorylation activates p38 MAPK- and Cdc42-mediated cell migration. The VEGFR2 phosphorylation site that mediates the Akt cell survival pathway is currently unknown. Figures adapted from [65] and [276].

1.4 Angiogenesis in disease

Unfortunately, insufficient or excessive angiogenesis can contribute to the development of a range of pathological conditions. For example, too little can lead to ischemic diseases such as stroke and coronary artery disease, whilst too much is associated with psoriasis, arthritis, diabetic blindness, and cancer [17]. This thesis is concerned with the latter.

1.4.1 Cancer

The term cancer encompasses a group of diseases characterised by the abnormal growth of cells into malignant neoplasms, or tumours, which are capable of spreading (metastasising) to different tissues around the body. It has been proposed that there are six 'hallmarks' of cancer that can be acquired to contribute to the progression of tumour cell growth and metastasis [92,93]. These are: 1) Sustaining proliferative signalling; 2) Evading growth suppressors; 3) Resisting cell death (apoptosis); 4) Enabling replicative immortality; 5) Inducing angiogenesis; 6) Activating invasion and metastasis [92,93].

1.4.1.1 Tumour Angiogenesis

Angiogenesis is critical for cancer progression as tumours are limited in growth and cannot metastasise until they acquire their own blood supply [23,94]. This led J. Folkman to propose, as early as 1971, that inhibiting tumour angiogenesis might be a valuable therapy against cancer [28,95]. When a tumour exceeds a few millimetres in diameter, hypoxia and nutrient-deprivation trigger, and in this case sustain, the angiogenic switch, meaning pro-angiogenic growth factors are persistently released in the tumour microenvironment [96,97]. This results in the induction of the same angiogenic signalling pathways as in normal angiogenesis, but due to their dysregulation, the arising vasculature is continuously remodelled, and is therefore leaky, tortuous and fragile [97,98]. Where mural cells have detached to expose the degrading BM, platelets become activated to release more angiogenic and permeability factors that enhance the response [97,98]. Tumour-associated fibroblasts (TAFs) then aberrantly deposit ECM, which is continuously remodelled by proteases to expose more growth factors [97,99]. To further escalate matters, even more stimulatory factors are released by TAFs,

infiltrating inflammatory cells (e.g. tumour-associated macrophages (TAMs) and neutrophils (both bone-marrow-derived myeloid cells)), and bone-marrow derived EPCs [97]. Tumour vessels additionally lack functional mural cells, meaning they can never fully reach quiescence and are more prone to regression [23]. Notably, in tumour angiogenesis, not only can blood vessels sprout from pre-existing ones, as in normal angiogenesis, but tumour cells can also co-opt the existing vasculature, and vessels can even form from differentiating tumour stem cells (vascular mimicry) [24,97,100]. Unsurprisingly, this does not stabilize the vasculature, but rather increases the likeliness of metastasis [97]. See **Figure 1.6**.

Clearly, tumour angiogenesis is a complex process whose aberrance is dependent on the contribution of multiple cell types. In fact, although once disregarded, the tumour microenvironment, or stroma, is now seen as similarly important for tumour progression and angiogenesis as the tumour (parenchymal) cells are themselves. Stromal cells include ECs, mural cells, TAFs, TAMs, EPCs, and lymphatic ECs, all of which can produce and/or respond to VEGF [58,101]. Below I have highlighted examples of how tumour and stromal cells contribute to the enhanced and aberrant tumour angiogenesis phenotype.

Tumour cells:

As we know, tumour cells signal to cells in their microenvironment in a paracrine manner to initiate angiogenesis in response to hypoxia. However, due to the abnormal and poorly perfused tumour vasculature that results, 'pockets' of hypoxia and acidosis persist throughout the tumour, creating a hostile environment in which pro-angiogenic factors are sustainably released to promote a vicious cycle of events [29]. Tumour cells not only produce VEGF, but respond to it to enhance their own survival, migration, proliferation, metastasis and epithelial-to-mesenchymal transition (EMT), and thus promote tumourigenesis [58]. Aside from VEGF, tumour cells additionally release many other pro-angiogenic factors that contribute to tumour growth and angiogenesis, including PlGF, VEGF-C, VEGF-D, PDGF-C, FGF1 or FGF2, ANG1, and ephrins A1 and A2 [58].

Tumour endothelial cells:

Pathologically high and persistent levels of VEGF and other growth factors have numerous consequences for ECs and angiogenesis, but ultimately they lead to hypersprouting and abnormal vessels [10,58]. Activated tumour ECs lose their polarity, and can detach from the BM and stack on top of each other, impeding blood flow [10]. They hypersprout, probably by increasing tip cell formation via DLL4, and become leaky through increasing their number of fenestrations, and widening their junctions, partly through a loss in differential VE-cadherin mobility [10,102]. This increase in permeability builds interstitial hypertension, impairs perfusion, and allows for leukocyte extravasation and tumour cell invasiveness [58,101]. Recently, EC metabolism has been pinpointed as a regulator of angiogenesis that is also influential in the context of a tumour. ECs rely on glycolysis for their metabolism, which is enhanced in response to VEGF via the upregulation of PFKFB3 [103,104]. This provides energy to increase EC proliferation and tip cell locomotion through inducing rapid actin remodelling in filopodia and lamellipodia [103,104]. The pharmacological inhibition of PFKFB3 has been shown to block tumour growth *in vivo* [104,105].

Mural cells:

Like in the physiological situation, tumours and their microenvironment release PDGF-B to recruit pericytes, but frequently tumour vessels have loose EC-pericyte associations and inadequate pericyte coverage, possibly due to a VEGF-dependent increase in ANG2 [58,106,107]. Those pericytes that do attach to the endothelium may have an abnormal shape, extend their processes into the stroma, and express less contractile markers [10]. Interestingly, it has been shown that breast cancer cell-derived VEGF enhances mural cell migration through a VEGFR1/NRP1/Akt-dependent pathway, although how this impacts on tumour vessel mural cell coverage is unclear [58,108]. Pericyte abnormalities ultimately ensure tumour vessels keep remodelling and never reach maturity, and thus disrupt blood flow and increase tumour cell intravasation and metastasis, for example [10,109].

Tumour associated fibroblasts (TAFs):

Signalling from tumour cells promotes the differentiation of tissue-resident fibroblasts into myofibroblasts and then into TAFs [110]. In contrast to myofibroblasts, TAFs can no longer revert to normal fibroblasts, are anti-apoptotic, and are generally more pro-tumourigenic [110]. TAFs are important regulators of tumour angiogenesis as they produce pro-angiogenic growth factors, allow them to be stored within the ECM they lay down, and release MMPs that make them available [110]. They have also been implicated in the recruitment of EPCs and stimulation of tumour growth through their secretion of stromal cell-derived factor (SDF)1 (CXCL12) [111].

Bone marrow-derived cells (BMDCs):

VEGF recruits bone-marrow derived EPCs (non-haematopoietic) and $CXCR4^+$ myeloid cells (haematopoietic) to the hypoxic tissue, where their CXCR4 receptor is bound by SDF1-α from perivascular myofibroblasts [58,112,113]. This enables EPCs to differentiate into contributing ECs (postnatal vasculogenesis), and pro-angiogenic monocytes and macrophages to become residents of the perivascular space, respectively [58,112,113]. Indeed, inflammatory cells, which additionally include mast cells, eosinophils, neutrophils, and dendritic cells, have an important role in tumour angiogenesis, having been initially ineffective at fighting the tumour [110]. By this point, they have been shown to release pro-angiogenic factors and ECM proteinases, and even suppress cytotoxic T-cell activity [110]. As an example, TAMs that resemble M2-type macrophages promote tumour growth and metastasis through their release of PlGF [114]. Given that inflammatory cells are now promoting, rather than suppressing, tumour growth and angiogenesis, tumours have rather bleakly been described as ‘wounds that do not heal’ [115].

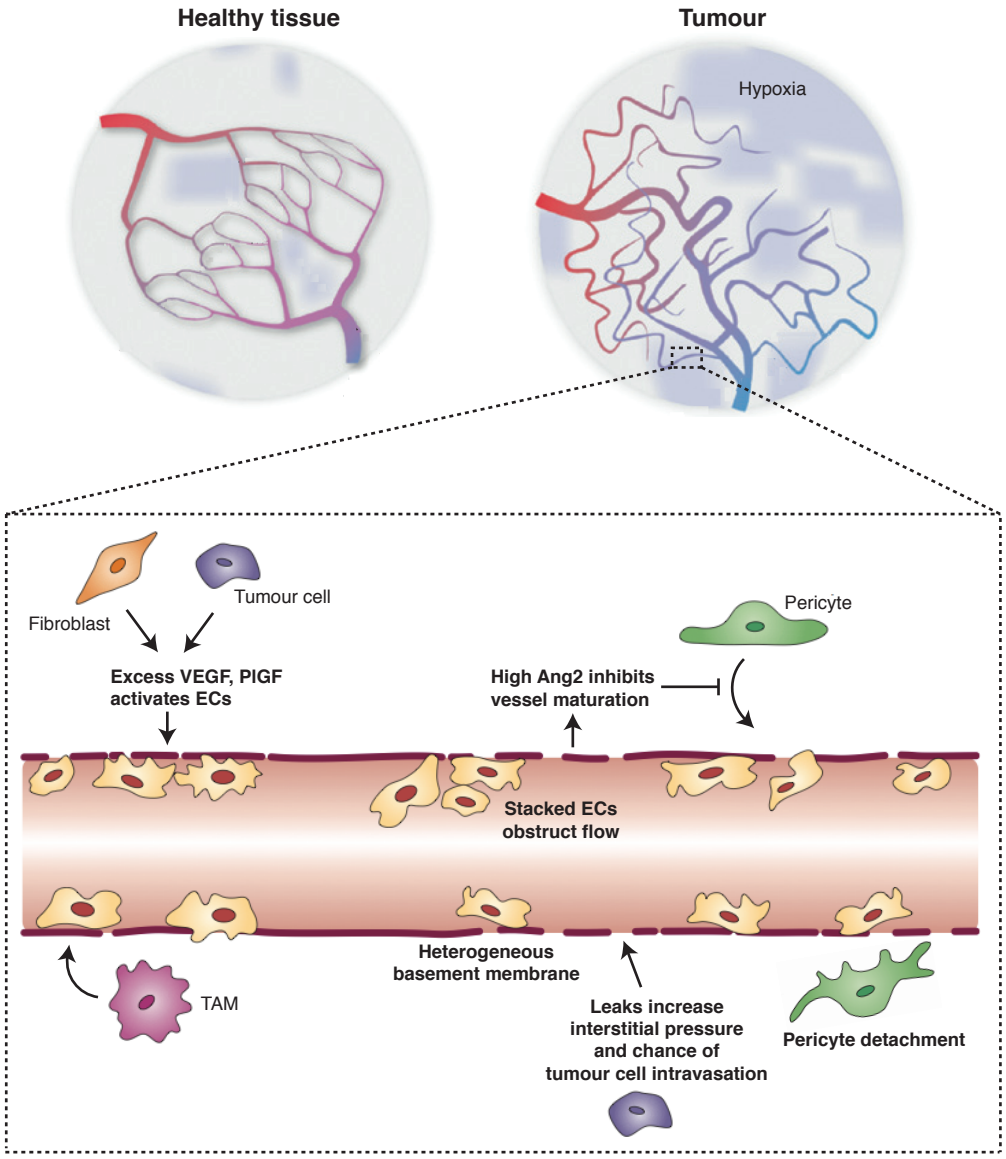

Figure 1.6: Tumour angiogenesis. In comparison to blood vessels in healthy tissues, those in tumours are leaky, tortuous, and fragile, due to dysregulated angiogenesis that is continuously remodelled. For example, excess growth factor release from tumour cells, platelets, tumour-associated fibroblasts, and infiltrating inflammatory cells (e.g. tumour-associated macrophages,TAMs)) maintains elevated angiogenesis. Persistently activated endothelial cells (ECs) begin to lose their polarity, stacking on top of each other to obstruct blood flow. Basement membrane coverage is disrupted and pericytes have looser and sparser associations with the endothelium. Widened endothelial junctions promote leakiness and therefore an increase in interstitial pressure, and a greater chance of leukocyte extravasation and tumour cell intravasation. Figure adapted from [10].

1.4.1.2 Metastasis

Metastasis is the spreading of tumour cells from the primary tumour neoplasm to one or more secondary locations around the body. It is reliant on tumour cells developing the ability to invade into a surrounding blood/lymphatic vessel (intravasation), travel through and survive in the bloodstream, and exit the circulation to colonise a distant site (extravasation) (reviewed in [116]). Relatively few tumour cells will eventually colonise given the difficulty in overcoming all of these barriers, but over time they may accumulate and grow to ultimately cause organ dysfunction. It is this reason that metastasis is seen as the primary cause of morbidity and mortality in most cancer patients. Different cancers are characterised by their differing metastatic potential, and the differential locations at which metastases form, thus partly explaining why particular cancer types are more aggressive and less treatable than others. The variability in metastatic outcome can be explained by a long-standing concept in cancer research known as 'seed and soil', theorised by Stephen Paget in 1889 [117]; the idea being that tumour cells or 'seeds' are spread around but can only survive and grow if they arrive in the optimum environment or 'soil' [116]. The type of cancer cell and the microenvironment at potential secondary sites will thus determine the degree of metastasis. This again highlights the importance of the stroma in coordinating tumour progression, as tumour cells are more likely to thrive in a more accommodating secondary environment, now termed the metastatic niche, which is dependent on the stromal components. Tumour cells are known to interact with this niche, releasing ECM molecules such as periostin and tenascin C, and inducing their sustained release from stromal cells, to ultimately promote colonisation [118]. A distinct population of tumour cells with stem cell properties, known as cancer stem cells (CSCs), are likely initiators of metastatic colonisation, given their ability to adapt to new environments [118]. Interestingly, in support of the seed and soil hypothesis, a 'pre-metastatic niche' may be primed for colonisation even before the tumour cells arrive. For example, VEGFR1+α4β1-integrin+ BMDCs were found to home to future metastatic sites of B16 melanoma and Lewis lung carcinoma (LLC) cells 4-6 days prior to them, clustering on fibronectin to facilitate tumour cell attachment and liberate stimulatory growth factors such as VEGF [119].

Metastasis, requiring blood vessels for intra- and extra-vasation, is heavily dependent on tumour angiogenesis at both primary and secondary sites. Not only do tumour cells have a nearby blood supply through angiogenesis, vessel co-option and vascular mimicry, but they also have a greater chance of intravasation due to the inherent leakiness of the vessels in this context. Clearly, the fact that angiogenesis is directly linked to metastasis, both of which are hallmarks of cancer, highlights the importance of angiogenesis and its potential as a target in cancer therapy.

1.4.1.3 Anti-angiogenic cancer therapy

Since J. Folkman [95] first proposed that targeting tumour angiogenesis might be a therapeutically beneficial strategy to treat cancer, a number of anti-angiogenic drugs have been clinically approved for the treatment of different tumour types, all of which disrupt the VEGF pathway [120,121]. This is unsurprising, given VEGF's key role in driving angiogenesis, its increased expression in most solid tumours, and the various successes of its inhibition in animal models to suppress tumour growth [122]. The drugs include: bevacizumab (Avastin®), ziv-aflibercept (Zaltrap®), sunitinib (Sutent®), sorafenib (Nexavar®), pazopanib (Votrient®), axitinib (Inlyta®), vandetanib (Caprelsa®), everolimus (Afinitor®), regorafenib (Stivarga®), and cabozantinib (Cometriq®) [58,121,123]. As an example, bevacizumab, the most widely used of these, is a humanised monoclonal antibody targeted against VEGF that has improved survival in patients with metastatic colorectal cancer and non–small-cell lung cancer when combined with chemotherapy [57,121]. It has also been approved for use with interferon-α to treat metastatic renal cancer, in the treatment of breast and ovarian cancers, and as a monotherapy for the treatment of patients with recurrent glioblastoma [38,58,120,121]. The rest of the approved antagonists can inhibit VEGF signalling by acting as a decoy receptor for VEGF family members, targeting tyrosine kinases or reducing VEGF production by blocking the mammalian target of rapamycin (mTOR) pathway [121].

Unfortunately, the results obtained with these drugs have been modest, with overall patient survival increasing by only a few months at best, and in some cases tumour growth and metastasis actually becomes more aggressive after administration [57,120]. Moreover, somewhat predictably given VEGF's ubiquity,

severe side effects such as renal toxicity, bleeding, arterial thromboembolic events, wound healing complications, gastrointestinal perforation and vessel regression in organs have been reported [124]. The ineffectiveness of these therapies has mainly been attributed to different mechanisms of resistance that tumours and their vasculature either have intrinsically or acquire to 'escape' treatment. Intrinsic resistance is likely observed in vasculature that has already matured, since VEGF-targeted therapies are more effective in newly forming vessels in pre-clinical models [122,125,126]. The tumour microenvironment that is inherently insensitive to VEGF targeting may also already have a high degree of redundancy of other pro-angiogenic signals, may not be dependent on angiogenic vessel growth, or the vessels might have already undergone invasive/metastatic co-option [125]. Acquired resistance may take the form of: an increase in tumour hypoxia causing increased growth factor release, enhanced tumour cell survival under stress, alternative mechanisms of tumour vascularisation (e.g. vessel co-option, vascular mimicry, intussusception), an upregulation of ECM components that can sequester active VEGF around the tumour microenvironment, a change in the dominant VEGF isoform, an increase in infiltrating pro-angiogenic BMDCs and stromal cells, increased pericyte coverage for vessel maturation, and a decrease in VEGF-dependence through an upregulation of other pro-angiogenic pathways [58,120-122,125-128].

Recently, it has been proposed that simultaneously blocking multiple pro-angiogenic pathways might be an effective strategy for overcoming these compensatory mechanisms; a concept that that has been upheld in various pre-clinical studies that co-target pathways such as VEGF/VEGFR, PDGFR, ANG2, FGF, DLL4/NOTCH, β3-integrin and neuropilin-1 [38,129-135]. As a consequence, new drugs against other angiogenic targets (e.g. integrin antagonists) have been in clinical trials, and may prove to be effective co-therapies that produce fewer side effects in the future. Additionally, R. K. Jain [136] has proposed that angiogenic therapy could be used to correct abnormal tumour vessel structure and function in order to improve the delivery and efficacy of chemotherapeutic drugs [24,124]. Indeed, this may be why the use of angiogenesis inhibitors in combination with chemotherapy has improved survival in many cases, although similar successes of the drugs used alone leave this

open to debate [122]. The therapeutic outcome with anti-angiogenic inhibitors is dependent on a multitude of other factors, including the type of cancer being treated, the stage of disease, the setting of drug administration (neo-adjuvant or adjuvant), the specificity and dose of inhibitor, and the physiology of the patient [122]. Clearly, to produce more therapeutically beneficial results in the future, all of these factors must be considered carefully to meet the requirements of each individual case.

1.5 More Molecular players in angiogenesis

1.5.1 Integrins

Integrins are a family of heterodimeric transmembrane (TM) glycoproteins, expressed in virtually every cell, that act as cell adhesion receptors for ECM proteins and immunoglobulin superfamily molecules [137,138]. They are involved in the promotion of cell attachment and migration on the surrounding ECM, as well as the regulation of cell proliferation, differentiation, and survival [137,139]. There are at least 24 distinct integrin α-β heterodimers that form from one of 18 α and one of 8 β subunits, each of which consist of an extracellular domain, a single TM region, and a short cytoplasmic tail [140,141] **(Figure 1.7)**. Different integrins have different ligand specificity; some bind a single ligand, others bind several, and many recognise short peptide sequences in their ligands. For example, αvβ3, α5β1, αIIbβ3, αvβ6 and α3β1, all recognise the Arginine-Glycine-Aspartic acid tripeptide, or RGD motif [137,142]. Typically, when integrins are ligated they exist in an unbent active conformation to promote a high avidity state, but when they are unligated they are in a bent inactive low avidity state, and can initiate apoptosis [137,143,144]. Integrins are capable of bi-directional signalling, meaning they can respond to intracellular stimuli, which initiate conformational changes that influence how the extracellular heads interact with ligands in their environment ('inside-out' signalling), and they can also mediate the transmission of extracellular signals across the plasma membrane to the intracellular signalling machinery ('outside-in' signalling) [140,141]. Although they have no intrinsic enzymatic or kinase activity, integrins can cluster at the plasma membrane and recruit scaffolding, adapter, and signalling proteins, including kinases, which feed through different signalling pathways to regulate different cellular processes. Through this mechanism, and by more direct interactions, integrins can enhance the activity of receptor tyrosine kinases, such as those activated by VEGF, FGF, and epidermal growth factor (EGF) [143]. The recruited scaffolding and adapter proteins at integrin adhesion sites form a clustered network known as a focal adhesion (FA), which links to the actin cytoskeleton to regulate cell migration in response to the environment [145].

Integrins regulate many physiological processes, but they also play an important role in promoting cancer through their functioning in different cells of the tumour microenvironment. Tumour cell proliferation, migration, survival, and invasion are all regulated by integrins, thereby affecting neoplasm growth and metastasis. Indeed, expression of integrins αvβ3, αvβ5, α5β1, α6β4, α4β1 and αvβ6, in several tumour cell types correlates with disease progression and decreased patient survival [139]. In addition, tumour-supporting processes such as angiogenesis, lymphangiogenesis, desmoplasia (fibrous/connective tissue growth) and inflammation are all regulated by integrins expressed in cells including ECs, mural cells, fibroblasts, BMDCs, inflammatory cells, and platelets [139]. Through their interactions with their extracellular ligands, integrins also regulate proteases and control ECM remodelling, which is essential for these processes [139,143]. The targeting of integrins in the tumour microenvironment is therefore viewed as a promising potential therapeutic approach for cancer treatment.

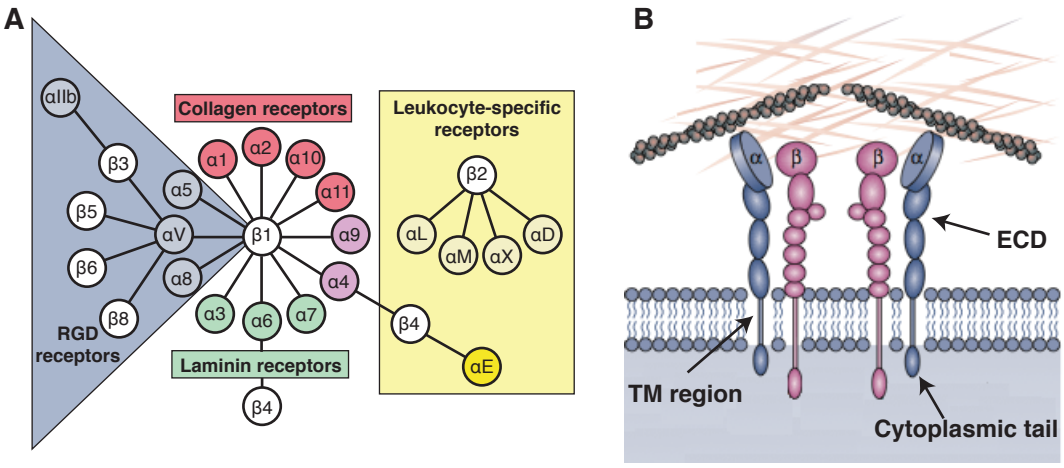

Figure 1.7: Integrin subunits and structure. A Diagram showing the different mammalian integrin subunits and their associations. There are at least 24 distinct integrin α-β heterodimers that form from one of 18 α and one of 8 β subunits. Different integrins have different ligand specificity. For example, αvβ3-integrin and α5β1-integrin recognise the Arginine-Glycine-Aspartic acid tripeptide, or RGD motif. Figure adapted and redrawn from [141]. **B** Integrin subunits consist of an extracellular domain (ECD), a single transmembrane (TM) region, and a short cytoplasmic tail. Figure adapted from [137].

1.5.1.1 Integrins and their ligands

The extracellular heads of activated integrins are capable of binding one or more ECM components or counter-receptors on adjacent cell surfaces [140]. The number of integrin ligands is extensive, but their recognition depends on the context of their location and integrin expression and activation. In blood vessels, integrins may, for example, be expressed on the luminal and abluminal side of ECs, where they may bind different ECM proteins, or on the surface of circulating blood cells, where they may recognise endothelial molecules like intercellular adhesion molecule-1 (ICAM-1) and vascular cell adhesion molecule-1 (VCAM-1) to mediate blood cell transmigration [138]. Cells in the tumour microenvironment that bind the ECM express integrins that recognise ECM proteins such as collagen, fibronectin, vitronectin, laminin, von Willebrand factor (vWF), fibrinogen, fibrillin, and thrombospondins [138,140]. Integrins have specificity for their ligands through recognising distinct peptide sequences in different ligands, such as the RGD motif already mentioned, and others such as EILDV, REDV, and LDV-type motifs [139,140]. This enforces cells expressing certain integrin heterodimers to reside within the ECM at locations rich in their specific ligand components [143]. As well as integrins being able to recognise multiple ligands, many ligands also display multivalency for their integrin counterparts, and often comprise several subunits that contain at least one recognition site [138]. For example, fibronectin binds α4β1-, α5β1-, and αvβ3-integrins among others [138,140]. See **Figure 1.8.** This may result in a high avidity scenario, where a dense ECM simultaneously crosslinks and clusters many integrins to enhance signalling potential [138]. The spatial dynamics of integrin associations ultimately determines how cells sense and respond to their environment, and thus dictates their migratory and invasive capacity [143]. Integrins therefore have a profound influence on angiogenesis and tumour cell invasion and metastasis, even helping determine the metastatic niche through their ligand specificity for particular ECM environments [143,146]. Integrin-ligand interactions also regulate cell survival; those that are ligated relay survival signals, and those that are not help initiate apoptotic pathways through anoikis (apoptosis occurring in response to cellular detachment) or integrin-mediated death (IMD - apoptosis occurring in response to unligated integrin recruitment and activation of caspase-8) [139]. Integrins therefore dynamically respond to their environment to manage this balance. Important to tumour

progression and ineffective therapeutic targeting, some tumour cells are resistant to IMD through loss of caspase-8, or an anchorage-independent αvβ3-integrin-SRC-mediated survival pathway [147,148]. Finally, integrin ligation can regulate cell proliferation by, for example, controlling the expression of cell cycle proteins like cyclin D1 and cyclin-dependent kinase inhibitors [139,149]. Again, integrin-mediated proliferation can contribute to tumour progression, as shown in a study where αvβ3-integrin overexpression promoted anchorage-dependent heregulin-induced breast cancer cell proliferation [150].

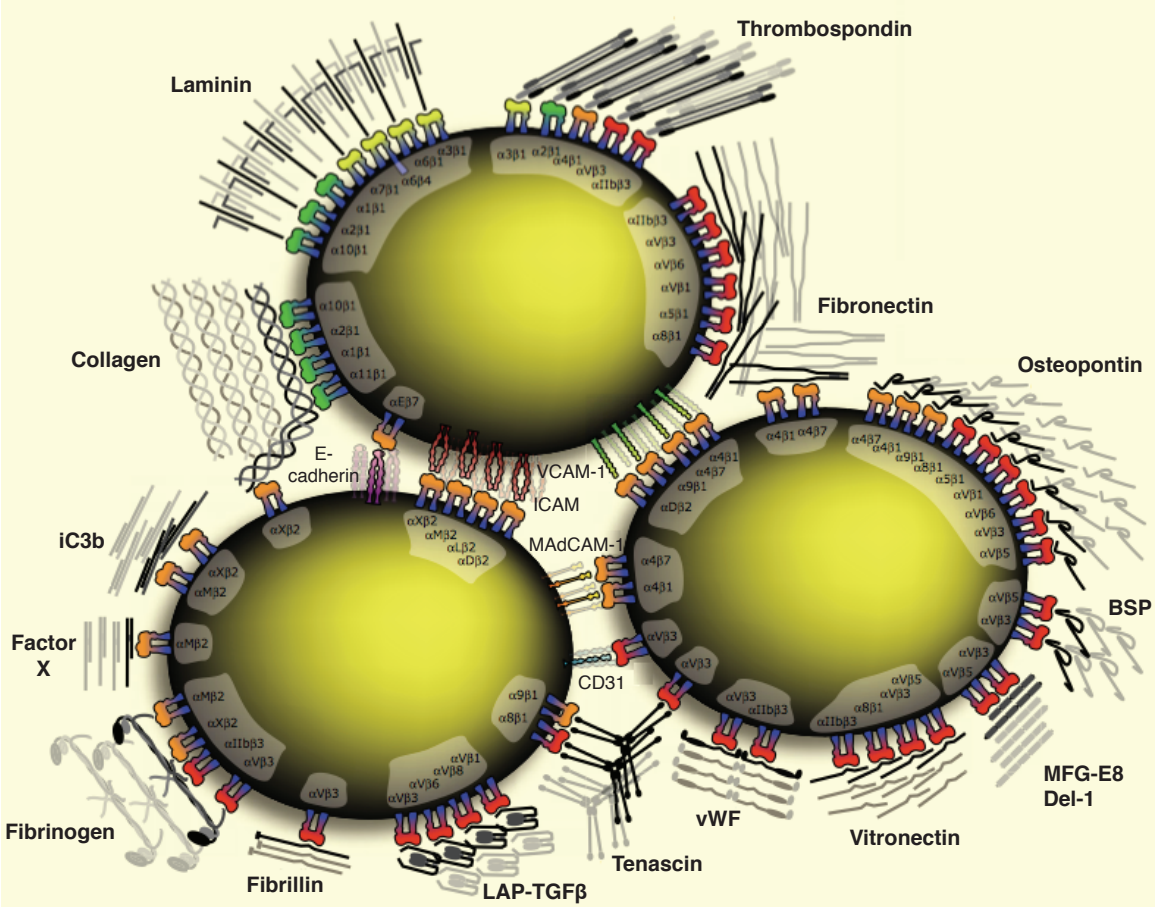

Figure 1.8: Integrin ligands. As well as integrins being able to recognise multiple ligands, many ligands also display multivalency for their integrin counterparts. The diagram shows the major integrin-ligand combinations. Figure adapted from [140].

1.5.1.2 Integrin activation - 'inside-out' signalling

Integrins are activated for ligand binding by inside-out signalling, which causes a conformational change that allows integrin extracellular domains to expose the ligand-binding site. This conformational change is known as 'affinity modulation' for a single integrin molecule as its affinity for its ligand is increased, but when multiple integrins and ligands are involved, as is predominantly the case in biological systems, 'avidity modulation' is the preferred term [138]. Structurally, activation begins when the non-covalently associated cytoplasmic tails and TM helices of the α and β subunits are unclasped and separated. Subsequently, the extracellular head of the integrin, which is typically bent towards the cell membrane in a closed conformation, is moved away from the membrane in a 'switchblade motion' through a conformational change in the extracellular domains that causes the two 'legs' to elongate. This 'intermediate' state can be opened further to permit access to larger ligands by swinging out the headpiece [138]. These transient conformational states are in equilibrium, dynamically changing in response to the environment (**Figure 1.9**). Reviewed in more molecular detail in [151,152].

Two major proteins that interact with, and activate, integrins via their cytoplasmic tails are worth mentioning here: talin and kindlin. Briefly, both talin and kindlins (there are three) are required for complete integrin activation by binding mainly to the membrane proximal NPxY peptide motif or the membrane distal NxxY motif respectively on the β integrin cytoplasmic tail via one of their FERM sub-domains, and thus displacing the β subunit's complex with the α subunit [138,153]. Talin itself is an actin-binding protein (ABP), but it also binds focal adhesion proteins including vinculin and the Rap1-interacting adapter molecule (RIAM), which interacts with the GTPase Rap1 to promote talin's binding to, and activation of, the β integrin cytoplasmic tail [138,153]. Talin is further primed for integrin activation through binding PIP_2 near the membrane, which shifts talin's inhibitory rod domain to expose its FERM-domain-containing head domain [138,153]. Like talin, kindlin contains three FERM sub-domains, but the F2 domain is interrupted by a Pleckstrin Homology (PH) domain [153]. Kindlin binding to integrins is thought to enhance the effect of talin-binding and promote the fully open and extended conformation, although this is not the case for kindlin1/2 binding of β1-

integrin [153,154]. It is also important to note that growth factors, particularly VEGF, have been implicated in integrin activation [155]. Interestingly, inside-out integrin activation can be inhibited by proteins such as Dok1, ICAP1, and filamin, which compete with talin for its integrin binding site, potentially to release talin from the integrin cytoplasmic tail to promote outside-in signalling [153,156].

1.5.1.3 Integrins and focal adhesion complexes

As the main intermediaries between the ECM and the intracellular actin cytoskeleton, integrins are essential for the transduction of biochemical and biophysical signals in the external environment to actin-myosin-mediated force generation [145]. This profoundly affects cell migration, which is governed by tightly regulated adhesions forming to cause actin-directed leading edge protrusion, and releasing to allow cell contraction at the rear [156]. Integrins indirectly link with, and polymerise, actin at adhesion sites through the recruited and clustered scaffolding and adapter proteins that make up focal adhesion (FA) complexes. FA complexes are dynamic; they constantly assemble and disassemble (turn over) in response to their external environment, at a rate that dictates the dynamics of cell adhesion and migration [157]. Several hundred FA proteins can be additively recruited at integrin-ECM adhesion sites, all of which are collectively referred to as the integrin 'adhesome' [158]. Some examples include those that directly bind both integrins and actin (actin-binding proteins, ABPs), such as talin, filamin, tensin, and α-actinin, and those that indirectly link integrins to actin, such as vinculin and Integrin Linked Kinase (ILK) [159]. In these cases, vinculin is an ABP that links to integrins via talin or paxillin, and ILK is an integrin-binding protein that links to actin via PINCH and parvin [156,159].

FA complexes do not just regulate physical properties of cells and tissues by building and severing this mechanical integrin-actin linkage; they also coordinate different cellular responses through signalling, including acto-myosin-mediated force generation required for migration, as many of the constituent proteins are kinases or other signalling molecules [160]. Some signalling pathways in the context of FA complexes will be discussed below, but the complexity of the integrin adhesome will be discussed in more detail later.

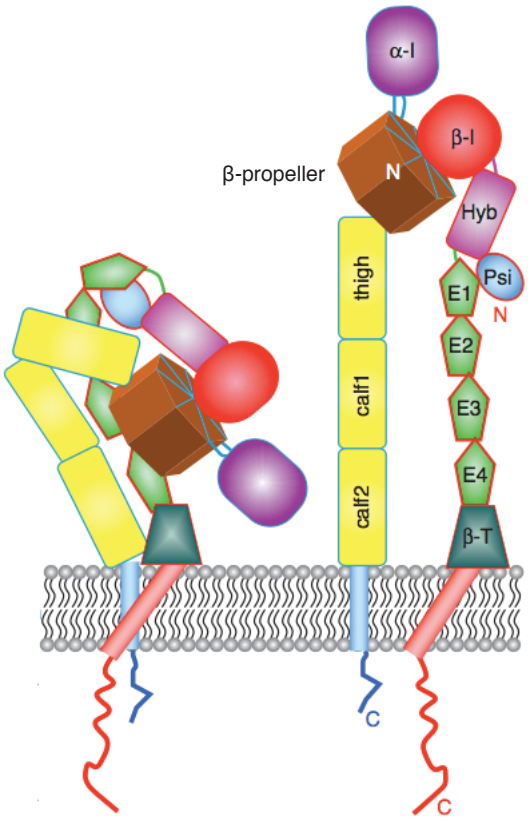

Figure 1.9: Integrin inside-out activation. Schematic of an example integrin (αxβ2) in its bent and upright conformations. Activation begins when the non-covalently associated cytoplasmic tails and transmembrane helices of the α and β subunits are unclasped and separated. Subsequently, the extracellular head of the integrin, which is typically bent towards the cell membrane in a closed conformation, is moved away from the membrane in a 'switchblade motion' through a conformational change in the extracellular domains that causes the two 'legs' to elongate. This 'intermediate' state can be opened further to permit access to larger ligands by swinging out the headpiece. These transient conformational states are in equilibrium, dynamically changing in response to the environment. Figure adapted from [152].

1.5.1.4 Integrin 'outside-in' signalling

As those activated integrins with an open conformation and high affinity for their ligands engage in ECM binding, they become stabilised and clustered to promote the high avidity state for more binding, but also increase outside-in signalling potential [153]. Clustered integrins recruit FA proteins to their cytoplasmic tails to form nascent adhesions, which may either disassemble or mature into more stable FAs [153]. Many of the different FA proteins are able to function in various signalling pathways that influence processes including cell migration, proliferation, differentiation, and survival [153], but for the purpose of this thesis we will concentrate on some of the roles of just a few.

A major signalling protein in FA complexes is the non-receptor tyrosine kinase, FAK, which is recruited to integrins early in outside-in signalling. It is activated after binding integrins directly, or via talin or paxillin, through autophosphorylation of its Y397 [159]. This creates a binding site for the SH2 domain of SRC, another non-receptor tyrosine kinase, which further phosphorylates and activates this SRC-FAK complex [159,161]. The activated SRC-FAK complex can potentiate lots of signalling pathways, but of particular interest is its role in activating the Rho family GTPases Rac1 and Cdc42 by modulating the balance of activity of particular GTPase activating proteins (GAPs) and guanine nucleotide exchange factors (GEFs) [156]. Active Rac1 is involved in promoting the protrusion of lamellipodia, which are actin projections at the leading edge of cells, whilst active Cdc42 is more involved in the extension of filopodia, the 'microspike' actin projections that extend beyond lamellipodia [153]. Rac1 and Cdc42 work through activating the Arp2/3 complex via different effector proteins (including N-WASP and WAVE1, respectively), causing it to nucleate and polymerise actin in the lamellipodia and filopodia [162]. They are therefore major drivers of cell spreading and migration. As well as the SRC-FAK complex, a number of other FA signalling proteins, including paxillin and p130 CRK-associated substrate (p130Cas), can also ultimately affect Rac1- and Cdc42-regulated actin remodelling [153,156,159]. It is also worth noting that SRC, and other SRC-family kinases, can additionally directly bind the cytoplasmic tail of integrins via its SH3 domain to activate downstream signalling molecules [156,161]. The other most common Rho family GTPase, RhoA, is actually suppressed by Rac and SRC-

FAK in leading edge protrusions, but is activated elsewhere by other means, whilst Rac1 is inhibited, to promote FA assembly and the formation of contractile acto-myosin fibres (stress fibres), which are more associated with contracting the rear of the cell during migration [153,162]. Clearly, this antagonistic relationship between the Rho family GTPases highlights the need for their proper spatiotemporal regulation by integrin outside-in signalling in order to effectively coordinate migration [153]. For a recent more detailed review on their relationship in this context, see [163]. See **Figure 1.10**.

Many of the above integrin-regulated FA signalling proteins can feed into other signalling pathways that influence other cellular processes. Of noteworthy mention is their synergistic effect with growth factor receptors. For example, FAK, SRC and other adapters like SHC and GRB2 are involved in enhancing growth factor receptor signalling cascades such as the MAPK or PI3K-Akt pathways [143,161]. Integrins have also been reported to directly interact with, and reciprocally cross-activate, growth factor receptors [138]. A major example of this is the interaction between αvβ3-integrin and VEGFR2, which will be discussed in more detail later. The indirect and direct cross-talk between integrins and growth factor receptors in different cells of the tumour microenvironment is hugely important for the enhanced signalling that contributes to tumour progression [139].

1.5.1.5 Integrin trafficking

It is important to note that integrin function is dependent on its levels on the cell surface available for ligand binding, which is determined by the degree of its expression and trafficking. Indeed, proteomics data have revealed that there are many proteins associated with receptor trafficking mechanisms present in the integrin adhesome, indicating the importance of trafficking to adhesion function [164]. The different processes involved in trafficking: integrin endocytosis, sorting, recycling, and degradation, must therefore be carefully regulated to optimise integrin signalling and function. Otherwise, disrupted integrin trafficking may contribute to cancer progression. The molecular detail of integrin trafficking goes beyond the scope of this thesis, but for a recent review, see [165].

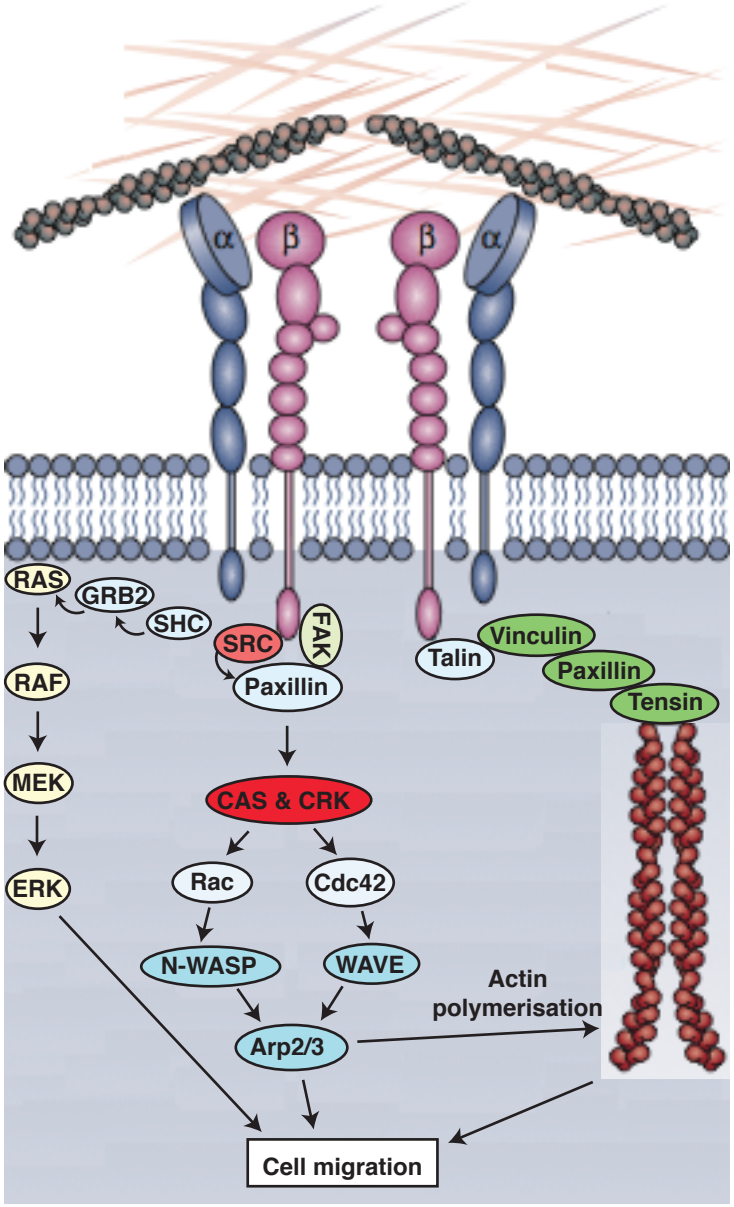

Figure 1.10: Integrin outside-in signalling. Activated and ligated integrins are able to recruit focal adhesion proteins that function in different signalling pathways. For example, a SRC-FAK complex can be recruited and activated at the integrin cytoplasmic tail, which potentiates signalling through Rac and Cdc42. Rac and Cdc42 in turn activate the Arp2/3 complex via different effector proteins, causing it to nucleate and polymerise actin, and therefore promote cell migration. FAK, SRC and other adapters like SHC and GRB2 are also involved in enhancing growth factor receptor signalling cascades, such as the RAS-RAF-MEK-ERK pathway. Figure adapted from [137].

1.5.1.6 Integrins in angiogenesis

The importance of certain integrins in angiogenesis can be highlighted by their differential expression in angiogenic and quiescent vessels, and their functional significance in various angiogenesis *in vitro* and *in vivo* models [166]. Integrins regulate angiogenesis through their expression in multiple contributing cell types, including ECs, pericytes, BMDCs, and fibroblasts. Those implicated in angiogenesis (with their canonical ligands in brackets) include: α1β1 and α2β1 (collagen), α4β1 and α5β1 (fibronectin), α6β1 and α6β4 (laminin), α9β1 (osteopontin), αvβ3 and αvβ5 (vitronectin), all of which are expressed by ECs, and αvβ8, which is expressed by glial cells in the brain [24,137,167]. With the exception of α6β4, this divides angiogenic integrins into two categories: αv-integrins and β1-integrins. As well as angiogenic sprouting being controlled by endothelial integrins dynamically adhering to the ECM, it is also affected by other integrin-dependent mechanisms. Very briefly, integrins can additionally regulate the expression and activity of different pro- and anti-angiogenic growth factors, receptors, cytokines, and proteases, affecting processes such as cell migration, proliferation, cell-cell interactions, and ECM remodelling [166]. Their ability to influence so many angiogenic factors has led to the suggestion that they act as 'hubs' that coordinate a variety of signalling pathways [166]. Once newly formed blood vessels have invaded their microenvironment, integrins also play a role in their maturation through regulating interactions between ECs, pericytes and the BM [24]. Furthermore, especially in tumour angiogenesis, integrins promote the adhesion of infiltrating BMDCs to the ECs [24].

1.5.1.6 αvβ3-integrin

αvβ3-integrin (αvβ3) is an RGD motif-recognising integrin that can bind a whole range of ECM ligands including fibronectin, fibrinogen, fibrillin, tenascin, osteopontin, vWF, and thrombospondin, but its major ECM ligand is vitronectin [137,140,146]. Important for research involving αvβ3, the β3 subunit can only pair with αv and αIIb, the latter of which is not expressed in ECs, meaning the αvβ3 heterodimer alone is influenced by manipulations in β3 in ECs [141]. This contrasts with the αv subunit, which can pair with both β3 and β5 in ECs, and β1, β6, and β8 elsewhere [141].

αvβ3 has probably received the most attention of the endothelial integrins in the angiogenesis field, ever since it was found to be upregulated in ECs in neoangiogenic vessels, yet expressed at low levels in quiescent vasculature [168]. Indeed, it is found widely expressed on blood vessels of human tumour biopsies, but not on vessels in normal tissues [137]. This finding alone not only highlighted αvβ3's importance in angiogenesis, but also hinted at its potential as a more specific anti-angiogenic target than the more ubiquitous VEGF pathway. Indeed, early studies demonstrated the effectiveness of the LM609 function-blocking monoclonal antibody against αvβ3, and the RGDfV (EMD66203) cyclic peptide antagonist of both αvβ3 and αvβ5, in inhibiting neovascularisation in different *in vivo* models, including tumour angiogenesis in a human breast cancer model [168-172]. These promising findings led to the development of another antagonistic RGD-mimetic cyclic peptide of αvβ3 and αvβ5, EMD121974, which also suppressed angiogenesis *in vitro* [173,174] and *in vivo* [175,176], and entered clinical trials as an anti-angiogenic drug under the commercial name of cilengitide [177]. Whilst cilengitide was well tolerated in patients and produced some anti-tumour efficacy, unfortunately in 2013 it failed its Phase III clinical trial when used in combination with standard chemo/radio-therapy for the treatment of the highly vascularised and aggressive brain cancer, glioblastoma multiforme, having failed to improve overall patient survival [178,179]. This, along with various pre-clinical data highlighted below suggested that αvβ3 may have both pro-and anti-angiogenic roles depending on its context, and its inhibition may induce counteracting mechanisms of resistance [180].

1.5.1.6.1 αvβ3-integrin as a pro-angiogenic molecule

The early antagonistic studies described above certainly implicate αvβ3 as a pro-angiogenic factor, their successes attributed in part to an increase in EC apoptosis following the unligation of αvβ3 and αvβ5 to vitronectin [181-184]. Also, aside from the well-documented roles of integrins in regulating different processes that contribute to angiogenesis, αvβ3 can be singled out in particular as a positive regulator of the main angiogenesis receptor, VEGFR2 [185-191]. Specifically, Soldi et al. [189] discovered that in HUVECs when αvβ3 is bound to vitronectin, and in the presence of VEGF, it can co-immunoprecipitate with, and cross-activate VEGFR2, enhancing phosphorylation of its intracellular tyrosine

residues to increase signalling through PI3K and promote EC migration and proliferation. Masson-Gadais et al. [188] confirmed these results, additionally finding elevated downstream activation of p38MAPK and FAK in response to αvβ3 cross-talk with VEGFR2, but specifically when αvβ3 was clustered and activated, which was not required in Soldi et al.'s study. Interestingly, Byzova et al. [155] additionally found a reverse scenario, where VEGF-stimulation activated αvβ3 via VEGFR2 and its PI3K activity. This prompted Byzova's laboratory to make use of knock-in 'DiYF' mice which expressed β3-integrin containing mutations in its Y747 and Y459 cytoplasmic tail residues, located in the integrin-activating motifs NPxY and NxxY, respectively [186]. Despite having normal embryogenesis and adult vasculature, these DiYF mice had significantly impaired tumour growth and angiogenesis in both prostate and melanoma subcutaneous cancer models. Furthermore, the defective β3 tyrosine phosphorylation in DiYF ECs resulted in the loss of VEGF-dependent β3-VEGFR2 interactions on vitronectin, and a significant reduction in both VEGFR2 phosphorylation and β3 activation, as well as decreased EC adhesion and migration [186]. In a subsequent study, the same laboratory identified that the VEGF-induced β3-VEGFR2 cross-talk was mediated by Src, which is activated downstream of VEGFR2 to cause β3 tyrosine phosphorylation, promoting a high avidity state, and β3-VEGFR2 complex formation, which in turn enhances VEGFR2 phosphorylation [187]. Moreover, they more recently found that the interaction between β3 and VEGFR2 is a direct one between their cytoplasmic tails, which is enhanced by β3 Y747 phosphorylation [191]. Gong et al. [192] have since shown the importance of Sprouty4 in regulating β3-VEGFR2 cross-activation, finding its overexpression to inhibit Src's phosphorylation of β3. Furthermore, a recent study by Ravelli et al. [193] implicated gremlin, a bone morphogenic protein antagonist, as a novel non-canonical ligand for VEGFR2, finding it stimulated the formation of VEGFR2-αvβ3 complexes to promote an angiogenic phenotype. These studies suggest that there is a reciprocal, and synergistic, relationship between β3 and VEGFR2, which is pro-angiogenic *in vitro* and in the context of a tumour (**Figure 1.11**). Indeed, the combination of cilengitide and a VEGFR2 antagonist in a pre-clinical cancer model inhibited tumour angiogenesis and progression significantly more than either antagonist alone [194]. This has led to the development of a dual-specific inhibitor that simultaneously binds αvβ3 and VEGFR2 and inhibits

angiogenesis *in vitro* and *in vivo* to a greater degree than mono-specific inhibitors, although it has not entered clinical trials [195].

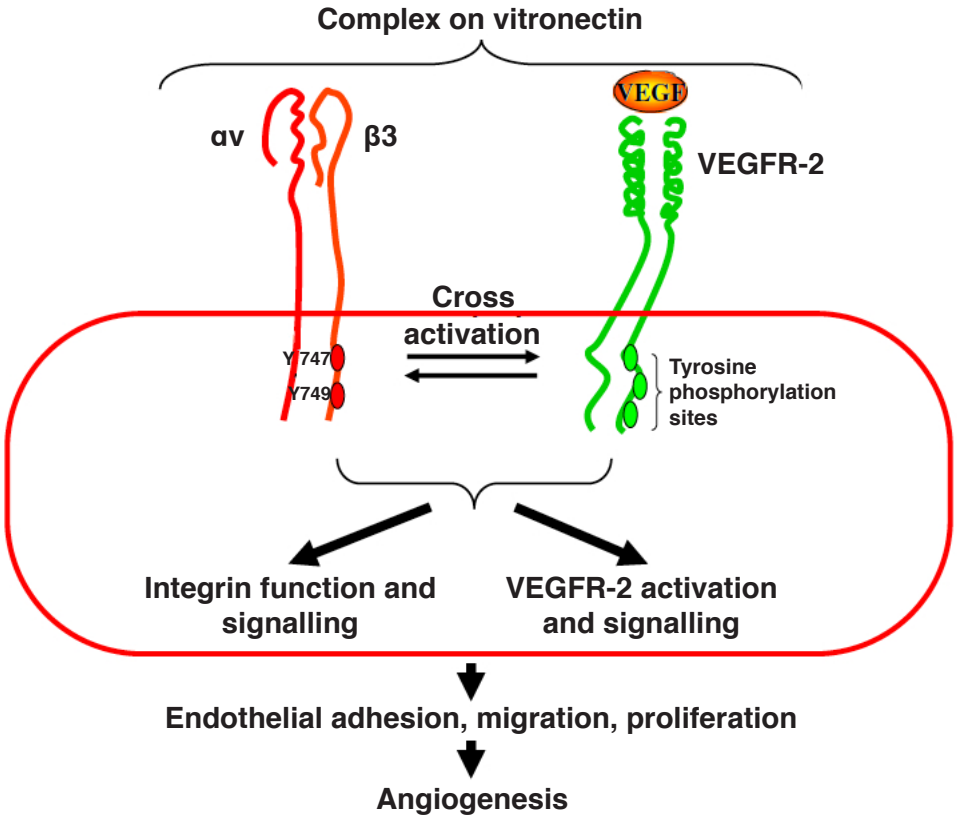

Figure 1.11: αvβ3-integrin cross-talk with VEGFR2. When endothelial β3-integrin is engaged with vitronectin in the presence of VEGF, VEGFR-2 and αvβ3 cross-activate each other by means of tyrosine (Y) phosphorylation, enhancing pro-angiogenic intracellular signalling cascades. Diagram adapted from [190].

1.5.1.6.2 αvβ3-integrin as an anti-angiogenic molecule

In contrast to these studies implicating αvβ3 as a pro-angiogenic factor, global β3 knock-out (β3-NULL) mice, although not displaying obvious developmental vascular defects [196], had significantly enhanced tumour growth and angiogenesis compared to wild-type (WT) littermates following subcutaneous injection of melanoma and lung carcinoma cells [197]. Interestingly, the β3-NULL ECs overexpressed VEGFR2, and in a follow-up study by Hodivala-Dilke's laboratory [134], the increased tumour growth and angiogenesis in the β3-NULL mice, as well as enhanced EC migration and proliferation, were deemed dependent on elevated VEGFR2 signalling. Similarly, in a separate study they showed an increase in VEGF-dependent blood vessel permeability, another facet of angiogenesis, in β3-NULL mice, which was also reversible by VEGFR2 inhibition [198]. The same laboratory later additionally implicated Rac1 in a potential compensatory pathway, as its induced endothelial depletion was only effective in inhibiting tumour growth and angiogenesis in β3-NULL mice [199]. Together, all this work implies that the global and constitutive loss of β3 enhanced angiogenesis through a developmental compensatory mechanism involving elevated VEGFR2 signalling and possibly an increased dependence on Rac1. Adding further complexity, however, the group later discovered that low doses (ie. nanomolar concentrations) of cilengitide also stimulated tumour growth and angiogenesis in a VEGFR2-dependent manner, and specifically promoted Rab4a-mediated VEGFR2 recycling and increased αvβ3's presence in peripheral FAs in ECs [200]. Furthermore, Alghisi et al. [201] found that cilengitide actually induced αvβ3 activation in HUVECs adhered to β1 ligands. This therefore showed that angiogenic compensation was not restricted to constitutive genetic β3 ablation, but also dependent on the dose of αvβ3 antagonist and its effects on non-canonical ligands. A further potential mechanism of compensation was observed by Robinson et al. [202], who showed that, in β3-NULL ECs, the VEGF co-receptor, NRP1, increased its expression and association with VEGFR2 to enhance signalling through ERK1/2. The inhibition of NRP1 when β3 was present at normal levels had a minimal effect on angiogenesis, but in the β3-NULL model, and when β3 was targeted by cilengitide, NRP1 inhibition became effective at reducing *ex vivo* VEGF-mediated aortic ring microvessel sprouting, and/or EC migration, and VEGFR2-mediated signalling [202]. Furthermore, the authors

reported co-immunoprecipitation between αvβ3 and NRP1, suggesting a mechanism whereby αvβ3 normally sequesters NRP1 away from VEGFR2 to prevent its enhancement of pro-angiogenic signalling [202]. A mutant form of β3 lacking part of its cytoplasmic tail (β3Δ722), though still able to dimerise and engage ligands, hindered the interaction between β3 and NRP1, but increased NRP1-VEGFR2 associations, promoting the potential importance of β3's cytoplasmic tail in this regulatory mechanism. The study therefore showed that angiogenesis in constitutive β3-NULL, constitutive β3-EC-NULL and cilengitide-treated models were dependent on NRP1 and its interactions with VEGFR2. However, a more detailed analysis of β3-NRP1 interplay is required to find out how β3 regulates NRP1; something that this thesis attempts to address.

Overall, one can conclude from the findings outlaid so far that it appears αvβ3 plays pro- and anti-angiogenic roles depending on its context [180]. The constitutive global removal of β3 enhances angiogenesis, suggesting an anti-angiogenic role, but is probably due to developmental compensation involving, at the least, VEGFR2, NRP1, and Rac1. Global removal of β3 complicates matters, as we are unable to determine whether β3 removal in different contributing cell types (e.g. pericytes, BMDCs, platelets, tumour cells) differentially affects angiogenesis [180]. Furthermore, we are not able to dissect out the specific contribution of the αIIbβ3 heterodimer, highly expressed by platelets, in angiogenesis, which, like αvβ3, would also be affected by β3 removal in a global knockout model [180]. In more clinically relevant models exploring the effect of αvβ3 antagonists on angiogenesis, further dichotomy in αvβ3's angiogenic role has arisen. Whilst cilengitide inhibited angiogenesis in some pre-clinical models [173-176,202], its use at low doses produced the opposite effect, which was dependent on VEGFR2 activity [200]. The dose of inhibitor therefore also has some bearing on αvβ3's angiogenic role. αvβ3's cross-activation of VEGFR2 positively regulates angiogenesis, an effect that is reversed in the DiYF model containing globally mutated integrin-activating tyrosine phosphorylation sites on β3's cytoplasmic tail, and by phosphorylated peptides that mimic the same site [186,191]. The DiYF model therefore contrasts with the β3-NULL model in angiogenic outcome and its lack of compensation through VEGFR2 overexpression, maybe because the integrin is still present and can still function

to some degree [202,203]. However, there is no evidence for this, except for the fact that the DiYF mutants do not display severe platelet defects and extended bleeding times like the β3-NULL mice [196,203]. The difference between the two models could also be partly related to cell survival; cells with unligated αvβ3 can undergo apoptosis through anoikis or IMD, which may contribute to the reduction in angiogenesis in DiYF mice, but, paradoxically, a reduction in β3 expression can decrease apoptosis, and so increased cell survival may play a part in the β3-NULL phenotype [144,203,204]. The potential mechanisms of resistance observed in the β3-NULL model involving NRP1 and VEGFR2 suggest that β3's interactions with other molecules might be influential in governing angiogenic outcome (ie. β3-VEGFR2 interactions seem pro-angiogenic, whilst β3-NRP1 interactions appear anti-angiogenic) [180]. It therefore may be important to further explore the significance of β3 interactions with conventionally pro- or anti-angiogenic molecules. Indeed, it has already been reported that the anti-angiogenic activity of tumstatin, a proteolytic fragment of collagen IV in the ECM, in tumour growth is dependent on interactions with αvβ3 [205], which may be a factor in promoting the anti-angiogenic DiYF phenotype [203]. A potential compensatory pathway through the increased angiogenic function of other integrins must also be carefully studied as a mechanism of resistance in response to different forms of β3 targeting [203].

1.5.1.6.3 Cell-specific functions of αvβ3-integrin

Given that the context of αvβ3 targeting seems so important, and due to the emergence of research on more specific drug targeting methods (e.g. the use of nanoparticles as delivery vehicles [206]), more emphasis has been placed on dissecting out the cell-specific contributions of αvβ3 to angiogenesis. Taverna et al. [207], for example, discovered that transplanting WT bone marrow into β3-NULL mice restored normal tumour growth and angiogenesis, promoting the importance of BMDCs in the β3-NULL phenotype [180]. Through transplanting β3-NULL bone marrow into β3-WT mice, it was later discovered that the lack of β3 in bone marrow may lead to enhanced angiogenesis through a greater degree of EPC mobilisation from the bone marrow, although most of the new vessels were non-functional [208]. Feng et al. [209] also demonstrated the significance of β3 expression by BMDCs in angiogenesis, finding WT bone marrow to rescue the

defective angiogenesis displayed by DiYF mice. Here, suppressed angiogenesis in the DiYF mice correlated with impaired CXCR4+ myeloid BMDC recruitment and retention at angiogenic sites via their improper adhesion and transmigration, rather than a change in release from the bone marrow [209]. This therefore, again, highlights the polarisation of αvβ3 angiogenicity in different contexts. More careful analysis of specific types of BMDCs is required to interpret these results properly, although Feng et al. did rule out a significant contribution of platelets to the DiYF phenotype [209]. In this regard, tissue-specific genetic targeting of β3 using the Cre-Lox system has progressed our understanding of myeloid and platelet expression of β3 [210]. Specifically, Morgan et al. [210] found that the depletion of β3 in platelets, despite disrupting hemostasis, had no effect on tumour growth, whereas a deficiency of β3 in myeloid cells enhanced tumour growth, although not necessarily due to angiogenesis. The endothelial contribution of αvβ3 to tumour growth and angiogenesis was reported by our laboratory in a publication released in 2014 (see **List of publications**) [211]. Here, we used β3-floxed mice crossed to two different endothelial-specific Cre lines: Tie1-Cre, in which floxed targets are constitutively deleted in Tie1+ cells (β3-EC-NULL); and Pdgfb-iCreER^{T2}, in which floxed targets are depleted in Pdgfb+ cells in an inducible fashion by the administration of 4-hydroxy-tamoxifen (OHT) (β3-EC-inducible depletion (ID)). This enabled us to compare the effects of a long-term reduction of β3 in ECs (an EC-specific imitation of the β3-NULL model) with an acute endothelial β3 depletion induced at a particular time (a genetic mimic of antagonist administration). We found that whilst the constitutive loss of β3 in ECs had no effect, an acute depletion successfully reduced tumour growth and angiogenesis when induced preventatively, but not in pre-established tumours. However, the suppressed responses were only observed for a transient period of time before longer-term depletion became ineffective. Our study therefore concluded that the timing of targeting, as well as the length of inhibition, were further critical factors in determining the effectiveness of targeting β3. Importantly, though, long-term endothelial β3 targeting did not result in increased tumour growth and angiogenesis, suggesting that enhanced pathological angiogenesis in the β3-NULL model is due to the contribution of non-ECs [211]. Therefore, due to an initial benefit in targeting β3 that was eventually overcome, it appears that there is still scope for the use of β3 as an effective anti-angiogenic

target, especially if we specifically target it in ECs, but only if we can prevent the acquisition of resistance. In our paper, we found that long-term targeting correlated with increased VEGFR2 surface levels, decreased expression of β5, reduced levels of FAK, and a misbalance in FAK phosphorylation, the latter two of which have been implicated in enhanced tumour growth and angiogenesis recently [212]. However, more work is required to properly decipher common mechanisms of escape to genetic and pharmacological long-term endothelial β3 targeting [213,214].

It is imperative not to forget the role of αvβ3 in tumours when considering targeting it in anti-angiogenic cancer therapy. Indeed, there is evidence to suggest that it may function differently in different tumours. For example, although it is upregulated in the vasculature of most tumours, in angiosarcomas endothelial β3 expression decreases during malignant transformation [180]. Moreover, there are conflicting reports over the contribution of β3, as expressed by tumour cells, to tumour growth and angiogenesis. For example, Lorger et al. [215] found that αvβ3 activation in tumour cells enhanced tumour angiogenesis and metastasis in the brain, whilst Kaur et al. [216], showed that the expression of αvβ3 in ovarian cancer cells reduced tumour growth and metastasis. Additionally, De et al. [217] discovered that active and clustered αvβ3 on tumour cells promoted the production of VEGF via p66 Shc phosphorylation to enhance tumour angiogenesis in prostate and breast cancers. This study is particularly relevant to the failure of αvβ3 therapies, as the effect was observed even in response to the LM609 αvβ3 function-blocking antibody. Furthermore, an adhesion-independent role of αvβ3 in tumour progression was discovered by Desgrosellier et al. [147]. Here, unligated αvβ3 in IMD-resistant tumour cells increased anchorage-independent tumour cell survival and metastasis via Src. Thus, the potential adverse effects of αvβ3 targeting in different patients and cancer types must be properly scrutinised in order to make informed decisions about the correct use of antagonists. For comprehensive reviews on αvβ3 and other integrins in tumour cells, see [139,143,146].

1.5.1.6.4 Conclusions on αvβ3-integrin

Careful consideration of the multiple factors that influence αvβ3's role in angiogenesis is essential for us to improve the therapeutic results achieved with antagonists. Such improvements may rely on enhancing the specificity of antagonists to certain parts of the αvβ3 molecule in particular cell types at the optimal time, using the correct dose, and simultaneously targeting other compensatory pathways to counter therapy resistance. With regard to the latter, which may prove most therapeutically effective, co-targets must be carefully chosen based on how significant and common their mode of resistance is in different clinically relevant models, how they interplay with αvβ3 and other pathways, and whether their targeting produces unwanted adverse effects. This thesis will be further exploring the joint roles of αvβ3 and NRP1 to pathological angiogenesis, with a view to determining whether NRP1 would present itself as one such candidate.

1.5.2 Revisiting the integrin adhesome

Since the recent proteomic profiling of the integrin adhesome in human and mouse fibroblasts [218-220], mesenchymal stem cells [221], and chronic myelogenous leukemia cells [222,223], we have gained greater insight into its cell-, integrin- or ECM-specific molecular complexity, but still have limited understanding about its functional significance in different contexts, how it is dynamically assembled, disassembled, and regulated, and how its composition differs *in vivo*, and in different cell types and conditions [164]. Moreover, there is still some confusion over the specific terms for different focal adhesion complexes. Proteins that make up the adhesome have in this thesis hitherto been referred to as FA proteins, and their clustered arrangement at integrin adhesion sites has been described as a FA complex. However, this is a simplification, as the general consensus is that the proteins can be arranged in four classical types of adhesion complex: nascent adhesions, focal complexes, focal adhesions and fibrillar adhesions, as well as the less conventional podosomes and invadopodia (**Figure 1.12**) [156,224]. These classical types vary in their location, lifespan, and composition. Nascent adhesions are the smallest type that form at the lamelliopodial side of the cell to promote membrane protrusion; they either rapidly disassemble or mature into focal contacts, which have a slightly slower rate of turnover [156,157]. Focal contacts in turn can mature into larger, more elongated focal adhesions, which have a slower turnover still. FAs can support forward movement through their linkage to actin stress fibres that propagate contractile force, but can also disassemble at the rear of the cell to aid cell retraction [218]. Fibrillar adhesions are long, stable structures found parallel to bundles of fibronectin, mainly in fibroblasts [156,157]. To achieve coordinated cell migration, there must be a cooperative balance in the workings of these complexes, which depends on the specific adhesion conditions. For example, Schiller et al. [220] found that cells with restricted expression of either αv- or β1-integrins formed distinct adhesion complexes that regulated different mechanical transduction events. α5β1-integrins induced the formation of nascent adhesions, activated the Rac1/Wave/Arp2/3 pathway at membrane protrusions, and generated actomyosin force through the RhoA-ROCK-myosin II pathway, whereas αv-integrins accumulated in areas of high tension and promoted the formation of large FAs that were more involved in mediating the structural reinforcement of

actin stress fibres via GEF-H1, the formin mDia, and RhoA [164,220]. Indeed, work from Rossier et al. [225] showing that activated β3-integrins are immobilised in large FAs, whilst activated β1-integrins are capable of rearward movement, may imply a similar distinction in αvβ3 and α5β1 specifically, even though they are both fibronectin-binding integrins. On this matter, Roca-Cusachs et al. [226] found that α5β1 clusters were important in maintaining the strength of adhesion to fibronectin under high forces, whereas αvβ3 had a weaker association with fibronectin, but was more involved in the structural reinforcement of linkages to the cytoskeleton and enabling mechanotransduction. Regardless, it seems that both integrins are required to cooperatively enable cells to adapt cellular contractility to the rigidity of the ECM [145].

The proteomics data for the adhesome from different sources have expanded the pre-existing adhesome database, consisting of 232 proteins accumulated by microscopy and protein interaction assays, by two- to three-fold [164]. However, a large proportion of the additional proteins from each proteomics study are a context-specific subset related to the cell type, ECM substrate and integrin components, that need to be dissected further [164,227]. This suggests that there may be a group of canonical adhesome components, and many more additional non-canonical proteins that are more labile [164]. However, it is important to emphasise that protein associations within the adhesome are dynamic, or ‘switchable’, and not necessarily universal [157,228]. Furthermore, much of the work on the adhesome has been carried out on cells adhered to 2D surfaces, and so is not entirely representative [157]. A major discovery from adhesome proteomics studies is that many proteins recruited to maturing integrin adhesions do so in a myosin II-dependent manner, and contain LIN-11, Isl1, and MEC- 3 (LIM) domains (e.g. zyxin and paxillin), which are believed to be important for force mechanotransduction in stress fibres [164,218,219]. More recently, Robertson et al. [229] proteomically profiled the phospho-adhesome and found a number of known and novel phosphorylated proteins that contribute to adhesion signalling, including cyclin-dependent kinase 1 (CDK1), whose inhibition reduces adhesion complex formation. Interestingly, the activity of CDK1 has been shown to be enhanced by increased αvβ3-integrin expression to promote migration, and members of the CDK family are known to regulate proteins such as paxillin and

filamin-A [229-232]. These proteomics studies, combined with super-resolution microscopy and higher resolution mass spectrometry imaging in the future should build us a clearer picture of adhesion complex structure and dynamics in different cells and adhesion types [164].

For the sake of clarity, a summary of the mechanotransductive role of integrin-mediated-cell-ECM adhesions, including examples of canonical adhesome proteins, is as follows: integrins activated by talin and kindlins attach to the ECM to form adhesions. At the leading edge of a cell, these engaged integrins recruit a small number of proteins in a myosin II-independent fashion, including FAK, SRC, paxillin, and p130Cas to form nascent adhesions, where signalling is generally directed through Rac1 and Cdc42 to promote cell motility via Arp2/3-mediated actin polymerisation in lamellipodia and filopodia [145,157,159,218]. Nascent adhesions keep turning over quickly during membrane protrusion, but they may also undergo a tension-dependent maturation into larger focal complexes that reside at the interface between the lamellipodia and the lamella, and subsequently focal adhesions, which endure longer and are more associated with high RhoA activity and the generation of contractile force through their stabilised connection to the actin cytoskeleton [145,163]. Adhesion complex maturation involves the recruitment of additional proteins such as vinculin, which stabilises the link between talin and actin, and the RhoA-mDia-mediated elongation of actin, which is bundled by α-actinin, and further complexed with the adapter proteins zyxin, tensin, and VASP [218]. The integrin adhesion machinery is mechanosensitive to tension generated intracellularly by myosin II activity or by external forces (e.g. the rigidity of the ECM) [157]. In response to these forces, tension-sensitive FA proteins change conformation to expose binding sites for non-tension-sensitive proteins, and thus promote adhesion maturation [218]. Tension further amplifies maturation through the activation of FAK and SRC, which can phosphorylate paxillin and p130Cas to form binding sites for SH2-containing proteins [218]. Cells therefore modulate FA composition and signalling for a spatially and temporally regulated mechanotransductive response to applied forces [145]. A stiff ECM, or high myosin II activity, will promote adhesion maturation and therefore the generation of RhoA-ROCK-dependent acto-myosin contractile force, but a more compliant ECM will block this to enhance nascent

adhesion-mediated membrane protrusion [145,157]. Myosin II and ECM rigidity therefore have key roles in coordinating a balance between the protrusive and contractile activity of a cell [145]. FA-mediated contractile force reflects back on the ECM, pulling on it to alter its structure and organisation, and thus allowing cells to continue mechanosensing their environment [145]. Actomyosin contractility also contributes to FA disassembly by presenting FAs with disassembly factors, and ultimately retracts the cell rear to complete the migration cycle [233]. FA disassembly may also be regulated by other factors, such as PIP_2 levels, but, like FA assembly, is still a poorly understood process [234].

Aside from those mentioned, other 'core' canonical FA components that frequent proteomics data are believed to include filamin, ILK, LASP, and IQGAP, although we still do not know if these components differ in other cell types under different conditions [164]. Unsurprisingly, improper functioning of adhesome proteins is characteristic of different diseases, particularly cancer, and increasing evidence suggests that components of the adhesome may be interesting novel therapeutic targets. See [160] for a review. More detailed sub-chapters on some FA components relevant to this thesis follow below.

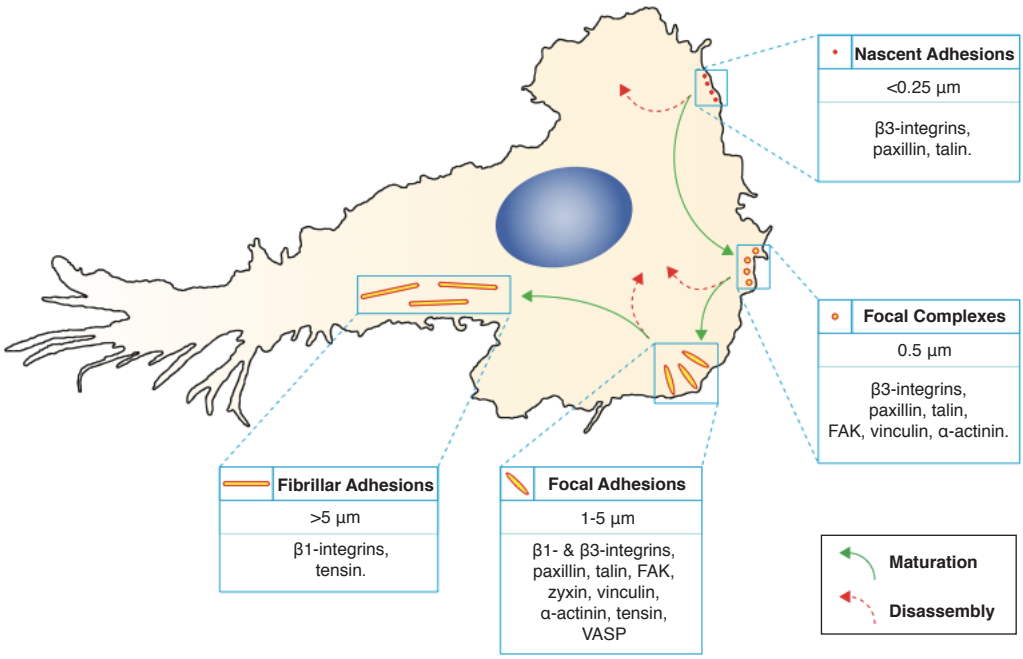

Figure 1.12: Classical focal adhesion structures. The general consensus is that proteins of the adhesome can be arranged in four classical types of adhesion complex: nascent adhesions, focal complexes, focal adhesions and fibrillar adhesions. These structures localise to different areas of the cell, and are characterised by their size and rate of turnover, which is determined by the rates of their maturation and disassembly. The hierarchy of maturation (green arrows) and disassembly (red arrows) are depicted. Figure adapted from [156].

1.5.2.3 Filamin A

Filamin A, belonging to the family of filamins, is a multi-domain homodimeric protein that cross-links actin, and contributes to its anchorage to the ECM [235,236]. Indeed, not just ABPs, filamins can bind a range of other molecules including receptors, ion channels, transcription factors, and scaffolding, signalling, and adhesion proteins [236]. In response to tension, filamins, like other FA proteins, can undergo conformational changes that can change their affinity for binding partners and expose binding sites for other components [236]. This has led to the speculation that filamins play a role in mechanosensing the environment to confer cells with mechanical properties and influence processes like cell spreading and migration [236,237].

In non-muscle cells, filamin A is known to co-localise with filamentous(F)-actin along, and at the end of, stress fibres, and can also concentrate at filopodia and lamellopodia during cell spreading, and at adhesion sites following force application to cells [235,236,238]

As mentioned briefly earlier, filamins compete with talin, and also kindlins, for their binding site on integrins, inhibiting their activation [159]. However, migfilin, a LIM-domain-containing protein can reverse this effect [159,239]. Filamins increase their binding to integrins in response to myosin II-dependent force production and external shear, which can expose the integrin binding site in filamins, but also cause the release of the filamin A-associated Rho GAP (FilGAP), a Rac inactivator [159,240,241]. This is important, for example, for the suppression of Rac1 activity at later stages of adhesion, as, here, activated FilGAP can inhibit the formation of Rac-dependent lamellipodia [163,242]. Interestingly, filamin A can also inhibit Rac at the latter stages of adhesion through a pathway involving IQGAP and RacGAP1 [163,243]. Presumably, since it takes myosin II-dependent force for filamins to bind integrins, and the recruitment of LIM-domain-containing proteins like migfilin is also dependent on myosin II, the inhibitory effect of filamins on integrin activation may be offset.

1.5.2.4 Non-muscle myosin II (NM-II)

Members of the non-muscle myosin II (NM-II) family are conventional F-actin-based molecular motors involved in regulating the organisation and force-generation of the cytoskeleton [244]. Their name is actually a misnomer since members are expressed in cardiac, skeletal, and smooth muscle cells, but in much smaller amounts than sarcomeric myosins [244]. There are three NM-II isoforms in vertebrates: myosin IIA, myosin IIB, and myosin IIC, which consist of two copies each of heavy chains, essential light chains, and regulatory light chains [245]. Myh9, Myh10, and Myh14 genes encode the heavy chains of myosin IIA, IIB, and IIC, respectively, which contain binding sites for both ATP and actin in their N-terminal globular domain [245]. Phosphorylation of the regulatory light chains by Ca^{2+}-MLCK or Rho-ROCK pathways triggers NM-II activation and its higher-order assembly into a bipolar complex, which slides between actin filaments of opposing polarity towards their plus-ends via ATP hydrolysis to generate tension and contractile forces and cross-link them [244]. Myosin IIA and IIB appear to have slightly different, yet overlapping, roles in cell migration. Myosin IIA is mainly localised at the front of cells and in protrusions, although not at their leading edge, as nascent adhesion formation is NM-II-independent, whilst myosin IIB is missing from protrusions, but more associated with the centre and rear of migrating cells [244]. Loosely, myosin IIA supports FA formation and protrusion at the front, and the formation of actomyosin stress fibres at the rear. Myosin IIB is more involved in the stabilisation and contraction of these stress fibres [244]. These isoforms therefore work in tandem to coordinate cell adhesion and directional migration. They are, however, involved in many other processes, including vesicular transport, endocytosis, exocytosis, and cytokinesis, and can contribute to different diseases when functioning improperly [244].

1.5.2.5 Paxillin

Paxillin is a multi-domain signalling scaffold protein recruited to integrin adhesions early on [246]. It is capable of promoting FA formation through binding an array of different scaffolding and signalling proteins via its many modules, which includes four LIM domains, in a manner that is regulated by phosphorylation of its multiple tyrosine, threonine and serine phosohorylation

sites [247,248]. Specifically, phosphorylated tyrosine is known to provide additional docking sites for protein binding [248]. Key interactants of paxillin include the kinases FAK, Src, and ILK, phosphatases, ABPs like vinculin, and GAPs and GEFs of the Rho GTPases [156,246,248]. The diversity in paxillin's interactions likely suggests an ability to dynamically regulate FA turnover and migration [246]. Of noteworthy mention is that the phosphorylation of paxillin (Y31 and Y118) enhances its association with FAK in nascent adhesions, which significantly increases FA formation and size, and keeps FA turnover in check [249]. Like that of FAK, paxillin's regulation of Rho GTPases via various GAPs and GEFs has also been deemed greatly important for cell motility, having been described as a 'Rac hub' [248,250]. Also, in addition to its role in FA formation and signalling, paxillin has been shown to be important for the disassembly of FAs, as paxillin-deficient fibroblasts have significantly impaired FA disassembly [251].

Recently, German et al. [252] discovered that reduced expression of paxillin increased the migration of human umbilical vein ECs (HUVECs), and stimulated angiogenesis during development and in response to tumour-derived factors *in vivo*. This effect correlated with, and was mimicked by, reduced NRP2 expression, and overexpression of NRP2 prevented the effect [252]. Interestingly, this study contrasts with work by Yang et al. [253], who showed a reduction in VEGF-induced HUVEC migration and *in vitro* tube formation in paxillin-knockdown cells. However, although Yang et al.'s tube formation assay was performed in matrigel, it appears as though their HUVECs were cultured on poly-L-lysine, which promotes integrin-independent adhesion. This contrasts with German et al.'s HUVEC culturing on 1% gelatin, and so might explain these dichotomous findings.

1.5.3 Neuropilins

The neuropilins (NRPs), consisting of neuropilin-1 (NRP1) and neuropilin-2 (NRP2), are single-pass TM glycoproteins that are primarily involved in the nervous and cardiovascular systems [27]. Although originally identified as adhesion molecules, NRPs also act as receptors for class 3 semaphorins (a family of secreted polypeptides with major roles in axon guidance), and for members of the VEGF family [69,254]. However, they are more specifically referred to as co-receptors as they lack their own catalytic activity but mediate signalling responses when complexed with other receptors (ie. plexins in the case of semaphorins; VEGF receptors in the case of VEGFs) [27,255,256]. NRP1 and NRP2 share a similar domain structure and have an overall amino acid homology of 44%, but can generally be divided by their functional significance in different processes, as highlighted by mutant mouse studies. These have shown that whilst NRP1 is essential for neural and cardiovascular development, NRP2 is dispensable for blood vessel patterning, but more associated with neuronal path-finding and lymphangiogenesis [27,255-259]. NRPs play roles in other physiological and pathological processes, and, aside from their regulation of the above receptors, are also notable for their influence on cell migration, adhesion, and permeability. Importantly, they are highly expressed in different tumours, and have been implicated in tumour growth and angiogenesis *in vivo* [69,133,255].

1.5.3.1 Structure and isoforms of neuropilins

NRPs are made up of an N-terminal extracellular domain, a TM domain, and a small cytoplasmic tail. Their extracellular domain consists of a1/a2 domains that can bind semaphorins, b1/b2 domains that can bind $VEGF_{165}$, heparin, and semaphorins to some extent, and a c domain that mediates oligomerisation [27,69,260]. The cytoplasmic tail, consisting of 44 and 43 amino acids for NRP1 and NRP2, respectively, contains an SEA amino acid motif at its C-terminus (in NRP1 and the NRP2a isoform) which recognises the PSD-95/Dlg/ZO-1 (PDZ) domain of synectin, otherwise known as GAIP-interacting protein (GIPC1) (**Figure 1.13**) [27,69,260,261].

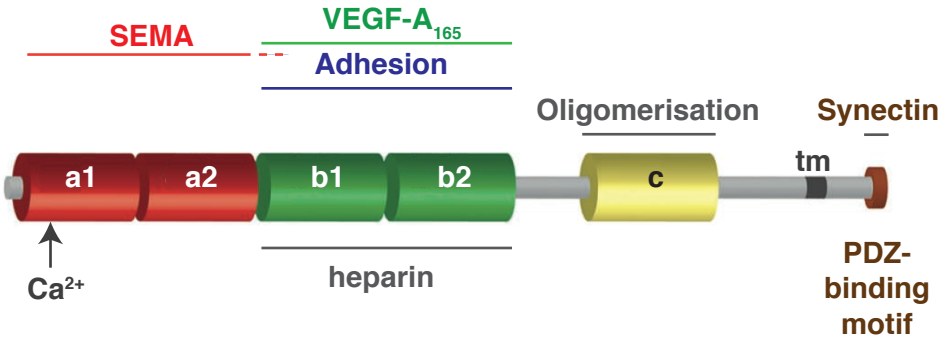

Figure 1.13: Neuropilin domain organisation. Neuropilins are made up of an N-terminal extracellular domain, a transmembrane (tm) domain, and an intracellular domain. The extracellular domain consists of a1/a2 domains that can bind semaphorin-3 (SEMA), b1/b2 domains that are involved in adhesion and can bind VEGF-A_{165} and heparin/heparan sulfate, and a C domain that mediates interactions with other receptors. The last three amino acids of the cytoplasmic domain (SEA) confer binding to the PDZ domain-containing protein synectin. Figure adapted from [260].

The NRP1 gene comprises 17 exons that code for the full-length protein of 933 amino acids. Alternative splicing of the gene results in one membrane-bound isoform (Δexon16) that retains normal functionality, and four mRNA isoforms that lack the c domain and cytoplasmic tail, and, although only two of these have been reported to translate into soluble(s)NRP1 protein isoforms, likely act as decoy receptors [69]. There are two major NRP2 membrane-bound forms, NRP2a and NRP2b, the latter of which only shares 11% homology in its TM domain and cytoplasmic tail with that of the former, and sNRP2 also exists [69]. Both NRPs are post-translationally glycosylated at varying degrees depending on the cell type. A high-molecular-weight glycosylated species of NRP1 (>250 kDa) is known to exist in addition to the normal species in some tumour cell lines, vSMCs and ECs [69].

1.5.3.2 The neuropilin ligands

Of the semaphorins, Sema3A binds NRP1 with the highest affinity, whilst Sema3F is the best-characterised NRP2 ligand [69]. $VEGF_{165}$ can bind both NRPs, and, as discussed previously, has the most signalling potential of the VEGFs, possibly due to its ability to promote NRP1-VEGFR2 complex formation [68,69]. Whilst the other major VEGF-A isoforms are theoretically capable of binding NRP1, $VEGF_{121}$ cannot promote NRP1-VEGFR2 complex formation, and $VEGF_{189}$ and $VEGF_{206}$ are sequestered in the ECM [68,69]. $VEGF_{165}$'s affinity for NRP1 is enhanced by the presence of heparin, NRP1 density, and CS-GAG glycosylation of NRP1 [69,262]. Other VEGF family members have additionally been shown to bind NRP1, including VEGF-B, VEGF-E, and PlGF-2 for NRP1, and VEGF-C and VEGF-D for both NRPs [69].

1.5.3.3 Neuropilin-1

NRP1 plays an essential role in vascular development, highlighted by the fact that NRP1-knockout (NRP1-NULL) mice die *in utero* with severe vascular defects, and NRP1 overexpression, also embryonic lethal, causes the excessive growth of leaky, haemorrhagic blood vessels [27,263,264]. Moreover, NRP1 is highly expressed in the endothelium of growing blood vessels, and in other cell types of the angiogenic microenvironment, such as neural progenitor cells and macrophages in the hindbrain [27,265]. Interestingly, early on in endothelial tip

cell research, Gerhardt et al. [266] used NRP1-NULL mice to demonstrate that NRP1 is required for tip cell guidance in the developing hindbrain. More recently, Fantin et al. [265] found, through the use of constitutive and OHT-inducible cell-specific knockout mice, that while the specific expression of NRP1 in neural progenitors and macrophages was redundant for normal embryonic brain angiogenesis, endothelial NRP1 was essential, even though its EC depletion was inefficient due to inadequate Cre recombination. The impairment in Cre recombinase efficiency was actually favourable, though, as it resulted in remaining NRP1+ ECs to preferentially adopt the tip cell position, thus suggesting that endothelial NRP1 cell autonomously promotes tip cell function [265]. The specific role of NRP1's cytoplasmic tail has also been investigated in blood vessel development through the use of mice that lack this portion of the NRP1 molecule (NRP1Δcyto). Fantin et al. [267] showed that NRP1's cytoplasmic tail is dispensable for developmental angiogenesis, but important for the spatial separation of retinal arteries and veins, as the NRP1Δcyto mice displayed increased artery-vein crossings. This therefore suggests that NRP1's membrane-anchored extracellular domain alone is sufficient for regulating blood vessel development [267]. Lanahan et al. [268] additionally reported a redundancy of the cytoplasmic tail in pathological angiogenesis using oxygen-induced retinopathy and skin wounding mouse models, but instead found it to be required for arteriogenesis. More recently, two separate groups discovered that mice expressing NRP1 unable to bind VEGF overcame embryonic lethality but had defective postnatal angiogenesis, suggesting NRP1's binding of VEGF is non-essential for embryonic blood vessel development, but important later on [269,270].

These studies have therefore all shown NRP1 to be important for blood vessel formation during development in one form or another. However, the exact molecular mechanism of NRP1 action in adult vascular endothelium during physiological and pathological angiogenesis is not yet clear. We have seen from earlier that Robinson et al. [202] reported no effect on *ex vivo* microvessel sprouting when targeting NRP1 alone, and that pathological angiogenesis in Lanahan et al.'s [268] study was independent of NRP1's cytoplasmic tail, therefore suggesting NRP1's role in these processes is negligible. However,

Raimondi et al. [271] recently found that inducible endothelial NRP1 depletion inhibited oxygen-induced retinopathy in pups, and Fantin et al. [269] implicated the VEGF-binding domain of NRP1 as important for this pathological neovascularisation of the retina in pups as well, but also for angiogenesis-dependent tumour growth, thus putting us into doubt over NRP1's exact role in pathological angiogenesis. Research over the last 10 years or so has broadly split NRP1's endothelial function into two categories; its role in regulating VEGFR2 biology, and its VEGFR2-independent role, which is partly related to its roots as an adhesion molecule. These categories will be explored further below.

1.5.3.3.1 VEGFR2-dependent roles of neuropilin-1

NRP1 can form a receptor complex with VEGFR2 upon $VEGF_{165}$ binding, and also reciprocally enhance the affinity of VEGF-A_{165} for VEGFR2, thereby altogether enhancing VEGFR2 phosphorylation and signalling, and promoting EC migration [68,256,272-279]. The VEGF-NRP1-VEGFR2 tri-partite complex likely forms through $VEGF_{165}$ bridging between the two receptors, binding VEGFR2's core VEGF homology region via its cysteine knot motif and NRP1's b domain via its C-terminal moiety [69,256]. However, Prahst et al. [280] have reported that the VEGFR2-NRP1 association is also dependent on NRP1's cytoplasmic tail, suggesting that intracellular interactions may also be important [69]. In HUVECs, NRP1 enhances VEGF-mediated VEGFR2 Y1175 phosphorylation, as shown by a significant reduction in phosphorylation following NRP1 siRNA-mediated knockdown in two separate studies, although ERK1/2 phosphorylation was unaffected [272,273]. However, a NRP1-directed antibody, which specifically inhibits VEGF binding to NRP1, the expression of a NRP1 Y297A mutant deficient in VEGF binding, and the expression of a mutant NRP1 lacking its cytoplasmic tail (NRP1Δcyto), all had no such effect on VEGFR2 phosphorylation, suggesting that the NRP1-VEGFR2 interaction and the role of the NRP1 cytoplasmic tail does not directly affect VEGFR2 activation in HUVECs [133,272,273]. Both NRP1 knockdown and the expression of NRP1Δcyto did abrogate p130Cas phosphorylation and endothelial migration, however, suggesting a VEGF-dependent role for NRP1 in regulating migration via FA function [272]. This involvement of NRP1 in the phosphorylation of p130Cas was mediated by Pyk2 phosphorylation, but was independent from the

phosphorylation of FAK at its major phosphorylation site, Y397 [69,272]. Instead, NRP1 knockdown and the expression of the NRP1 Y297A mutant suppressed the VEGF-induced phosphorylation of FAK at Y407, which is also known to be regulated by Pyk2 [69,273,281]. This suggests that NRP1 potentially mediates signalling through a Pyk2/FAK407/p130Cas pathway, although how much this depends on VEGFR2 activation is unclear [256]. The $VEGF_{165}$-induced association of NRP1 with VEGFR2 has additionally been implicated in activating p38MAPK, another known positive regulator of migration [133,275]. NRP1's effect on EC migration is striking, as targeting NRP1 in different ways has consistently reduced EC migration to a high degree in a number of different studies, but, interestingly, VEGF-induced HUVEC proliferation and survival, as regulated through the PLCγ/ERK and Akt signalling cascades, appear to be largely independent of NRP1 and its association with VEGFR2 in these cells [69,133,272-275,282]. However, more recently, Raimondi et al. [271] reported reduced VEGF-induced phosphorylation of PLCγ/ERK and Akt in human dermal microvascular ECs (HDMECs) upon NRP1 siRNA knockdown, indicating a discrepancy between EC types. Furthermore, arterial ECs and heart tissue from NRP1Δcyto mice were shown to exhibit dampened phosphorylation of VEGFR Y1175 and ERK1/2 in response to VEGF, though this is more congruent with NRP1's role in arteriogenesis, as mentioned above, which appears to require a greater degree of ERK1/2 signalling [268]. Overall, consistent results in HUVECs show that NRP1 regulates VEGF-induced EC migration and signalling through p38MAPK, p130Cas, and FAK407 in a manner that is dependent on its interaction with VEGF and VEGFR2, and its cytoplasmic tail, but not necessarily on VEGFR2 activation (**Figure 1.14A**). It is also worth mentioning that NRP1 has additionally been implicated in VEGF/VEGFR-2-mediated endothelial permeability [283].

There is now mounting evidence to suggest that a major role for NRP1 is to mediate the endocytosis and trafficking of VEGFR2, and therefore regulate its signalling in this way. In primary murine aortic ECs, Salikhova et al. [284] showed that $VEGF_{165}$ induced the clathrin-mediated endocytosis of NRP1 and VEGFR2 together, and that NRP1 trafficking to EEA1+ early endosomes was dependent on the presence of its cytoplasmic binding partner, synectin, which is known to

drive receptor internalisation via the molecular motor, myosin VI [285]. Lanahan et al. [82] subsequently found that synectin and myosin VI were also required for VEGF-induced VEGFR2 trafficking to EEA1+ early endosomes in these cells. Without the synectin-myosin VI complex, VEGFR2 Y1175 phosphorylation and downstream signalling through ERK1/2 and Akt was impaired due to delayed VEGFR2 trafficking away from the phosphatase PTP1b at the plasma membrane, but was, interestingly, here, not related to associations with NRP1 [82]. The synectin-myosin VI-dependent trafficking of VEGFR2 was additionally shown to be important for arterial morphogenesis [82]. Ballmer-hofer et al. [80] then, through the use of overexpressed VEGFR2, NRP1 and fluorescently-tagged-Rab proteins in porcine aortic ECs (PAEs), which lack endogenous VEGFR expression, found that $VEGF_{165}$ stimulated NRP1-VEGFR2 complexes to recycle to the plasma membrane through Rab5, Rab4, and Rab11 vesicles. However, without the NRP1-VEGFR2 association, VEGFR2 was shuttled down a degradation pathway through Rab7 vesicles, and without NRP1's C-terminal synectin-binding motif (SEA), VEGFR2 no longer trafficked through Rab11 vesicles and was degraded faster [80]. The presence of NRP1 resulted in elevated phosphorylation of VEGFR2 Y1175, PLCγ, and p38MAPK. PLCγ and p38MAPK phosphorylation was impaired by loss of NRP1's cytoplasmic tail, and full p38MAPK phosphorylation was even dependent on NRP1's SEA synectin-binding motif [80]. Consistent with these results, the defective arteriogenesis and VEGFR2/ERK phosphorylation observed previously in NRP1Δcyto mice in Lanahan et al. [268]'s study was ascribed to the lack of a link between NRP1-VEGFR2 and synectin that resulted in delayed VEGFR2 trafficking from Rab5 to EAA1+ endosomes and therefore prolonged exposure to PTP1b. Interestingly, a recent study by Koch et al. [286] showed that if NRP1 is presented to VEGFR2 in *trans* (ie. from one EC to another), then VEGFR2 endocytosis was arrested, and its signalling via ERK was delayed, compared to NRP1 expressed on the same cell.

Together, this work therefore points to a role for NRP1 in enhancing VEGF-induced VEGFR2 endocytosis and recycling, and thus signalling, via its cytoplasmic tail's interaction with the PDZ domain of synectin (**Figure 1.14B**). Indeed, we know from earlier that VEGFR2 can continue signalling from endocytic vesicles, which enhances signalling responses [80-86,91]. However,

since these studies were carried out in aortic/arterial ECs, which did not necessarily endogenously express NRP1 and VEGFR2, it is not clear how physiologically relevant these results are, and whether they translate to HUVECs or microvascular ECs. Given Fantin et al.'s [267] and Lanahan et al.'s [268] *in vivo* results with NRP1Δcyto mice, it has been proposed that NRP1-mediated VEGFR2 trafficking, and therefore high levels of ERK1/2 signalling, are only required for arteriogenesis, and not for angiogenesis [287]. Exactly how NRP1 influences VEGF-induced signalling overall is still unclear, especially as there appears to be differences between that in HUVECs, microvascular ECs and aortic/arterial ECs that may also be related to angiogenic vs arteriogenic effects [268]. We also do not know the exact function of NRP1's cytoplasmic tail in either angiogenic or arteriogenic contexts. Can it directly or indirectly activate VEGFR2? Does it universally regulate VEGFR2 signalling by promoting its trafficking? Does it have additional binding partners other than synectin? And how does its VEGFR2-dependent role integrate with its other functions?

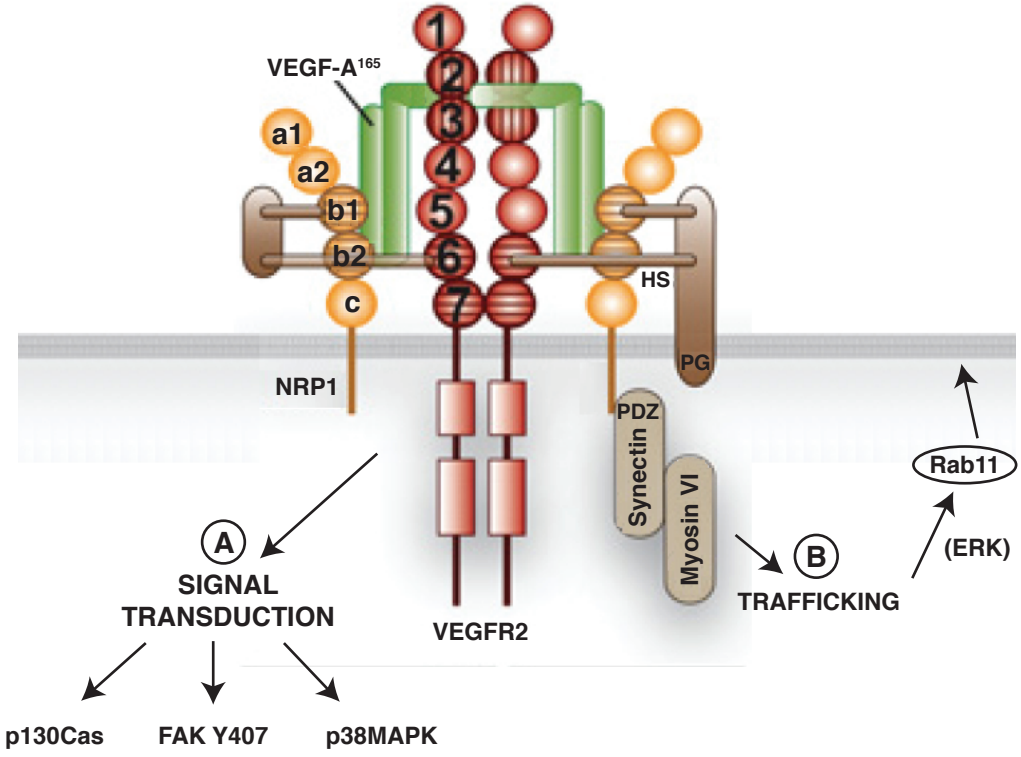

Figure 1.14: Neuropilin-1's VEGFR2-dependent roles. Neuropilin-1 (NRP1) can form a receptor complex with VEGFR2 upon VEGF-A_{165} binding, and also reciprocally enhance the affinity of VEGF-A_{165} for VEGFR2. **A** As a result, NRP1 can regulate VEGF-induced EC migration and signalling through p38MAPK, p130Cas, and FAK407. **B** Also, when in this complex, NRP1 can enhance VEGF-induced VEGFR2 endocytosis and recycling through Rab11-positive vesicles, and thus enhance ERK1/2 signalling, via its cytoplasmic tail's interaction with the PDZ domain of synectin. Figure adapted from [276].

1.5.3.3.2 VEGFR2-independent roles of neuropilin-1

Fantin et al. [269] recently investigated the significance of VEGF binding to NRP1 for angiogenesis *in vivo* using mice with a Y297 mutation in the VEGF-binding pocket of NRP1's b1 domain. Though this resulted in NRP1 hypomorphism, and therefore reduced NRP1 expression, NRP1-VEGF binding was successfully perturbed, and, importantly, the NRP1 Y297 mice were able to overcome the mid-gestation lethality of NRP1-NULL mice [269]. More recently, a different NRP1 VEGF-binding-deficient mutant mouse line that expressed normal levels of NRP1 also survived, and with normal vasculature, therefore meaning NRP1 does not appear to influence embryonic blood vessel formation through binding VEGF [270]. The mice did, however, display defects in postnatal angiogenesis in the retina [270]. In further support of a VEGF-independent role for NRP1 in embryonic blood vessel formation, the vascular phenotype in mutant mice that only express their equivalent of the non-NRP1-VEGFR2 complex-inducing VEGF, $VEGF_{121}$, was also less severe than NRP1-NULL mice, although this phenotype was more attributed to differential VEGF-ECM binding ability than the loss of NRP1 binding [27,66]. Regardless, these studies prove that NRP1 can function independently of its binding to VEGF to regulate embryonic blood vessel formation *in vivo*, though NRP1-VEGF binding is more required for postnatal angiogenesis.

The original discovery of NRP1 as an adhesion receptor is suggestive of its VEGF-independent endothelial role partly being related to adhesion [254]. Indeed, siRNA knockdown of NRP1, but not of VEGFR2, impaired HUVEC adhesion to gelatin, fibronectin and laminin, suggesting NRP1 regulates EC attachment in a VEGFR2-independent manner [282]. Consistent with this hypothesis to some degree, Valdembri et al. [288] showed that NRP1 promoted human umbilical artery EC (HUAEC) adhesion to fibronectin, although not type I collagen, vitronectin or laminin, in a manner that was dependent on NRP1's SEA synectin-binding motif, and the fibronectin-binding integrin, α5β1, and was, importantly, independent of VEGF [288]. The authors specifically found that this function of NRP1 was mediated through its interaction with α5β1 via its extracellular domain at adhesion sites, and its promotion of α5β1 trafficking via synectin (which can interact with both NRP1 and α5β1) and subsequent recycling

to the membrane [288]. This could have profound implications for angiogenesis, particularly given NRP1's significance in tip cells, and the importance of a fast turnover of α5β1-positive nascent FAs for EC migration [266,288].

In agreement with NRP1's involvement with integrin function, as discussed earlier, it is possible that αvβ3 normally interacts with NRP1 to prevent its pro-angiogenic interactions with VEGFR2, which may be why the loss of β3 increases NRP1-VEGFR2 interactions and elevates angiogenesis [202]. However, this does not take into account NRP1's clear VEGFR2-independent role. It is therefore important to properly evaluate both NRP1's VEGR2-dependent and -independent functions when αvβ3 is targeted to have a greater insight into its endothelial mechanism of action.

Recently, there has been further support for NRP1's function in adhesion. Seerapu et al. [289] immunoprecipitated NRP1 from murine heart ECs and used proteomics to identify binding partners. They found, for example, the heavy chains of NM-IIA and NM-IIB to associate with NRP1 with and without the presence of VEGF, and filamin A and α-enolase to co-associate only when VEGF was present [289]. NRP1 co-localised with filamin A in vesicles in response to VEGF in a manner dependent on its cytoplasmic tail, and additionally associated with another FA protein, p130Cas, but in vesicular punctae, and not FAs, suggesting it was a recycling fraction of p130Cas [289]. NRP1Δcyto ECs migrated slower than WT ECs in a VEGF-induced wound-closure model, and FA assembly and disassembly were impaired in NRP1Δcyto ECs, as viewed by live TIRF imaging mCherry-tagged-kindlin-2 dynamics [289]. This therefore suggested that in heart ECs, NRP1, via its cytoplasmic tail, interacts with FA proteins mainly along their trafficking pathway, and resides in FAs only transiently, but regulates FA turnover, and thus EC migration [289]. The authors speculated that NRP1 may be regulating FA turnover by promoting the trafficking of FA components via its cytoplasmic link to synectin and myosin VI [289]. NRP1's role in FA dynamics may also be supported by its VEGF-induced phosphorylation of FAK407 and p130Cas, which may or may not be mediated by VEGFR2.

In a separate study, Raimondi et al. [271] discovered that, independent of VEGF/VEGFR2, NRP1 promoted fibronectin-stimulated actin remodelling and phosphorylation of paxillin Y118 via the non-receptor tyrosine kinase, ABL1. In response to fibronectin, NRP1 formed a complex with ABL1, which was required for ABL1's phosphorylation of paxillin, and for the promotion of HMDEC, HUVEC and mouse lung EC migration on fibronectin. NRP1 itself also co-associated with phosphorylated paxillin at peripheral cell areas resembling FAs, further supporting a potential role for NRP1 in FAs [271]. Concordant with these results, both physiological and pathological angiogenesis in the perinatal retina were inhibited by treatment with an ABL1 inhibitor, Imatinib; pathological angiogenesis was affected in a similar manner to that observed in inducible EC-specific NRP1 knockout murine pups [271]. The authors hypothesised that, given NRP1's cytoplasmic tail is not required for angiogenesis, its extracellular domain likely influences ABL1's effect on paxillin, but possibly in an indirect manner through interactions with fibronectin-binding integrins [271].

Fantin et al. [290] most recently found that NRP1, again independent of VEGF stimulation, promoted fibronectin-stimulated Cdc42-dependent actin remodelling and filopodia formation in endothelial tip cells, thereby supporting angiogenic sprouting. This fit with Raimondi et al.'s [271] work nicely, as fibronectin-stimulated Cdc42 activation was dependent on ABL1 activity, suggesting that a NRP1-ABL1 complex directly activates Cdc42 [290] (**Figure 1.15**). The authors additionally proved that NRP1 was not required for genetic tip cell identity, meaning NRP1 purely promoted tip cell function by promoting Cdc42 activation [290].

Other VEGFR2-independent roles for NRP1 aside from adhesion have also been reported. For example, its fusion to the EGFR promoted EC migration in response to VEGF [278]. NRP1 mediated VEGF-induced, but VEGFR2-independent EC survival via synectin, which activated Akt and subsequently inactivated p53 pathways and FoxOs, and activated p21 [291]. NRP1 also reportedly binds VEGFR1, potentially to compete against its binding with VEGFR2 [292]. Furthermore, we must not forget the role of NRP1 in other cell

types, as PDGF-BB-stimulated migration and signalling via p130Cas was significantly decreased when NRP1 was inhibited in vSMCs [293].

The aforementioned studies have provided substantial evidence for VEGFR2-independent roles for NRP1 in regulating angiogenesis that is mainly related to its role in EC adhesion. Though NRP1's VEGF binding capability was not required for embryonic blood vessel formation, it is likely that generally both NRP1's VEGFR2-dependent and -independent functions are required to work together to coordinate effective EC activity to meet the requirements of a particular scenario. However, again, the studies were predominantly performed in developmental angiogenesis models, meaning further physiological and pathological angiogenesis analyses are required in adult mice to properly distinguish NRP1's function in these different contexts. Similarly, NRP1's projected role in regulating focal adhesions must be pursued further in different cell types and under different conditions, before we can fully understand the mechanisms behind this alleged function.

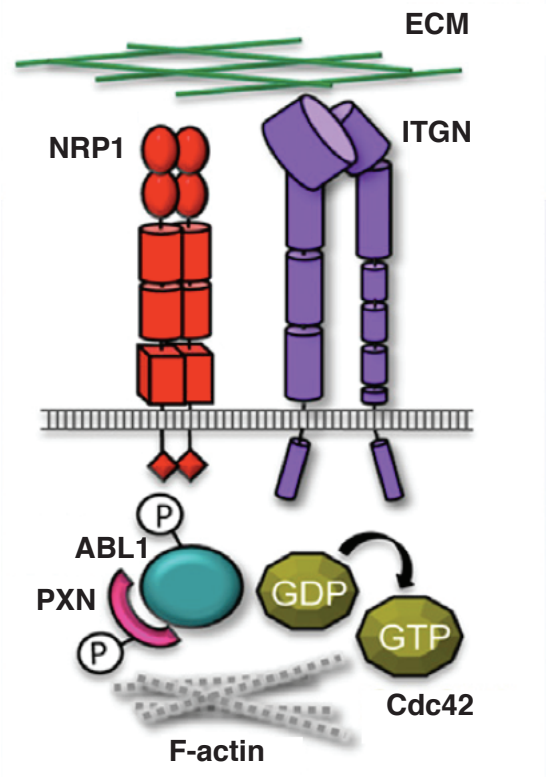

Figure 1.15: Projected model of neuropilin-1's adhesion-dependent role. Fantin et. al. [ref] have proposed that neuropilin-1 (NRP1) mediates the extracellular matrix (ECM)- dependent activation of ABL1 and Cdc42, thereby promoting filopodia formation and actin remodelling in endothelial tip cells. Figure adapted from [290].

1.5.3.3.3 NRP1 in cancer

NRP1 is seen as a potentially good target in cancer therapy; not only is it overexpressed in a wide range of cancer cell lines and human tumours, but targeting NRP1 with monoclonal antibodies, siRNAs, inhibitory peptides, soluble NRP1, and small molecule inhibitors of the NRP1-VEGF interaction, inhibits pro cancer phenotypes such as tumor cell migration, adhesion, and survival, as well as tumour growth and angiogenesis in various pre-clinical models [69,124,133,294-304]. In rectal carcinoma patients, treatment with bevacizumab increased NRP1 expression in cancer cells, suggesting NRP1 may be involved in a compensatory escape mechanism following VEGF targeting [124,305]. In support of this, blocking the VEGF-binding domain of NRP1 with a monoclonal antibody, whilst only mildly affecting VEGFR2 signalling, strongly reduced tumour growth and vessel organisation in an additive manner when combined with anti-VEGF antibody therapy [133]. Interestingly, this effect was not dependent on NRP1's expression in the tumour cells, but rather due to an inhibition of the tumour vasculature, although other studies have contested the notion that NRP1's role in tumour growth is solely related to vascularisation [69,133]. Nevertheless, the study further implicates the importance of VEGFR2-independent roles for NRP1, but in pathological angiogenesis [69]. In agreement, NRP1 expression was found to promote invasiveness of melanoma cells through both VEGFR2-dependent and -independent mechanisms [306]. Also, NRP1 promoted pancreatic cancer cell growth, survival, and invasion via its interaction with β1-integrin, [307] and, in another study, NRP1 stimulated tumour growth by increasing fibronectin fibril assembly in the tumour microenvironment via associations with synectin and ABL to augment α5β1 activity [308]. Clearly, NRP1's VEGFR2-independent functions cannot be overlooked when deciding on NRP1-based cancer therapies.

The use of small molecule inhibitors that target the NRP1-VEGF interaction may have promise as a novel cancer therapeutic strategy [69,299]. EG00229 and EG3287 are current peptidomimetics of portions of the $VEGF_{165}$ molecule, which have demonstrated efficacy in inhibiting VEGFR2 phosphorylation and EC migration, and EG3287 has additionally been shown to inhibit cancer cell adhesion and migration, and even enhance chemosensitivity by interfering with

integrin-dependent survival pathways [274,299,300]. Promisingly, they have provided a basis for the design of further inhibitors that may have clinical efficacy in the future, especially when used in combination with antagonists against other molecules [69,299].

1.5.3.3.4 Conclusions on neuropilin-1

We have gained great insight into the roles of NRP1 in the endothelium, the significance of its cytoplasmic tail, its VEGF-binding ability, and its potential promise as an anti-cancer target. However, the mass of information on NRP1's contribution to blood vessel formation is complex, given NRP1's differential effects in different contexts. Though the global and endothelial expression of NRP1 is essential for vascular development and endothelial tip cell function, NRP1's cytoplasmic tail is dispensable for developmental angiogenesis, and its role in VEGF binding is not required for embryonic blood vessel formation, but more involved in postnatal angiogenesis. NRP1's synectin-dependent promotion of VEGFR2 trafficking and prolonged ERK signalling appears to be important for arteriogenesis, but not developmental angiogenesis, which is likely more influenced by a combination of other VEGFR2-dependent and -independent functions of NRP1. It has been proposed that during angiogenesis, given that endothelial tip cells express very high levels of VEGFR2 and are exposed to high VEGF concentrations, they likely do not require prolonged NRP1-mediated VEGFR2/ERK signalling, but are rather more reliant on a VEGFR2-dependent and -independent induction of migration [287]. On the other hand, arteriogenesis, which involves luminal expansion, for example, may be more limited in VEGF availability, and so requires NRP1 to enhance and prolong VEGFR2 signalling by inceasing its recycling [287]. This may partly explain the overall differences observed in NRP1-mediated signalling properties between EC types (ie. due to their inherent predisposition for regulating different blood vessel formation processes), though this whole theory needs exploring further. More clarity is also needed on how NRP1's VEGFR2-dependent and adhesion-dependent functions cooperate to regulate angiogenesis. Moreover, information on the roles of NRP1 in adult physiological and pathological angiogenesis is still lacking. There is therefore a requirement for further work on NRP1's significance and mechanisms of action in these contexts.

1.6 Research Aims and Objectives

Following the discovery that NRP1's role in angiogenesis becomes more influential, and thus targetable, in the complete absence of β3 [202], this project was developed to examine whether the same phenomenon exists in a more physiologically relevant model than β3-NULL mice, and whether it impacts on tumour progression and angiogenesis. Coupled with this major objective, since αvβ3 was reported to associate with NRP1 and potentially control its function in ECs, this project also aimed to elucidate whether, and how, αvβ3-integrin might regulate neuropilin-1's role in this new model. Any data collected would help us determine whether targeting both molecules together might be a promising anti-angiogenic therapeutic approach in the future.

In line with the above, more specific aims are outlined below:

1. Determine the effect of an endothelial-specific NRP1 depletion on tumour growth, angiogenesis and metastasis in WT and β3-integrin-heterozygous (β3-HET) mice
2. Determine the effect of the loss of NRP1's cytoplasmic tail on tumour growth, angiogenesis and metastasis in WT and β3-HET mice
3. Assay for potential differences in EC behaviour following the targeting of β3 and/or NRP1
4. Elucidate a molecular mechanism of how β3 and NRP1 interplay, and how β3 regulates NRP1's function, in ECs
5. Determine whether simultaneously targeting both β3 and NRP1 inhibits tumour growth and angiogenesis in mice

2. Materials and methods

2.1 Reagents (and antibodies)

VEGF-A^{164} (the mouse equivalent of human VEGF-A_{165}), used for stimulating mouse lung microvascular ECs, was made in-house according to the protocol published by Krilleke et al. [309]. All chemicals were from Sigma-Aldrich (Poole, UK) unless otherwise indicated. All primary and secondary antibodies used are presented in **Table 2.1** and **Table 2.2**, respectively.

2.2 Animals

All animals were on a mixed C57BL6/129 background. β3-integrin-heterozygous (β3-HET) mice, which have one β3-NULL allele [196], were acquired from β3-WT X β3-HET breeding pairs. Neuropilin-1 (NRP1)-floxed mice [258], which contain loxP sites flanking exon 2 of the Nrp1 gene, were purchased from The Jackson Laboratory (Bar Harbor, Maine, USA). The β3-integrin-floxed allele was generated by gene target insertion of embryonic stem cells that resulted in the insertion of loxP sites flanking exon 1 of the itgb3 (β3-integrin) gene [210]. Pdgfb-iCreERT^2 mice [310] were provided by Marcus Fruttiger (UCL, London, UK). NRP1-floxed/floxed ($^{fl/fl}$), $\beta3^{fl/fl}$, and NRP1/β3-double$^{fl/fl}$ mice were bred with Pdgfb-iCreERT^2 mice in order to generate each different floxed Cre-positive (and Cre-negative) animal. Mice lacking NRP1's cytoplasmic tail (NRP1Δcyto) [267] were provided by Christiana Ruhrberg (UCL, London, UK), and were crossed with β3-WT and β3-HET mice to acquire β3-WT-NRP1Δcyto and β3-HET-NRP1Δcyto animals. Littermate controls were used for all *in vivo* experiments. All experiments were performed in accordance with UK Home Office regulations and the European Legal Framework for the Protection of animals used for scientific purposes (European Directive 86/609/EEC).

Table 2.1 List of primary antibodies:

Anti-	Clone/Cat. #	Conjugate	Host	Reactivity used	Source	Application
α1-integrin	HMα1 / 142603	PE	Hamster (IgG)	Mouse	Cambridge Bioscience	FC
α2-integrin	DX5 / 12-5971-63	PE	Rat (IgM)	Mouse	eBioscience	FC
α5-integrin	eBioHMα5-1 / 12-0493-81	PE	Hamster (IgG)	Mouse	eBioscience	FC
α5-integrin	#4705		Rabbit	Mouse	Cell Signalling Technology	WB
αV-integrin	RMV-7 / 12-0512-81	PE	Rat (IgG1)	Mouse	eBioscience	FC
β1-integrin	eBioHMb1-1 / 12-0291-81	PE	Hamster (IgG)	Mouse	eBioscience	FC
β3-integrin	2C9.G3 / 12-0611-82	PE	Hamster (IgG)	Mouse	eBioscience	FC
β3-Integrin	#4702		Rabbit	Mouse	Cell Signalling Technology	WB
β5-integrin	KN52 / 12-0497-41	PE	Mouse (IgG1, κ)	Mouse	eBioscience	FC
Akt	#9272		Rabbit	Mouse	Cell Signalling Technology	WB
Phospho Akt	#4060		Rabbit	Mouse	Cell Signalling Technology	WB
Biotin	3D6.6		Mouse	Mouse	Jackson Immunoresearch	IP
BS1-lectin	L2895	FITC		Mouse	Sigma	ARA
CD31	ER-MP12		Rat	Mouse	Abd Serotec	ECS
CD31	390 / 12-0311-82	PE	Rat (IgG2a, κ)	Mouse	eBioscience	FC
CD146	EPR3208		Rabbit	Mouse	Abcam, Cambridge, UK	IHC
Endomucin	V.7C7		Rat	Mouse	Santa Cruz Biotechnology	IHC
ERK1/2 (p44/42 MAPK)	137F5 / #4695		Rabbit	Mouse	Cell Signalling Technology	WB
Phospho ERK1/2	D13.14.4E #4370		Rabbit	Mouse	Cell Signalling Technology	WB
VEGFR2	AVAS 12α1	PE	Rat (IgG2a, κ)	Mouse	BD Pharmingen	FC
FAK	#3285		Rabbit	Mouse	Cell Signalling Technology	WB
Phospho FAK (Y407)	#OPA1-03887		Rabbit	Mouse	Thermo Scientific	WB
Filamin A	ab76289		Rabbit	Mouse	Abcam	WB
GAPDH	14C10 / #2118		Rabbit	Mouse	Cell Signalling Technology	WB

Histone H3	D1H2 / #4499		Rabbit	Mouse	Cell Signalling Technology	WB
HSC-70	B-6 / sc-7298		Mouse	Mouse	Santa Cruz Biotechnology	WB
ICAM-2	#MCA2295EL		Rat	Mouse	AbD Serotec	ECS
ICAM-2	3C4 (mlc2/4) / 53-1021-80	Alexa®-488	Rat (IgG2a, κ)	Mouse	eBioscience	FC
IgG Isotype control	eBio299 Arm / 12-4888-81	PE	Hamster	Mouse	eBioscience	FC
IgG1 isotype control	M1-14D12	PE	Rat	Mouse	eBioscience	FC
IgG1, κ isotype control	P3.6.2.8.1	PE	Mouse	Mouse	eBioscience	FC
IgG2a, κ isotype control	G155-178	PE	Mouse	Mouse	BD Biosciences	FC
IgM isotype control	eBRM / 12-4341-81	PE	Rat	Mouse	eBioscience	FC
Myosin 9	#3403		Rabbit	Mouse	Cell Signalling Technology	WB
Neuropilin 1	D62C6 / #3725		Rabbit	Mouse, Human	Cell Signalling Technology	WB, IP
Neuropilin 1	AF566		Goat	Mouse	R&D Systems	ICC, IP
p130cas	#610271		Mouse	Mouse	BD Biosciences	WB
Phospho p130cas	#4011		Rabbit	Mouse	Cell Signalling Technology	WB
p38 MAPK	#9212		Rabbit	Mouse	Cell Signalling Technology	WB
Phospho p38 MAPK	3D7 / #9215		Rabbit	Mouse	Cell Signalling Technology	WB
Paxillin	ab32084		Rabbit	Mouse	Abcam	ICC, WB
Phospho Paxillin (Y118)	#2541		Rabbit	Mouse	Cell Signalling Technology	ICC, WB
SP-1	#5931		Rabbit	Mouse	Cell Signalling Technology	WB
VE-Cadherin	eBioBC13 / 12-1441-80	PE	Rat (IgG1)	Mouse	eBioscience	FC
VEGFR2	AVAS 12α1	PE	Rat (IgG2a, κ)	Mouse	BD Biosciences	FC
VEGFR2	55B11 / #2479		Rabbit	Mouse, Human	Cell Signalling Technology	WB, IP
Phospho VEGFR-2 (Y1175)	19A10 / #2478		Rabbit	Mouse	Cell Signalling Technology	WB
Vimentin	D21H3 / #5741		Rabbit	Mouse	Cell Signalling Technology	WB

Table 2.1: Abbreviations - Aortic ring assay (ARA), EC sorting (ECS), Flow cytometry (FC), Immunocytochemistry (ICC), Immunohistochemistry (IHC), Immunoprecipitation (IP), and Western blotting (WB).

Table 2.2 List of secondary antibodies:

Anti-	Cat. #	Conjugate	Host	Source	Application
Goat	A-21222	Alexa®-488	Rabbit	Invitrogen	ICC
Goat	A-21223	Alexa®-594	Rabbit	Invitrogen	ICC
Mouse	715-035-151	HRP	Donkey	Jackson Immunoresearch	WB
Rabbit	A-21206	Alexa®-488	Donkey	Invitrogen	IHC, ICC
Rabbit	711-035-152	HRP	Donkey	Jackson Immunoresearch	WB
Rat	11035	Dynabeads	Sheep	Invitrogen	ECS
Rat	A-21209	Alexa®-594	Donkey	Invitrogen	IHC

Table 2.1: Abbreviations - EC sorting (ECS), Immunocytochemistry (ICC), Immunohistochemistry (IHC), Immunoprecipitation (IP), and Western blotting (WB).

2.3 Mouse genotyping

2.3.1 PCR genotyping

Ear or tail snips from mice were digested overnight (o/n) at 56°C in 100 µL ear/tail snip lysis buffer (50 mM Tris-HCl pH 8.5, 10 mM EDTA pH 8.0, 100 mM NaCl, 0.2% SDS) supplemented with 100 µg/mL proteinase K in separate wells of a 96-well PCR plate (Fisher Scientific). DNA was subsequently precipitated by adding 100 µL isopropanol to each well, shaking the plate to mix, and centrifuging the plate at 1400 × g for 30 mins. Isopropanol was removed by gently inverting the plate, and the DNA pellet was dried at 37°C for about 2 hrs. DNA was then resuspended in 200 µL TE buffer (10 mM Tris-HCl pH7.5, 1 mM EDTA) and left to solubilise o/n at room temperature (RT).

PCR reactions were then performed for the relevant transgenic mice in a 96-well block thermal cycler PCR machine (Bioer Technology, Binjiang, China), as detailed below.

2.3.1.1 β3-integrin-knockout PCR

PCR analysis of the β3-NULL allele, which was originally created by replacing a 1.4 kb HindIII fragment of the β3 gene (in exons I and II) with a 1.7 kb targeting construct containing a PGK-neomycin (neo)-resistance cassette [196], was carried out using the following oligonucleotide primers:

Common forward primer 1:	5’ – CTTAGACACCTGCTACGGGC – 3’
Reverse primer 2:	5’ – CACGAGACTAGTGAGACGTG – 3’
Reverse primer 3:	5’ – CCTGCCTGAGGCTGAGTG – 3’

The forward primer 1, which recognises DNA 5’ of the PGK-neo cassette, was used in two separate PCR reactions with each of the other reverse primers (2 and 3). Primer 2 is neo-specific and primer 3 is wild-type specific, meaning an amplification product of a reaction involving primers 1 and 2 corresponds to the β3-NULL allele, whilst that of a reaction involving primers 1 and 3 corresponds to the β3-WT allele. PCR amplified products produced in both reactions therefore corresponds to DNA from β3-HET mice.

For each PCR reaction involving primers 1 and 2, 0.4 µL of DNA was mixed with 10 µL MegaMix-Blue (Microzone, Haywards Heath, UK), and primers 1 and 2 (used at a final concentration of 1 µM). For each PCR reaction involving primers 1 and 3, 0.4 µL of DNA was mixed with 10 µL MegaMix-Blue, and primers 1 and 3 (used at a final concentration of 0.4 µM). PCR reaction conditions were as follows: initialisation step at 95°C for 15 min; followed by 35 amplification cycles of denaturation at 95°C for 30 sec, extension at 60°C for 45 sec, and annealing at 72°C for 90 sec; and terminated with a final elongation step at 72°C for 10 min. PCR products are 538 base pairs (bp) long (β3-NULL allele) and 446-bp (wild-type).

2.3.1.2 β3-integrin-floxed PCR

PCR analysis of the β3-floxed allele was carried out using the following oligonucleotide primers:

Forward primer:	5’ – TTGTTGGAGGTGAGCGAGTC – 3’
Reverse primer:	5’ – GCCCAGCGGATCTCCATCT – 3’

For each PCR reaction, 0.8 µL of DNA was mixed with 10 µL MegaMix-Blue, and the forward and reverse primers (used at a final concentration of 0.8 µM). PCR reaction conditions were as follows: initialisation step at 95°C for 2 min; followed by 35 amplification cycles of denaturation at 95°C for 30 sec, extension at 56°C

for 30 sec, and annealing at 72°C for 30 sec; and terminated with a final elongation step at 72°C for 8 min. PCR products are 182-bp (β3-WT), 272-bp ($\beta3^{fl/fl}$).

2.3.1.3 NRP1-floxed PCR

PCR analysis of the NRP1-floxed allele was carried out using the following oligonucleotide primers:

Forward primer: 5' – AGGTTAGGCTTCAGGCCAAT – 3'
Reverse primer: 5' – GGTACCCTGGGTTTTCGATT – 3'

For each PCR reaction, 0.8 µL of DNA was mixed with 10 µL MegaMix-Blue, and the forward and reverse primers (used at a final concentration of 0.8 µM). PCR reaction conditions were as follows: initialisation step at 94°C for 3 min; followed by 35 amplification cycles of denaturation at 94°C for 30 sec, extension at 65°C for 1 min, and annealing at 72°C for 1 min; and terminated with a final elongation step at 72°C for 2 min. PCR products are 550-bp (NRP1-WT), 738-bp ($NRP1^{fl/fl}$).

2.3.1.4 Pdgfb.CreER PCR

PCR analysis of the Pdgfb.CreER allele was carried out using the following oligonucleotide primers:

Forward primer: 5' – GCCGCCGGGATCACTCTC – 3'
Reverse primer: 5' – CCAGCCGCCGTCGCAACT – 3'

For each PCR reaction, 0.8 µL of DNA was mixed with 10 µL MegaMix-Blue, and the forward and reverse primers (used at a final concentration of 1 µM). PCR reaction conditions were as follows: initialisation step at 94°C for 4 min; followed by 34 amplification cycles of denaturation at 94°C for 30 sec, extension at 57.5°C for 45 sec, and annealing at 72°C for 1 min; and terminated with a final elongation step at 72°C for 10 min. PCR product is 443-bp if positive for Pdgfb.CreER.

2.3.1.5 NRP1Δcyto PCR

PCR analysis of the NRP1Δcyto allele was carried out using the following oligonucleotide primers:

Forward primer:	5' – CCTTTTGATGGACATGTGACCTGTAGC – 3'
Reverse primer:	5' – CACCAGGTCTGATTGAAGAGAAGG – 3'
Δcyto reverse primer:	5' – ATGGTACCTTGAGCATCTGACTTCTG – 3'

For each PCR reaction, 1 µL of DNA was mixed with 8 µL MegaMix-Blue, forward primer (used at a final concentration of 1 µM), reverse primers (used at a final concentration of 0.5 µM), and betaine (used at a final concentration of 0.4 M). PCR reaction conditions were as follows: initialisation step at 94°C for 2 min; followed by 34 amplification cycles of denaturation at 94°C for 40 sec, extension at 60°C for 45 sec, and annealing at 72°C for 1 min; and terminated with a final elongation step at 72°C for 10 min. PCR products are 550-bp (NRP1-WT) or 660-bp (NRP1Δcyto).

2.3.2 Agarose gel electrophoresis

PCR products were separated on a 1.8% agarose gel, apart from those from the NRP1Δcyto PCR, which were separated on a 2% agarose gel. To make these gels, the corresponding agarose (Fisher Scientific, Loughborough, UK) amounts to a final volume of 200 mL were weighed in grams and dissolved in 100 mL distilled water (dH_2O) by microwaving for 2-3 mins. Another 96 mL distilled water was then added to this dissolved agarose to aid faster cooling, along with 4 mL of 50X TAE buffer (0.5 M Tris, 1 M acetic acid, 50 mM EDTA pH 8.0) and 10 µL of ethidium bromide (Fisher Scientific). This gel solution was poured into a large gel tank (Alpha Laboratories, Eastleigh, UK) containing well-forming combs that meet the demand for the number of PCR samples. The entire PCR product (~10 µL) from each reaction was loaded into each well of the gel and separated at 100 V for ~1 hr. Gel bands were visualised under UV light and photographed using a BioDoc-It Transiluminator (UVP, Cambridge, UK).

2.4 *In vivo* tumour growth assays

Syngeneic mouse melanoma (B16F0, ATCC; mycoplasma free) or mouse lung carcinoma (CMT19T, CR-UK Cell Production; mycoplasma free) cells (1×10^6) were injected subcutaneously in the flank of age-matched experimental and littermate control mice. 12-20 days after injection mice were sacrificed by cervical dislocation, tumour sizes were measured in two dimensions using a digital caliper, and tumour samples were fixed in 4% paraformaldehyde (PFA) o/n for histological analysis. For prevention studies in Pdgfb-iCreER^{T2} mice (**Figure 3.2, Appendix Figure 1**), slow release (5 mg, 21-day release) tamoxifen pellets (Innovative Research of America, Sarasota, Florida, USA) were implanted subcutaneously into the scruff of the neck 3 days prior to tumour cell injection. For intervention studies (**Figure 3.7**), pellets were implanted after 10 days of initial tumour growth. Tumour volumes (mm^3) were calculated according to the formula: length × width^2 × 0.52 [311].

2.5 Immunohistochemical analyses

2.5.1 Tumour samples

Post-fixation, tumours were washed in PBS for a further 24 hrs, and then bisected at the midline. Samples were dehrydrated by successively placing them through ethanol solutions of increasing concentrations (50-100%), followed by Histoclear (Sigma), and were then embedded in paraffin. Paraffin blocks were sectioned using a microtome (HM 355 S, Microm, Bicester, UK) into 5 µm sections (with the cut tumour face toward blade), which were mounted onto glass slides and dried at 37°C o/n. Prior to immuno-staining, sections were de-paraffinised in Histoclear, and rehydrated through successive solutions of ethanol of decreasing concentrations (100%-50%) and left in PBS. Heat-mediated antigen retrieval was performed by boiling sections in sodium citrate buffer (10 mM tri-sodium citrate, 0.05% Tween®-20, pH 6) for 20 mins. They were then allowed to cool, washed in PBLEC (1 mM $CaCl^2$, 1 mM $MgCl^2$, 0.1 mM $MnCl^2$, 1% Tween-20) (3X15 mins), and blocked using drops of serum-free protein block solution (Dako, Ely, UK) at 37°C in a humidified chamber for 30 mins. Sections were incubated with primary antibody (Ab) (diluted in PBLEC) at 4°C o/n, washed in PBS 0.1% Triton X-100 (Sigma, Dorset, UK) (3X15 mins), and then incubated

with secondary Ab (diluted in PBLEC) at RT for 2 hrs. After 2X15 mins washes in PBS 0.1% Triton, 1X15 min wash in PBS, sections were stained with 0.1% Sudan Black (Sigma) for 10 mins, rinsed in water, and mounted with Prolong Gold containing DAPI (Life Technologies, Warrington, UK). Images were acquired on an Axioplan (Zeiss, Cambridge, UK) epifluorescent microscope and tissue area was quantified using Image J™ software available at the National Institutes of Health website. Primary antibodies: rat anti-endomucin (clone V.7C7, used at 1:500, Santa Cruz Biotechnology, Santa Cruz, CA, USA); rabbit anti-CD146 (clone EPR3208, used at 1:500, Abcam, Cambridge, UK). Secondary antibodies: donkey anti-rat Alexa®-594 and donkey anti-rabbit Alexa®-488 conjugates (Invitrogen, Paisley, UK), both used at 1:500.

Blood vessel density was assessed by counting the total number of endomucin-positive vessels per mm^2 across entire midline tumour sections from age-matched, size-matched tumours. For tumour sections from the intervention studies (**Figure 3.7**) vessels around the perimeter of the sections were counted in order to avoid the necrotic centres of tumours.

2.5.2 Lung samples from metastasis experiment

Lungs were embedded in paraffin post-fixation as described above for tumour samples, except lungs were not bissected, and 10 µm sections were prepared instead of 5 µm. Prior to hematoxylin and eosin (H&E) staining, sections were de-paraffinised in Histoclear, and rehydrated through successive solutions of ethanol of decreasing concentrations (100%-50%) and left in dH_2O. Sections were then stained with haematoxylin for 2 mins, rinsed with running tap water, and submerged in a solution of 1% HCl in 70% EtOH for 30 sec. After washing in dH_2O for 10 mins, sections were then placed in 2% sodium bicarbonate for 2 mins, dH_2O for 2 mins, and stained with eosin for 30 sec. Then, sections were dehydrated in 70% EtOH for 10 sec, 2X95% for 2 mins, 2X100% for 2 mins, and placed in Histoclear for 10 mins, before mounting with DePeX (BDH Laboratory Supplies, Poole, UK). Images were acquired on an Axioplan (Zeiss) epifluorescent microscope using the colour camera (AxioCam HRc, Zeiss).

2.6 *Ex vivo* aortic ring assay

This assay was performed by following the protocol outlined by Baker et al. [312]. In summary, thoracic aortae were dissected from 6- to 9-week-old adult mice, cut into rings approximately 0.5 mm in width, and incubated in serum-free media (Opti-MEM™, Invitrogen) at 37°C o/n. Each ring was then embedded in separate wells of a 96-well plate containing 1 mg/mL of collagen I (Millipore, Watford, UK), which was polymerised by leaving the plate at 37°C for 30 mins. Rings were fed with fresh Opti-MEM™ supplemented with 2.5% FBS and VEGF (30 ng/mL) (where indicated) at 37°C every 3 days. After 6-10 days, rings were fixed with 4% PFA, permeabilised with 0.2% Triton and stained with FITC-conjugated BS-1 lectin. A Zeiss inverted microscope (Zeiss Axiovert 40 CFL) was used to count sprouting microvessels and obtain images of the rings. Endothelial protein depletion in aortic rings from Pdgfb-iCreER^{T2} mice was induced in culture with 1 µM 4-hydroxytamoxifen (OHT). For the intervention study (**Figure 3.6**), protein depletion in ECs was induced in culture with 1 µM OHT 4 days after VEGF-induced sprouting had been established, and the microvessel sprouts were quantified after an additional 4 days of VEGF-stimulation.

2.7 *In vivo* metastasis experiment

2.7.1 Attempt at Luciferase-tagging CMT19TF1 cells

2.7.1.1 Lentivirus production in HEK293 cells

HEK-293 cells were seeded at 1×10^6 cells per well in 6-well plates in DMEM high glucose + 10% FBS (without penicillin/streptomycin) and left o/n at 37°C. The following day cells were transfected with 1 µg pLenti-II-CMV-Luc-IRES-GFP lentiviral vector (Abm, Huntingdon, cat no. V010127), 750 ng of the packaging plasmid psPAX (Addgene, Teddington, UK), and 250 ng of the envelope plasmid pMD2.G (Addgene), using lipofectamine 2000 (Thermo Scientific). For transfection, these reagents were first mixed in serum-free OptiMEM® for 30 mins at RT and then applied slowly to the cells, before leaving them at 37°C for 12-15 hrs. The media was then replaced with DMEM high glucose + 10% FBS + 100 units/mL penicillin/streptomycin. The following day, lentivirus was harvested by collecting the conditioned media and storing at 4°C o/n, whilst replenishing the media for the cells. A second harvest was collected the following day, pooled with

that from the previous day, and centrifuged at 1400 × g to remove cell debris. The conditioned media was then aliquoted into cyrovials (Thermo Scientific) and stored at –80°C until use.

2.7.1.2 Lentiviral transduction of CMT19TF1 cells

Mouse lung carcinoma cells enriched for their ability to metastasise to the lung (CMT19TF1) were seeded at 2×10^4 cells per well in 6-well plates, and a volume of lentivirus predicted to give 100% transduction efficiency was added to the media (DMEM high glucose + 10% FBS + 100 units/mL penicillin/streptomycin), along with 8 µg/mL hexadimetherine bromine (polybrene, Sigma). After leaving cells at 37°C for 48 hrs, the media was replaced and successful transduction was confirmed by observed green fluorescent cells under an inverted Axiovert (Zeiss) microscope. These cells were then trypsinised and expanded in culture under antibiotic selection (500 µg/mL G418).

2.7.1.3 Reverse transcription PCR to detect luciferase expression

Lentiviral-transduced-CMT19TF1 cells, and non-transduced cells (as a control), were pelleted, resuspended in RNAbee (Amsbio, Abingdon, UK), and stored at –80°C until use. RNA was the extracted using a SV Total RNA isolation kit (Promega, Southampton, UK). cDNA was created by reverse transcription using Superscript II (Thermo Scientific) following the manufacturer's supplied protocol.

PCR analysis of luciferase was carried out on the cDNA using the following oligonucleotide primers:

Forward primer: 5' – GTTCGTCACATCTCATCTACCTCC – 3'
Reverse primer: 5' – CTTTAGGCAGACCAGTAGATCCAG – 3'

For each PCR reaction, 50 ng of DNA was mixed with 10 µL MegaMix-Blue, and the forward and reverse primers (used at a final concentration of 0.8 µM). PCR reaction conditions were as follows: initialisation step at 95°C for 3 mins; followed by 39 amplification cycles of denaturation at 95°C for 10 sec, extension at 55°C for 30 sec, and annealing at 72°C for 30 sec; and terminated with a final elongation step at 72°C for 1 mins. PCR products were separated by gel electrophoresis on a 1.8% agarose gel.

2.7.1.4 Bioluminescence imaging

To confirm luciferase tagging of CMT19TF1 cells *in vivo*, 1×10^6 lentiviral-transduced CMT19TF1 cells, and B6-LV1 cells (previously tagged with luciferase) were injected subcutaneously in the flank of WT mice. After a few days of growth, mice were injected i.p. with 0.1 cc of a 1 mg/mL luciferin (Promega) and bioluminescence was detected in the mice using the *In vivo* Xtreme BI 4MP machine (Bruker, Coventry, UK).

2.7.2 *In vivo* metastasis experiment

CMT19TF1 cells (1×10^6) were injected subcutaneously in the flank of age-matched experimental and littermate control mice. 20 days after injection, tumours were resected, and slow release (5 mg, 21-day release) tamoxifen pellets were implanted subcutaneously into the scruff of the neck. After 12 further days, mice were sacrificed by cervical dislocation, and their lungs were inflated with 4% PFA, and left in 4% PFA o/n prior to histological analysis by H&E (see **2.5.2 Lung samples from metastasis experiment**).

2.8 Mouse tumour endothelial cell isolation

Tumours were dissected and placed in Hank's Balanced Salt Solution (HBSS) (Thermo Scientific). They were minced and enzymatically digested for 1 hr at 37°C under gentle agitation in HBSS containing 0.2% collagenase IV (Invitrogen), 0.01% hyaluronidase and 0.01% DNase I. The cellular digests were passed through 19 gauge needles, filtered through a 70 µm mesh (Fisher Scientific), and centrifuged for 5 mins at 400 x g. After centrifugation, cells were resuspended in HBSS containing 2% bovine serum albumin (BSA) and 0.6% sodium citrate. Cell yield was determined in a hemocytometer and viability assessed by trypan blue exclusion. Anti-CD31 (AbD Serotec, Oxford, UK) -coupled Dynabeads® (Invitrogen) were incubated at a ratio of 30 beads per target cell (estimated at 1% of total cell count) at 4°C for 25 mins with occasional agitation. Bound cells were separated from unbound cells on a magnet and were washed 3X in HBSS containing 0.1% BSA and 0.6% sodium citrate. Bound cells were lysed in electrophoresis sample buffer (ESB; 65 mM Tris-HCl, pH 7.4, 60 mM sucrose, 3% SDS) and prepared for Western blot analysis.

2.9 Cell isolation and/or culture

2.9.1 Mouse lung microvascular endothelial cell culture

Primary mouse lung ECs were cultured in MLEC media: a 1:1 mix of Ham's F-12:DMEM medium (low glucose) (Invitrogen) supplemented with 20% fetal bovine serum (FBS) (HyClone, Invitrogen), 100 units/mL penicillin/streptomycin (Invitrogen), 2 mM glutamax (Invitrogen), 50 μg/mL heparin (Sigma), and 25 mg of endothelial mitogen (AbD Serotec). To induce target gene deletion in Pdgfb-iCreER^{T2}-floxed cell lines, cells were grown for 48 hrs in medium supplemented with 500 nM OHT.

Immortalised mouse lung ECs were cultured in IMMLEC media, which is identical to MLEC media, except for the exclusion of endothelial mitogen and that FBS was supplemented only to 10%. Tissue culture flasks for routine sub-culture were always pre-coated with 0.1% gelatin (type A from porcine skin, ~300g bloom). Immortalised ECs were used between passages 5-20, and were routinely checked by flow-cytometry for surface expression of ICAM2, CD31, and VECAD (see **2.12 Flow Cytometry**, and **Figure 4.1**) to ensure they retained their normal EC characteristics. For experimental analyses, tissue culture plates and flasks were coated overnight at 4°C with one or more of the following, as specified below: 0.1% gelatin, Purecol (COLI) (Nutacon B.V., the Netherlands), human plasma fibronectin (FN) (Millipore) and mouse multimeric vitronectin (VN) (Patriecell Ltd, Nottingham, UK).

2.9.2 Mouse lung microvascular endothelial cell isolation and immortalisation

Primary mouse lung endothelial cells were isolated from adult mice as described previously by Reynolds & Hodivala-Dilke [313]. In summary, lungs were removed aseptically from adult mice and collected in Ham's F12 medium. They were then rinsed in 70% ethanol, minced with scalpels, and enzymatically digested in PBS containing 0.1% collagenase I (Invitrogen) at 37°C for 1 hr. The cellular digests were passed through 19 gauge needles three times, filtered through sterile 70 μm filters (Fisher Scientific), and centrifuged for 5 mins at 300 × g. Cells were resuspended in MLEC media by gentle pipetting, plated into a well of a 6-well-plate previously coated with a mixture of COLI (30 µg/mL) and gelatin (0.1%),

and incubated at 37°C o/n. The following day, cells were washed two times with PBS to remove red blood cells. Intracellular adhesion molecule-2 (ICAM-2)-positive ECs were then selected for by magnetic activated cell sorting (MACS): Cells were incubated with rat-anti-mouse ICAM-2 (Abd Serotec) (1:1000 in PBS) for 30 mins at 4°C, washed with PBS and then incubated with sheep-anti-rat IgG coated magnetic beads (2 μl bead/mL of MLEC medium) for another 30 mins at 4°C. After 3XPBS washes to remove unbound beads, cells were detached with 0.25% trypsin:EDTA (Invitrogen), resuspended in MLEC media, collected in an eppendorf™ tube and put on a magnet. The supernatant was discarded and the ECs attached to the beads were resuspended in fresh medium and plated into a new well of a previously coated (as above) 6-well-plate. When cells neared confluency, a second positive sort was performed in order to enhance EC purity.

For immortalisation, ECs were treated with polyoma-middle-T-antigen (PyMT) retroviral transfection as described previously by Robinson et al. **[09]**. Briefly, PyMT conditioned medium was collected from cultured packaging GgP+E cells, filter sterilised using a 0.45 µm filter, and stored at –80°C until use. Following two rounds of ICAM-2-positive selection, primary ECs in six-well plates were treated with the preserved PyMT conditioned medium supplemented with 8 µg/mL polybrene for 6 hrs at 37°C. PyMT conditioned medium was removed and replaced with complete growth medium. This same procedure was repeated the following day. Cells were observed and passaged for 4 weeks to ensure their immortalisation.

2.9.3 Human umbilical vein endothelial cell culture

HUVECs were cultured in EBM-2 media supplemented with the SingleQuots™ kit (Lonza, Slough, UK).

2.9.4 Other cell culture

CMT19T, CMT19TF1, B16F0, and B6-LV1 cancer cells, and HEK293 cells were cultured in high glucose DMEM (Invitrogen) supplemented with 10% FBS and 100 units/mL penicillin/streptomycin.

2.10 Flow-cytometry

For flow-cytometric analysis, cells were trypsinised, resuspended in fluorescence-activated cell sorting (FACS) buffer (1% FBS in PBS + 1 mM $CaCl^2$ + 1 mM $MgCl^2$), and labelled with one of the following antibodies (all used at 1:200 and, unless stated otherwise, purchased from eBioscience, Hatfield, UK): PE-anti-mouse Flk1/VEGFR2 (BD Biosciences, Oxford, UK), PE-anti-mouse CD49a (Cambridge Bioscience, Cambridge, UK); PE-anti-mouse CD49b; PE-anti-mouse CD49e; PE-anti-mouse CD51; PE-anti-mouse CD29; PE-anti-mouse CD61; PE-anti-mouse integrin beta 5; PE-anti-mouse CD31; FITC-anti-mouse ICAM2; PE-anti-mouse VECAD; appropriate PE/FITC labelled isotype-matched controls were from eBioscience. In the case of VEGFR2 analysis, cells were stimulated with 30 ng/mL VEGF at 37°C over a timecourse before trypsinisation.

2.11 Western blot analysis

For the analysis of VEGFR2, NRP1, β3-integrin, ERK1/2, p130cas, FAK, Akt, and p38MAPK in MLECs, cells were seeded at 2×10^5 cells per well in 6-well plates coated with 0.1% gelatin, 10 µg/mL FN, 10 µg/mL COLI, and 2 µg/mL VN. For paxillin analysis, ECs were seeded at the same density, but on plates coated with only 10 µg/mL FN in PBS. 24 hrs later, cells were starved for 3 hrs in serum-free OptiMEM®. VEGF was then added to a final concentration of 30 ng/mL cells were lysed at the indicated times (see relevant figures) in ESB. Lysed cells were scraped off their plates using rubber policeman, transferred to eppendorf™ tubes containing acid-washed glass beads (Sigma), homogenised in a Tissue Lyser (Qiagen, Sussex, UK) at 50 Hz for 2 mins, and centrifuged at 12,000 × g for 10 mins at RT. Lysates were analysed for protein concentration using the BioRad DC protein assay (BioRad, Hemel Hempstead, UK). NB: see other method sections for sample preparation for other assays that required Western blot analysis. 15–30 µg of protein from each sample was loaded onto 8–10% polyacrylamide gels and subjected to SDS-PAGE. For paxillin analysis, samples were loaded onto a 4-12% gradient gel for better resolution. The protein was transferred to a nitrocellulose membrane (Whatman® Protran®, Sigma) and incubated for 1 hr in 5% milk powder/PBS plus 0.1% Tween-20 (PBSTw), followed by an overnight incubation in primary Ab diluted 1:1000 in 5%

BSA/PBSTw at 4°C. The blots were then washed 3X with PBSTw and incubated with the relevant horseradish peroxidase (HRP)-conjugated secondary Ab (Dako) diluted 1:2000 in 5% milk/PBSTw, for 1 hr at RT. Chemiluminescence was detected on a Fujifilm LAS-3000 darkroom (Fujifilm UK Ltd, Bedford, UK). Antibodies (all used at 1:1000 and purchased from Cell Signalling Technology, unless noted otherwise): anti-phospho (Y1175) VEGFR2 (clone 19A10); anti-VEGFR-2 (clone 55B11); anti-Neuropilin-1 (cat no. 3725); anti-β3-integrin (cat no. 4702); anti-phospho (Thr202/Tyr204) p44/42 MAPK Erk1/2 (clone D13.14.4E); anti-total p44/42 MAPK Erk1/2 (clone 137F5); anti-phosho (Y410) p130cas (cat no. 4011); anti-p130cas (Cat no. 610271, BD Biosciences); anti-phospho (Y407) FAK (#OPA1-03887, Fisher Scientific); anti-FAK (cat no. 3285); anti-HSC70 (clone B-6, Santa Cruz Biotechnology); anti-phospho (Y118) paxillin (cat no. 2541); anti-paxillin (ab32084; Abcam); anti-GAPDH (14C10, cat no. 2118); anti-SP1 (cat no. 5931); anti-histone H3 (D1H2, cat no. 4499); anti-vimentin (D21H3, cat no. 5741); anti-phospho p38 MAPK (cat no. 9215); anti-p38 MAPK (cat no. 9212); anti-phospho Akt (cat no. 4060); anti-Akt (cat no. 9272); anti-myosin 9 (cat no. 3403); anti-filamin a (ab76289; Abcam); anti-α5-integrin (cat no. 4705).

Densitometric readings of band intensities for Western blots were obtained using Image J™. Band densities for total protein were normalized to HSC-70/GAPDH levels, and densities for phosphorylated protein were normalised to the corresponding total protein levels to make quantitative measurements of protein expression levels.

2.12 Cell surface biotinylation assay

Cells were plated o/n at a density of 8×10^5 in 6 cm dishes, coated with 0.1% gelatin, 10 µg/mL FN, 10 µg/mL COLI, and 2 µg/mL VN. After starvation, cells were moved to an ice bath, washed twice with ice-cold SBS (Soerensen Buffer, 14.7 mM KH_2PO_4, 2 mM Na_2HPO_4 and 120 mM Sorbitol pH 7.8), and left in the second wash for 10 mins. All of the SBS was then removed before adding 1 mL of ice-cold SBS pH 7.8 containing 0.3 mg/mL EZ-Link NHS-SS-biotin (Fisher Scientific) per dish for 30 mins. After a further two washes in ice-cold SBS pH 7.8, the unreacted biotin was quenched for 10 mins by incubation with ice-cold SBS pH 7.8 containing 100 mM glycine. Cells were then washed twice with ice-cold

SBS pH 7.8 and left in Opti-MEM™ supplemented with 2 μg/mL heparin for 5 mins before stimulation with 30 ng/mL VEGF for 5, 15, 30 and 60 minute time-points at 37°C to allow internalisation of biotinylated plasma membrane proteins. Internalisation was stopped by bringing the cells back to the ice bath, washing twice in ice-cold SBS pH 8.2, and leaving them in the second wash for 5 mins. The biotin still present on cell-surface molecules was cleaved off by incubating the cells with 50 mM of membrane impermeable disulphide reducing agent TCEP (tris-(2-carboxyethyl)phosphine; Sigma) in ice-cold SBS pH 8.2 for 25 mins. Unstimulated cells not treated with TCEP were used as controls. Cells were washed twice with ice-cold SBS pH 8.2 and then lysed in 0.2 mL/dish of RIPA buffer (20 mM Tris pH 7.4, 50 mM NaCl, 0.1% SDS, 1% Triton, 1% Deoxycholate, 1% NP40) containing phenylmethanesulfonylfluoride (PMSF, Sigma) (~1 mM) and Halt® Protease and Phosphatase inhibitor (1:100) (Fisher Scientific). Cells were scraped off their dishes using rubber policeman, transferred to eppendorf™ tubes containing acid-washed glass beads, homogenised in a Tissue Lyser at 50 Hz for 2 mins, and centrifuged at 12,000 × g for 10 mins at 4°C. Biotinylated proteins were then immunoprecipitated by incubating them with 3 μg of a mouse-anti-mouse-biotin Ab (Jackson Immunoresearch, Newmarket, UK) coupled to magnetic dynabeads (using the Dynabeads® Ab Coupling Kit (Invitrogen)) on a rotator o/n at 4°C. Immunoprecipitated complexes were washed three times with 0.2 mL of RIPA buffer, and once in PBS, before being added to, and boiled in, 1X NuPAGE® LDS sample buffer containing reducing agent (Invitrogen), ready for separation on an 8% acrylamide gel and Western blotting.

2.13 Immunoprecipitation assays

Cells were grown to 80-90% confluency in 15 cm dishes, coated with 10 μg/mL FN in PBS. After starvation in OptiMEM® for 3 hrs, cells were stimulated with 30 ng/mL VEGF for 10 mins (+VEGF), or for the indicated times, at 37°C. Cells were then placed on ice, washed two times with PBS, and lysed in 0.5 mL/plate of RIPA buffer (20 mM Tris pH 7.4, 50 mM NaCl, 0.1% SDS, 1% Triton, 1% Deoxycholate, 1% NP40) containing PMSF (~1 mM) and Halt® Protease and Phosphatase inhibitor (1:100). Lysates were centrifuged at 12,000 × g for 10 mins at 4°C. 400 μg of total protein from each sample was IP'd by incubating them with protein-G Dynabeads® (Invitrogen) coupled to the relevant Ab on a

rotator o/n at 4°C. IP'd complexes were washed three times with 0.2 mL of RIPA buffer, and once in PBS, before being added to, and boiled in, 1X NuPAGE® sample reducing agent (Life Technologies), ready for SDS-PAGE prior to Western blotting (to detect co-associations (co-IP)), silver staining, or mass spectrometry analysis (first experiment). A rabbit-anti-mouse-VEGFR2 Ab (clone 55B11, Cell Signalling Technology) was used for the VEGFR2 IP. The NRP1 IP that was initially used to detect β3-co-association and for the first mass spectrometry experiment was carried out using a rabbit-anti-mouse-Neuropilin-1 (cat no. 3725) Ab. A rabbit-anti-mouse-β3-integrin (cat no. 4702) was used for the β3 IP. The NRP1 IP for the second mass spectrometry experiment and the other NRP1 co-IPs was carried out using a goat-anti-mouse Neuropilin-1 Ab (AF566, R&D Systems). Prior to subjecting the NRP1 IP'd samples to mass spectrometry analyses, a fraction of them were separated by SDS-PAGE on a 10% polyacrylamide gel, which was subsequently silver stained using the Pierce® Silver Stain Kit (Fisher Scientific) to confirm uniform IP efficiency between samples.

2.14 Adhesion Assays

2.14.1 Static adhesion

96-well plates were coated overnight at 4°C with 10 µg/mL COLI, 10 µg/mL FN, 10 µg/mL laminin-I (LN), or 2 µg/mL VN in PBS, or a mixture (MIX) containing 10 µg/mL COLI, 10 µg/mL FN, and 2 µg/mL VN in 0.1% gelatin was also used. The wells were then washed with PBS, and blocked for 1 hr at RT with 1% BSA in PBS, before a final wash in PBS. Prior to seeding, cells were starved for 3 hrs in Opti-MEM®, trypsinised, and resuspended in serum-free OptiMEM®. They were then seeded in serum–free OptiMEM® at a concentration of 1×10^4 cells/well for 90 mins at 37°C. Plates were washed three times gently by immersion in a bucket of PBS, and any excess volume was removed. Cells were fixed with 4% formalin for 10 mins, stained with methylene blue for 30 mins, washed for 15 mins under running water and air-dried. Dye was extracted with 50%ethanol:50% 0.1N HCl and the absorbance of each well was measured at 610 nm.

2.14.2 Adhesion on various matrix concentrations

96-well plates were coated overnight at 4°C with serial dilutions of VN or FN. The wells were then washed with PBS, and blocked for 1 hr at RT with 1% BSA in PBS. Prior to seeding, cells were starved for 3 hrs in Opti-MEM®, trypsinised, and resuspended in serum-free OptiMEM®. They were then seeded in serum–free OptiMEM® at a concentration of 3×10^4 cells/well for 90 mins at 37°C. Plates were tapped vigorously on the bench top and wells were washed thoroughly using a multi-channel pipette. Cells were fixed with 4% formalin, stained with methylene blue for 30 mins, washed for 15 mins under running water and air-dried. Dye was extracted with 50%ethanol:50% 0.1N HCl and the absorbance of each well was measured at 610 nm.

2.14.3 Cell spreading assay

6-well plates were coated overnight at 4°C with 10 µg/mL FN. The wells were then washed with PBS, and blocked for 1 hr at RT with 1% BSA in PBS. Prior to seeding, cells were starved for 3 hrs in Opti-MEM®, trypsinised, and resuspended in serum-free OptiMEM®. They were then seeded in serum–free OptiMEM® at a concentration of 70×10^5 cells/well for 6 hours at 37°C. Plates were washed three times gently by immersion in a bucket of PBS, and any excess volume was removed. Cells were fixed with 4% formalin for 10 mins, stained with methylene blue for 30 mins, washed for 15 mins under running water and air-dried. Phase contrast photographs were taken using an inverted Axiovert (Zeiss) microscope and cell surface areas were measured using ImageJ™ software.

2.15 Migration assays

2.15.1 Random migration assay

ECs were starved in OptiMEM® for 3 hrs, trypsinised and seeded at 1.5×10^4 cells/well in 24-well plates coated with 10 µg/mL FN in PBS, and allowed to adhere for 3 hrs. The media was then replaced with OptiMEM® + 2% FBS, and half of the wells were supplemented with 30 ng/mL VEGF. One phase-contrast image/well was taken live every 10 mins in a fixed field of view using an inverted Axiovert (Zeiss) microscope for 15 hrs at 37°C and 4% CO_2. Individual cells were

then manually tracked using the ImageJ™ cell tracking plugin, and the speed of random migration was calculated in µm moved/hr.

2.15.2 Wound closure assay

ECs were seeded at 4×10^5 cells/well in 6-well plates coated with 10 µg/mL FN in PBS, and cultured until the next day, by which time they had reached confluency. Cells were serum starved for 3 hrs in OptiMEM® before scratching the confluent monolayer with a P200 pipette tip. Phase contrast images of scratches were then captured and the media was changed to OptiMEM® containing 30 ng/mL VEGF. After 24 hrs, cells were fixed for 10 mins with 4% formaldehyde and scratches were imaged again. The degree of scratch wound closure was quantified by measuring the gap between cells in three areas per field using Axiovision (Zeiss) software, taking an average, and calculating the length change between time points.

2.16 Cell fractionation assay

ECs were seeded in plates coated with 0.1% gelatin, 10 µg/mL FN, 10 µg/mL COLI, and 2 µg/mL VN. 24 hrs later, cells were starved for 3 hrs in serum-free OptiMEM®, and either stimulated with 30 ng/mL VEGF or not. Cells were then trypsinised and centrifuged at 500 × g. Cell fractionation was carried out following the 'Subcellular protein fractionation kit for cultured cells' (Fisher Scientific) protocol exactly, and samples were prepared for Western blotting.

2.17 Immunocytochemistry

Either primary or immortalised ECs were seeded at 1.5×10^5 cells/well in six-well plates on acid-washed and oven-sterilised glass coverslips, coated with 10 µg/mL FN in PBS and cultured until the next day. Cells were starved for 3 hrs in serum-free OptiMEM®, and either stimulated with 30 ng/mL VEGF at 37°C for 10 mins (+VEGF), or not at all (–VEGF). Cells were then fixed in 4% formaldehyde for 10 mins, washed in PBS, permeabilised with 0.5% NP40 in PBS, blocked in 0.1% BSA+0.2% Triton in PBS, and incubated with primary antibody diluted 1:100 in PBS for 1 hr at RT. After further PBS washes, cells were incubated with the relevant Alexa-Fluor®-conjugated secondary antibody (Invitrogen) diluted 1:500

in PBS for 45 min at RT. Coverslips were washed in PBS again before they were mounted on slides with Prolong® Gold containing DAPI (Invitrogen). To stain for filamentous-(F) actin, Alexa-Fluor®-568–phalloidin (Invitrogen) was used 1:300 in PBS at the secondary-antibody incubation stage. To look at β3-integrin fluorescently, 1×10^6 ECs were transfected with a GFP-tagged β3-integrin cDNA expression construct (provided by Dr Maddy Parsons, King's College London, London, UK) by nucleofection prior to seeding on coverslips at 1.5×10^5 cells/well. Antibodies (all used at 1:100) were: anti-phospho (Y118) paxillin (Cell Signaling Technology, cat. no. 2541); anti-paxillin (ab32084, Abcam); anti-neuropilin-1 (AF566, R&D Systems). NRP1-PXN co-localisation was quantified using the Coloc2 ImageJ™ plugin to determine the Pearson's correlation coefficient. Focal adhesion sizes were measured using ImageJ™ software.

2.18 Mass spectrometry analyses

Mass spectrometry experiments were carried out by the Fingerprints Proteomics Facility, Dundee University, Dundee, UK. In the first experiment, after NRP1 IP'd samples were confirmed for their uniform NRP1 IP efficiency by silver staining (see above), the remainder of the samples were again separated by SDS-PAGE and sent off to the facility as gel fragments lane by lane. They were then subjected to 1D nano liquid chromatography tandem mass spectrometry (1D nLC-MS/MS) using an LTQ Orbitrap analysis. In the second experiment, after NRP1 IP'd samples were confirmed for their uniform IP efficiency by silver staining, the remainder of the NRP1-IP'd dynabead samples were boiled in ESB buffer and separated on a magnet. The samples in ESB buffer were then sent off to the facility for label-free quantitative mass spectrometry. Peptides were identified and quantified using MaxQuant software using the Andromeda peptide database. To achieve label-free quantitative results, 3 biological repeats were pooled and each of these pooled samples was analysed via 3 technical repeats through the spectrometer. Peptides present in at least 2 samples were hierarchically clustered by clustering median log(LFQ) values by city-block distance using Cluster 3.0 software (available for download from http://bonsai.hgc.jp/~mdehoon/software/cluster/software.htm), and presented with Java TreeView (available from http://jtreeview.sourceforge.net).

2.19 Focal adhesion enrichment

ECs were starved in serum-free OptiMEM® for 3 hrs and seeded at 6×10^6 cells/plate in 10 cm plates that were previously coated with 10 µg/mL FN in PBS o/n at 4°C and blocked in 1% BSA in PBS for 1 hr at RT. Cells were allowed to adhere for 90 mins to allow for mature FAs to form and either stimulated with 30 ng/ml VEGF at 37°C for 10 mins (+VEGF) or not at all (–VEGF). Cells were washed in PBS + 1 mM $CaCl^2$ + 1 mM $MgCl^2$ (PBS++) and incubated with 0.5 mM Dithiobis(succinimidyl propionate) (DSP) and 0.05 mM 1,4-di-[30-(20-pyridyldithio)-propionamido] butane (DPP) diluted in PBS++ for 5 mins to cross-link FAs to the plate. This reaction was quenched with 1 M Tris-HCl pH 7.5 before cells were lysed in RIPA for 30 mins on ice with occasional agitation. RIPA was collected without scraping, and the plates were blasted with a high-sheer flow jet of distilled water to remove cell debris. Cross-linked proteins were eluted with 2 mL dithiothereitol (DTT) buffer (25 mM Tris-HCl pH 7.5, 10 mM NaCl, 0.1% SDS, 100 mM DTT) for 1 hr at 60°C in a sealed and humidified chamber. 8 mL of acetone was added to this solution and left overnight at –20°C to allow the proteins to precipitate. Samples were then centrifuged at 13,000 × g for 40 mins, and the acetone layer removed. The pellet was resuspended in ESB ready for Western blot analysis (or mass spectrometry analysis in a separate project).

2.20 Focal adhesion tracking

1×10^6 ECs were transfected with a GFP-tagged paxillin cDNA-expression-construct (kindly provided by Dr Maddy Parsons, KCL, London, UK) and a fraction of these were seeded on acid-washed and oven-sterilised glass coverslips, coated with 10 µg/mL FN in PBS, in wells of a 6-well plate. Cells were cultured for ~48 hrs before they were starved in serum-free OptiMEM® for 3 hrs. In turn, individual coverslips were separately transferred to OptiMEM® + 2% FBS + 30 ng/mL VEGF was added. An Axiovert (Zeiss) inverted microscope was then used to take live images of the GFP-paxillin-positive focal adhesions in a selected field of view every 2 mins for 1 hr at 37°C + 4% CO_2. Assembly and disassembly was quantified by manually tracking leading and trailing edges of focal adhesions using the MTrackJ plugin for Image J™.

2.21 Statistical analysis

Significant differences between means were evaluated by Student's-t-test. $P<0.05$ was considered statistically significant. For flow cytometric analysis of integrins, relative differences were deemed significant if they were greater than 2-fold.

3. Investigating the dual importance of αvβ3-integrin and neuropilin-1 in tumour growth and angiogenesis

3.1 Like β3-integrin-knockout mice, β3-integrin-heterozygous mice have significantly increased angiogenesis and tumour growth relative to their wild-type littermates

As described earlier, it was previously shown that tumour growth and angiogenesis were significantly enhanced in β3-integrin-knockout (β3-NULL) mice [134,197,202]. Though these results were surprising at the time, given αvβ3's upregulation in neo-angiogenic vasculature and various successes with αvβ3 antagonists in pre-clinical models, it has since become clear that angiogenic phenotypes that arise in response to αvβ3 targeting are determined by the context in which αvβ3 is targeted [180]. It was postulated that the β3-NULL phenotype was caused, in part, by a developmental upregulation of VEGFR2, and increased NRP1-VEGFR2 associations [134,202]. Since interactions between αvβ3 and VEGFR2 are important for angiogenesis, the results obtained from a model in which β3 is completely absent and VEGFR2 levels are elevated are not physiologically relevant and difficult to interpret [186,191]. We therefore moved our analyses to β3-integrin-heterozygous (β3-HET) mice, which express roughly half the normal level of β3 (**see Chapter 4**), hypothesising that this would circumvent developmental changes arising from the complete loss of the protein, whilst at the same time maintaining, at least to a degree, interactions between β3 and VEGFR2 and/or NRP1. Using VEGF-induced aortic ring microvessel sprouting as a means of measuring angiogenesis in these models, we found that angiogenesis in the β3-HET model was enhanced compared to that in wild-type (WT) aortic rings, though not as markedly as in the β3-NULL model (**Figure 3.1**). Similarly, we also observed an increase in subcutaneous B16F0 melanoma allograft tumour growth in β3-HET mice, but again this effect was dampened compared to the increase seen in β3-NULL mice. Unsurprisingly, these data suggest that mechanisms of resistance to genetic β3 targeting still feature in the β3-HET model, though their effects are not as pronounced as when β3 is missing.

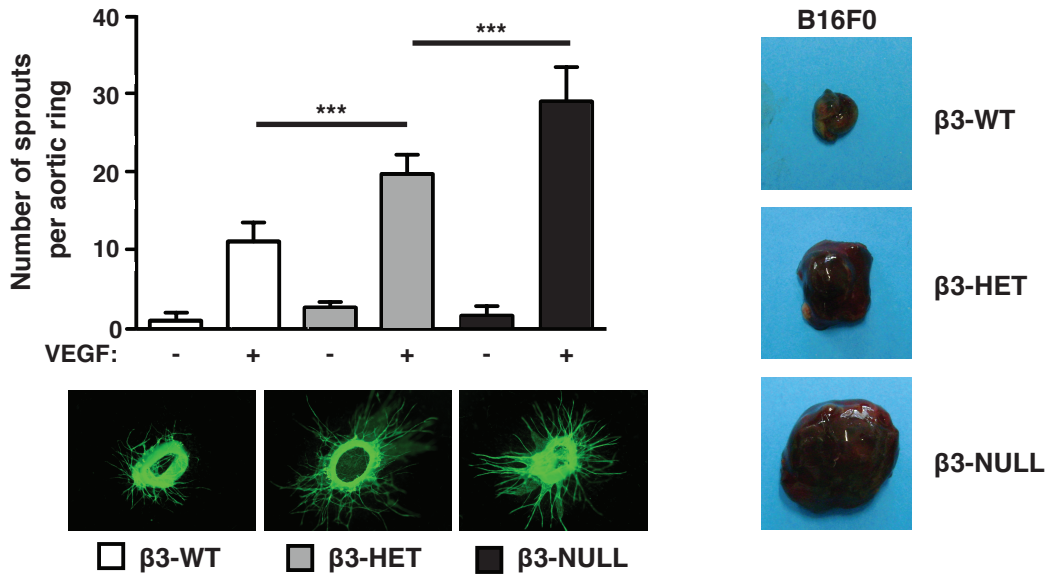

Figure 3.1: Like β3-integrin-null (β3-NULL) mice, β3-integrin-heterozygous (β3-HET) mice have significantly increased angiogenesis and tumour growth relative to their wild-type (β3-WT) littermates. Microvessel sprouting of aortic ring explants of the indicated genotypes. The bar chart shows the total number of microvessel sprouts per aortic ring after 6 days of VEGF-stimulation (mean +SEM from 3 independent experiments; n≥40 rings per genotype). Asterisks indicate statistical significance: ***, $P<0.001$; nsd = not significantly different. Unpaired two-tailed *t* test. The bottom panel shows representative images of aortic rings stained with FITC-conjugated BS1-lectin (an endothelial marker) from each genotype. The panel on the right shows representative examples of B16F0 melanoma allograft tumours from each genotype after 12 days of growth.

3.2 Tumour growth and angiogenesis in β3-integrin-heterozygous mice are sensitive to endothelial neuropilin-1 depletion

Robinson et al. [202] previously reported that targeting NRP1 with inhibitory peptides or siRNA inhibited angiogenesis in the β3-NULL model more substantially than when β3 was uninterrupted. However, we do not know if this phenomenon applies in the β3-HET model. Endothelial neuropilin-1 has been shown to be essential for normal embryonic brain angiogenesis [265], and its depletion inhibits postnatal pathological neovascularisation of the retina [271]. However, its significance in angiogenesis in adult models has never been investigated. We therefore wanted to combine these two objectives and determine the effect of an acute EC-specific depletion of NRP1 (NRP1-EC-ID) on tumour growth and angiogenesis in both β3-WT and β3-HET mice.

We crossed β3-WT and β3-HET mice to tamoxifen (OHT)-inducible Pdgfb-iCreER^{T2}/NRP1-floxed mice [258,310] and examined subcutaneous allograft tumour growth using both CMT19T cells **(Figure 3.2)** and B16F0 cells (**Appendix Figure 1**), as well as aortic ring sprouting (**Figure 3.3**). EC-NRP1 depletion, which was induced with OHT prior to tumour growth and aortic ring sprouting (meaning NRP1 was targeted in a preventative manner), had no effect on β3-WT responses, but significantly inhibited tumour growth and VEGF-induced microvessel sprouting in β3-HET mice. Tumour angiogenesis was also only significantly inhibited in β3-HET mice by depleting endothelial NRP1, although vessel morphology and pericyte coverage were normal (**Figure 3.2B**). These results are reminiscent of the increased angiogenic sensitivity to NRP1 targeting in the β3-NULL model reported previously [202], but additionally suggest that NRP1 function is perturbed by a reduction in, and not absence of, β3 expression, and that, as a result, specifically endothelial NRP1 becomes more targetable in the context of pathological angiogenesis. Compensation to long-term β3 targeting may therefore partly take the form of an increased importance for endothelial NRP1, meaning that NRP1 is normally regulated by β3, but only when β3 is properly expressed in ECs.

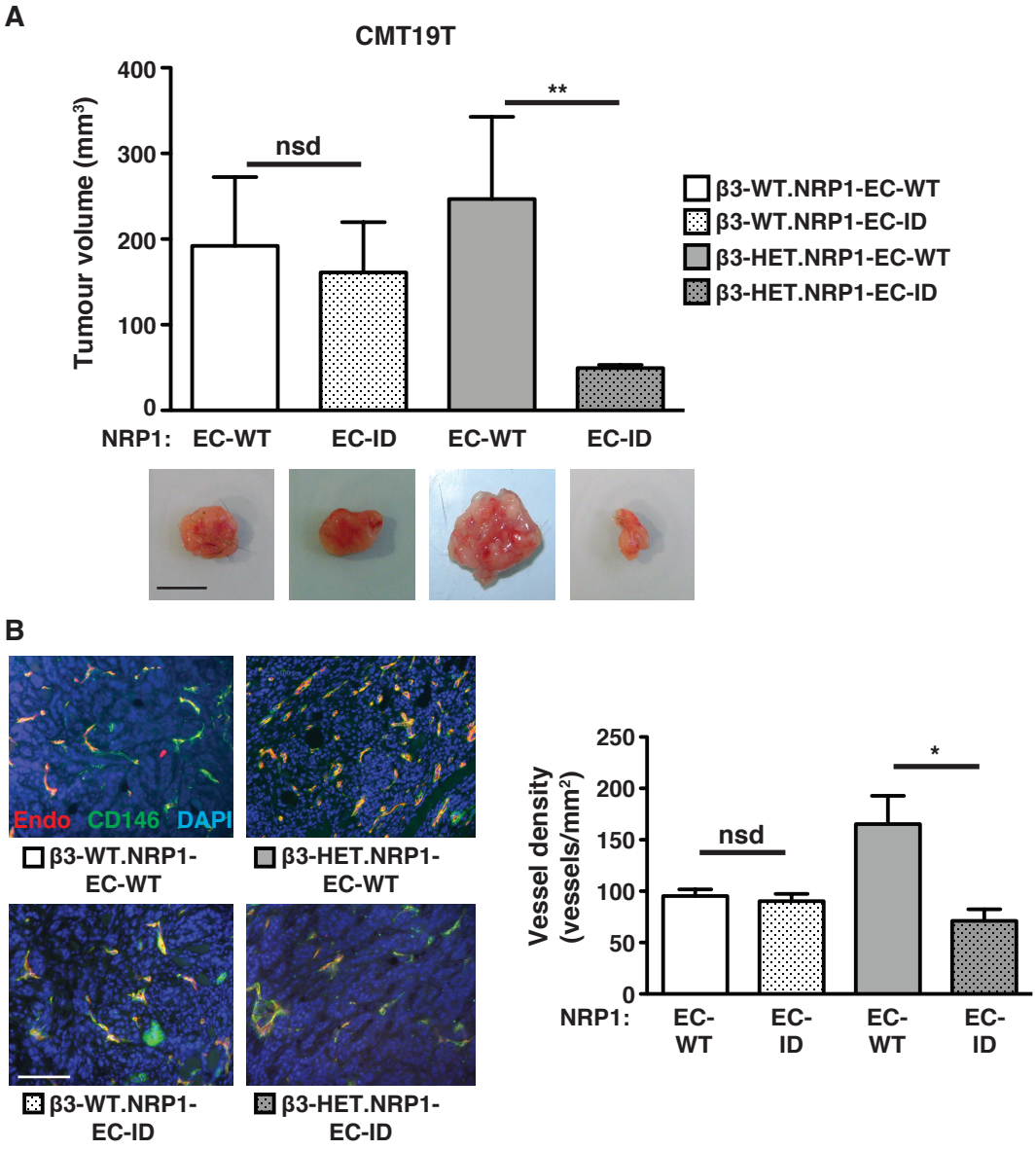

Figure 3.2: Tumour growth and tumour angiogenesis in β3-integrin-heterozygous mice are sensitive to endothelial neuropilin-1 depletion. A Tumour growth was measured in animals of the indicated genotypes. Mice were given subcutaneous injections of CMT19T tumour cells. To induce depletion of endothelial NRP1 (NRP1-EC-ID), 21-day slow-release OHT pellets were administered 3-days prior to tumour cell injection. OHT-treated Cre-negative (NRP1-EC-WT) littermates served as controls. Tumour volumes were measured after 12 days of growth (mean +SEM of 3 independent experiments; n≥10 animals per genotype). Representative pictures of tumour macroscopic appearances are shown. Scale bar = 10 mm. **B** Blood vessel density was assessed in tumours of the indicated genotypes by counting the total number of endomucin-positive vessels across tumour sections (mean +SEM; n≥10 sections per genotype). Representative micrographs of immunofluorescence staining for endomucin, an endothelial cell marker (Endo, red) and CD146, a pericyte marker (green) in tumour sections from each genotype are shown. DAPI (blue) was used as a nuclear counterstain. Scale bar = 100 µm. Asterisks indicate statistical significance: *, $P<0.05$; **, $P<0.01$; nsd = not significantly different. Unpaired two-tailed *t* test.

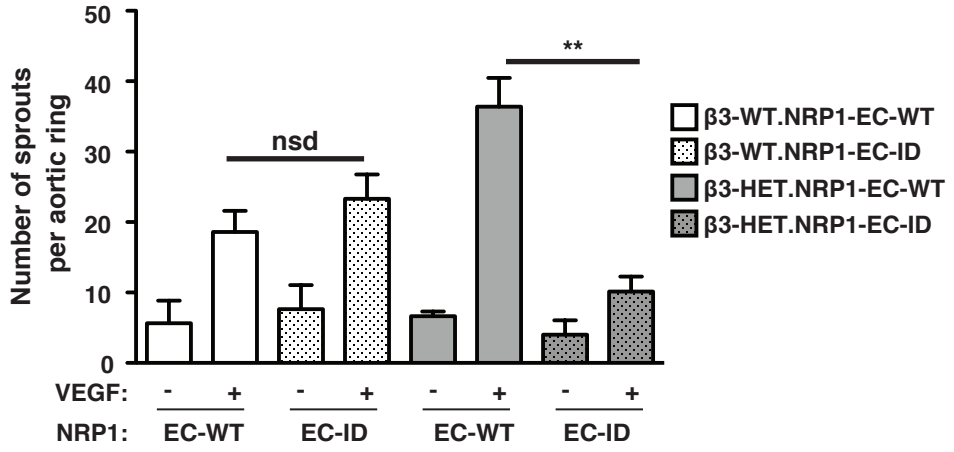

Figure 3.3: Angiogenesis in β3-integrin-heterozygous mice is sensitive to endothelial neuropilin-1 depletion. Microvessel sprouting of aortic ring explants of the indicated genotypes. To induce depletion of endothelial NRP1 (NRP1-EC-ID), 1 μM OHT was supplemented in culture. OHT-treated Cre-negative (NRP-EC-WT) rings served as controls. The bar chart shows the total number of microvessel sprouts per aortic ring after 6 days of VEGF-stimulation (mean +SEM from 3 independent experiments; n≥40 rings per genotype). Asterisks indicate statistical significance: **, $P<0.01$; nsd = not significantly different. Unpaired two-tailed *t* test.

3.3 Tumour growth and angiogenesis in β3-integrin-heterozygous mice are sensitive to the loss of neuropilin-1's cytoplasmic tail

NRP1's cytoplasmic tail is known to be dispensable for developmental and pathological angiogenesis, but more involved in arteriogenesis and arteriovenous patterning [267,268]. However, a potentially cooperative role between the cytoplasmic tail of NRP1 and β3 has never been studied in angiogenesis, or elsewhere. To narrow our mechanistic focus, we wanted to explore whether pathological angiogenesis in β3-HET mice is sensitive to the removal of NRP1's cytoplasmic tail.

We therefore crossed β3-WT and β3-HET animals with mice carrying a global deletion of NRP1's cytoplasmic tail (NRP1Δcyto) [267] and examined CMT19T subcutaneous allograft tumour growth **(Figure 3.4)** and aortic ring sprouting (**Figure 3.5**), as before. CMT19T tumour growth and microvessel sprouting were unaltered in β3-WT mice by the introduction of the NRP1Δcyto mutation, but both were inhibited in β3-HET-NRP1Δcyto mice. Although the loss of NRP1's cytoplasmic tail had a minor effect on tumour angiogenesis in β3-WT mice (**Figure 3.4B**), this did not translate to an overall difference in tumour growth (**Figure 3.4A**). As in EC-NRP1-ID tumours, pericyte coverage of tumour vasculature was not affected by a NRP1 cytoplasmic deletion (**Figure 3.4B**). We conclude from these results that NRP1's cytoplasmic tail is normally dispensable for pathological angiogenesis, but its role becomes significant when β3 expression is reduced. Thus, it is possible that β3 normally keeps the pro-angiogenic functioning of NRP1's cytoplasmic tail in check, but is unable to when insufficiently expressed.

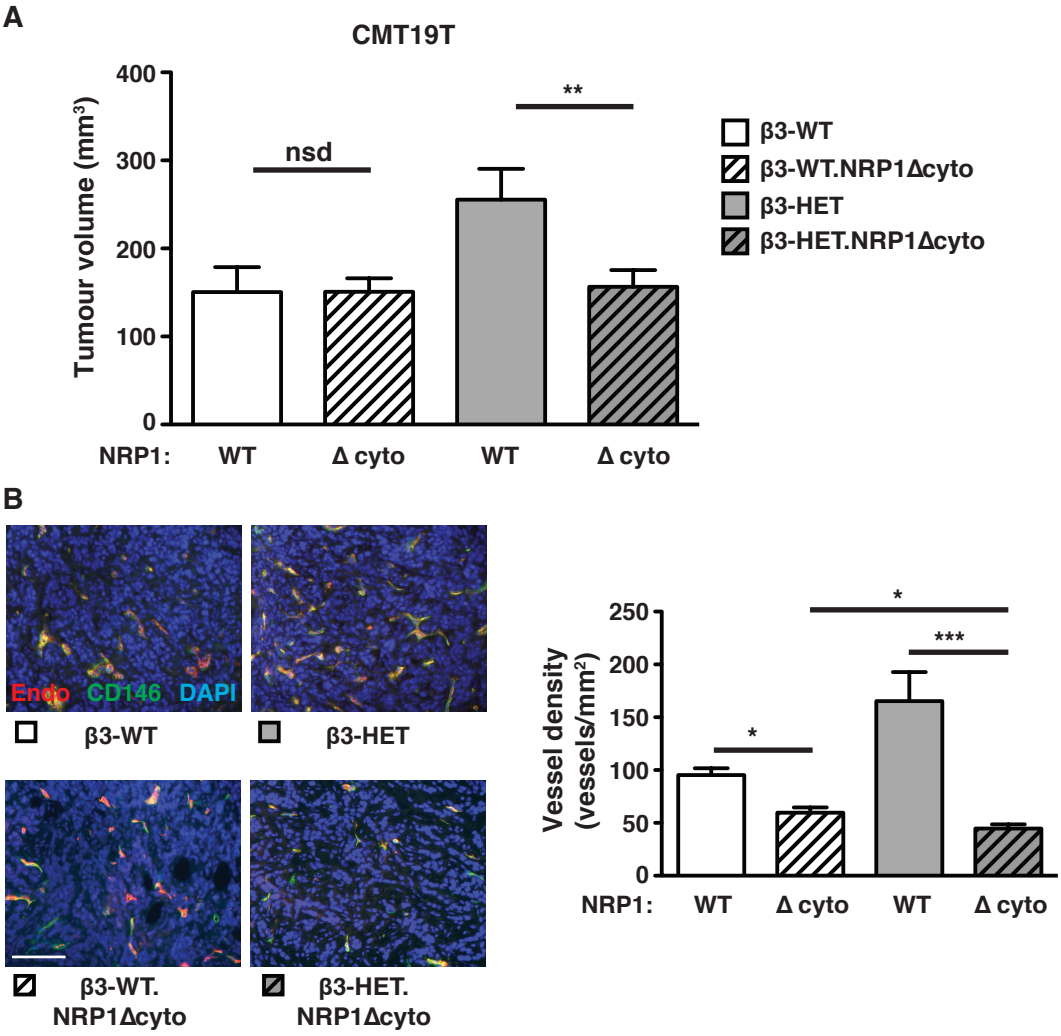

Figure 3.4: Tumour growth and tumour angiogenesis in β3-integrin-heterozygous mice are sensitive to the loss of neuropilin-1's cytoplasmic tail. A CMT19T tumour growth and angiogenesis were measured in animals of the indicated genotypes. In addition to their β3-integrin genetic status, mice were negative (NRP1WT) or positive (NRP1Δcyto) for the loss of NRP1's cytoplasmic tail. Mice were given subcutaneous injections of CMT19T cells and tumour volumes were measured 12 days later. The bar chart shows tumour volumes (mean +SEM of 3 independent experiments; n≥10 animals per genotype). **B** Blood vessel density was assessed by endomucin (red) and CD146 (green) staining (mean +SEM; n≥10 sections per genotype). DAPI was used as a nuclear counterstain (blue). Scale bar = 100 μm. Asterisks indicate statistical significance: *, $P<0.05$; **, $P<0.01$; ***, $P<0.001$; nsd = not significantly different. Unpaired two-tailed *t* test.

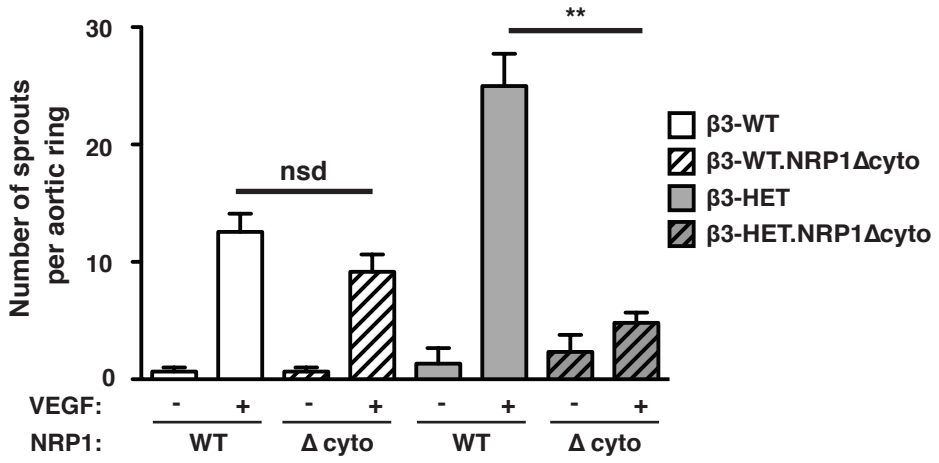

Figure 3.5: Angiogenesis in β3-integrin-heterozygous mice is sensitive to the loss of neuropilin-1's cytoplasmic tail. Microvessel sprouting of aortic ring explants of the indicated genotypes. The bar chart shows the total number of microvessel sprouts per aortic ring after 6 days of VEGF-stimulation (mean +SEM from 3 independent experiments; n≥40 rings per genotype). Asterisks indicate statistical significance: **, $P<0.01$; nsd = not significantly different. Unpaired two-tailed *t* test.

3.4 Simultaneous depletion of both endothelial β3-integrin and neuropilin-1 blocks pre-established tumour growth and angiogenesis

Whilst the data presented so far convincingly show that tumour growth and angiogenesis become sensitive to NRP1 disruption when there is reduced β3 expression, it is difficult to claim that targeting β3 and NRP1 together would be an effective anti-cancer strategy on this evidence alone. The β3-HET and NRP1Δcyto models do not accurately simulate β3/NRP1 targeting in a clinical scenario, as they feature a global and constitutive reduction, or perturbation, in β3 and NRP1, respectively. Furthermore, in the endothelial NRP1-targeted model, NRP1 depletion was induced before tumour growth and angiogenesis were established. These targeting methods are therefore preventative, and so are not representative of the clinical situation, where tumour growth and angiogenesis are already in motion. We therefore wanted to examine the effect of simultaneously targeting both β3 and NRP1 on already established tumour growth and angiogenesis, as a proof-of-concept for clinical intervention, using β3/NRP1-double-floxed mice crossed to those with OHT-inducible-Pdgfb-iCreER^{T2} transgenics.

First, we assessed the effect of such an intervention on angiogenesis in the aortic ring assay. VEGF-induced microvessel sprouting was initiated in aortic rings isolated from: 1) β3-floxed mice with (Cre-positive) and without (Cre-negative) Pdgfb-iCreER^{T2}; 2) NRP1-floxed mice with (Cre-positive) and without (Cre-negative) Pdgfb-iCreER^{T2}; or 3) double-floxed mice with (Cre-positive) and without (Cre-negative) Pdgfb-iCreER^{T2}. OHT was administered to all rings after 4 days of sprouting to induce endothelial depletion (EC-ID) in Cre-positive rings, and microvessels were quantified 4 days later. Only in rings from double-floxed Pdgfb-iCreER^{T2}-positive animals was further sprouting significantly inhibited (**Figure 3.6**). We then examined intervention in established vascularised tumours in mice of these same genotypes. CMT19T allografts were grown in the animals, as previously, but this time OHT was administered after 10 days of growth, before allowing the tumours to continue growing for another 10 days. In concordance with the intervention aortic ring studies, further tumour growth and angiogenesis were significantly inhibited in double-floxed Pdgfb-iCreER^{T2}-positive animals, but not in any of the other genotypes (**Figure 3.7**). These results therefore constitute

key pre-clinical evidence that suggests simultaneously targeting β3 and NRP1 may be a viable anti-angiogenic intervention strategy in cancer therapeutics.

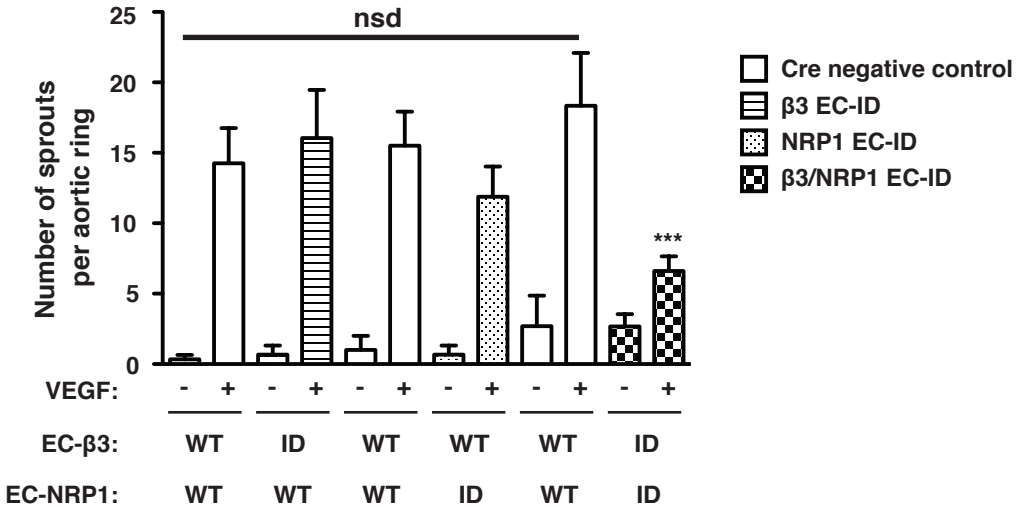

Figure 3.6: Simultaneous depletion of both endothelial β3-integrin and neuropilin-1 blocks pre-initiated microvessel sprouting. Microvessel sprouting of aortic ring explants of the indicated genotypes. To induce depletion of endothelial β3 and/or NRP1 (EC-ID), 1 μM OHT was supplemented in culture 4 days after VEGF-induced sprouting had been established. The bar chart shows the total number of microvessel sprouts per aortic ring after an additional 4 days of VEGF-stimulation (mean +SEM from 3 independent experiments; n≥40 rings per genotype). Asterisks indicate statistical significance: ***, $P<0.001$; nsd = not significantly different. Unpaired two-tailed *t* test.

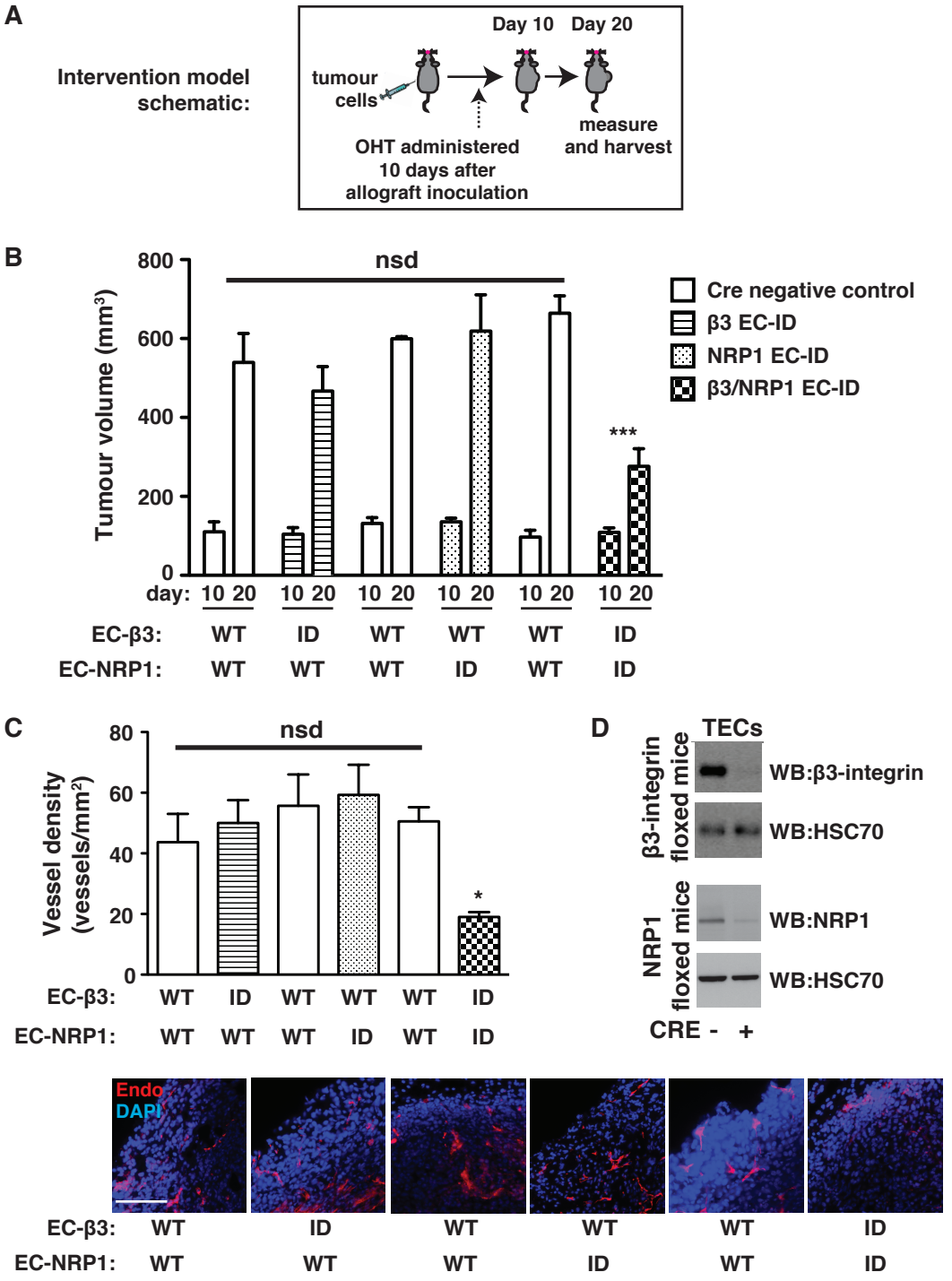

Figure 3.7: Simultaneous depletion of both endothelial β3-integrin and neuropilin-1 blocks pre-established tumour growth and angiogenesis. Tumour growth and angiogenesis were measured in animals of the indicated genotypes. **A** *Model schematic*: Mice were injected subcutaneously with CMT19T cells and 10 days later OHT was administered to induce depletion of endothelial β3 and/or NRP1 (EC-ID). After an additional 10 days (20 days in total) tumours were harvested. **B** The bar chart shows mean tumour volumes measured at days 10 and 20 (+SEM of 2 or more independent experiments; n≥10 animals per genotype). **C** Blood vessel density in 20-day tumours was assessed by counting the total number of endomucin-positive vessels around the periphery (within 150 µm of the edge of the tumour) of midline bisected tumour sections. The bar chart shows mean vessel number per mm^2 (+SEM). Representative micrographs of endomucin staining (red) are shown along the bottom. Scale bar = 50 µm. **D** Western blot showing representative depletion of β3-integrin and NRP1 in tumour endothelial cells (TEC) isolated from Cre-positive animals, compared to Cre-negative littermate controls. Asterisks indicate statistical significance: *, $P<0.05$; ***, $P<0.001$; nsd = not significantly different. Unpaired two-tailed *t* test.

3.5 The investigation of the dual importance of β3-integrin and neuropilin-1 in metastasis was unsuccessful

Our data show that targeting both β3 and NRP1 inhibits the growth and angiogenesis of tumours, but tumour progression also encompasses metastasis, which invariably is the cause of mortality in cancer patients. We therefore sought to determine whether a joint β3/NRP1 targeting strategy could also negatively regulate metastasis, and thus potentially improve patient survival in this way if used in the clinic. Our plan was to grow subcutaneous allografts, as before, but using a variant of the CMT19T cancer cell line, CMT19TF1, which we had previously shown to metastasise to the lung (not shown). We attempted to transduce this cell line with luciferase (Luc) in order to monitor the progress of metastasis formation using bioluminescence. However, although RT-PCR of the Luc gene appeared to show the presence of Luc cDNA in the transduced cells (**Appendix Figure 2A**), no bioluminescence signal was ever detected in mice injected with the alleged CMT19TF1-Luc cells (**Appendix Figure 2B**). Nevertheless, we pursued with the untagged CMT19TF1 cells, injecting them into mice of all the genotypes used in the intervention experiment, and allowing 20 days of growth. Tumours were then resected, and OHT was administered at this point to simulate β3 and/or NRP1 targeting in the adjuvant setting. After 12 more days, lungs from the animals were harvested and processed for immunohistochemical analysis. Surprisingly, no metastases were observed in lungs from any of the animals in two separate repeats of this experiment (**Appendix Figure 2D**). Since work from our laboratory previously identified lung metastases in both Cre-negative and Cre-positive Tie.Cre/β3-floxed mice (example shown in **Appendix Figure 2D**), we therefore conclude that this metastasis experiment did not work in our hands on these occasions. However, since the Tie1-Cre/β3-floxed mice display a constitutive deletion of β3, no administration of OHT is required in this case. It is therefore possible that the OHT used in our experiments may have inhibited the formation of metastases, though further investigation into this, and other reasons why our model failed, is required to avoid disappointment in the future.

3.6 Discussion

In a previous publication, we showed that the acute depletion of endothelial β3 only transiently inhibits tumour growth and angiogenesis, suggesting that specific mono-targeting strategies, though initially effective, are not so in the long-term, and therefore may benefit from the additional targeting of a compensatory pathway [211]. Unfortunately, although long-term endothelial β3 targeting in this particular study correlated with increased VEGFR2 surface levels, decreased expression of β5, reduced levels of FAK, and a misbalance in FAK phosphorylation, a conclusive mechanism of escape is yet to be elucidated in this case [211]. However, Robinson et al. [202] formerly showed that the total loss of β3 expression sensitises angiogenesis to NRP1 inhibition by siRNA or small peptides, suggesting that NRP1 may play a compensatory role when β3 has been missing for a long time, and pre-empting the idea that co-targeting αvβ3 and NRP1 might offer greater anti-angiogenic efficacy than their individual targeting. Though encouraging, these results were limited by the potential physiological irrelevance of a situation where β3 is globally and constitutively absent, and the complication of a developmental upregulation in VEGFR2 in the β3-NULL model. In order to gain a deeper mechanistic understanding of how β3 and NRP1 cooperate, and of the effect of their joint targeting in a more physiologically relevant model, we decided to move from β3-NULL mice to β3-HET mice, which feature a more subtle, albeit global, reduction in β3 expression. Like their knockout counterparts [134,197,202], β3-HET mice display enhanced tumour growth and angiogenesis, though not to such an elevated extent. This suggests that a compensatory resistance mechanism arises in this context in response to a constitutive reduction in β3, but not as aggressively as when β3 is constitutively absent. This contrasts with the long-term endothelial depletion of β3, which, despite not preventing mechanisms of escape, does not result in an elevated pathological response. Thus it is logical to assume that enhanced pathological angiogenesis in β3-HET mice is mainly due to the contribution of non-ECs. Even so, tumour growth and angiogenesis in β3-HET, but not WT, mice are sensitive to both the endothelial depletion of NRP1, and the global deletion of its cytoplasmic tail. This corroborates what Robinson et al. [202] previously showed in β3-NULL mice, but applies it to a more physiologically relevant model, extends the effect of targeting NRP1 to pathological angiogenesis, and implicates

NRP1's cytoplasmic tail as a major contributor to the effect. That both NRP1's endothelial depletion and lack of cytoplasmic tail had no effect on WT responses are also progressive findings. Endothelial NRP1 has previously been shown to be essential for embryonic brain angiogenesis [265] and postnatal pathological neovascularisation of the retina [271], but here we report a redundancy for endothelial NRP1 in VEGF-stimulated microvessel sprouting and pathological angiogenesis in adult mice, unless β3 is insufficiently expressed. Endothelial NRP1 is therefore non-essential for angiogenesis after development, at which point it may be held under control by β3, but if β3 levels drop, angiogenesis becomes dependent on NRP1 in ECs. Although our finding that NRP1's cytoplasmic tail is normally dispensable for angiogenesis is in agreement with previous studies [267,268], again we now report that its function becomes significant when β3 expression is reduced. Whilst we cannot rule out the effect of the deletion of NRP1's cytoplasmic tail in other cell types, this result implicates the cytoplasmic tail of NRP1 as a factor that dictates a significant pro-angiogenic response when β3 levels are reduced in ECs. The mechanistic basis behind β3's potential regulation of NRP1 in ECs must therefore be carefully analysed for greater clarity on this issue.

Our previous work has already shown that the acute endothelial depletion of β3 alone is unable to inhibit tumour growth and angiogenesis in pre-established tumours [211]. Now we report that the acute depletion of either β3 or NRP1 in ECs has no effect on tumour growth and angiogenesis, or on aortic ring microvessel sprouting, but when both β3 and NRP1 are simultaneously depleted, further tumour growth and angiogenesis, and microvessel sprouting, are blocked. This reinforces the notion that specifically targeting β3 in ECs is an effective anti-angiogenic approach, but that its results can be substantially improved by additionally targeting endothelial NRP1, which may otherwise contribute to an escape mechanism. That tumour growth can be inhibited by intervention is particularly exciting, as it strongly suggests that an anti-angiogenic approach involving the targeting of both molecules might offer improved therapeutic results in patients with advanced solid cancers over other strategies that have failed. The effect of β3/NRP1 dual targeting on metastasis in an adjuvant-like setting has so far proved elusive, but is the source of ongoing research in our laboratory. If co-

targeting the molecules additionally produces anti-metastastic effects, then the case for their further clinical investigation is strengthened. However, before antagonists can enter clinical trials as a joint therapy, a greater mechanistic understanding of how the two molecules cooperate is needed. Such an understanding might further implicate novel master regulators of the effect we have seen, or highlight particular portions of the molecules that should be targeted. Only then can we assuredly experiment with antagonists that impair the important processes involved. In the meantime, small molecule inhibitors directed against NRP1 are under development [274,299,300], which could be tested alongside existing or new αvβ3-integrin antagonists, although their effect on non-ECs that also contribute to tumour growth and angiogenesis must be considered carefully, as our results suggest that specifically targeting the molecules in ECs would be the most effective form of therapy. The small molecule inhibitors that have been produced so far target the VEGF-binding portion of NRP1, which, unlike the cytoplasmic tail, we do not know the significance of in pathological angiogenesis, although it would be interesting to find this out. We can also further explore the durability of a dual-targeted approach; it may be that additional mechanisms of escape arise in response to the long-term targeting of both molecules.

Nevertheless, our main priority in this project was to discover the mechanistic basis behind why NRP1 becomes more sensitive to perturbation with reduced β3 expression. This will now be explored in the following two chapters, which focus on NRP1's VEGFR2-dependent and VEGFR2-independent roles, respectively, both of which have been shown to be influenced by NRP1's cytoplasmic tail.

4. Investigating how αvβ3-integrin regulates neuropilin-1's VEGFR2-dependent role in endothelial cells

4.1 Polyoma-middle-T-antigen immortalised endothelial cells maintain their endothelial identity

In order to investigate the underlying molecular mechanisms associated with the phenotypes presented in the previous chapter, and specifically determine how β3 expression levels differentially affect NRP1 function, we employed polyoma-middle-T-antigen (pMT) immortalised murine lung microvascular ECs (MLECs) isolated from β3-WT, β3-WT.NRP1Δcyto, β3-HET and β3-HET-NRP1Δcyto mice. These pMT MLECs, which are well suited for assays that require large numbers of cells, have previously been utilised as models to study angiogenesis to great effect [202,211,314], but to confirm they maintain endothelial identity in our hands, we routinely analysed their surface levels of the EC markers VE-Cadherin, CD31, and ICAM-2 by flow cytometry. We consistently found them to display a significant enrichment in these markers compared to isotype controls (**Figure 4.1**).

4.2 VEGFR-2 expression levels are marginally elevated in β3-integrin-heterozygous endothelial cells

β3-NULL ECs display significantly upregulated VEGFR2 expression, a characteristic that may arise during development in response to the absence of β3, and may partly explain the enhanced tumour growth and angiogenesis seen in β3-NULL animals [134,197,202]. We therefore assessed total VEGFR2 levels in the four genotypes. In comparison to β3-NULL ECs, we noted only a small (not significant) trend of increased VEGFR2 levels in both β3-HET and β3-HET-NRP1Δcyto ECs (**Figure 4.2**). Since tumour growth and angiogenesis is reduced in β3-HET-NRP1Δcyto compared to β3-HET mice, this suggests that upregulated VEGFR2 is not necessary for elevated tumour growth and angiogenesis in β3-HET mice.

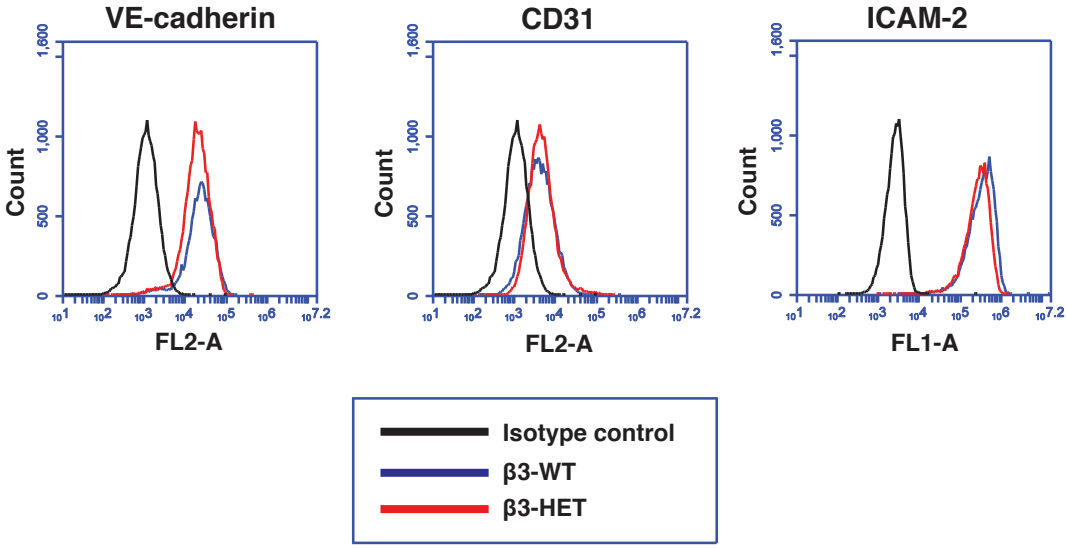

Figure 4.1: Polyoma-middle-T-antigen immortalised endothelial cells maintain their endothelial identity. Lung microvascular endothelial cells (ECs) were isolated and immortalised (polyoma-middle-T-antigen) from β3-WT and β3-HET mice. ECs were trypsinised and analysed by flow cytometry for surface levels of the EC markers VE-Cadherin, CD31, and ICAM-2. Median fluorescence intensity was measured after forward versus side scatter data were tightly gated around, and normalised to, an isotype control. Representative flow-cytometric histogram profiles of β3-WT and β3-HET ECs are shown.

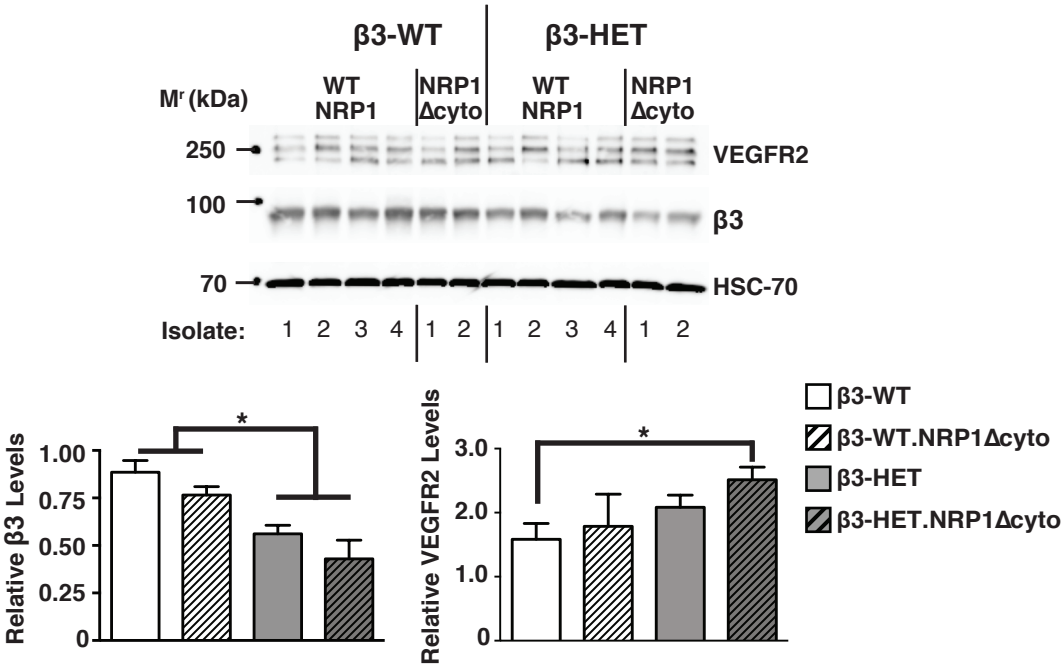

Figure 4.2: VEGFR-2 expression levels are elevated in β3-integrin-heterozygous endothelial cells. Lung microvascular endothelial cells (ECs) were isolated and immortalised (polyoma-middle-T-antigen) from β3-WT and β3-HET mice that were expressing either normal (WTNRP1) or cytoplasmic-tail deleted NRP1 (NRP1Δcyto). Multiple EC lysates of each genotype were Western blotted (WB) to examine total cellular levels of VEGFR2 and β3-integrin. HSC-70 was used as a loading control. Bar charts of densitometric analysis of mean (+SEM) changes between the four genotypes are shown below. Asterisks indicate statistical significance: *, P<0.05.

4.3 VEGFR2 activation and degradation patterns are no different between wild-type and β3-integrin heterozygous endothelial cells with and without neuropilin-1's cytoplasmic tail

Given that NRP1 is widely recognised as a regulator of VEGFR2 function [68,272-275,277,278], we wanted to determine whether β3 expression levels differentially affect known NRP1-mediated VEGFR2 responses. NRP1's cytoplasmic tail is important for driving VEGFR2 trafficking, which increases VEGFR2 phosphorylation and downstream signalling through ERK. Although this effect has only been observed in aortic/arterial ECs before, and been projected to be more associated with arteriogenesis than angiogenesis, we wondered whether it featured in our MLECs with normal or reduced β3 expression.

We started to address this objective by immunoblotting for changes in VEGFR2 phosphorylation, ERK1/2 phosphorylation, and total VEGFR2 levels over a time course of VEGF stimulation between β3-WT and β3-HET ECs with and without NRP1's cytoplasmic tail. Both extended (**Figure 4.3A**) and shortened (**Figure 4.3B**) time courses were used so we were able to discern subtle changes in timing patterns (**4.3A**) and, once we had this information, to simultaneously compare all four genotypes at the most crucial time points (**4.3B**). Importantly, like all other assays that require EC adhesion in this chapter, prior to their VEGF stimulation, ECs were allowed to adhere to a complex matrix containing gelatin, collagen I (COLI), fibronectin (FN), and vitronectin (VN), to ensure we were not perturbing VEGFR2 function by denying its interaction with β3, which relies on VN **[ref]**. Apart from the previously mentioned upregulation of VEGFR2 in the β3-HET ECs, no differences in patterns of VEGFR2 expression over the timecourses were observed between the ECs, with VEGFR2 levels steadily decreasing over time after VEGF stimulation in each case (**Figure 4.3A**). This suggests that the VEGFR2 protein is degraded over time in all four genotypes in a similar manner to that previously reported [88,200,315], indicating that VEGFR2 degradation was not affected by the loss of NRP1's cytoplasmic tail even with reduced β3 expression. Although VEGF-induced VEGFR2 phosphorylation was slightly elevated in β3-HET ECs, VEGFR2 phosphorylation, like degradation, was not significantly changed by the introduction of the NRP1Δcyto mutation in either β3-WT or β3-HET ECs. In contrast, VEGF-induced ERK1/2 phosphorylation was

sensitive to NRP1 cytoplasmic deletion in β3-HET ECs but not β3-WT ECs (**Figure 4.3B**). This may be suggestive of a slight disruption in NRP1 cytoplasmic tail-mediated VEGFR2 trafficking in β3-HET-NRP1Δcyto ECs, although we still cannot be sure that this change in ERK1/2 phosphorylation is not regulated independently from VEGFR2, especially given the lack of difference in VEGFR2 phosphorylation. Moreover, differences seem to be too subtle to fully explain the high degree of sensitivity of angiogenesis in β3-HET mice (relative to WT counterparts) to NRP1's cytoplasmic tail removal. Of additional noteworthy mention, NRP1 expression, like that of VEGFR2, was found to be slightly elevated in both β3-HET ECs, but also was increased in the Δcyto ECs (in both β3-WT and β3-HET cells) relative to those that expressed normal NRP1, arguing against the idea that *in vivo* phenotypes are influenced by changes in NRP1 expression.

Taken together, these results show that certain facets of previously recognised NRP1-mediated VEGFR2 trafficking are seemingly not dependent on NRP1's cytoplasmic tail in microvascular MLECs. However, as slightly enhanced ERK1/2 phosphorylation in β3-HET ECs is sensitive to the loss of NRP1's cytoplasmic tail, VEGFR2 trafficking will be further investigated later.

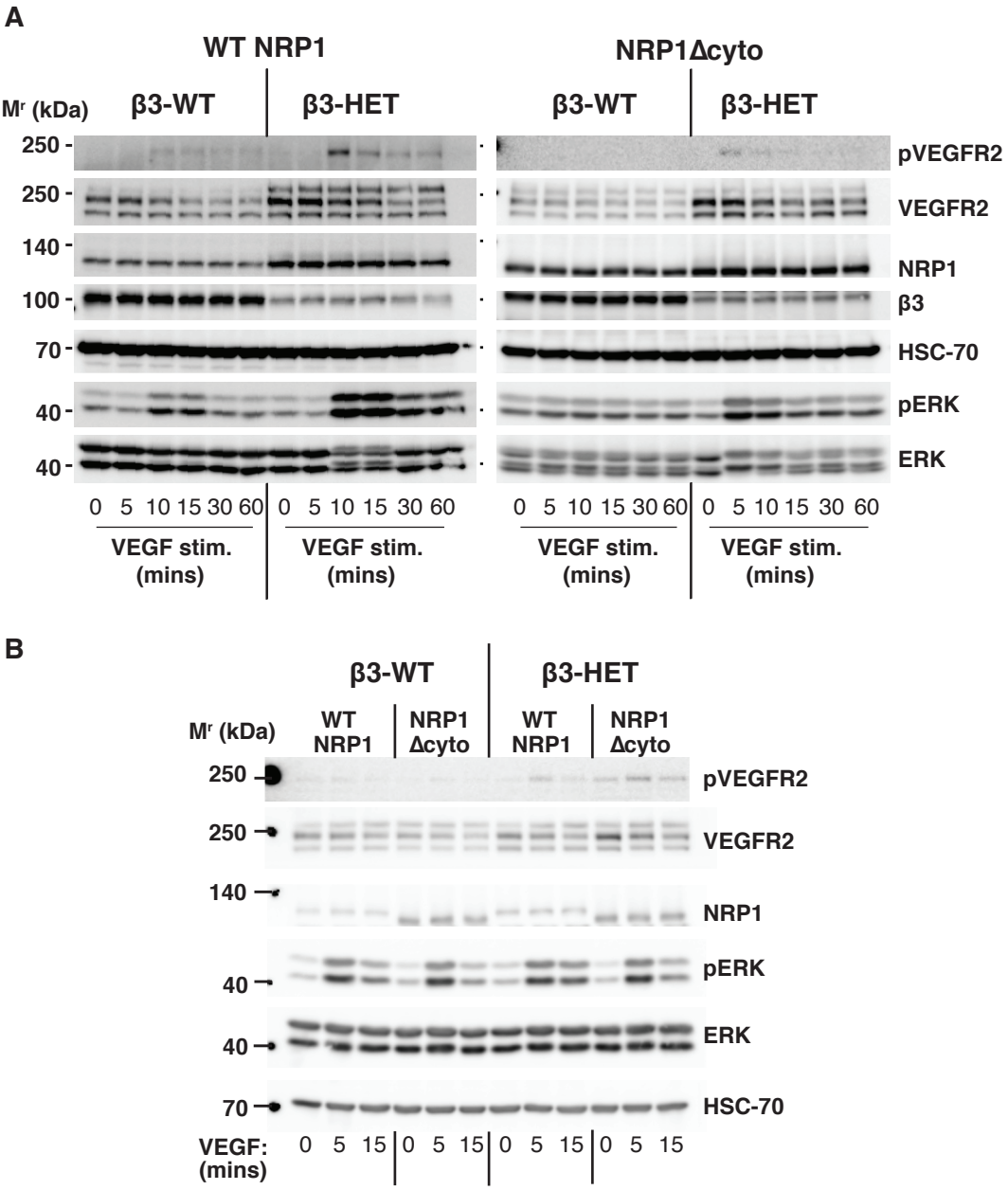

Figure 4.3: VEGFR2 degradation patterns and signalling through ERK are no different between wild-type and β3-integrin heterozygous endothelial cells with and without neuropilin-1's cytoplasmic tail. Lung microvascular endothelial cells (ECs) were isolated and immortalised (polyoma-middle-T-antigen) from β3-WT and β3-HET mice that were expressing either normal (WTNRP1) or cytoplasmic-tail deleted NRP1 (NRP1Δcyto). ECs were seeded overnight on a complex matrix containing gelatin, collagen, fibronectin and vitronectin, and were then stimulated with VEGF over: **A** an extended time course to examine protein degradation and signalling kinetics; **B** a shorter time course to enable comparison between all genotypes. ECs were lysed and blotted for levels of phosphorylated ('p'...) and total VEGFR2, NRP1, β3-integrin, and phosphorylated and total ERK1/2. HSC-70 was used as a loading control. Data are representative of 3 independent experiments.

4.4 Neuropilin-1-regulated VEGFR2 signalling is no different between wild-type and β3-integrin heterozygous endothelial cells with and without neuropilin-1's cytoplasmic tail

Besides investigating NRP1's reported regulation of VEGFR2/ERK signalling, we wanted to examine its role in other VEGF-induced signalling pathways in β3-WT and β3-HET microvascular MLECs to continue determining whether β3 levels differentially affect NRP1-mediated VEGFR2 function. Of particular interest was NRP1's involvement in the regulation of p130Cas phosphorylation, which, in HUVECs, is dependent on NRP1's cytoplasmic tail, and may be part of a NRP1-mediated signalling pathway that additionally involves FAK Y407 phosphorylation [272,273]. However, immunoblotting for phosphorylated and total p130Cas and FAK after ECs were stimulated with VEGF over extended (**Figure 4.4A**) and shortened (**Figure 4.4B**) time courses revealed no relative changes in phosphorylation of either molecule upon NRP1 cytoplasmic tail removal, even when β3 expression was reduced. It did appear, however, as though both total and phosphorylated levels of p130Cas and FAK were slightly reduced by the loss of NRP1's cytoplasmic tail in β3-WT and β3-HET ECs to a similar degree. Thus, although this does not translate to differences in phosphorylation relative to the amounts of total protein, NRP1's cytoplasmic tail may have some influence on these molecules, yet not in a way that explains the differential sensitivity of β3-WT and β3-HET mice to NRP1 targeting.

A mild reduction in p38MAPK activity following the prevention of NRP1's VEGF-binding ability in HUVECs and PAEs [133,275], and in PAEs expressing mutant NRP1 lacking its cytoplasmic tail [80], have previously been reported. Also, there have been reports of reduced Akt phosphorylation upon NRP1 siRNA knockdown in HDMECs [271], but not HUVECs [133,272,275] (except by a small molecule NRP1 inhibitor [274]). We therefore additionally examined phosphorylation of these molecules over a VEGF time course by immunoblotting, but again saw no changes that might explain why β3-HET mice are sensitive to NRP1 perturbation, whereas β3-WT mice are not (**Appendix Figure 3**). We therefore conclude that β3 levels do not differentially affect NRP1-mediated VEGF-induced signalling.

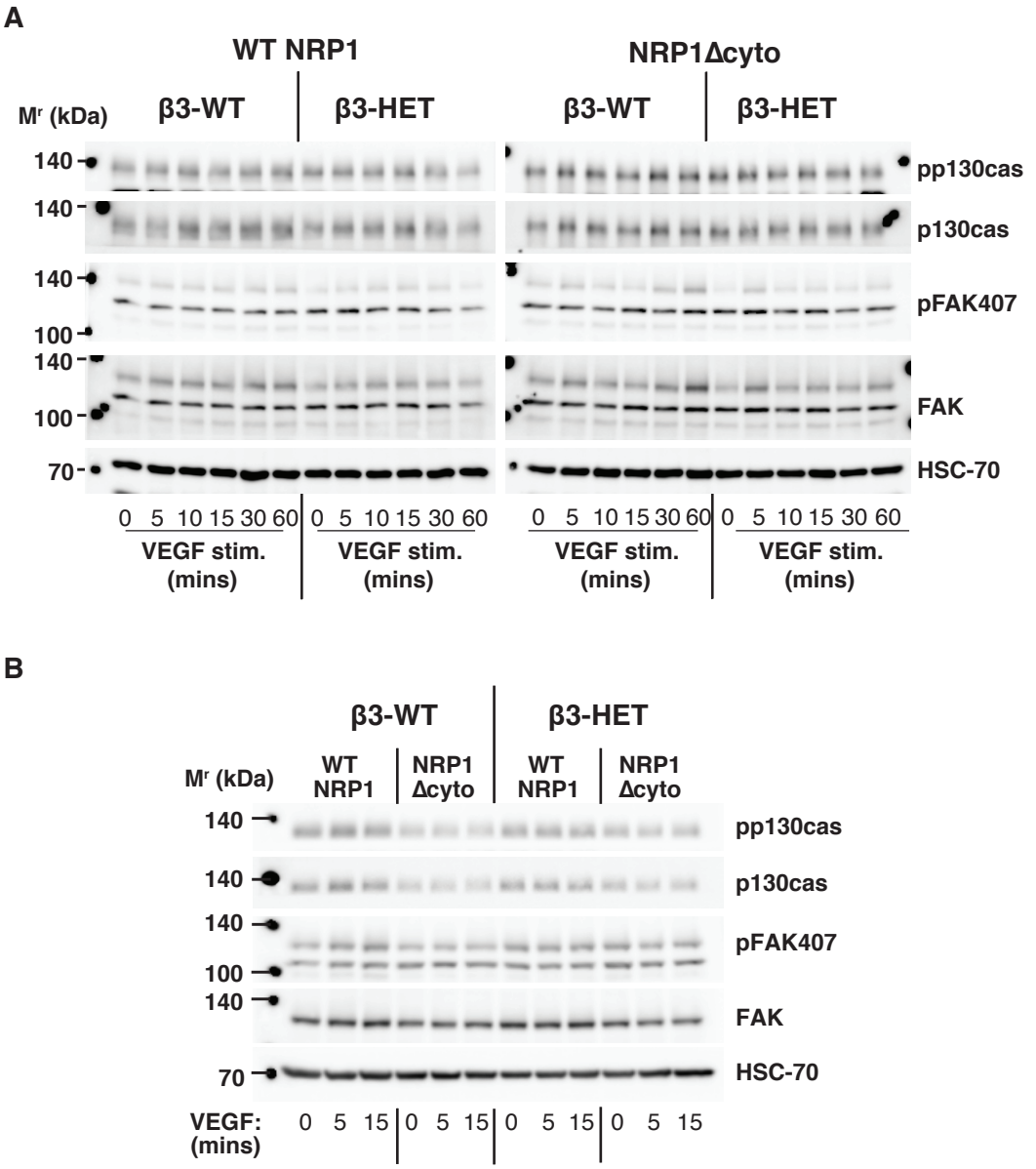

Figure 4.4: Neuropilin-1-regulated VEGFR2 signalling via p130Cas and FAK is no different between wild-type and β3-integrin heterozygous endothelial cells with and without neuropilin-1's cytoplasmic tail. Lung microvascular endothelial cells (ECs) were isolated and immortalised (polyoma-middle-T-antigen) from β3-WT and β3-HET mice that were expressing either normal (WTNRP1) or cytoplasmic-tail deleted NRP1 (NRP1Δcyto). ECs were seeded overnight on a complex matrix containing gelatin, collagen, fibronectin and vitronectin, and were then stimulated with VEGF over: **A** an extended time course to examine signalling kinetics; **B** a shorter time course to enable comparison between all genotypes. ECs were lysed and blotted for levels of phosphorylated ('p'...) and total p130cas, and phosphorylated (tyrosine 407) and total FAK. HSC-70 was used as a loading control. Data are representative of 3 independent experiments.

4.5 Cell surface biotinylation internalisation assays do not reliably measure VEGFR2 trafficking in pMT MLECs, but VEGFR2 surface levels do not appear different in β3-HET ECs with or without NRP1's cytoplasmic tail by flow cytometry

Whilst we saw no changes in VEGFR2 activation or degradation in NRP1Δcyto ECs with normal or reduced β3 expression, we did see a slight change in ERK1/2 phosphorylation between β3-HET and β3-HET-NRP1Δcyto ECs, which may reflect changes in VEGFR2 trafficking. It was therefore necessary to continue looking at different aspects of VEGFR2 trafficking in our MLECs. Our first approach was to monitor internalised VEGFR2 and NRP1 using a cell surface biotinylation assay that was previously used successfully by Remacle et al. [316]. In this assay, surface proteins are biotinylated and internalised with VEGF for different time points before the remaining biotin on cell surface proteins is stripped off using a membrane-impermeable reducing agent. Cells are then lysed and immunoprecipitated (IP'd) for biotin, and these IPs are immunoblotted for VEGFR2 and NRP1 to see their degree of internalisation at the different VEGF time points. Unfortunately, in our pMT ECs we were not able to achieve consistent results with the reducing agent MESNA, as shown by its inability to strip off remaining biotin in the 'stripped' internal control in pMT ECs, but not HUVECs (**Figure 4.5B**). This did not improve after continuous attempts to optimise the protocol, which involved trialling the temperature at which it was performed, the concentration of biotin, the timing of different incubation steps, the washing buffer, the lysis buffer, and the surface protein being examined. However, changing the reducing agent to TCEP did result in successful biotin stripping, though still not altogether reliably. We therefore cannot read too much into VEGFR2 and NRP1 internalisation results obtained with TCEP. An example of such an experiment is shown in **Figure 4.5C**, and the quantified degree of internalisation is presented in **Figure 4.5D**. Here, whilst biotin stripping in the control is somewhat effective in β3-HET ECs, it is not so in WT ECs, reducing the impact of this data. If one were to analyse this data, though, it looks as though VEGFR2 and NRP1 are internalised very quickly in WT ECs before their signal disappears, which may suggest their complete degradation or recycling, or more likely a combination of both. In β3-HET ECs, however, VEGFR2 and NRP1 are more slowly internalised, and their signals are lost more slowly, in a manner

similar to the degradation pattern observed before, although recycling may play a role here as well. In both β3-WT and β3-HET ECs lacking NRP1's cytoplasmic tail, NRP1 internalisation is again difficult to comment on due to the inefficiency of biotin stripping in the control. However, VEGFR2 is not internalised in either case, suggesting that NRP1's cytoplasmic tail is important for VEGFR2 endocytosis, although it is possible that the assay is too insensitive to pick up subtle signal changes. Due to the unreliability of this assay in pMT ECs, we were also not able to use it to specifically analyse VEGFR2/NRP1 recycling, despite attempts using the recycling inhibitor, primaquine (not shown).

As we were unable to accurately measure VEGFR2 trafficking by cell surface biotinylation, we turned to the analysis of VEGFR2 surface levels in trypsinised pMT LMECs over a time course of VEGF stimulation by flow cytometry (**Figure 4.5E**). Surface levels were similar between the four genotypes, with each showing an initial increase in surface levels upon stimulation that likely reflects the previously reported VEGFR2 mobilisation from an internal pool [88], and subsequently a general decrease over time, in line with various internalisation studies [88,89,200,315]. This therefore suggests that, ultimately, perturbing NRP1 function when there are normal or reduced β3 expression levels does not majorly affect net changes in VEGFR2 internalisation and recycling.

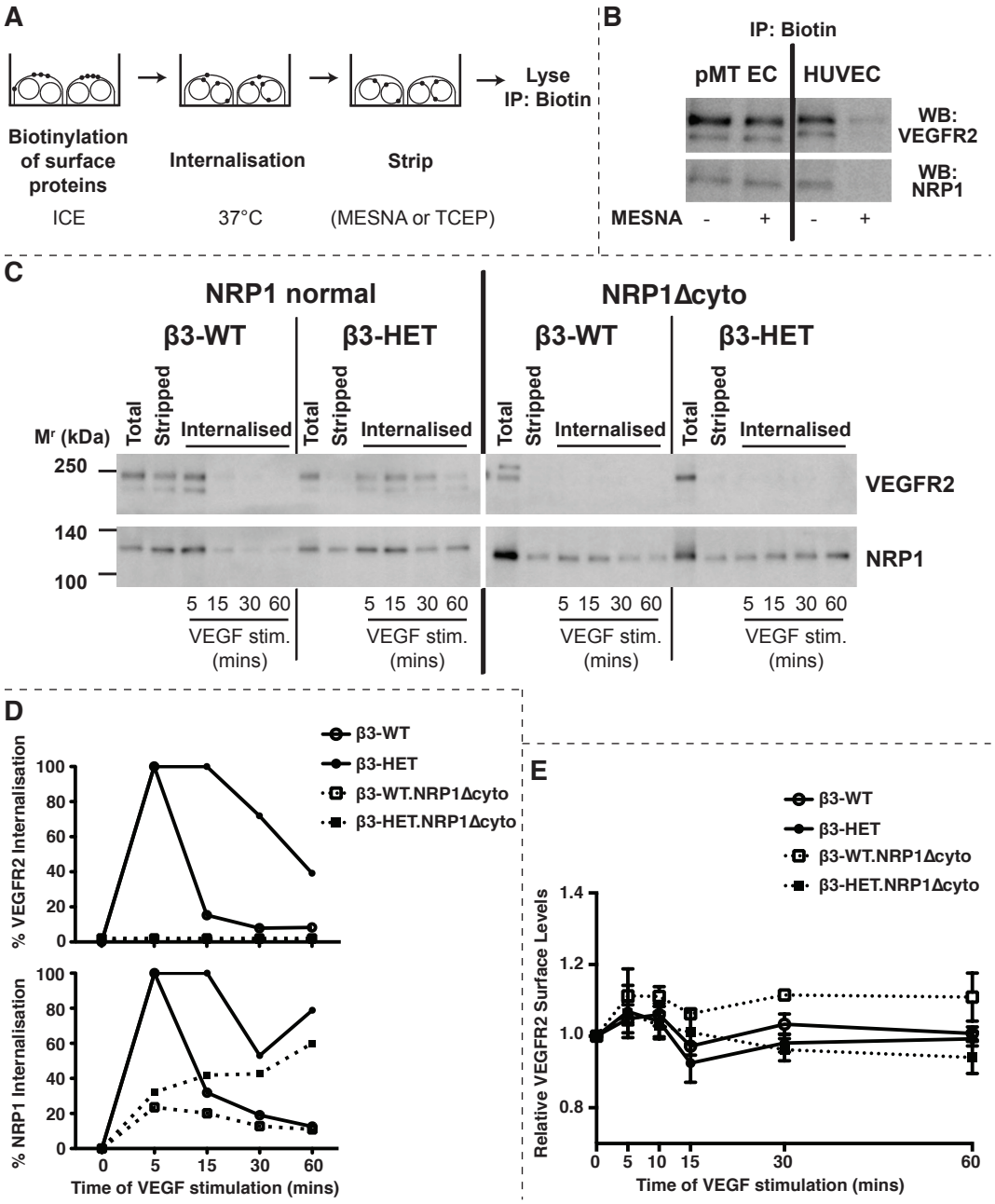

Figure 4.5: Cell surface biotinylation internalisation assays do not reliably measure VEGFR2 trafficking in pMT MLECs, but VEGFR2 surface levels do not appear different in β3-HET ECs with or without NRP1's cytoplasmic tail by flow cytometry. Lung microvascular endothelial cells (ECs) were isolated and immortalised (polyoma-middle-T-antigen) from β3-WT and β3-HET mice that expressed either normal or cytoplasmic-tail-deleted NRP1 (NRP1Δcyto). **A** *Biotinylation assay schematic* (adapted from [316]): Cell surface proteins of ECs seeded on a complex matrix containing gelatin, collagen, fibronectin and vitronectin, were biotinylated, internalised with VEGF for different time points, and the remaining biotin on cell surface proteins was 'stripped' off using a membrane-impermeable reducing agent (MESNA/TCEP). Cells were lysed and immunoprecipitated (IP'd) for biotin. **B** Western blot (WB) of biotin-pulldowns show MESNA effectively strips biotin off VEGFR2 and NRP1 in HUVECs, but not in pMT ECs. **C** WB of biotin IPs showing internalised VEGFR-2 and NRP1 over time of VEGF stimulation between the different transgenic pMT ECs. 'Total' surface protein (from cells not stimulated and not stripped), and protein from cells not stimulated with VEGF, but 'stripped' with TCEP, are shown as controls. **D** Graphs showing the internalisation of VEGFR2 and NRP1 over time stimulated with VEGF (mins) between the different ECs from ***C***. Internalisation is quantified as a percentage of the 'total' surface protein level from a densitometric analysis. **E** Following a VEGF time course, pMT ECs were trypsinised and analysed by flow cytometry for surface levels of VEGFR2. Median fluorescence intensity was measured, and normalised to, an isotype control. The graph shows the relative surface level of VEGFR2 (means ±SEM) relative to the 0 (non-stimulated) time point from 3 independent experiments.

4.6 There are no relative differences in neuropilin-1-VEGFR2 interactions between wild-type and β3-heterozygous endothelial cells

VEGF-induced interactions between VEGFR2 and NRP1 are elevated in β3-NULL ECs, and contribute to increased angiogenesis and ERK signalling in this model [202]. We therefore next examined this interaction in response to VEGF in β3-WT and β3-HET ECs by co-immunoprecipitation, first comparing different isolates to one another (**Figure 4.6A**), and then comparing association kinetics over a time course (**Figure 4.6B**). No significant changes in VEGFR2-NRP1 associations were observed in β3-HET ECs compared to β3-WT ECs, despite their upregulated expression of both proteins. In contrast to a previously published study [280], we saw that the VEGF-induced association between the two molecules was preserved in both β3-WT-NRP1Δcyto and β3-HET-NRP1Δcyto ECs (**Figure 4.6C**).

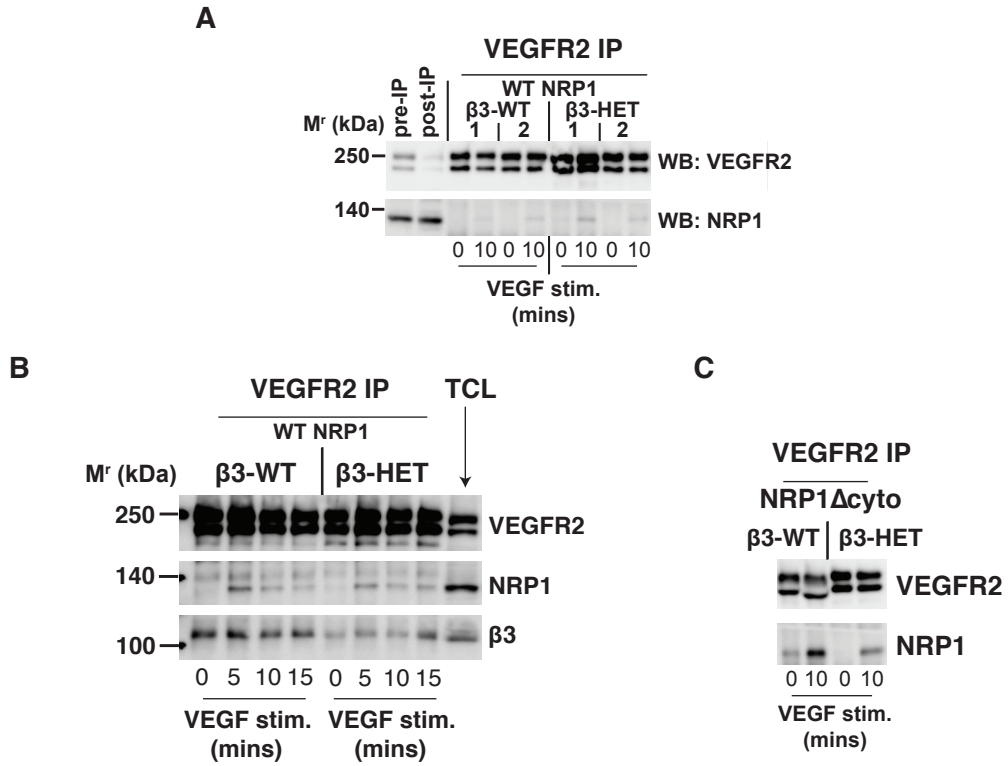

Figure 4.6: There are no relative differences in neuropilin-1-VEGFR2 interactions between wild-type and β3-heterozygous endothelial cells. Lung microvascular endothelial cells (ECs) were isolated and immortalised (polyoma-middle-T-antigen) from β3-WT and β3-HET mice that were expressing either normal (WTNRP1) or cytoplasmic-tail deleted NRP1 (NRP1Δcyto). ECs were seeded overnight on a complex matrix containing gelatin, collagen, fibronectin and vitronectin and stimulated with VEGF for the indicated amounts of time and then lysed and immunoprecipitated for VEGFR2 (VEGFR2 IP), before being blotted for NRP1 association. **A** Western blot showing VEGFR2-NRP1 associations in 2 separate isolates of β3-WT and β3-HET ECs either stimulated (10 mins) with VEGF or unstimulated (0 mins). Total cell lysates taken before the IP (pre-IP) and after the IP (post-IP) are shown as controls to confirm the efficiency of the IP. **B** Western blot showing VEGFR2-NRP1 associations over a VEGF time course. A total cell lysate (TCL) is shown for comparison. **C** Western blot showing VEGFR2-NRP1 associations from β3-WT and β3-HET ECs lacking NRP1's cytoplasmic tail.

4.7 Discussion

Since elevated tumour growth and angiogenesis in β3-NULL mice was dependent on upregulated VEGFR2 expression [134], and NRP1 has been shown to positively regulate VEGFR2, including via its cytoplasmic tail [68,80,268,272-275,277,278], we sought to determine whether β3 expression levels differentially regulate NRP1-mediated VEGFR2 function, and therefore explain why tumour growth and angiogenesis are sensitive to NRP1 perturbation in β3-HET, but not β3-WT mice.

In contrast to the β3-NULL model, we observed a relatively small upregulation in VEGFR2 expression in both β3-HET and β3-HET-NRP1Δcyto ECs. This suggests that enhanced VEGFR2 expression in ECs is not required for elevated tumour growth and angiogenesis in β3-HET mice. Moreover, it means that the reduction in tumour growth and angiogenesis in β3-HET-NRP1Δcyto mice occurs in spite of slightly enhanced VEGFR2 levels in ECs. Whilst we cannot rule out the role of VEGFR2 in other cell types that contribute to our *in vivo* phenotypes in β3-HET mice, there was no change in VEGFR2 expression in the acute EC-depleted β3 model in our previous publication, which displayed transiently reduced tumour growth and angiogenesis [211], and joint β3/NRP1 EC targeting inhibits pre-established tumour growth and angiogenesis, both implying that ECs can majorly influence our phenotypes.

In aortic/arterial ECs, NRP1 is known to complex with VEGFR2 in the presence of VEGF and enhance its trafficking away from a degradative pathway, but rather through recycling endosomes via NRP1's cytoplasmic tail's linkage to synectin/myosin VI [80,268]. This keeps VEGFR2 away from the phosphatase PTP1b and results in enhanced VEGFR2 and ERK1/2 phosphorylation [80,82,268]. Since NRP1's cytoplasmic tail was previously shown to be dispensable for angiogenesis, but more involved in arteriogenesis [268], NRP1's mediation of VEGFR2 recycling and enhanced ERK signalling has been proposed to be specific for arteriogenesis [287]. However, this role of NRP1 had never been examined in microvascular ECs, and we wondered whether it featured differentially between β3-WT and β3-HET ECs. No differences in VEGFR2 phosphorylation, surface levels, or degradation patterns were found

when NRP1 lacked its cytoplasmic tail in either β3-WT or β3-HET ECs. Moreover, there was no difference in VEGF-induced NRP1-VEGFR2 association between β3-WT and β3-HET ECs. However, whilst VEGF-induced ERK1/2 phosphorylation was not dependent on NRP1's cytoplasmic tail in β3-WT ECs, it was in β3-HET ECs. Overall, this implies that NRP1-mediated VEGFR2 trafficking does not occur to a significant extent in WT microvascular ECs, agreeing, perhaps, with the notion that it is more of an archetype of arteriogenesis, at least when β3 is sufficiently expressed. However, that there was a minor difference in ERK1/2 phosphorylation between β3-HET and β3-HET-NRP1Δcyto ECs may be indicative of a subtle increase in NRP1-dependent VEGFR2 recycling in β3-HET ECs that could not be detected in our analyses. Our biotinylation data may support this, given slight changes in VEGFR2 internalised signal between β3-WT and β3-HET ECs, although the unreliability of the assay in pMT ECs, and our unsuccessful attempts at extending it to monitor recycling, leaves this open to debate. As differences in ERK signalling were only minor, and we observed no other VEGFR2 trafficking-related changes, and furthermore, the change in ERK1/2 phosphorylation may have been mediated independent of VEGFR2, we did not pursue further with VEGFR2 recycling analyses. If we were to do so in the future, then perhaps it would be most worthwhile to use immunocytochemistry to monitor potential differences in VEGFR2 co-localisation with different Rab GTPase markers of recycling endosomes over a VEGF-stimulated timecourse between β3-WT and β3-HET ECs.

The lack of an effect on VEGF-induced ERK phosphorylation in β3-WT-NRP1Δcyto ECs is in agreement with other studies that saw no effect in response to different forms of NRP1 targeting in HUVECs, including using anti-NRP1 monoclonal antibodies [133], NRP1 siRNA knockdown [272], and a NRP1 mutant defective in VEGF binding [273]. However, there have been contradictions in this matter. Whilst the differences mentioned in aortic/arterial ECs that feature enhanced VEGFR2 trafficking may be explained by their inherent tendencies towards supporting arteriogenesis, minor reductions in ERK activation have also been observed in HUVECs in response to another NRP1 siRNA [282] or a small molecule NRP1 antagonist [274], and in HDMECs following NRP1 siRNA knockdown [271]. Clearly, the role that NRP1 plays in mediating VEGF-induced

ERK phosphorylation is dependent on the EC type and the method of NRP1 inhibition, and so the mechanistic basis behind these discrepancies must be further scrutinised.

As shown previously in HUVECs [272], but not arterial ECs or heart tissue [268], we observed no difference in VEGF-induced VEGFR2 Y1175 phosphorylation in ECs lacking NRP1's cytoplasmic tail, again suggesting a division in different cell types' predispositions for different processes, but this warrants further investigation. Nevertheless, in our microvascular ECs, this portion of NRP1 does not influence VEGFR2 activation under conditions of both normal and reduced β3 expression.

Since both total and phosphorylated levels of p130Cas and FAK were marginally reduced by the loss of NRP1's cytoplasmic tail in β3-WT and β3-HET ECs to a similar degree, this does not support the previously reported relative reduction in phosphorylation of each molecule in response to NRP1 targeting in HUVECs [272,273]. Nor does it explain the differential sensitivity of tumour growth and angiogenesis in β3-WT and β3-HET mice to NRP1 targeting. Furthermore, unlike previous studies in other cell types [80,133,271,274,275], we observed no obvious changes in Akt or p38MAPK activation in either β3-WT or β3-HET microvascular ECs.

Perhaps partly explaining the absence of differences in NRP1-mediated VEGFR2 trafficking and signalling in our different ECs, unlike β3-NULL ECs, we found no change in VEGF-induced NRP1-VEGFR2 interactions in β3-HET ECs compared to β3-WT ECs. The interactions we detected were also not dependent on NRP1's cytoplasmic tail in our cells, unlike results published by Prahst et al. [280], which showed that the PDZ domain of NRP1 was required for NRP1-VEGFR2 interactions in PAEs and HUVECs. Again, this may point to distinctions in NRP1's role between EC types, and should be a matter for further investigation.

Overall, although our cultured transgenic microvascular ECs are not perfect mimics of ECs in pathological angiogenesis, results garnered from them indicate that the increased sensitivity of tumour growth and angiogenesis to perturbations

in NRP1 in β3-HET mice cannot be explained by NRP1's VEGFR2-dependent function, despite potential subtle changes in VEGFR2 trafficking.

5. Investigating how αvβ3-integrin regulates neuropilin-1's VEGFR2-independent role in endothelial cells

5.1 Examining adhesion and cell spreading properties of β3-integrin-wild-type and heterozygous endothelial cells with and without neuropilin-1's cytoplasmic tail

Intriguingly, recent studies have shown that NRP1's contribution to angiogenesis is not limited to its binding of VEGF [269,270], and that its regulation of the process can be mediated by FN [271,290]. Indeed, prior to its description as a VEGF co-receptor, NRP1 was identified as a surface protein mediating cell adhesion [254], and Valdembri et al. [288] later found it to promote HUVEC adhesion to FN, but not COLI, VN or LN, in a manner dependent on NRP1's SEA synectin-binding motif and α5β1 [288]. As our transgenic models included manipulations of both NRP1 and αvβ3, whose canonical ligand is VN, we examined adhesion of our β3-WT, β3-WT.NRP1Δcyto, β3-HET and β3-HET-NRP1Δcyto pMT ECs to a range of concentrations of VN or FN (**Figure 5.1A**). Unsurprisingly, compared to β3-WT and β3-WT-NRP1Δcyto ECs, β3-HET and β3-HET-NRP1Δcyto ECs showed reduced adhesion to VN over a range of concentrations tested, although, in this assay, the same was also true for their adhesion to FN, indicating that the heterozygous expression of β3 reduces adhesion to both its VN and FN ligands, regardless of a deletion in NRP1's cytoplasmic tail. In contrast to Valdembri et al's [288] study, the loss of NRP1's cytoplasmic tail had no obvious effect on microvascular EC adhesion to FN, with normal or reduced β3 expression. Having established working concentrations of ECM components, we tested the ECs' adhesion to saturating concentrations of a range of matrices, normalising the data to the degree of adhesion to FN (which universally bound the most cells), since we would later be analysing other EC processes that we did not want to be influenced by differences in adhesion to low concentrations of ECM components (**Figure 5.1B**). The only clear difference noted on saturating matrix concentrations in these types of assays was the expected reduction in adhesion of β3-HET and β3-HET-NRP1Δcyto ECs to matrices containing VN. Since ECs were only allowed to adhere over a short time (90 minutes) in these assays, we also examined long-term cell spreading of our

four cell lines to 10 µg/ml FN, a saturating concentration which effectively promotes adhesion and migration of a number of cell types (**Figure 5.1C**) [317-319]. Cell spreading on FN after 6 hours was similar in all four genotypes, meaning the subtle differences in adhesion between genotypes were negligible if the ECs were allowed enough time to adhere to saturating FN concentrations. Importantly, this gives us the opportunity to measure EC migration on this component over a longer period of time without the added complexity of differences in EC adhesion (see later).

5.2 Examining surface levels of integrins in β3-integrin-wild-type and heterozygous endothelial cells with and without neuropilin-1's cytoplasmic tail

Although there were only relatively subtle differences in adhesion of our four transgenic cell lines to VN and FN, we still wondered whether reduced β3 expression levels cause changes in other integrins. Since NRP1 is known to interact with a number of integrins [202,288,307], they may be involved in allowing NRP1 to be more sensitive to perturbation in β3-HET ECs.

We therefore used flow cytometry to examine the surface expression of various EC integrin subunits in our pMT ECs (**Figure 5.2** and **Appendix Figure 4**). Consistent with the adhesion data, αv- and β3-integrin levels were significantly higher in β3-WT and β3-WT-NRP1Δcyto ECs compared to their β3-HET counterparts. Whilst α1, β1 and β5 surface levels were unchanged, we observed a small increase in α2 surface expression in β3-HET ECs. Most notably, however, α5 surface levels were lower in ECs expressing reduced levels of β3-integrin, which might partially account for their reduced adhesion to FN. The molecular consequences of these changes in integrin surface levels in β3-HET ECs on NRP1 function would therefore be interesting to dissect to further ascertain whether they contribute in any way to our *in vivo* phenotypes.

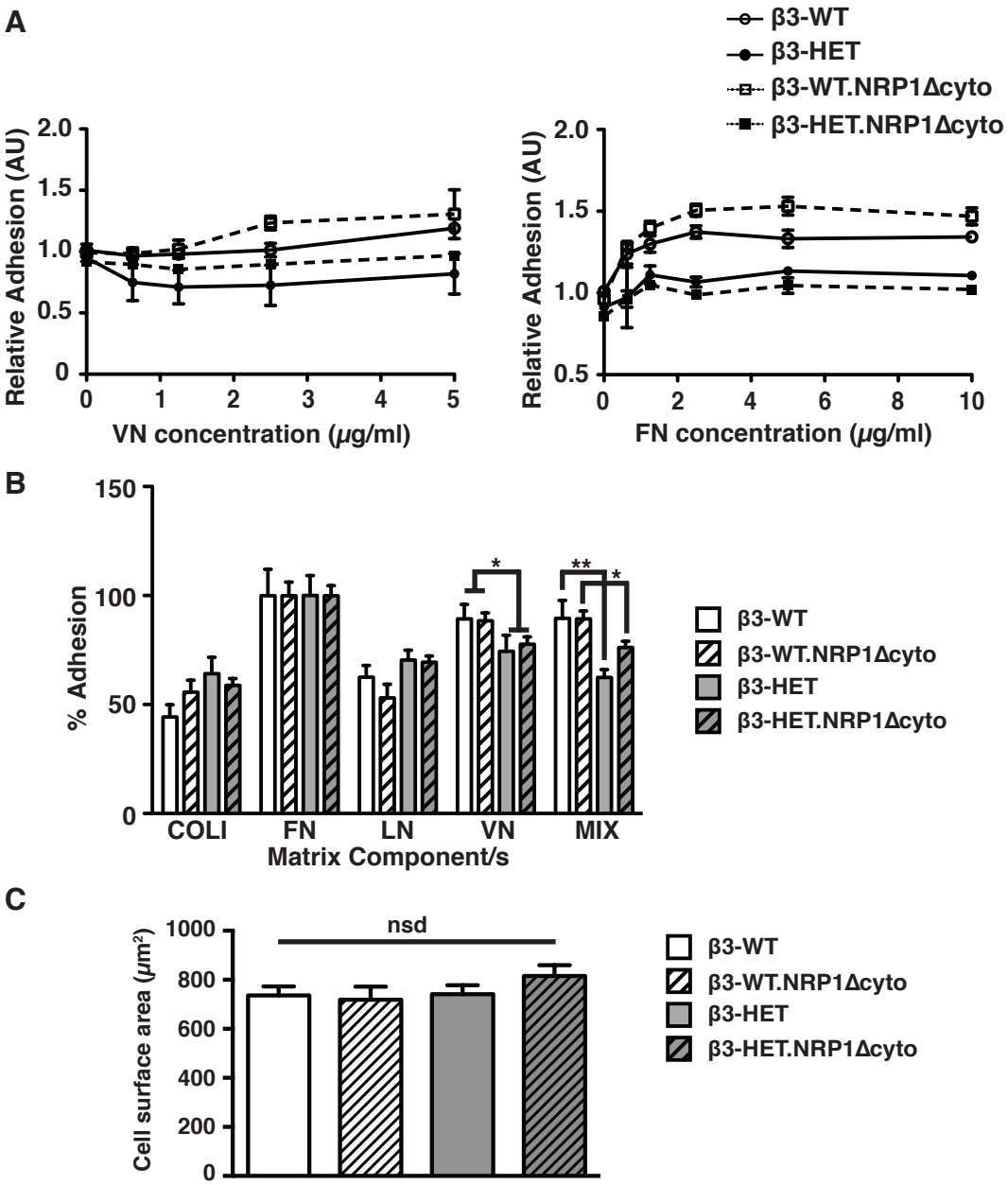

Figure 5.1: Examining adhesion and cell spreading properties of β3-integrin-wild-type and heterozygous endothelial cells with and without neuropilin-1's cytoplasmic tail. A ECs of the indicated genotypes were plated on increasing concentrations of FN or VN. After 90 minutes plates were washed and remaining cells were fixed and stained. Dye was extracted and measured spectophotometrically. The graph shows mean (±SEM) number of cells that remained attached to the plate after the procedure. **B** ECs of the indicated genotypes were seeded on collagen type I (COLI), fibronectin (FN), laminin (LN), vitronectin (VN), or a complex mixture of COLI, FN, VN and gelatin (MIX) for 90 minutes. Unattached cells were washed off, and the remaining cells were fixed and stained. Dye was extracted and measured spectophotometrically. The bar chart shows the percentage of cell adhesion to each component relative to FN (means +SEM from 3 independent experiments). **C** 70□10^5 cells of the indicated genotypes were plated for 6 hours on 10 μg/ml FN in 6-well plates. Phase contrast photographs were taken and cell surface areas were measured using ImageJ™ software. The bar chart represents mean (+SEM) surface area quantified from multiple images (n ≥ 50 cells per genotype). Asterisks indicate statistical significance: *, P<0.05; **, P<0.01; ***, P<0.001; nsd = not significantly different. Unpaired two-tailed t test.

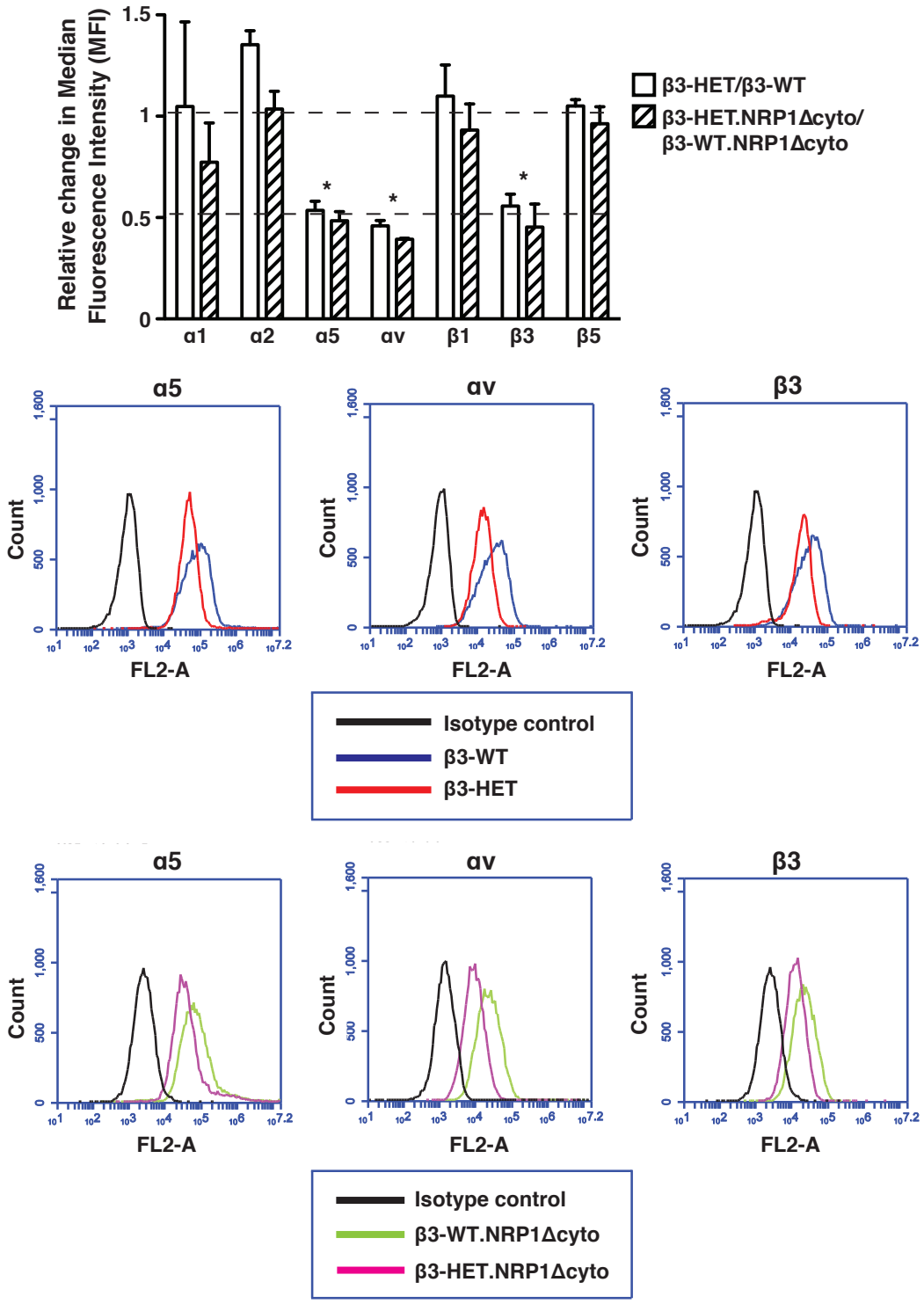

Figure 5.2: Examining surface levels of integrins in β3-integrin-wild-type and heterozygous endothelial cells with and without neuropilin-1's cytoplasmic tail. ECs of the indicated genotypes were measured for their surface expression of endothelial integrin subunits by flow-cytometry. Median fluorescence intensity (MFI) was measured after forward versus side scatter data were tightly gated around, and normalised to, an isotype control. The bar chart shows the relative change in MFI of β3-HET compared to β3-WT ECs or of β3-HET.NRP1Δcyto ECs compared to β3-WT.NRP1Δcyto ECs (means +SEM from 3 independent experiments). *Relative changes were deemed significant with a 2-fold change. Representative flow-cytometric histogram profiles are shown below for significantly changed integrins.

5.3 VEGF-induced migration in β3-integrin-heterozygous endothelial cells is dependent on neuropilin-1

It has been widely reported that targeting NRP1 in different ways reduces the migration of multiple EC types [68,272-275]. As EC migration is a key part of angiogenesis, we wanted to determine the effect of reduced β3 expression levels on EC migration in response to VEGF stimulation. Importantly, we wondered whether β3-WT and β3-HET EC migration are differentially affected by the loss of NRP1's cytoplasmic tail, as was the case for ERK1/2 phosphorylation, and therefore help explain our *in vivo* phenotypes.

Since NRP1, α5β1-integrin and αvβ3 all promote adhesion to FN [141,288], we set out to measure the migration of our four pMT EC lines on this matrix component, confident that our results would not be complicated by differences in cell spreading (see earlier). We examined both random (**Figure 5.3A**) and directed (**Figure 5.3B**) migration in cells following their long-term (ie. overnight) adhesion to a saturating concentration of FN. Both types of migration assays revealed enhanced baseline and VEGF-induced migration in β3-HET ECs, compared to β3-WT ECs. Unlike β3-WT ECs, β3-HET ECs were sensitive to NRP1 disruption, in a manner reminiscent of the tumour growth and angiogenesis phenotypes in mice of these genotypes. This therefore suggests that aberrant integrin-directed migration contributes to pathological angiogenesis in our models. Migration appears to be regulated by β3 expression levels, but, at least in these transgenic pMT microvascular ECs, is only dependent on NRP1's cytoplasmic tail when β3 levels are reduced.

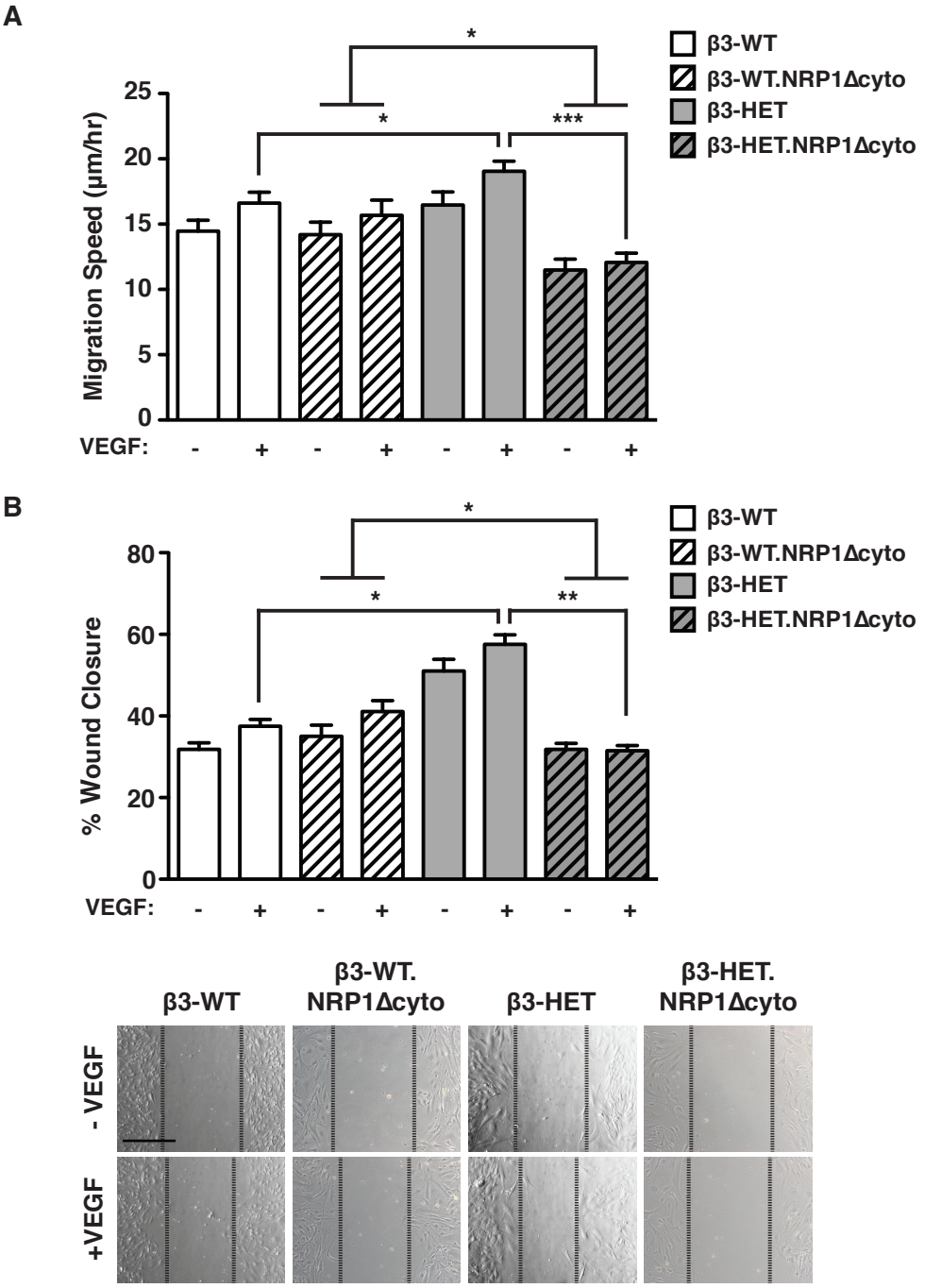

Figure 5.3: VEGF-induced migration in β3-integrin-heterozygous endothelial cells is dependent on neuropilin-1. A ECs were firmly attached to FN coated dishes and then imaged live for 15 hours in low serum medium ±VEGF. Individual cells were tracked every 10 minutes over this period using ImageJ™. The bar chart shows the EC migration speed of each of the indicated gentoypes (mean +SEM from 3 independent experiments; n=50 cells per condition). **B** ECs were plated onto FN coated dishes overnight. After 3 hours of starvation a scratch wound was created and cells were incubated in low serum medium ± VEGF for 24 hours. The bar chart shows the percentage closure of the scratch 'wound' as a result of directed cell migration (means +SEM from 3 independent experiments; n=27 for each condition). Representative images of scratch wound closure at 24 hours are shown below. Scale bar = 200μm. Asterisks indicate statistical significance: *, $P<0.05$; **, $P<0.01$; ***, $P<0.001$; nsd = not significantly different. Unpaired two-tailed *t* test.

5.4 Neuropilin-1's sub-cellular localisation is proportionally similar between β3-integrin-wild-type and heterozygous endothelial cells

Taking steps towards deciphering how β3 expression levels influence the sensitivity of EC migration to NRP1 perturbations, we first examined NRP1's distribution in subcellular compartments in β3-WT and β3-HET ECs after cell fractionation, looking for obvious signs of changes in NRP1 localisation (**Figure 5.4**). Immunoblotting for NRP1 and markers of the different fractions revealed no clear differences in NRP1 sub-cellular localisation between the ECs, other than the previously noted trend toward overexpression of the protein in β3-HET ECs.

5.5 Neuropilin-1's localisation at the ends of actin filaments is altered in stimulated β3-integrin-depleted endothelial cells

NRP1 is known to localise at adhesion sites, and co-associate with FA-associated proteins [271,288,289]. We therefore next immunolocalised NRP1 alongside filamentous (F)-actin staining in cells plated on FN overnight. These cells included our pMT β3-WT and β3-HET MLECs (**Figure 5.5A**) and primary MLECs that were isolated from β3-floxed-Pdgfb-iCreER^{T2}-negative (β3-WT) and -positive animals (**Figure 5.5B**), which were supplemented with OHT in culture to induce the depletion of β3 in the Cre-positive ECs (β3-EC-ID). In all of these ECs, the lack of VEGF-stimulation resulted in NRP1 localised to mature FA-like structures, which were found at the plus-ends of F-actin fibres. Whilst this localisation was maintained after VEGF stimulation in the pMT and primary β3-WT ECs, in VEGF-stimulated β3-HET and primary β3-EC-ID ECs, NRP1 only very rarely localised to these sites. These changes therefore intriguingly highlight a potential mechanism whereby β3 expression levels control NRP1's localisation to FA-like structures in a manner sensitive to VEGF stimulation.

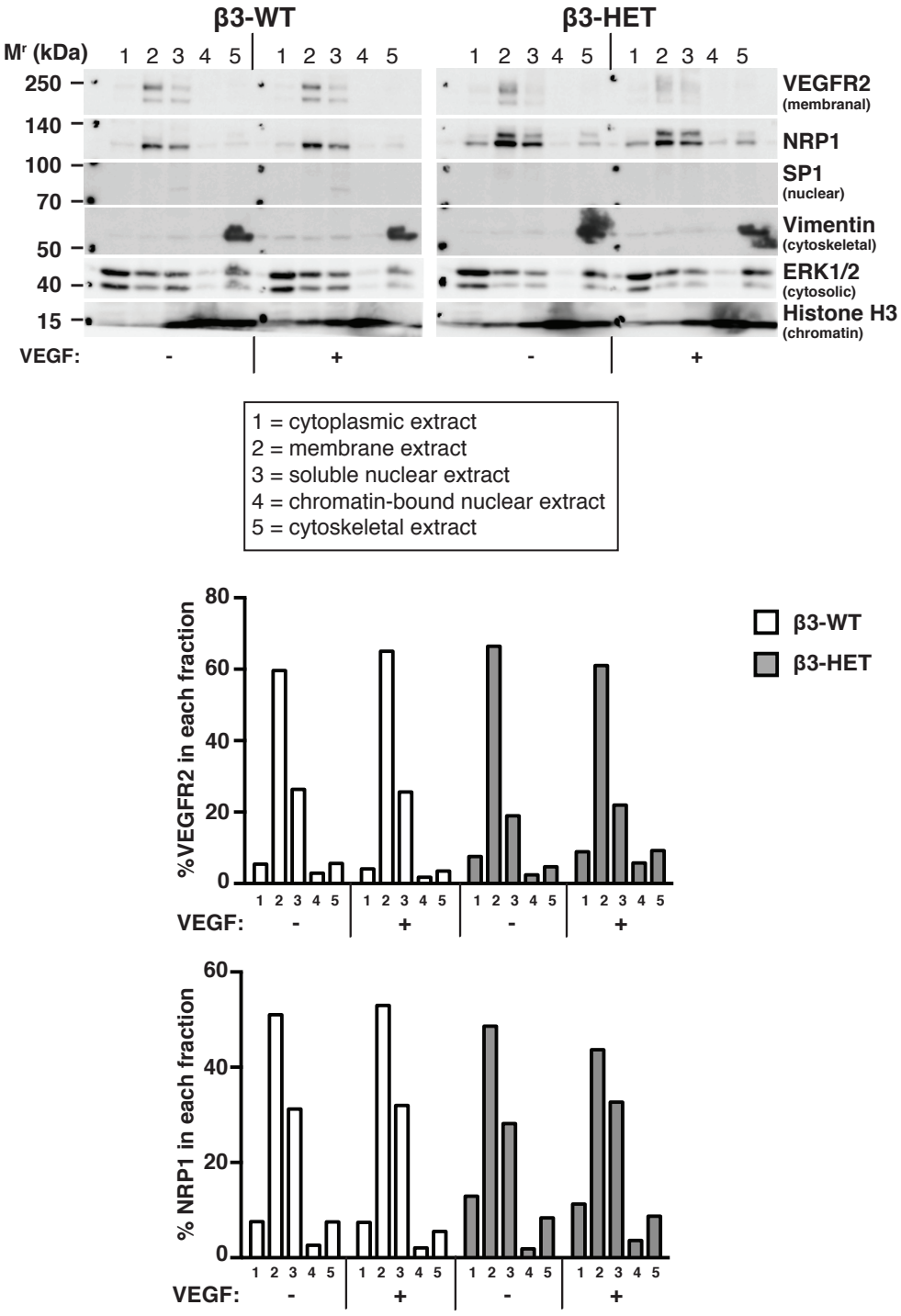

Figure 5.4: Neuropilin-1's sub-cellular localisation is proportionally similar between β3-integrin-wild-type and heterozygous endothelial cells. β3-WT and β3-HET ECs were subjected to a cell fractionation experiment following ±VEGF treatment for 10 minutes. Fractionated samples were then analysed by Western blot (WB) for the indicated proteins. 1=cytoplasmic extract; 2=membrane extract; 3=soluble nuclear extract; 4=chromatin-bound nuclear extract; 5=cytoskeletal extract. Protein markers for each sub-cellular compartment were included as controls. Data are representative of 2 independent experiments. The bar charts represent the relative proportion (%) of VEGFR2 or NRP1 present in each fraction determined by ImageJ™ densitometry.

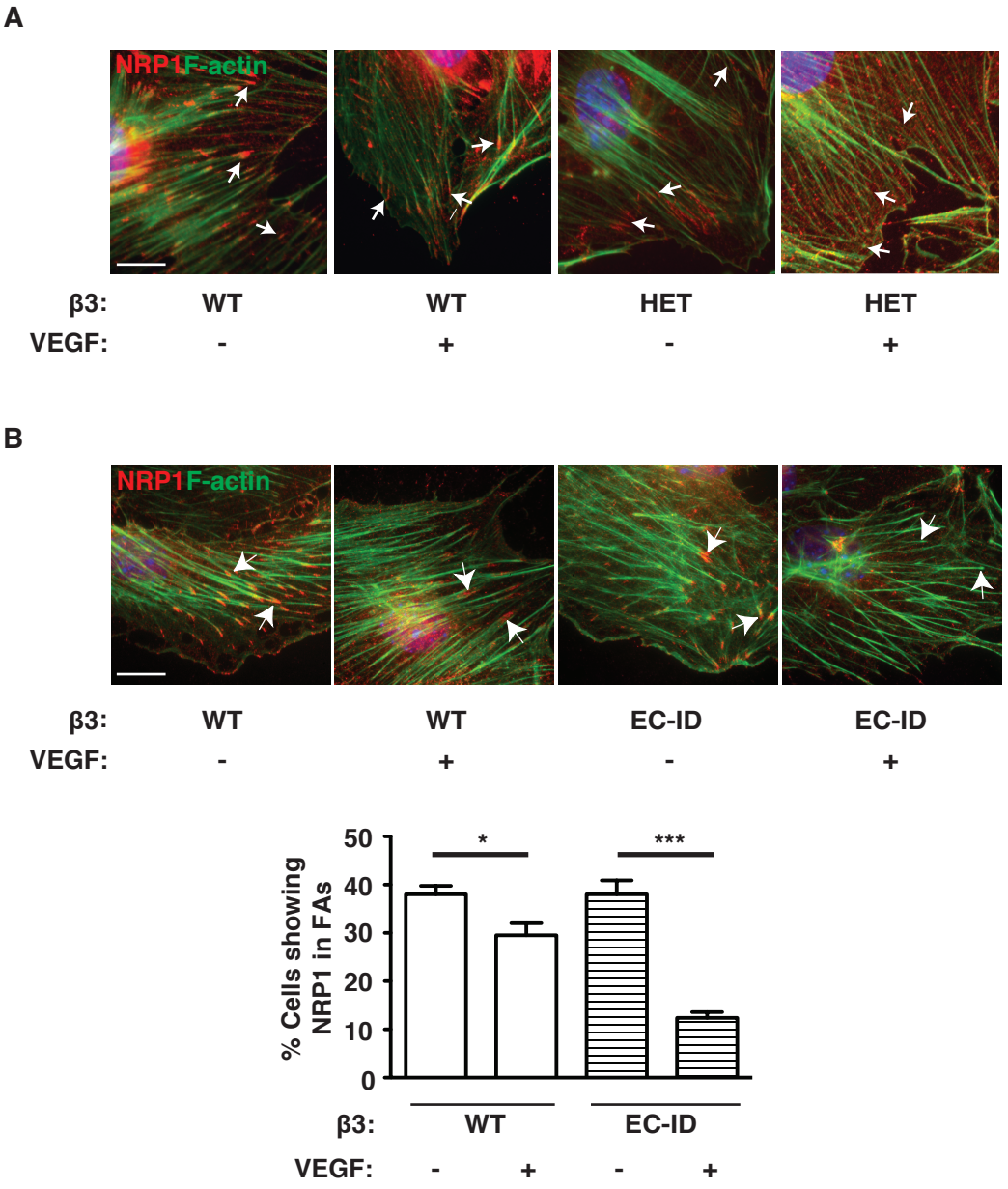

Figure 5.5: Neuropilin-1's localisation at the ends of actin filaments is altered in stimulated β3-integrin-depleted endothelial cells. ECs of the indicated genotypes were seeded overnight onto FN-coated glass coverslips, starved for 3 hours in serum-free medium, and stimulated with VEGF for 10 minutes. Cells were fixed and stained with phalloidin for filamentous actin (F-actin - green), and immunostained for neuropilin-1 (NRP1- red). White arrows point to the ends of actin filaments. **A** The above was carried out on β3-WT and β3-HET polyoma-middle-T-antigen-immortalised lung microvascular ECs. Scale bar = 20 μm. **B** The above was carried out on primary lung microvascular ECs that were isolated from β3-floxed-Pdgfb-iCreER^{T2}-negative and -positive animals. Tamoxifen (OHT) was administered after pure EC-populations were achieved to induce β3-integrin depletion (β3-EC-ID). Scale bar = 20 μm. The bar chart shows the percentage of cells within the population showing NRP1 staining at the end of actin filaments (mean +SEM; n≥50 cells per condition).

5.6 β3-integrin and neuropilin-1 co-localise in the same structures, but their interaction is weak

Given this β3-regulated effect on NRP1 localisation we wondered whether β3 is also present in the same FA-like structures, so we set about immunolocalising β3 and NRP1 in our ECs. Unfortunately, antibodies raised against β3 produced a lot of background signal (even in β3-NULL cells, not shown), so instead we transfected β3-WT ECs with a GFP-tagged β3-integrin cDNA expression construct and plated them on FN overnight (**Figure 5.6A**). NRP1 did indeed co-localise with β3 in FA-like structures in these ECs.

β3 and NRP1 were previously shown to co-associate in HUVECs in a manner that was enhanced by VEGF stimulation [202]. Here, we examined their co-association in β3-WT and β3-HET pMT ECs using an IP of NRP1 (**Figure 5.6B**) and of β3 (**Figure 5.6C**) to detect co-immunoprecipitation (co-IP) in both directions. Using the NRP1 IP we detected an association with β3, albeit a weak one, which did not appear to change in β3-WT ECs with VEGF stimulation or between unstimulated β3-WT and β3-HET ECs, taking the overexpression of NRP1 and reduced expression of β3 in β3-HET ECs into account. However, NRP1-β3 co-IP looks slightly reduced in the β3-HET sample following VEGF stimulation. When the β3 IP was used, we observed a slight increase in β3's association with NRP1 following VEGF stimulation in β3-WT ECs, but again found VEGF to cause a reduced association between the molecules in β3-HET samples. These results are suggestive of a VEGF-dependent reduction in interactions between β3 and NRP1 only in β3-HET ECs, and are therefore in synchronisation with our immunolocalisation studies. However, IP co-association of the molecules was weak in both directions and changes were only subtle, suggesting that the interaction between them is not direct. Moreover, trends between β3-WT and β3-HET samples are difficult to interpret given the overexpression of NRP1 in β3-HET ECs.

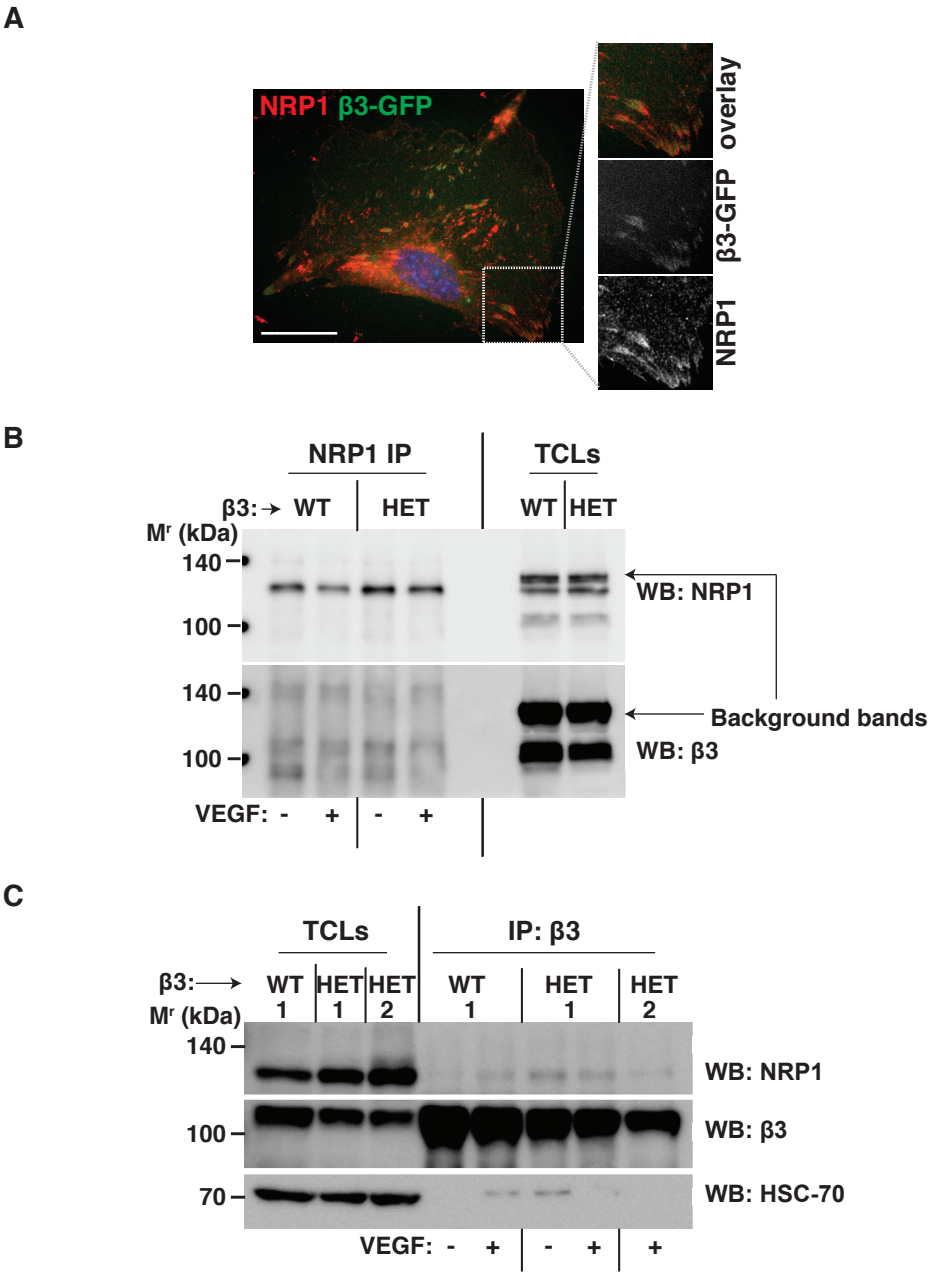

Figure 5.6: β3-integrin and neuropilin-1 co-localise in the same structures, but their interaction is weak. A β3-WT ECs were transfected with a β3-integrin-GFP construct (green) and seeded on FN-coated coverslips. 48 hours later, cells were fixed and immunostained for NRP1 (red). Split channel close-ups are shown to depict β3-integrin/NRP1 co-localisation. Scale bars = 10 μm. **B,C** β3-WT and β3-HET ECs were seeded overnight on a complex matrix containing gelatin, collagen, fibronectin and vitronectin, and were then stimulated with VEGF and lysed and immunoprecipitated for: **B** NRP1 (NRP1 IP), before blotting for β3 association, or **C** β3 (β3 IP), before blotting for NRP1 association. Total cell lysates (TCLs) are shown as controls, and HSC-70 served as a loading control. NB: In **B**, β3 was immunoblotted before NRP1, which explains why the β3, and β3 background, bands are present on the NRP1 WB. In **C**, 2 separate isolates of β3-HET ECs stimulated with VEGF were IP'd (HET 1 and 2).

5.7 Myosin 9 co-associates with neuropilin-1 less in β3-heterozygous endothelial cells

Due partly to the weakness of β3-NRP1 associations, which may suggest an indirect interaction between the two molecules, and partly to our desire to explore NRP1's protein associations when there are different β3 expression levels, we decided to use proteomics to examine NRP1's binding partners in β3-WT and β3-HET EC samples in an unbiased way. We wondered whether we could identify proteins whose association with NRP1 changes between the samples upon VEGF stimulation in a way that reflects β3's supposed regulation of NRP1 localisation to FA-like structures. Using an anti-NRP1 antibody (raised against NRP1's cytoplasmic tail), we immunoprecipitated NRP1 in unstimulated (-V) and VEGF-stimulated (+V) β3-WT and β3-HET ECs and, after confirming the uniform efficiency of the IPs between samples by silver staining them following their separation by SDS-PAGE (**Figure 5.7A**), we subjected these samples to 1D nano liquid chromatography tandem mass spectrometry (1D nLC-MS/MS). To compare the effect of VEGF stimulation on NRP1's protein associations between β3-WT and β3-HET ECs, we ordered our results by the fold change between the ratios of β3-WT+V/-V and β3-HET+V/-V Mascot protein scores (**Table 5.1**). Though this is not quantitative data, we still get a general idea of the number of peptide hits in each sample. Unexpectedly, we did not find many NRP1-binding proteins that are associated with focal adhesions. However, after we had carried out this experiment, Seerapu et al. [289] published a study in which LC-MS/MS was used to identify NRP1's protein associations in murine heart ECs. Here, a different anti-NRP1 antibody (raised against NRP1's extracellular portion) was used to IP NRP1, and FA proteins were identified, such as filamin a, which directly interacted with NRP1 via its cytoplasmic tail [289]. We therefore surmised that by using an anti-NRP1 antibody targeted against the cytoplasmic tail, interactions at this part of the molecule may be masking the ability of the antibody to bind NRP1, especially as we had previously used the anti-NRP1 antibody that Seerapu et al. [289] used to immunolocalise NRP1 in FA-like structures. We therefore decided to repeat our experiment with this other antibody (NB: proteins in **bold** in **Tables 5.1** and **5.2** are present in both experiments). However, before attempting this, we did note that, like in Seerapu et al.'s [289] study, our NRP1-associated protein data included the NM-IIA and NM-IIB heavy chain proteins,

myosin 9 and myosin 10, both of which had very high Mascot scores that were not only reduced in the β3-HET samples relative to those of β3-WT, but were raised after VEGF stimulation to a much lower degree in the β3-HET sample compared to the β3-WT sample. This trend in NRP1-myosin 9 association was subsequently confirmed by co-IP (**Figure 5.7B**). Since NM-II proteins are involved in the force generation associated with mature FAs, the reduction in NRP1-myosin 9 assocation in VEGF-stimulated β3-HET ECs compared to stimulated β3-WT ECs does loosely connect with NRP1's change in localisation away from FA-like structures in the stimulated β3-HET cells. However, since the level of NRP1-myosin 9 association does not change much between unstimulated and stimulated β3-HET ECs, this phenomenon does not appear to tell the whole story.

Table 5.1: Mass spectrometry results of neuropilin-1-immunoprecipitated β3-WT and β3-HET endothelial cell samples (first experiment).

Gene	Protein	Mass spectrometry Mascot score normalised to that of NRP1						
		WT-V	WT+V	HET-V	HET+V	WT+V/ WT-V	HET+V/ HET-V	Fold change HET/WT
Sfpq	Splicing factor, proline- and glutamine-rich	0.46	0.07	0.49	0.38	0.15	0.78	5.06
Rnp1	RNA recognition motif, RNP-1; Heterogeneous nuclear ribonucleoprotein M	0.52	0.14	0.56	0.48	0.27	0.86	3.18
Nono	Isoform 1 of Non-POU domain-containing octamer-binding protein	0.32	0.08	0.37	0.26	0.26	0.69	2.65
Ei3e	Eukaryotic translation initiation factor 3 subunit E	0.17	0.09	0.25	0.36	0.54	1.43	2.64
Ei4g1	Isoform 1 of Eukaryotic translation initiation factor 4 gamma 1	0.60	0.28	0.86	0.94	0.47	1.08	2.31
Ei3c	Eukaryotic translation initiation factor 3 subunit C	0.44	0.33	0.42	0.58	0.75	1.41	1.89
Hnrnph1	Heterogeneous nuclear ribonucleoprotein H	0.43	0.26	0.31	0.34	0.60	1.10	1.83
Dhx9	Isoform 1 of ATP-dependent RNA helicase A	0.17	0.14	0.23	0.32	0.80	1.39	1.73
Pcbp2	poly(rC)-binding protein 2 isoform 4	0.13	0.08	0.24	0.23	0.63	0.97	1.53
G3bp1	Ras GTPase-activating protein-binding protein 1	0.39	0.31	0.46	0.57	0.80	1.22	1.52
Ddx1	ATP-dependent RNA helicase DDX1	0.38	0.33	0.56	0.72	0.87	1.29	1.49
Ei3h	Eukaryotic translation initiation factor 3 subunit H	0.27	0.22	0.22	0.27	0.82	1.21	1.47
Prrc2a	protein PRRC2A isoform 2	0.17	0.10	0.25	0.20	0.56	0.82	1.45
Rps3	40S ribosomal protein S3	0.30	0.27	0.27	0.35	0.91	1.31	1.44
Rpsa	40S ribosomal protein SA	0.22	0.22	0.16	0.22	0.99	1.41	1.42
Fam120a	Constitutive coactivator of PPAR-gamma-like protein 1	0.54	0.47	0.53	0.65	0.87	1.23	1.41
Myl12a	**myosin light chain, regulatory B-like**	0.27	0.38	0.07	0.14	1.40	1.91	1.37
Fam83d	Isoform 1 of Protein FAM83D	0.27	0.29	0.17	0.25	1.07	1.46	1.36
Hnrnpa1	Isoform Long of Heterogeneous nuclear ribonucleoprotein A1	0.20	0.17	0.17	0.19	0.82	1.10	1.34
Ybx1	Nuclease-sensitive element-binding protein 1	0.33	0.21	0.29	0.25	0.64	0.85	1.33
Gulp1	Isoform 1 of PTB domain-containing engulfment adapter protein 1	0.25	0.26	0.20	0.27	1.03	1.36	1.33
Hsp90ab1	Heat shock protein HSP 90-beta	0.17	0.20	0.09	0.14	1.20	1.58	1.32
Caprin1	caprin-1 isoform c	0.35	0.30	0.46	0.51	0.85	1.10	1.30
Eps15	Isoform 1 of Epidermal growth factor receptor substrate 15	0.52	0.67	0.17	0.29	1.29	1.66	1.29
Rplp0	**60S acidic ribosomal protein P0**	0.18	0.19	0.10	0.13	1.06	1.35	1.28
Fxr1	Isoform C of Fragile X mental retardation syndrome-related protein 1	0.71	0.54	0.67	0.65	0.76	0.97	1.27
Rnp1	RNA recognition motif, RNP-1; Poly-adenylate binding protein, unique domain	0.61	0.55	0.74	0.85	0.90	1.15	1.27
Igf2bp2	Isoform 1 of Insulin-like growth factor 2 mRNA-binding protein 2	0.23	0.24	0.28	0.37	1.06	1.33	1.26

Ei3b	Eukaryotic translation initiation factor 3 subunit B	0.23	0.24	0.29	0.38	1.05	1.32	1.26
Usp10	Isoform 1 of Ubiquitin carboxyl-terminal hydrolase 10	0.25	0.19	0.33	0.30	0.73	0.91	1.24
Mov10	Putative helicase MOV-10	0.40	0.34	0.53	0.55	0.84	1.04	1.23
Rps15a	40S ribosomal protein S15a	0.13	0.23	0.13	0.28	1.70	2.09	1.23
Dhx29	ATP-dependent RNA helicase Dhx29	0.13	0.11	0.32	0.34	0.89	1.08	1.22
Prrc2b	protein PRRC2B isoform 1	0.24	0.24	0.24	0.29	0.99	1.19	1.21
Ei2s1	Eukaryotic translation initiation factor 2 subunit 1	0.18	0.18	0.20	0.25	1.04	1.26	1.21
Rtcb	tRNA-splicing ligase RtcB homolog	0.35	0.37	0.50	0.64	1.06	1.28	1.21
Elavl1	ELAV-like protein 1	0.24	0.27	0.31	0.41	1.11	1.33	1.20
Eif3i	Eukaryotic translation initiation factor 3 subunit I	0.15	0.17	0.15	0.19	1.12	1.30	1.17
Pabp1	Polyadenylate-binding protein 1	1.20	1.07	1.28	1.31	0.89	1.03	1.16
Rhamm1, Hmmr	Isoform RHAMM1 of Hyaluronan mediated motility receptor	0.37	0.53	0.29	0.46	1.46	1.59	1.09
Ddx5	Probable ATP-dependent RNA helicase DDX5	0.26	0.31	0.28	0.36	1.19	1.28	1.08
Paics	Multifunctional protein ADE2	1.47	1.60	0.78	0.90	1.09	1.15	1.06
Upf1	Isoform 1/2 of Regulator of nonsense transcripts 1	0.96	0.89	1.05	1.02	0.92	0.98	1.06
Tubb5	**Tubulin beta-5 chain**	0.18	0.27	0.14	0.21	1.51	1.56	1.03
Ap1b1	AP-1 complex subunit beta-1	0.80	1.21	0.52	0.81	1.52	1.55	1.02
Nrp1	**Neuropilin-1**	1.00	1.00	1.00	1.00	1.00	1.00	1.00
Ap2a1	Isoform B of AP-2 complex subunit alpha-1	1.93	2.44	1.02	1.28	1.27	1.25	-1.02
Hspa5, Grp78	78 kDa glucose-regulated protein	0.17	0.21	0.19	0.24	1.27	1.24	-1.02
Rps19	40S ribosomal protein S19	0.12	0.12	0.19	0.18	0.99	0.93	-1.07
Eif2s2	Eukaryotic translation initiation factor 2 subunit 2	0.15	0.21	0.18	0.24	1.42	1.33	-1.07
Ap2b1	Isoform 1 of AP-2 complex subunit beta	1.78	2.54	1.21	1.61	1.43	1.33	-1.07
Nufip2	Isoform 1 of Nuclear fragile X mental retardation-interacting protein 2	0.50	0.39	0.50	0.36	0.77	0.72	-1.07
Rps17	40S ribosomal protein S17	0.10	0.10	0.18	0.16	0.97	0.90	-1.08
Eif3d	Eukaryotic translation initiation factor 3 subunit D	0.32	0.40	0.34	0.40	1.26	1.15	-1.09
Ddx6	Probable ATP-dependent RNA helicase DDX6	0.14	0.23	0.27	0.39	1.60	1.45	-1.10
Eif3m	Eukaryotic translation initiation factor 3 subunit M	0.20	0.27	0.17	0.20	1.35	1.20	-1.12
Eif3l	Eukaryotic translation initiation factor 3 subunit L	0.31	0.38	0.43	0.48	1.25	1.11	-1.12
Cltc	**Clathrin heavy chain 1**	1.00	1.13	0.46	0.45	1.13	0.99	-1.14
Tbk1	Serine/threonine-protein kinase TBK1	0.48	0.68	0.27	0.33	1.43	1.25	-1.14
Reps1	Isoform 1 of RalBP1-associated Eps domain-containing protein 1	0.49	0.82	0.25	0.35	1.68	1.41	-1.19
Ddx3x	ATP-dependent RNA helicase DDX3X	0.37	0.50	0.52	0.56	1.34	1.09	-1.23

Arhgap29	Isoform 1 of Rho GTPase-activating protein 29	0.18	0.39	0.13	0.22	2.09	1.68	-1.25
Ap2m1	AP-2 mu	0.87	1.38	0.54	0.68	1.59	1.27	-1.25
Tbkbp1	Isoform 2 of TANK-binding kinase 1-binding protein 1	0.17	0.18	0.16	0.12	1.01	0.78	-1.29
C14orf166	UPF0568 protein C14orf166 homolog	0.16	0.25	0.30	0.35	1.55	1.17	-1.33
Hnrnpf	Isoform 1 of Heterogeneous nuclear ribonucleoprotein F	0.26	0.31	0.24	0.21	1.22	0.87	-1.39
Ap2a2	AP-2 complex subunit alpha-2	1.39	2.29	0.82	0.90	1.65	1.09	-1.51
Rps3a	**40S ribosomal protein S3a**	0.22	0.33	0.30	0.29	1.46	0.95	-1.54
Gapdh	**Glyceraldehyde-3-phosphate dehydrogenase**	0.23	0.37	0.21	0.20	1.56	0.93	-1.67
Carm1	Isoform 2 of Histone-arginine methyltransferase CARM1	0.19	0.27	0.13	0.11	1.43	0.80	-1.79
Actg1	**Actin, cytoplasmic 2**	1.61	3.52	0.81	0.98	2.19	1.21	-1.80
Myh9	**Myosin-9**	4.40	13.92	1.81	3.06	3.17	1.69	-1.87
Shank3	SH3 and multiple ankyrin repeat domains protein 3	0.16	0.36	0.10	0.11	2.16	1.08	-1.99
Tardbp, Tdp43	TAR DNA-binding protein 43	0.17	0.30	0.17	0.15	1.81	0.88	-2.05
FLJ45252	Uncharacterized protein FLJ45252 homolog	0.35	0.38	0.23	0.11	1.09	0.49	-2.21
Myh10	**Myosin-10**	1.10	5.08	0.40	0.72	4.61	1.83	-2.53
Msn	Moesin	0.13	0.42	0.12	0.15	3.34	1.25	-2.67
Fscn	Fascin	0.07	0.26	0.13	0.16	3.46	1.29	-2.67
Myo1c	**Isoform 1 of Myosin-Ic**	0.61	1.66	0.38	0.35	2.70	0.92	-2.94
Rasip1	**Ras-interacting protein 1**	0.17	0.40	0.13	0.08	2.32	0.63	-3.67
Ckap4	Cytoskeleton-associated protein 4	0.08	0.31	0.07	0.06	3.79	0.95	-4.01
Gsn	**Isoform 2 of Gelsolin**	0.09	0.68	0.05	0.04	7.73	0.74	-10.38
Aak1	Isoform 1 of AP2-associated protein kinase 1	0.50	0.84		0.30	1.68		
Ago2	Protein argonaute-2		0.16	0.36	0.41		1.12	
Anxa2	**Annexin A2**		0.35	0.13	0.15		1.21	
Ap2s1	AP-2 complex subunit sigma	0.19	0.23	0.11		1.21		
Ascc3	Activating signal cointegrator 1 complex subunit 3 isoform 2	0.08		0.19	0.14		0.76	
Atxn2l	Isoform 2 of Ataxin-2-like protein	0.24		0.36	0.29		0.80	
Ddx17	Isoform 1 of Probable ATP-dependent RNA helicase DDX17	0.22		0.21	0.27		1.26	
DHX15	putative pre-mRNA-splicing factor ATP-dependent RNA helicase DHX15 isoform 1	0.11		0.20	0.19		0.93	
Eif2s3x	Eukaryotic translation initiation factor 2 subunit 3, X-linked			0.23	0.25		1.09	
Eif3a	Eukaryotic translation initiation factor 3 subunit A	0.38		0.63	0.77		1.23	
Eif4a1	Eukaryotic initiation factor 4A-I	0.19		0.19	0.33		1.71	
Eif4a2	Isoform 1 of Eukaryotic initiation factor 4A-II	0.19		0.17	0.25		1.46	

Eif4a3	Eukaryotic initiation factor 4A-III	0.25		0.23	0.26		1.15
Eif4g2	Eukaryotic translation initiation factor 4 gamma 2 isoform 2	0.23	0.16		0.53	0.69	
Eif4g3	Isoform 4 of Eukaryotic translation initiation factor 4 gamma 3	0.15		0.42	0.41		0.99
Eps15l1	Isoform 3 of Epidermal growth factor receptor substrate 15-like 1	0.26			0.16		
FAM98A	Protein FAM98A	0.08		0.28	0.38		1.35
Fmr1	Isoform ISO3 of Fragile X mental retardation protein 1 homolog		0.27	0.36	0.48		1.33
G3bp2	Isoform A of Ras GTPase-activating protein-binding protein 2	0.27		0.31	0.35		1.12
Gnb2l1	Guanine nucleotide-binding protein subunit beta-2-like 1			0.15	0.19		1.25
Hdlbp	Vigilin			0.20	0.11		0.53
Hnrnpa2b1	Isoform 3 of Heterogeneous nuclear ribonucleoproteins A2/B1	0.15		0.24	0.30		1.25
Hnrnph2	Heterogeneous nuclear ribonucleoprotein H2	0.32		0.20	0.23		1.14
Larp1	Isoform 1 of La-related protein 1	0.17		0.32	0.39		1.20
Larp4	La-related protein 4			0.23	0.20		0.86
Mmrn2	Isoform 1 of Multimerin-2	0.34	0.49			1.46	
Prrc2c	Isoform 5 of Protein PRRC2C	0.19		0.29	0.33		1.13
Pura	Transcriptional activator protein Pur-alpha	0.20		0.15	0.09		0.63
Rbm14	Isoform 1 of RNA-binding protein 14	0.17		0.19	0.10		0.51
Rps18	40S ribosomal protein S18		0.20	0.22	0.28		1.27
Rps5	40S ribosomal protein S5	0.22		0.18	0.20		1.10
Rps6	40S ribosomal protein S6	0.07		0.22	0.15		0.68
Rps8	40S ribosomal protein S8	0.20		0.25	0.27		1.07
Rrbp1	Isoform 3 of Ribosome-binding protein 1	0.20		0.16	0.12		0.75
Spag9	Isoform 2 of C-Jun-amino-terminal kinase-interacting protein 4	0.36	0.48			1.31	
Synj1	Synaptojanin-1 isoform a	0.27	0.30			1.10	
Tdrd3	Isoform 2 of Tudor domain-containing protein 3	0.25	0.11		0.30	0.42	
Tmod3	**Tropomodulin-3**	0.06	0.35			5.51	
Top3b	DNA topoisomerase 3-beta-1			0.26	0.29		1.13
Tpm3	**Isoform 2 of Tropomyosin alpha-3 chain**	0.07	0.72		0.08	10.44	
Tpm4	**Tropomyosin alpha-4 chain**	0.06	0.38			6.08	
Ybx3	Y-box-binding protein 3	0.14		0.19	0.20		1.06
Zc3h7a	Zinc finger CCCH-type containing 7A	0.21		0.21			
Zo1	Tight junction protein ZO-1 isoform 2		0.30	0.03			

NB: **Genes/proteins in bold = also present in second NRP1 IP mass spectrometry experiment.** Genes/proteins underlined = of special interest.

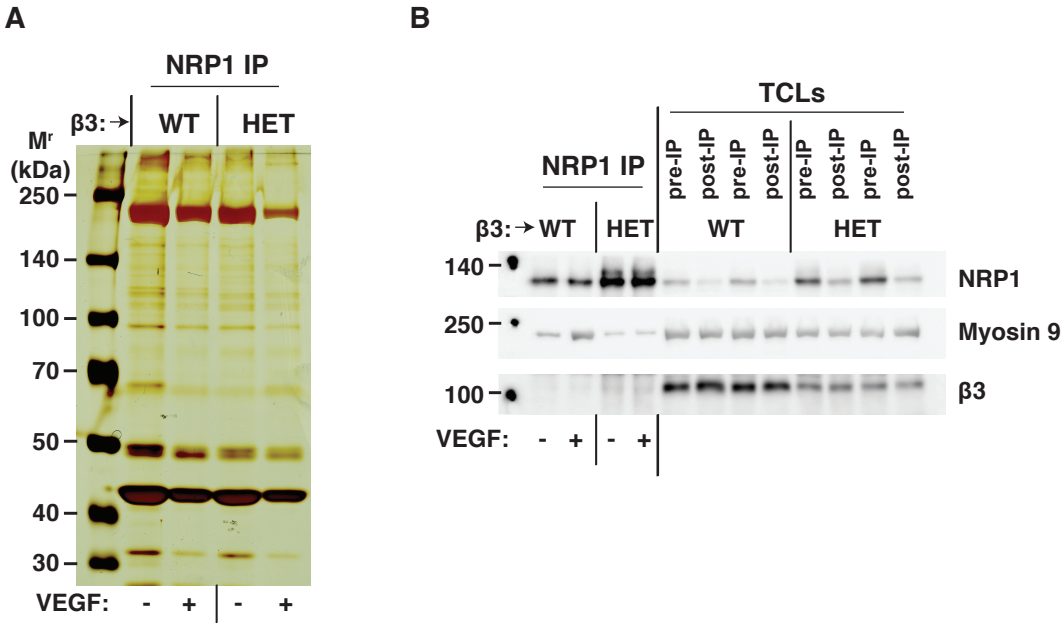

Figure 5.7: Myosin 9 confirmed to co-associate with neuropilin-1 less in β3-heterozygous endothelial cells. A β3-WT and β3-HET ECs were seeded overnight on fibronectin, treated ±VEGF, and lysed and immunoprecipitated for NRP1 (NRP1 IP). IP'd samples were separated by SDS-PAGE for **A** Silver staining, and **B** Western blotting. Total cell lysates taken before the IP (pre-IP) and after the IP (post-IP) are shown as controls to confirm the efficiency of the IP.

5.8 Many of the proteins that are appear differentially associated with NRP1 between β3-wild-type and β3-heterozygous endothelial cells are related to the cytoskeleton

We set about repeating the proteomic analysis of NRP1-associated proteins by immunoprecipitating NRP1 in unstimulated (-V) and VEGF-stimulated (+V) β3-WT and β3-HET ECs using the anti-NRP1 antibody from Seerapu et al.'s [289] study. This time, after confirming the uniform efficiency of the IPs between samples by silver staining (not shown), the samples were subjected to label-free quantitative mass spectrometry in order to more accurately compare data between samples. Results were ordered by the fold change between the ratios of β3-WT+V/-V and β3-HET+V/-V label-free quantification (LFQ) values to compare the effect of VEGF stimulation on NRP1's protein associations between β3-WT and β3-HET ECs (**Table 5.2**). LFQ values were also hierarchically clustered to group NRP1-associated proteins that appeared between samples in similar trends (**Figures 5.8** and **5.9**).

In contrast with our previous mass spectrometry experiment, this time we were able to detect many of the proteins reported to associate with NRP1 by Seerapu et al. [289], including myosin 9, myosin 10, filamin a, α-enolase, and eukaryotic elongation factor 1 α1 (underlined in **Table 5.2**). We also identified NRP1-associated proteins that were present in both of our mass spectrometry experiments that used different anti-NRP1 antibodies for NRP1 immunoprecipitation, noting similar trends between samples for almost all of them (**Table 5.3**).

From the hierarchical clustering analysis we noticed that many of the proteins that appear differentially associated with NRP1 between β3-WT and β3-HET ECs are functionally related to the cytoskeleton (**Figures 5.9A-E**). To our surprise, in complete contrast with the first experiment, myosin 10 appeared to associate with NRP1 more in the β3-HET samples (**Figure 5.9A**). However, the trend in myosin 9-NRP1 associations between samples was similar to that observed previously, and clustering revealed a number of other proteins associating with NRP1 in a similar pattern (ie. reduced NRP1 associations in β3-HET ECs) (**Figure 5.9B**). These included some that we identified in the previous experiment, such as Ras

interacting protein 1, actin cytoplasmic 2, unconventional myosin 1c, and tropomodulin-3, as well as various other actin- and myosin-related proteins.

Of particular interest to us were clustered groups that show proteins that appear to associate with NRP1 much less in VEGF-stimulated β3-HET ECs (**Figures 5.9C-D**). This included the FA protein filamin a, a result that is congruent with NRP1's localisation away from FA-like structures in stimulated β3-HET ECs. Also reduced in stimulated β3-HET EC samples was IQGAP1, which, along with filamin a, has previously been implicated in Rac1 deactivation at β1-integrin activation sites to regulate cell migration [243].

We further noted NRP1-associated proteins that were different upon VEGF stimulation in both β3-WT and β3-HET ECs (**Figures 5.9F-H**). Amongst these was α-enolase, which, like that previously reported, more prevalently bound to NRP1 in stimulated ECs [289], although this effect was slightly dampened in β3-HET samples.

We conclude that reduced β3 expression causes changes in NRP1's association with many proteins and is further influenced by VEGF stimulation. Almost all of the proteins identified associate with NRP1 less in β3-HET ECs, and most that have a clear trend in reduced NRP1 associations in both β3-HET samples are actin- and myosin-related proteins. Myosin 10 and myosin 9 are part of different NM-II molecules that play distinct, but complementary roles in coordinating cell migration [244]. Since myosin 10, which is involved in the stabilisation and contraction of actin stress fibres, is increased in β3-HET samples, whilst myosin 9, which is more involved in FA formation, is decreased, it is possible that this misbalance in association with NRP1 contributes to the enhanced migration of β3-HET ECs that is sensitive to NRP1 disruption. However, the change in myosin 10 was opposite to that observed in the previous experiment, and the lack of a clear difference in NRP1's association with these molecules between unstimulated and stimulated β3-HET samples does not reflect NRP1's immunolocalisation phenotype. The FA proteins filamin a and IQGAP1 associate with NRP1 in a way more fitting with NRP1's localisation away from FA-like structures in stimulated β3-HET ECs, since they are both reduced in these

samples. As both filamin a and IQGAP1 are involved in regulating cell migration through Rac1 deactivation [243], it is possible that NRP1's association with them is important in dictating EC migration outcome, thus presenting a possible reason why NRP1 becomes more targetable when β3 expression is reduced. Overall, these observations, coupled with the changes in NRP1's mobilisation away from the ends of actin filaments upon VEGF-stimulation, suggest that β3 regulates NRP1's localisation to, and association with, components of the cytoskeleton.

Table 5.2: Quantitative mass spectrometry results of neuropilin-1-immunoprecipitated β3-WT and β3-HET endothelial cell samples (second experiment).

Gene	Protein	LFQ value normalised to that of NRP1						
		WT-V	WT+V	HET-V	HET+V	WT+V/ WT-V	HET+V/ HET-V	Fold change HET/WT
Gng5	Guanine nucleotide-binding protein	0.23	0.12	0.03	0.05	0.50	1.53	3.06
Tpm4	**Tropomyosin alpha-4 chain**	0.54	0.21	0.11	0.13	0.38	1.12	2.94
Tpm3	**Tropomyosin alpha-3 chain**	1.82	1.33	0.34	0.58	0.73	1.73	2.37
Zo2	Tight junction protein ZO-2	0.33	0.11	0.08	0.06	0.33	0.74	2.23
Gapdh	**Glyceraldehyde-3-phosphate dehydrogenase**	0.50	0.53	0.36	0.70	1.07	1.94	1.81
Myl6	Myosin light polypeptide 6	1.97	1.60	0.68	0.99	0.81	1.45	1.79
Tpm1	Tropomyosin alpha-1 chain	0.39	0.36	0.09	0.13	0.93	1.43	1.55
Myh14	Isoform 2 of Myosin-14	5.54	3.86	4.62	4.78	0.70	1.04	1.49
Grn	Granulins	0.73	0.60	0.47	0.52	0.83	1.13	1.35
Rpl13a	60S ribosomal protein L13a	0.10	0.06	0.04	0.03	0.61	0.77	1.27
Plec	Plectin	3.64	2.26	1.86	1.39	0.62	0.75	1.20
Krt71	Keratin, type II cytoskeletal 71	0.03	0.03	0.02	0.03	0.98	1.14	1.17
Sipa1	Signal-induced proliferation-associated protein 1	0.04	0.02	0.02	0.01	0.58	0.65	1.11
Capza2	Capza2 F-actin-capping protein subunit alpha 2	0.64	0.56	0.38	0.37	0.88	0.97	1.10
Myo1c	**Unconventional myosin-Ic**	0.78	0.71	0.38	0.37	0.90	0.99	1.09
Serpinh1	Serpin H1	0.13	0.09	0.18	0.13	0.67	0.71	1.07
Rasip1	**Ras-interacting protein 1**	0.06	0.05	0.04	0.03	0.76	0.81	1.07
Rplp0	**60S acidic ribosomal protein P0**	0.26	0.24	0.15	0.14	0.93	0.96	1.03
Myh10	**Myosin-10**	3.97	3.97	6.32	6.52	1.00	1.03	1.03
Rpl6	60S ribosomal protein L6	0.05	0.04	0.03	0.02	0.79	0.81	1.02
Cald1	Caldesmon 1	1.48	1.19	0.57	0.46	0.80	0.82	1.02
Tmod3	**Tropomodulin-3**	0.29	0.31	0.18	0.19	1.07	1.08	1.01
Dbn1	Isoform E2 of Drebrin	0.09	0.08	0.05	0.05	0.92	0.93	1.01
Nrp1	**Neuropilin-1**	1.00	1.00	1.00	1.00	1.00	1.00	1.00
Actg1	**Actin, cytoplasmic 2**	166.25	172.15	109.54	110.31	1.04	1.01	-1.03
Myl12a	**Myosin light chain, regulatory B-like**	1.53	2.25	0.58	0.82	1.47	1.42	-1.03
Capza1	Capza1 F-actin-capping protein subunit alpha 1	0.25	0.26	0.21	0.21	1.05	1.01	-1.04
Flii	Protein flightless-1 homolog	0.22	0.18	0.15	0.12	0.81	0.77	-1.05

Actc1	Actin, alpha cardiac muscle 1	2.37	3.72	0.65	0.96	1.57	1.47	-1.07
Actbl2	Beta-actin-like protein 2	38.52	41.16	21.77	20.61	1.07	0.95	-1.13
Capzb	F-actin-capping protein subunit beta	0.30	0.33	0.22	0.21	1.10	0.94	-1.18
Myh9	**Myosin-9**	226.75	246.90	159.30	146.76	1.09	0.92	-1.18
Myo6	Unconventional myosin-VI	0.05	0.05	0.05	0.04	0.95	0.77	-1.24
Rpl18	60S ribosomal protein L18	0.05	0.03	0.04	0.02	0.65	0.52	-1.25
Myo1b	Unconventional myosin-Ib	0.11	0.12	0.08	0.07	1.12	0.89	-1.26
Myo1e	Unconventional myosin-Ie	0.10	0.11	0.08	0.07	1.13	0.88	-1.28
Rpl7	60S ribosomal protein L7	0.07	0.06	0.05	0.03	0.91	0.63	-1.44
Rps3	**40S ribosomal protein S3**	0.11	0.18	0.05	0.05	1.70	1.17	-1.46
Flna	Filamin a	0.12	0.11	0.11	0.07	0.93	0.58	-1.59
Spnb2	Spectrin beta chain, non-erythrocytic 1	0.08	0.06	0.08	0.04	0.78	0.47	-1.66
Spna2	Spectrin alpha chain, non-erythrocytic 1	0.22	0.23	0.21	0.14	1.07	0.64	-1.67
Myo18a	Unconventional myosin-XVIIIa	0.48	0.47	0.54	0.28	0.97	0.52	-1.88
Iqgap1	Ras GTPase-activating-like protein IQGAP1	0.04	0.06	0.04	0.03	1.45	0.69	-2.09
Hspa5	78 kDa glucose-regulated protein	0.15	0.38	0.17	0.17	2.48	1.00	-2.47
Hspa8	Heat shock cognate 71 kDa protein	0.20	0.65	0.15	0.16	3.18	1.13	-2.82
Gsn	**Gelsolin**	0.02	0.09	0.03	0.02	3.68	0.85	-4.33
Tuba1b	Tubulin alpha-1B chain	0.15	0.68	0.16	0.17	4.46	1.02	-4.36
Eno1	Alpha-enolase	0.02	1.18	0.02	0.20	58.82	13.03	-4.51
Tubb5	**Tubulin beta-5 chain**	0.04	0.16	0.06	0.04	3.75	0.69	-5.40
Anxa2	**Annexin A2**	0.20	1.34	0.15	0.16	6.61	1.03	-6.40
Mtap4	Microtubule-associated protein 4	0.03	0.04	0.17	0.03	1.38	0.18	-7.54
Hsp90aa1	Heat shock protein HSP 90-alpha	0.03	0.31	0.03	0.03	8.97	1.18	-7.59
Eef1a1	Eukaryotic elongation factor 1-alpha 1	0.26	1.32	0.27	0.18	5.10	0.64	-7.93
Cfl1	Cofilin-1	0.01	0.16	0.01	0.01	12.15	1.07	-11.38
Lmna	Prelamin-A/C	0.02	0.81	0.01	0.02	32.79	2.01	-16.34
Jup	Junction plakoglobin	0.30	5.31	0.53	0.53	17.43	1.01	-17.29
Eef2	Elongation factor 2	0.03	0.51	0.03	0.03	19.87	1.13	-17.52
Uba52	Ubiquitin-60S ribosomal protein L40	0.17	1.82	0.26	0.13	11.01	0.48	-22.91
Dsp	Desmoplakin	0.42	8.94	0.50	0.46	21.46	0.92	-23.44
Calm2;Calm1;Calm3	Calmodulin	0.02	1.12	0.01	0.01	66.65	1.32	-50.37
Actn4	Alpha-actinin-4	0.06	0.29			5.18		
Ahnak	Ahnak Desmoyokin	0.04	0.08			2.09		

Aldoa	Fructose-bisphosphate aldolase A	0.12	1.10		0.60	9.10	
Arpc4	Actin-related protein 2/3 complex subunit 4	0.01	0.09		0.01	7.01	
Atp5b	ATP synthase subunit beta, mitochondrial		0.08		0.02		
Cltc	**Clathrin heavy chain 1**	0.04	0.07			1.88	
Eppk1	Epiplakin	0.07	1.30		0.03	17.59	
Hal	Histidine ammonia-lyase	0.02	0.14		0.02	5.93	
Hist1h2al	Histone H2A type 2-C		0.44		0.04		
Hist1h4a	Histone H4		1.31		0.03		
Hspa1a	Heat shock 70 kDa protein 1A		0.33		0.05		
Ldha	L-lactate dehydrogenase A chain		0.31		0.17		
Lima1	LIM domain and actin-binding protein 1	0.06		0.05	0.04		0.91
Lrrfip1	Leucine-rich repeat flightless-interacting protein 1	0.06	0.04		0.03	0.70	
Naca	Nascent polypeptide-associated complex subunit alpha	0.01	0.03			3.16	
Pgk1	Phosphoglycerate kinase 1		0.20		0.06		
Pkm2	Pyruvate kinase PKM	0.03	0.39		0.11	11.37	
Ptbp1	Polypyrimidine tract-binding protein 1	0.02	0.05			3.03	
Rpl10a	Ribosomal protein		0.05	0.04	0.04		0.91
Rpl12	60S ribosomal protein L12	0.03	0.03			1.09	
Rpl4	60S ribosomal protein L4	0.05		0.03	0.03		0.87
Slc25a4	Plakophilin-1		0.16	0.03			
Tgm1	Protein-glutamine gamma-glutamyltransferase K		0.06		0.01		
Tpi1	Triosephosphate isomerase		0.40	0.02	0.10		6.30
Tpm1	Tropomyosin alpha-1 chain	0.09		0.03	0.03		1.04

NB: **Genes/proteins in bold = also present in first NRP1-IP mass spectrometry experiment.** Genes/proteins underlined = of special interest.

Table 5.3: Comparison of common hits from mass spectrometry of neuropilin-1-immunoprecipitated β3-WT and β3-HET EC samples between first and second experiments.

Gene	Protein	LFQ value normalised to that of NRP1 (second experiment)				Mass spectrometry Mascot score normalised to that of NRP1 (first experiment)			
		WT-V	WT+V	HET-V	HET+V	WT-V	WT+V	HET-V	HET+V
Tpm4	**Tropomyosin alpha-4 chain**	0.54	0.21	0.11	0.13	0.06	0.38		
Tpm3	**Tropomyosin alpha-3 chain**	1.82	1.33	0.34	0.58	0.07	0.72		0.08
Gapdh	Glyceraldehyde-3-phosphate dehydrogenase	0.50	0.53	0.36	0.70	0.23	0.37	0.21	0.20
Myo1c	**Unconventional myosin-Ic**	0.78	0.71	0.38	0.37	0.61	1.66	0.38	0.35
Rasip1	Ras-interacting protein 1	0.06	0.05	0.04	0.03	0.17	0.40	0.13	0.08
Rplp0	**60S acidic ribosomal protein P0**	0.26	0.24	0.15	0.14	0.18	0.19	0.10	0.13
Myh10	**Myosin-10**	3.97	3.97	6.32	6.52	1.10	5.08	0.40	0.72
Tmod3	**Tropomodulin-3**	0.29	0.31	0.18	0.19	0.06	0.35		
Nrp1	**Neuropilin-1**	1.00	1.00	1.00	1.00	1.00	1.00	1.00	1.00
Actg1	**Actin, cytoplasmic 2**	166.25	172.15	109.54	110.31	1.61	3.52	0.81	0.98
Myl12a	**Myosin light chain, regulatory B-like**	1.53	2.25	0.58	0.82	0.27	0.38	0.07	0.14
Myh9	**Myosin-9**	226.75	246.90	159.30	146.76	4.40	13.92	1.81	3.06
Rps3	40S ribosomal protein S3	0.11	0.18	0.05	0.05	0.22	0.33	0.30	0.29
Gsn	**Gelsolin**	0.02	0.09	0.03	0.02	0.09	0.68	0.05	0.04
Tubb5	Tubulin beta-5 chain	0.04	0.16	0.06	0.04	0.18	0.27	0.14	0.21
Anxa2	**Annexin A2**	0.20	1.34	0.15	0.16		0.35	0.13	0.15
Cltc	**Clathrin heavy chain 1**	0.04	0.07			1.00	1.13	0.46	0.45

NB: **Genes/proteins in bold = those with similar trends between experiments.**

: relatively high value in group of comparison

: relatively low value in group of comparison

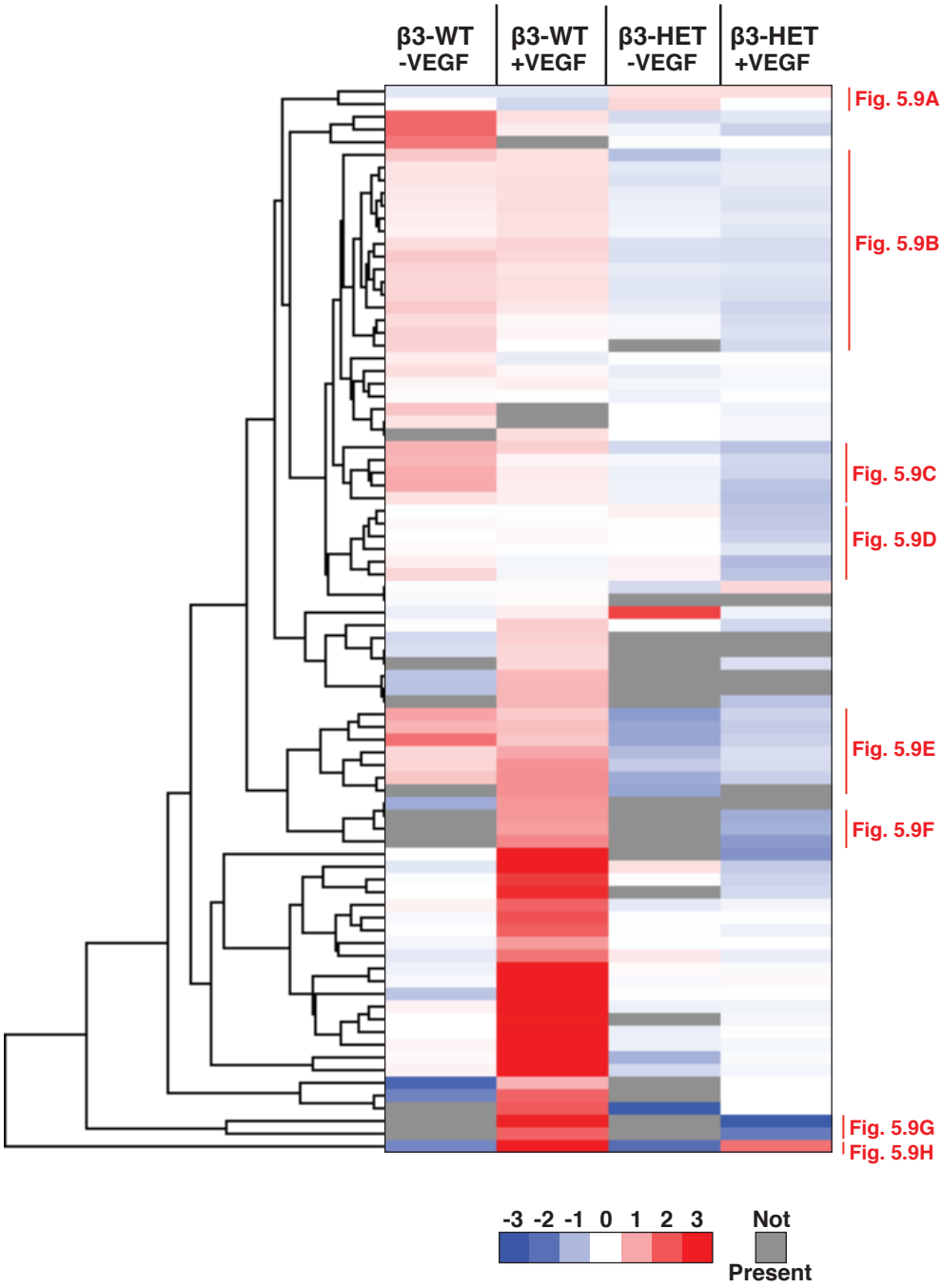

Figure 5.8: Quantitative mass spectrometry analysis of neuropilin-1-immunoprecipitated samples highlights differential neuropilin-1 associations between β3-wild-type and β3-heterozygous endothelial cells. β3-WT and β3-HET ECs were seeded overnight on fibronectin, treated ±VEGF, and lysed and immunoprecipitated for NRP1. Samples were subjected to label-free quantitative mass spectrometry analysis. Peptides present in at least 2 samples were hierarchically clustered by clustering median log(LFQ) values by city-block distance. The analysis is further dissected in Figures 9A-H. Particular clusters subsequently focussed on are highlighted in red on the right side.

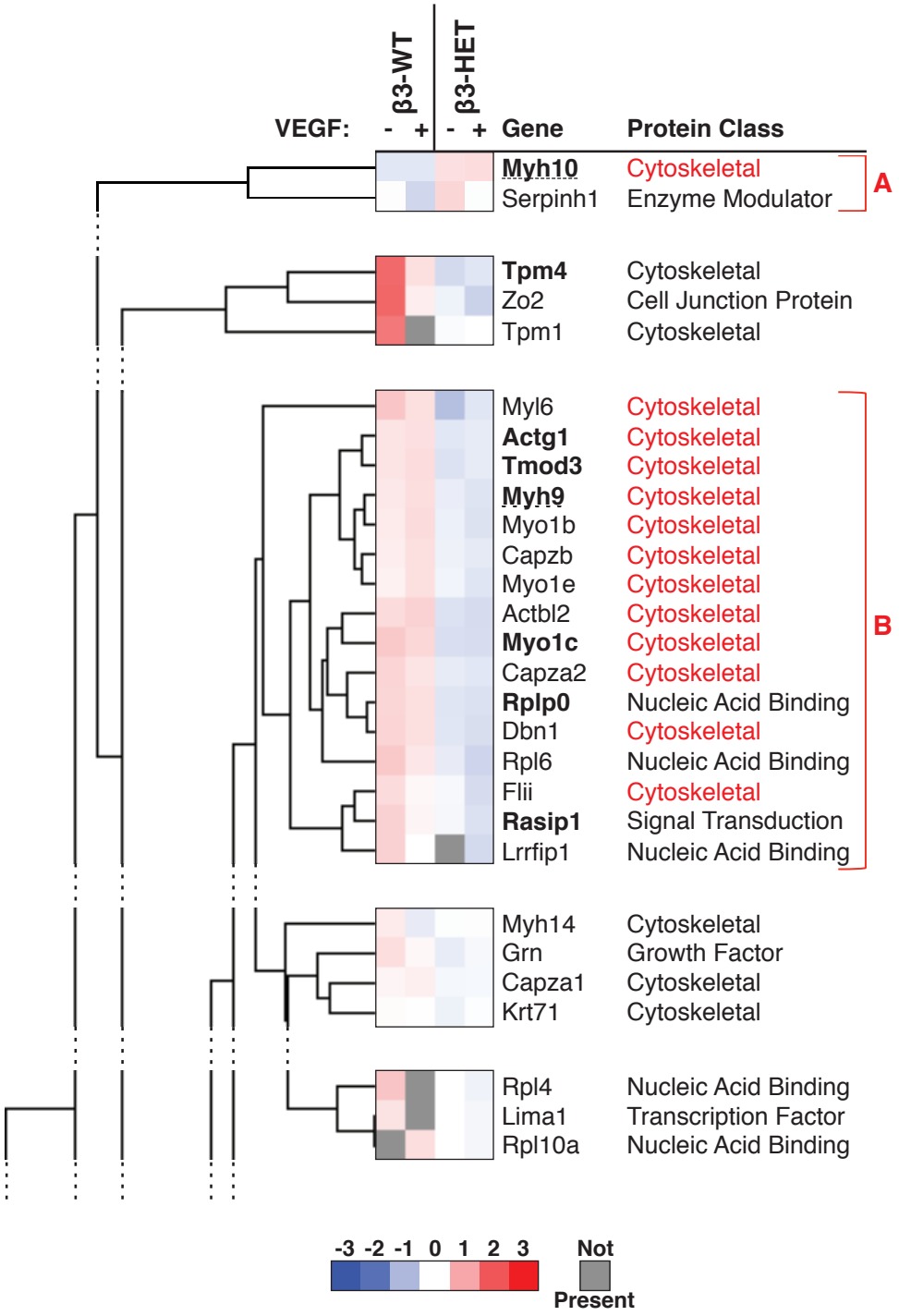

Figure 5.9: Quantitative mass spectrometry analysis of neuropilin-1-immunoprecipitated samples highlights differential neuropilin-1 associations between β3-wild-type and β3-heterozygous endothelial cells. β3-WT and β3-HET ECs were seeded overnight on fibronectin, treated ±VEGF, and lysed and immunoprecipitated for NRP1. Samples were subjected to label-free quantitative mass spectrometry analysis. Peptides present in at least 2 samples were hierarchically clustered by clustering median log(LFQ) values by city-block distance. **A** Top 2 proteins highlighted have enhanced NRP1 associations in β3-HET ECs. **B** Predominantly cytoskeletal proteins have enhanced NRP1 associations in β3-WT ECs and decreased associations in β3-HET ECs. **NB: Genes in bold = protein also present in first NRP1 IP mass spectrometry experiment.** Genes underlined = of special interest.

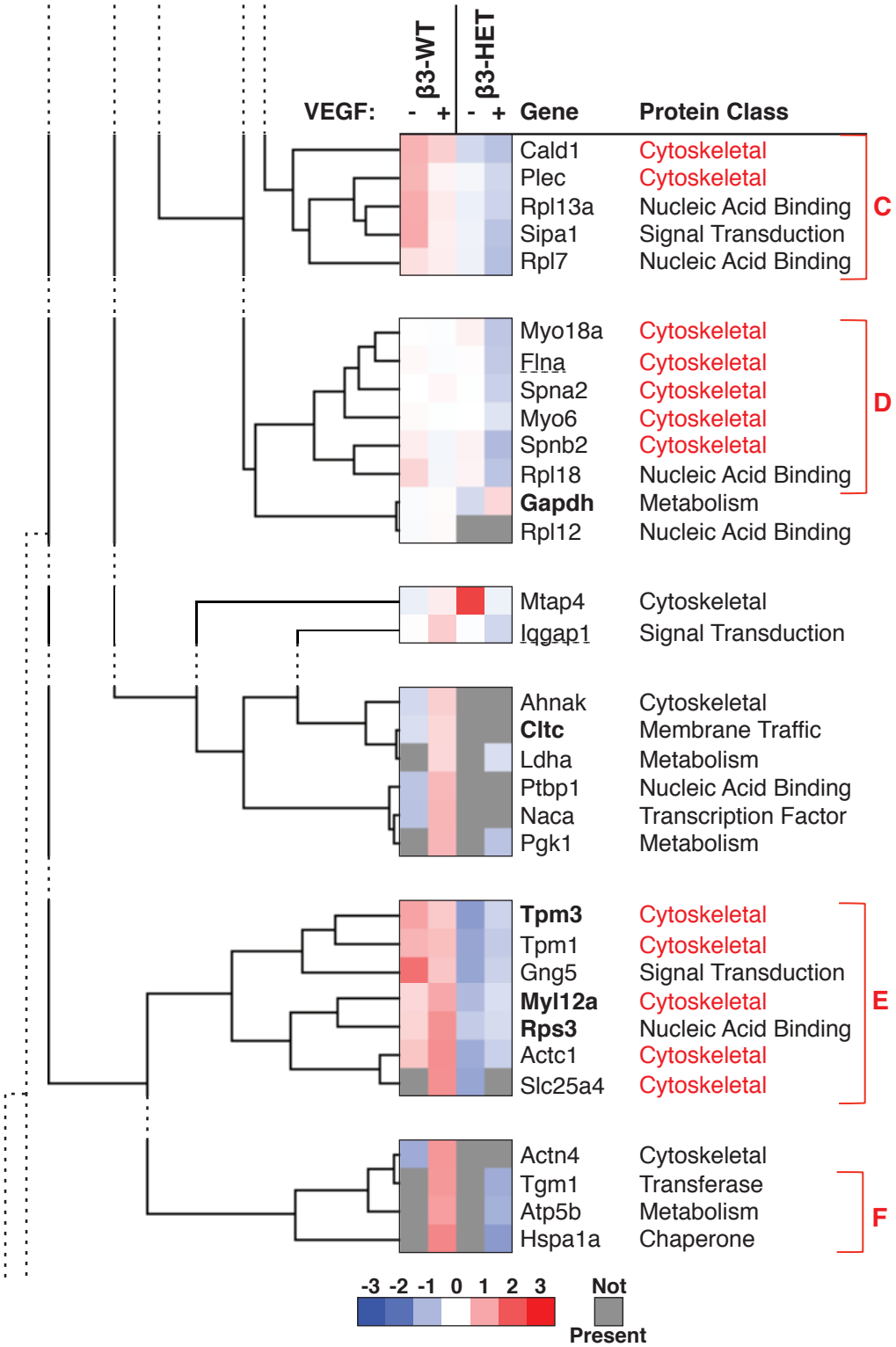

Figure 5.9: Quantitative mass spectrometry analysis of neuropilin-1-immunoprecipitated samples highlights differential neuropilin-1 associations between β3-wild-type and β3-heterozygous endothelial cells. β3-WT and β3-HET ECs were seeded overnight on fibronectin, treated ±VEGF, and lysed and immunoprecipitated for NRP1. Samples were subjected to label-free quantitative mass spectrometry analysis. Peptides present in at least 2 samples were hierarchically clustered by clustering median log(LFQ) values by city-block distance. **C** Proteins highlighted have enhanced NRP1 associations in β3-WT ECs -VEGF, but decreased associations in β3-HET ECs +VEGF. **D** Predominantly cytoskeletal proteins have decreased NRP1 associations specifically in β3-HET ECs +VEGF. **E** Predominantly cytoskeletal proteins have strongly enhanced associations in β3-WT ECs and strongly decreased associations in β3-HET ECs. **F** Proteins have enhanced associations in β3 WT ECs +VEGF and reduced associations in β3-HET ECs +VEGF. **NB: Genes in bold = protein also present in first NRP1 IP mass spectrometry experiment.** Genes underlined = of special interest.

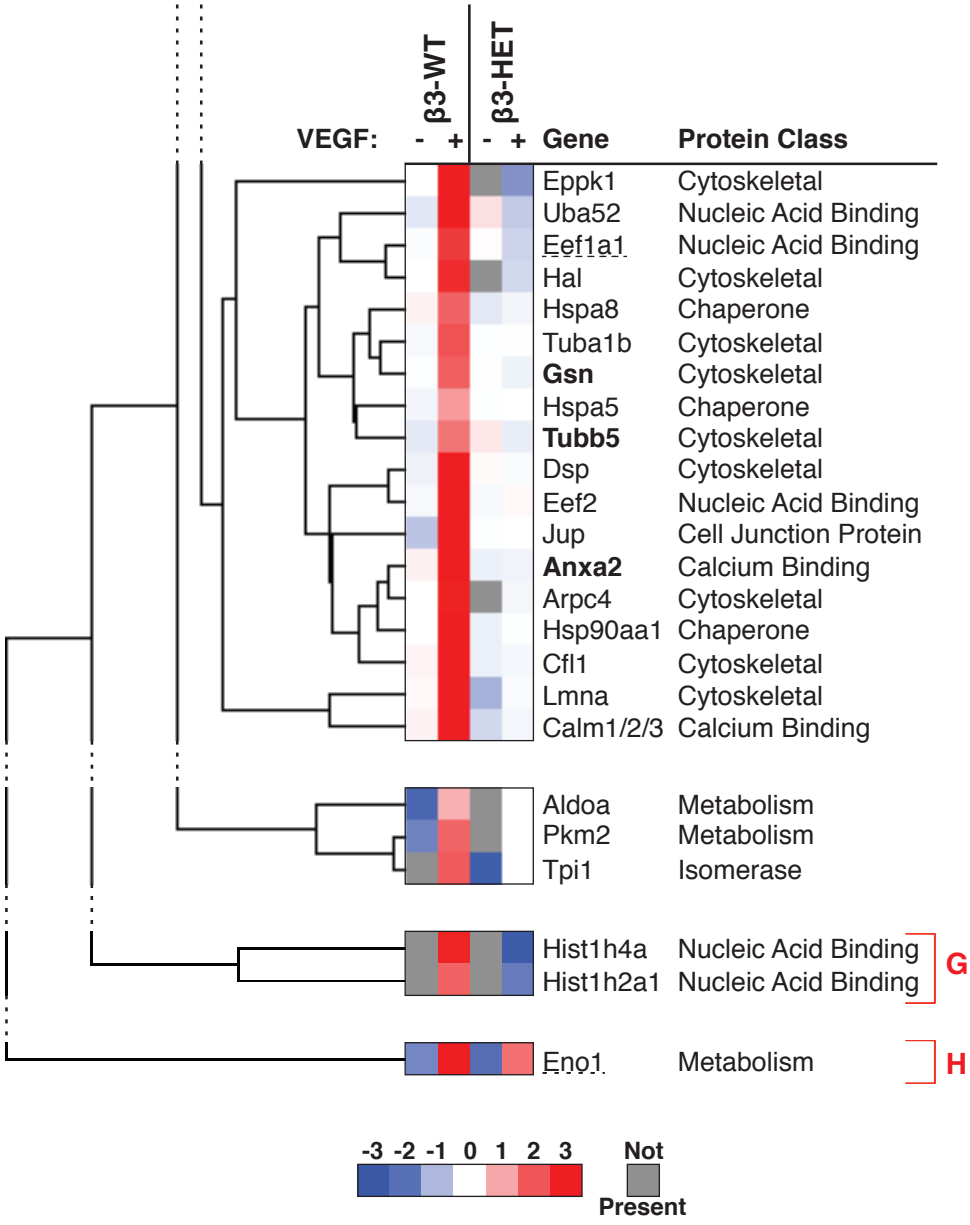

Figure 5.9: Quantitative mass spectrometry analysis of neuropilin-1-immunoprecipitated samples highlights differential neuropilin-1 associations between β3-wild-type and β3-heterozygous endothelial cells. β3-WT and β3-HET ECs were seeded overnight on fibronectin, treated ±VEGF, and lysed and immunoprecipitated for NRP1. Samples were subjected to label-free quantitative mass spectrometry analysis. Peptides present in at least 2 samples were hierarchically clustered by clustering median log(LFQ) values by city-block distance. **G** Proteins have strongly enhanced NRP1 associations in β3 WT ECs +VEGF and strongly reduced associations in β3-HET ECs +VEGF. **H**α-enolase has enhanced associations in both β3-WT and β3-HET ECs stimulated with VEGF. **NB: Genes in bold = protein also present in first NRP1 IP mass spectrometry experiment.** Genes underlined = of special interest.

5.9 Examining neuropilin-1's associations within the endothelial adhesome

Since mass spectrometry revealed that many of the proteins that changed their associations with NRP1 between β3-WT and β3-HET ECs were related to FAs and the cytoskeleton, we further investigated the association of NRP1 with such proteins that might be relevant to our phenotypes by co-IP. Following the IP of NRP1 using the same antibody as the second mass spectrometry experiment, we initially looked again at associations with myosin 9, as well as with filamin a, and α5-integrin (**Figure 5.10Ai**). We decided on α5-integrin as NRP1 is known to interact with α5β1 and control its trafficking in ECs [288], because the surface expression of α5 is reduced in β3-HET ECs, and because filamin a and IQGAP1, which we have established to associate with NRP1, are known to be recruited to active β1 sites [243]. We additionally examined NRP1's associations with the FA proteins FAK and p130Cas (**Figure 5.10Aii)**, whose phosphorylation is known to be regulated by NRP1 [272,273]. p130Cas is also known to co-localise with NRP1 in vesicular punctae [289]. Unfortunately, these co-IP experiments were not consistent, meaning the effect of VEGF stimulation and/or reduced β3 expression does not conclusively alter NRP1's associations with these molecules. In the experiments shown in **Figure 5.10A**, NRP1 was IP'd in both pMT immortalised and primary β3-WT and β3-HET MLECs, although not uniformly between unstimulated and VEGF-stimulated pMT EC samples, for reasons unknown. Taking this into account, there were no obvious differences in NRP1 co-association between samples for any of the molecules tested. This includes myosin 9-NRP1 association, which we previously showed was reduced in β3-HET ECs, although a different anti-NRP1 antibody was used for the IP. However, myosin 9-NRP1 association was reduced in stimulated primary β3-HET ECs, suggesting that results with myosin 9 may be inherently variable. Repeats of the NRP1-filamin a co-IP experiment are shown in **Figure 5.10B** to confirm that no differences in NRP1 co-association were observed for this molecule per amount of NRP1 IP'd. However, experimental repeats with the other molecules were even more inconsistent (not shown). Whilst we found NRP1's association with myosin 9 and filamin a to not change in the way predicted from mass spectrometry, we can confirm that NRP1 does associate with a range of FA molecules, including α5-integrin, filamin a, FAK, and p130Cas [288,289]. To further support NRP1's placement within the endothelial adhesome, we used a

method previously employed by Schiller et al. [219,220] in fibroblasts to establish and enrich mature integrin-dependent FAs in β3-WT and β3-HET ECs. Eluted FA-enriched samples were analysed for NRP1 content by Western blotting (**Figure 5.10C**). We detected similar amounts of NRP1 in the adhesomes from unstimulated and VEGF-stimulated β3-WT and β3-HET ECs. This therefore confirms that NRP1 is present in the endothelial adhesome, but does not provide further insight into the difference in NRP1 localisation in stimulated β3-HET ECs. A more detailed analysis of the FA-enriched samples has been conducted in a separate project, but we can confirm here that the samples have been validated for their enrichment for FA components as expected (not shown).

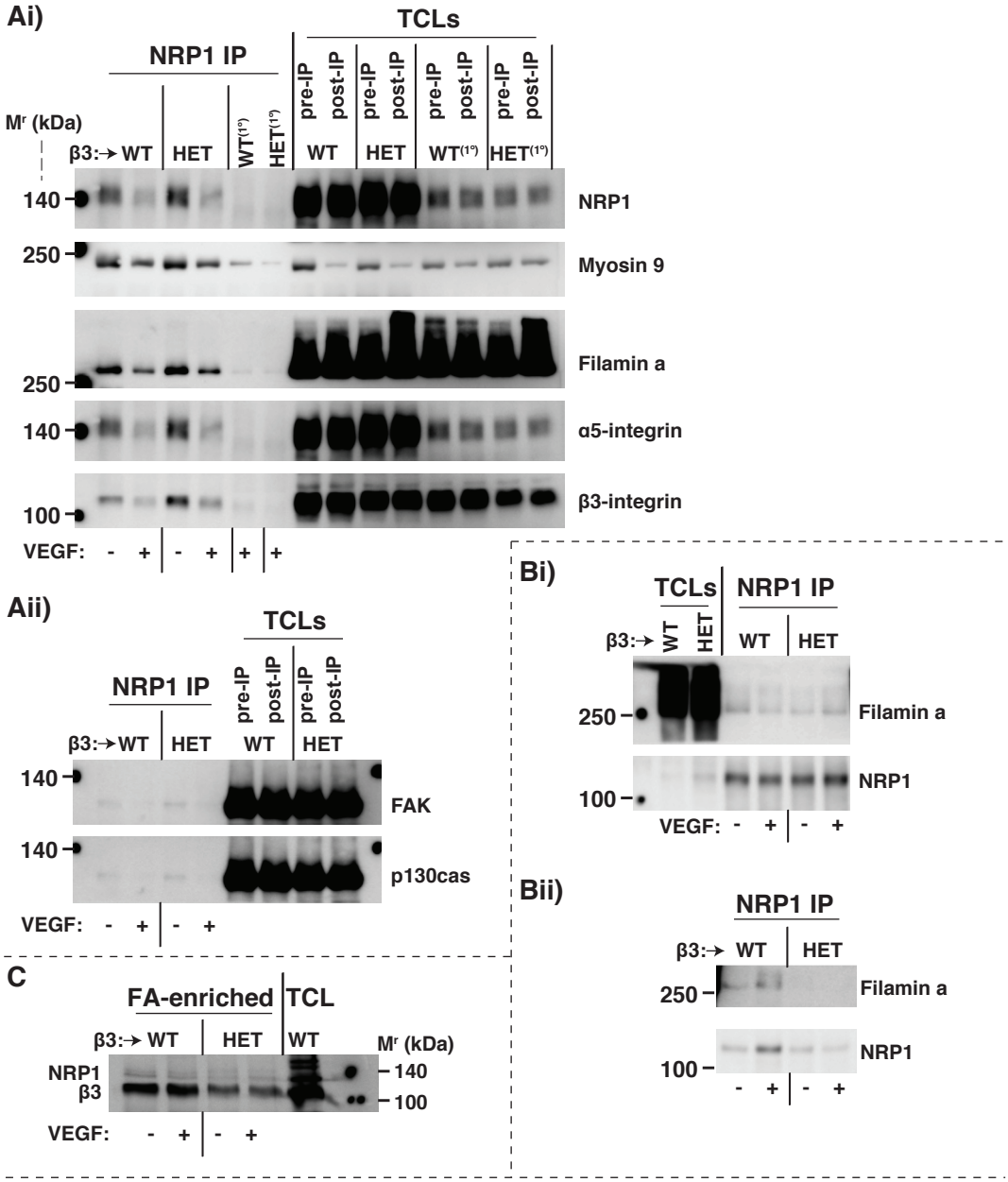

Figure 5.10: Examining neuropilin-1's associations within the endothelial adhesome. A,B β3-WT and β3-HET primary (1°) and polyoma-middle-T-antigen immortalised lung microvascular ECs were seeded overnight on fibronectin (FN), treated ±VEGF, and lysed and immunoprecipitated for NRP1 (NRP1 IP). IP'd samples were separated by SDS-PAGE for Western blotting. Total cell lysates taken before the IP (pre-IP) and after the IP (post-IP) are shown as controls to confirm the efficiency of the IP. **C** ECs were allowed to adhere to FN-coated dishes for 90 minutes to establish 'mature' integrin-dependent focal adhesions (FAs). FAs were chemically crosslinked to the plates and cells were lysed with RIPA buffer. Non-crosslinked proteins and other cellular components were rinsed away under high-sheer flow. FA-enriched complexes were eluted and subjected to SDS-PAGE for Western blot analysis. A total cell lysate (TCL) is shown for comparison. Data are representative of 3 independent experiments.

5.10 Neuropilin-1's co-localisation with paxillin-positive focal adhesions is lost upon stimulation with VEGF in only β3-heterozygous endothelial cells

Whilst the examination of NRP1 associations in β3-WT and β3-HET ECs by co-IP/Western blot was inconclusive, and could not explain NRP1's localisation away from the ends of actin filaments in stimulated β3-HET ECs, the consistent link between NRP1 and the adhesome led us to speculate that there may be NRP1-regulated changes in FA dynamics that are too subtle to be detected by co-IP. Indeed, NRP1 has previously been implicated in FA turnover [289], as well as FN-stimulated paxillin (PXN) phosphorylation [271]. We therefore turned our attention to examining NRP1 alongside PXN, first by immunolocalising them in β3-WT and β3-HET ECs both with and without NRP1's cytoplasmic tail to further dissect the differences in EC migration observed previously (**Figure 5.11A**).

Immunocytochemistry of ECs plated overnight on FN showed a predicted co-localisation of total PXN and NRP1 in mature FAs in unstimulated β3-WT ECs. This co-localisation was maintained after 10 minutes of VEGF-stimulation. NRP1/PXN co-localisation in mature FAs was also apparent in unstimulated β3-HET ECs, but it was lost upon VEGF-stimulation, with NRP1 co-localising with PXN in vesicular structures instead. A similar pattern was observed in β3-HET-NRP1Δcyto ECs, except NRP1 also no longer co-localised with PXN in vesicles. β3-WT-NRP1Δcyto ECs displayed a relatively small loss of NRP1/PXN co-localisation in mature FAs after VEGF-stimulation (**Figure 5.11B**).

The sizes of paxillin-positive FAs were measured in all of the cell types to gain a static representation of the ramifications of FA turnover in the different ECs (**Figure 5.11C**). We noted that both β3-WT-NRP1Δcyto and β3-HET-NRP1Δcyto ECs contained slightly proportionally larger FAs than their counterparts with intact NRP1.

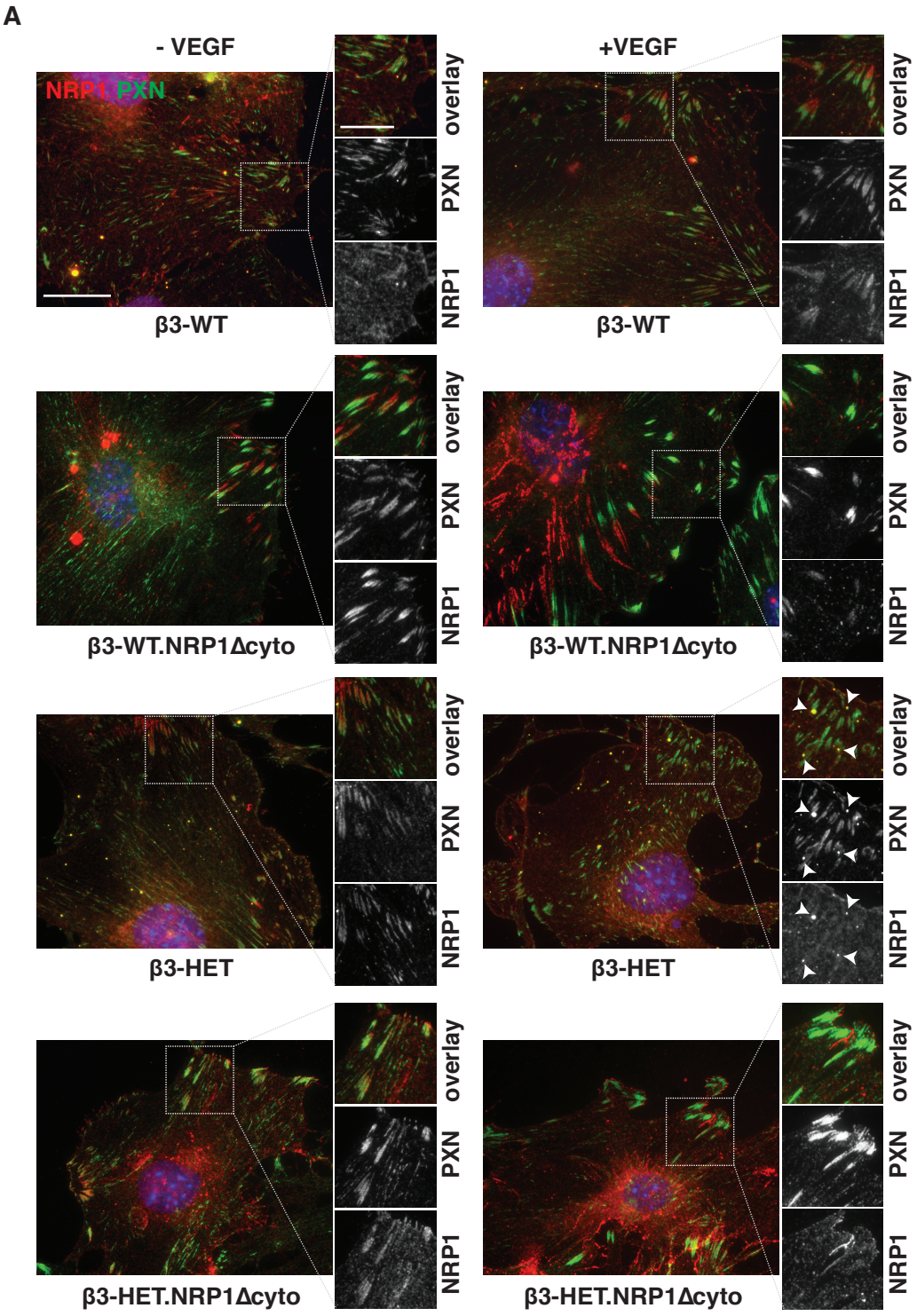

Figure 5.11: Neuropilin-1's co-localisation with paxillin-positive focal adhesions is lost upon stimulation with VEGF in only β3-heterozygous endothelial cells. A ECs of the indicated genotypes were seeded overnight on FN-coated glass coverslips. After 3 hours of starvation, cells were treated ±VEGF for 10 minutes in serum-free medium, then fixed and immunostained for total paxillin (PXN - green) and neuropilin-1 (NRP1 - red). Split channel close-ups are shown to depict PXN/NRP1 co-localisation in mature focal adhesions. White arrowheads in β3-HET close-up highlight PXN/NRP1 co-localisation in vesicles. Scale bar = 20 µm.

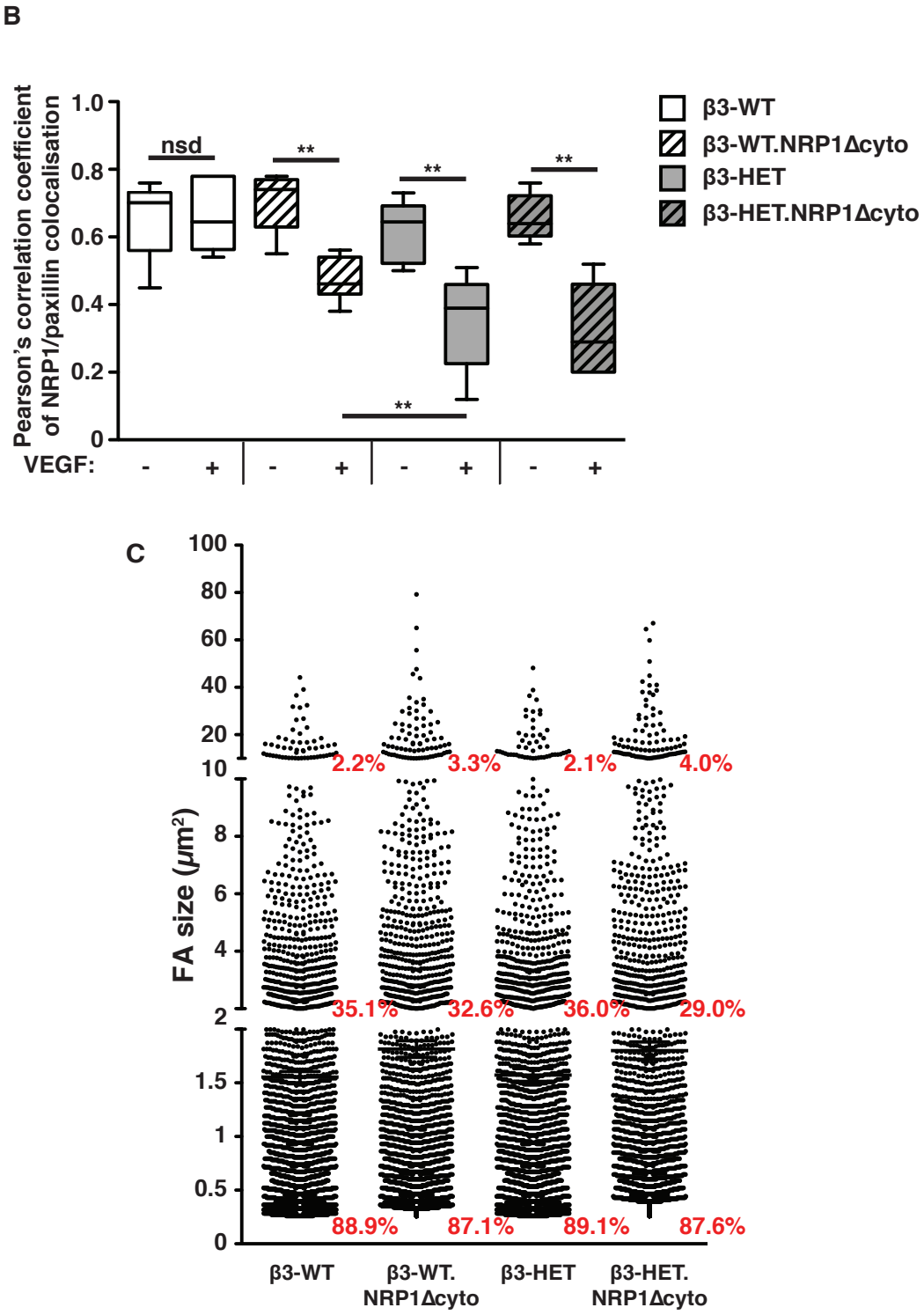

Figure 5.11: Neuropilin-1's co-localisation with paxillin-positive focal adhesions is lost upon stimulation with VEGF in only β3-heterozygous endothelial cells. ECs of the indicated genotypes were seeded overnight on FN-coated glass coverslips. After 3 hours of starvation, cells were treated ±VEGF for 10 minutes in serum-free medium, then fixed and immunostained for total paxillin and neuropilin-1. **B** The box and whisker plot shows Pearson's correlation coefficient of PXN/NRP1 colocalisation in each of the indicated genotypes in the indicated regions as determined using the ImageJ™ coloc2 plugin (means ± interquartile ranges and extreme values; n≥5 cells per genotype). **C** The size of FAs was quantified by using ImageJ to measure the area of PXN-positive FAs. The graph shows plotted values of FA size for each cell genotype (n≥10 cells per genotype, 1800 FAs per genotype in total). The percentage of FAs in different size ranges are indicated in red. Asterisks indicate statistical significance: *, $P<0.05$; **, $P<0.01$; nsd = not significantly different. Unpaired two-tailed *t* test.

5.11 Paxillin activation is sensitive to neuropilin-1 disruption in β3-integrin-heterozygous endothelial cells

We next pursued a potential β3-integrin-regulated NRP1 link with PXN activation by analysing the phosphorylation of PXN through Y118 by immunoblotting (**Figures 5.12A,B**) and immunocytochemistry (**Figure 5.12C**). PXN phosphorylation was substantially reduced in β3-HET-NRP1Δcyto ECs, but not β3-WT-NRP1Δcyto ECs, suggesting that PXN activation is only NRP1-dependent when β3-integrin levels are suppressed. This therefore reflects the tumour angiogenesis, and EC migration phenotypes observed previously, but unlike the mobilisation of NRP1 away from PXN-positive FAs, reduced PXN phosphorylation in β3-HET-NRP1Δcyto ECs was apparent in both non-VEGF-stimulated and VEGF-stimulated ECs.

5.12 Focal adhesion turnover is more sensitive to neuropilin-1 disruption in β3-integrin-heterozygous endothelial cells

Finally, through the live tracking of GFP-PXN in transfected cells, we monitored FA turnover by measuring the rates of FA assembly and disassembly (**Figure 5.13**). We noted that compared to β3-WT ECs, which displayed similar rates of FA assembly and disassembly, β3-HET ECs contained FAs that overall assembled and disassembled at a faster rate, thereby corresponding to an overall increase in FA turnover in these cells. However, in β3-WT-NRP1Δcyto and β3-HET-NRP1Δcyto ECs, whilst FA assembly rates were enhanced compared to that in β3-WT ECs, the corresponding rates of FA disassembly were significantly reduced, meaning net FA turnover is perturbed by the loss of NRP1's cytoplasmic tail. This effect was most pronounced in β3-HET-NRP1Δcyto ECs, and therefore the combination of β3 expression reduction and the absence of NRP1's cytoplasmic tail impairs FA turnover most efficaciously. Indeed, whilst FA disassembly rates between β3-WT and β3-WT-NRP1Δcyto ECs were not quite significantly reduced, the rates between β3-HET and β3-HET-NRP1Δcyto ECs were reduced significantly. These data reflect the differences in size of FAs between the cells reported earlier (ie. the small increase in FA size in the NRP1Δcyto ECs, which was greatest in the β3-HET-NRP1Δcyto ECs, is congruent with a net reduction in FA turnover). It is logical to connect the abnormally localised NRP1 away from mature FAs in VEGF-stimulated β3-HET

ECs, and the increased sensitivity of β3-HET ECs to NRP1-mediated PXN activation and FA turnover, to the EC migration phenotypes observed previously, since FA dynamics are inextricably linked to cell motility. Our data suggest that, in the presence of β3-integrin, EC migration is NRP1-independent; β3-integrin maintains NRP1 in mature FAs, thus ensuring a controlled migratory response to VEGF-stimulation. However, reduced levels of β3-integrin lead to changes in FA turnover and cell migration that are NRP1-dependent. Extrapolating further, these phenomena may help explain the enhanced sensitivity of tumour growth and angiogenesis to NRP1 perturbation when β3 expression is reduced, as well as the blockade of established tumour growth and angiogenesis in response to simultaneous endothelial β3/NRP1 inhibition.

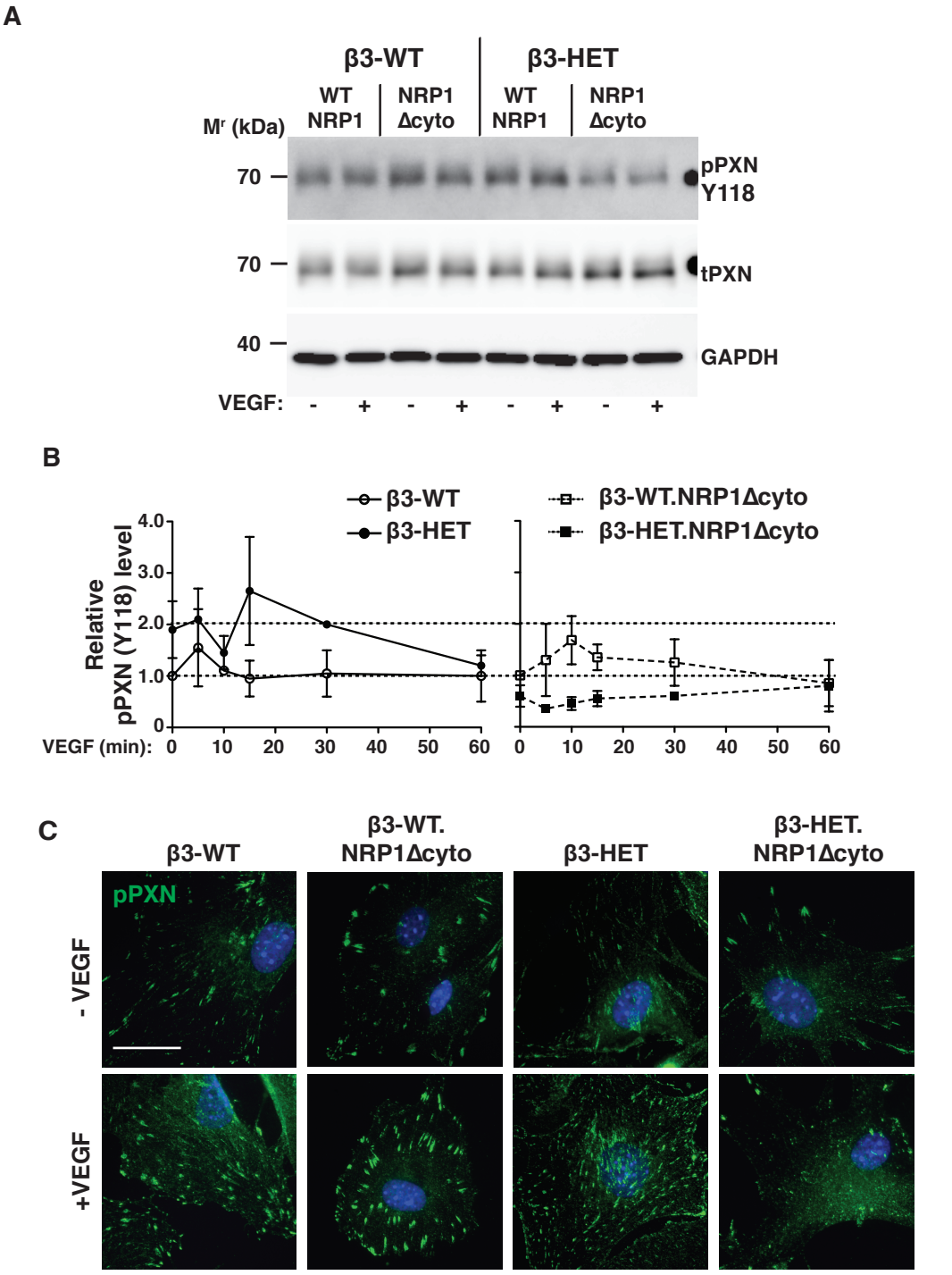

Figure 5.12: Paxillin activation is sensitive to neuropilin-1 disruption in β3-integrin-heterozygous endothelial cells. A ECs of the indicated genotypes were seeded overnight on FN. They were then starved for 3 hours and treated ±VEGF for 10 minutes in serum free medium. Cells were lysed and Western blotted (WB) for levels of phosphorylated (p) and total (t) PXN. GAPDH served as a loading control. Data are representative of 3 independent experiments. **B** The graph shows densitometry of pPXN relative to tPXN, as determined by Western blot, over an extended VEGF time course (means ±SEM from ≥3 independent experiments). **C** ECs that were seeded overnight onto FN-coated glass coverslips and stained for pPXN. ECs were starved for 3 hours and treated ±VEGF for 10 minutes in serum free medium. Cells were fixed and immunostained for pPXN (green). Scale bar = 10 μm.

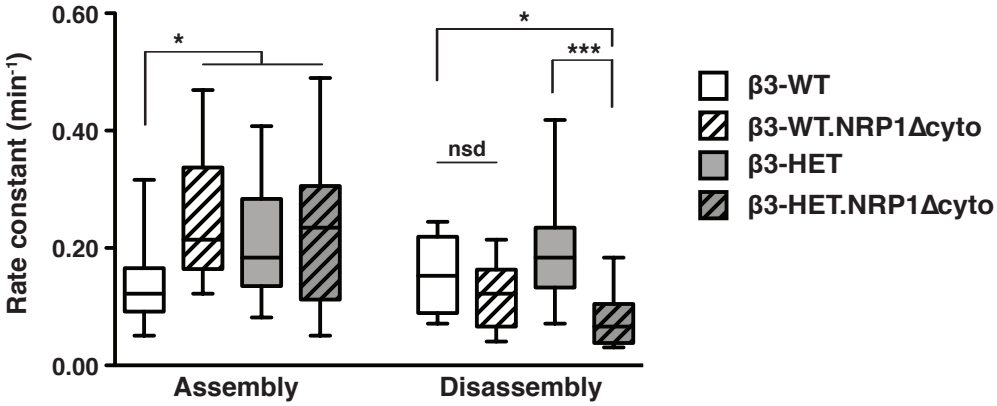

	Assembly vs disassembly (turnover)
β3-WT	nsd
β3-WT.NRP1Δcyto	**
β3-HET	nsd
β3-HET.NRP1Δcyto	***

Figure 5.13: Focal adhesion turnover is more sensitive to NRP1 disruption in β3-integrin-heterozygous endothelial cells. ECs were transfected with a PXN-GFP construct and seeded at a low density on FN-coated coverslips. 72 hours later cells were starved and then treated with VEGF in reduced serum medium. Representative cells were then imaged live (every 2 minutes) on an inverted fluorescence microscope for 1 hour to monitor focal adhesion (FA) turnover. The front and back ends of individual FAs were tracked over this period to measure FA assembly and disassembly using the ImageJ™ MTrack2 plugin. The box and whisker plot shows the rate of FA assembly or disassembly for each of the indicated genotypes (means ± interquartile ranges and extreme values; n≥20 FAs per genotype). The table below highlights the significance of net changes in FA assembly vs disassembly (turnover) for each EC genotype. Asterisks indicate statistical significance: *, $P<0.05$; **, $P<0.01$. ***, $P<0.001$; nsd = not significantly different. Unpaired two-tailed *t* test.

5.13 Discussion

Following our conclusion that disrupting NRP1 in β3-HET ECs did not sufficiently change VEGFR2 biology to account for the reduction in tumour growth and angiogenesis in β3-HET mice, we turned to the analyses of other NRP1 functions. Firstly, the adhesion of β3-HET pMT LMECs to αvβ3's canonical ligand, vitronectin, was reduced as expected, and was supported by a reduction in αv and β3 levels on the surface of these cells. Similarly, the adhesion of these β3-HET ECs to fibronectin was reduced, and may be related to their reduction in α5 surface levels as FN is a prominent ligand of α5β1, although β1 surface levels were unchanged. Contrary to previous findings in HUAECs [288], the absence of NRP1's cytoplasmic tail had no obvious effect on the adhesion of microvascular MLECs to FN when β3 was expressed at normal and reduced levels. This discrepancy may be related to the EC type, and possibly a disparity between tendencies toward either angiogenesis or arteriogenesis, as predicted for VEGFR2 function previously. Surface levels of α5 and β1 in β3-WT and β3-HET ECs lacking NRP1's cytoplasmic tail reflected those in the equivalent ECs expressing full-length NRP1. Though Valdembri et al. [288] showed that NRP1 internalises and recycles with α5β1 in ECs, they found no differences in α5β1 surface levels in ECs with NRP1 expression knocked-down, meaning our data is in agreement in this case. However, given the reduction in α5 surface levels in β3-HET ECs, it remains possible that α5β1 recycling may be perturbed in these cells. Like Valdembri et al.'s [288] study, no obvious differences in EC adhesion to VN, COLI or LN, were found in the absence of NRP1's cytoplasmic tail.

Whilst differences in EC adhesion were not especially enlightening, both random and directed migration of β3-HET, but not β3-WT, ECs were sensitive to NRP1 perturbation, thereby phenocopying the tumour growth and angiogenesis *in vivo* data from animals of the same genotypes. As angiogenesis is heavily dependent on EC migration, this suggests that migration significantly contributes to the *in vivo* phenotypes. Indeed, as β3-HET EC migration was elevated, enhanced tumour angiogenesis in the corresponding mice is likely not only due to the contribution of non-ECs. In contrast with a study by Seerapu et al. [289], who showed that NRP1Δcyto heart ECs had an impeded rate of scratch wound closure, β3-WT microvascular ECs lacking NRP1's cytoplasmic tail did not

migrate differently from those with full-length NRP1. This dichotomy again may be related to the EC type, as our results are more fitting with the normal EC migration observed in the angiogenic postnatal retina of NRP1Δcyto mice [267]. Although EC migration can be regulated by VEGFR2-dependent signalling, our previous analysis of VEGFR2 signalling pathways showed no obvious changes, other than NRP1-sensitive ERK1/2 signalling in β3-HET ECs, and so our attention was diverted towards NRP1's purported regulation of migration via its involvement with FA proteins [271,289].

We found that NRP1 is normally able to localise at mature PXN-positive FAs at the plus-ends of actin filaments and is retained at these sites following VEGF stimulation. Moreover, through the enrichment of FA complexes, we have, for the first time, placed NRP1 in the **endothelial** adhesome of both unstimulated and VEGF-stimulated β3-WT and β3-HET ECs. However, in β3-HET ECs with normal and cytoplasmic-tail-deleted NRP1, and to a lesser extent in β3-WT-NRP1Δcyto ECs, we found that VEGF-stimulation mobilises NRP1 away from mature FAs. This was also true in primary ECs with an induced depletion of β3, therefore highlighting a novel ability of β3 to regulate NRP1 by controlling its retention within mature FAs upon VEGF-stimulation. This regulation may occur through an indirect interaction between β3 and NRP1 in FAs, as although the two molecules co-localised in the same structures, their association by co-IP was weak, and β3 was not present in the mass spectrometry data of NRP1-immunoprecipitated samples. The slight reduction in NRP1's retention in mature FAs in β3-WT ECs missing NRP1's cytoplasmic tail suggests that the cytoplasmic portion of NRP1 is also important for the localisation of NRP1 at mature FAs. Though NRP1 has previously been shown to localise at both α5β1-positive adhesion sites and intracellular vesicles in HUAECs [288], Seerapu et al. [289] reported that in heart ECs NRP1 associated with FAs transiently, but was rather more associated with recycling FA components in vesicles following VEGF stimulation, and may regulate the trafficking of these proteins via its cytoplasmic tail's link to synectin. Since we found NRP1 still localised to mature FAs, and relatively little NRP1-PXN co-localisation in vesicles, following VEGF stimulation in β3-WT ECs, it seems possible that, in contrast to that in heart ECs, NRP1's regulation of FA proteins in vesicles does not readily occur when β3 is adequately expressed in

microvascular ECs. However, when β3 expression is reduced, NRP1 is mobilised from mature FAs in response to VEGF, and becomes co-localised with PXN in vesicles. NRP1 may therefore be much more involved in regulating the trafficking of FA components in β3-HET ECs, though this hypothesis is yet to be tested. The presence of NRP1 in Rab-11-positive recycling vesicles, and its association with FA proteins, was previously shown to be dependent on NRP1's cytoplasmic tail [268,289]. Here, although NRP1 without its cytoplasmic tail is mobilised away from mature FAs to some extent following VEGF stimulation, it also does not co-localise with PXN in vesicles, so this may agree with previous reports. Therefore, upon VEGF stimulation NRP1 may have different functions between β3-HET and β3-WT-NRP1Δcyto ECs that explain their differential migration. It would therefore be interesting to determine whether NRP1 differentially co-localises with Rab vesicle markers and FA proteins between the ECs after VEGF stimulation to gain further insight into this matter. On a related note, one thing we know from earlier is that NRP1 does not appear to be degraded differently over a VEGF timecourse between the ECs.

In further support of β3's regulation of actin/FA-localised NRP1, mass spectrometry identified mainly cytoskeletal, FA- and myosin-based proteins that associated with NRP1 to a lesser degree in β3-HET ECs. Of particular interest was NRP1's mis-balanced association with myosin 9/10 in β3-HET ECs, and the specific reduction in NRP1's association with filamin a and IQGAP1 in VEGF-stimulated β3-HET ECs. It is possible that, since myosin 9 and 10 are part of the NM-IIA and NM-IIB proteins that regulate distinct FA-related processes [244], NRP1's differential association with them in β3-HET ECs may result in their uncoordinated elevated migration, though this would be difficult to clarify in our transgenic ECs. In agreement with Seerapu et al.'s [289] mass spectrometry data, myosin 9 and myosin 10 associated with NRP1 in both unstimulated and VEGF-stimulated ECs, and α-enolase was more prevalently associated in VEGF-stimulated ECs. However, filamin a was equally associated with NRP1 in β3-WT unstimulated and VEGF-stimulated ECs, unlike the VEGF-dependent association previously reported [289]. As filamin a and IQGAP1, which are known to be involved in Rac1 deactivation at active β1 sites, had reduced associations with NRP1 in stimulated β3-HET ECs, this may fit with NRP1's localisation away from

mature FAs. NRP1 was previously identified to localise with α5β1 at adhesion sites, and regulate α5β1 trafficking via NRP1's cytoplasmic tail [288]. Together, these results point towards the possibility that reduced β3 expression inhibits NRP1 from associating with α5β1 (which might explain β3-HET ECs' reduction in α5 surface levels and adhesion to FN, possibly through defective α5β1 recycling), filamin a, and IQGAP1, thereby impacting on Rac1 activation and hence cell migration. Indeed, NRP1 has previously been shown to regulate Cdc42 activation, and thereby filopodia formation and actin remodelling in endothelial tip cells [290], so it would be interesting to additionally assess Rac1 activity in our ECs. Though we have recently established that total Rac1 levels do not change between β3-WT and β3-HET ECs (not shown), we are yet to examine Rac1 phosphorylation. NRP1's co-localisation with filamin a was previously shown to be dependent on NRP1's cytoplasmic tail in heart ECs [289], a finding that may be supported by our results showing NRP1 localised away from mature FAs in stimulated β3-WT-NRP1Δcyto ECs. Unfortunately, the co-association of NRP1 with α5, filamin a, myosin 9, FAK, and p130Cas in β3-WT and β3-HET ECs was too variable and/or inconclusive by co-IP to follow up our mass spectrometry data with any certainty. Though it is possible that the variability in myosin 9-NRP1 associations pertains to the 'stickiness' of the myosin molecule, we ultimately reasoned that NRP1's associations may be too dynamic in nature to be able to detect differences by co-IP, so we moved to the assessment of FA dynamics through paxillin activation and FA turnover, both of which have previously been reported to be regulated by NRP1 [271,289]. In the future, however, it would be interesting to further investigate NRP1's protein associations identified in the mass spectrometry data by immunocytochemistry.

Reflecting our EC migration phenotype, paxillin phosphorylation and FA disassembly were only impaired in β3-HET-NRP1Δcyto ECs. Compared to β3-WT ECs, net FA turnover was increased in β3-HET ECs, but decreased in β3-HET-NRP1Δcyto ECs, thus suggesting that EC migration is mainly dependent on FA turnover here. β3-WT-NRP1Δcyto ECs also displayed defective FA turnover, in agreement with Seerapu et al.'s [289] work, but not to the same extent as β3-HET-NRP1Δcyto ECs, and this did not translate to differences in migration in our microvascular ECs. This may be because paxillin phosphorylation was not

inhibited in β3-WT-NRP1Δcyto ECs, and therefore may still promote Cdc42 activation and concomitant EC migration in the way projected by Fantin et al. [290]. As NRP1's role in Cdc42 activation was reported recently (after this project had been completed), we have not yet clarified whether Cdc42 activation is regulated by NRP1-mediated PXN phosphorylation in our microvascular MLECs, but it would be interesting to do so in the future. Nevertheless, the inhibition of PXN phosphorylation in β3-HET-NRP1Δcyto ECs, and lack thereof in in β3-WT-NRP1Δcyto ECs, is in agreement with Raimondi et al. [271]'s prediction that NRP1's extracellular portion is responsible for ABL1-mediated paxillin activation via interactions with FN-binding integrins. It is therefore possible that β3 is one such FN-binding integrin that regulates NRP1-ABL1-mediated PXN phosphorylation (though we have yet to examine ABL1 activation in our ECs). However, since PXN phosphorylation is unaltered in β3-HET ECs, there appears to be redundancy built into the system such that the presence of either β3 or full-length NRP1 is sufficient to mediate adequate PXN activity. Perhaps another molecule can compensate for reduced β3 levels to regulate this function of NRP1 in a way dependent on NRP1's cytoplasmic tail. Indeed, α5β1-integrin, as a major FN-binding integrin that is regulated by NRP1's cytoplasmic tail, may be one such candidate, though the reduction in α5 surface levels in β3-HET ECs may argue against this. We do not yet know how NRP1's VEGF-induced mobilisation away from mature FAs and towards PXN-positive vesicles in β3-HET ECs links with FA turnover and PXN phosphorylation, but it could be that NRP1's role in regulating FA protein trafficking via its cytoplasmic tail is enhanced in β3-HET ECs, and results in faster FA turnover that, along with concomitant PXN phosphorylation [271], is sensitive to the removal of NRP1's cytoplasmic tail. Since NRP1's associations with filamin a and IQGAP1 were less prevalent in stimulated β3-HET ECs in the mass spectrometry data, this would mean that these FA-proteins are not trafficked by NRP1 in β3-HET ECs. They could even rather be blocked from deactivating Rac1 at active β1 sites, thereby further enhancing uncontrolled EC migration. To prove this theory, NRP1, filamin a, IQGAP1, and PXN would need to be co-localised with recycling vesicles and imaged over a time course, and Rac1 activation should be scrutinised, in our ECs. Moreover, it would be interesting to further explore the functional relationship between NRP1 and α5β1-integrin.

Overall, the increased sensitivity of β3-HET EC migration to the loss of NRP1's cytoplasmic tail may be caused by a number of factors, but it seems to be strongly related to β3-integrin's regulation of NRP1 function at FAs. When β3 is expressed at normal levels, NRP1 is stabilised in mature FAs, and has a negligible role in EC migration. On the other hand, when β3 expression is reduced, NRP1 is mobilised from mature FAs and EC migration becomes dependent on NRP1 via its involvement in FA turnover and concomitant PXN activation. This may therefore help explain the increased sensitivity of tumour growth and angiogenesis in β3-HET, but not β3-WT, mice to NRP1 perturbation.

6. Final Discussion and Future Work

6.1 Final Discussion

In this project we have shown that, in angiogenesis, NRP1 becomes more targetable, not only in the complete absence of β3-integrin (β3-NULL), as previously reported [202], but in a more physiologically relevant model that displays a more subtle, albeit global, reduction in β3 expression (β3-HET). This phenomenon additionally extends to pathological angiogenesis, as only in β3-HET mice does an endothelial depletion of NRP1, or the removal of NRP1's cytoplasmic tail, inhibit tumour growth and angiogenesis. Although NRP1 depletion in ECs in WT mice may affect embryonic brain angiogenesis [265] and postnatal pathological neovascularisation of the retina [271], that we observed no effect on β3-WT angiogenic responses suggests that the role of endothelial NRP1 in pathological angiogenesis is redundant in adult mice. The lack of an effect of the removal of NRP1's cytoplasmic tail on adult angiogenesis in β3-WT mice is, however, in agreement with that previously reported across the board [267,268]. Our *in vivo* and *ex vivo* angiogenic phenotypes correlated with the rates of random and directed migration of lung microvascular ECs isolated from mice of the same genotypes; only in β3-HET ECs was migration sensitive to the loss of NRP1's cytoplasmic tail. EC migration may therefore have a profound influence on tumour growth and angiogenesis in our models. Indeed, although the lack of a difference in tumour growth and angiogenesis in mice with a constitutive endothelial deletion of β3 [211] suggests that elevated tumour growth and angiogenesis in β3-HET mice is due to the role of non-ECs, β3-HET EC migration was enhanced in a similar manner to angiogenesis, and so endothelial migration cannot be ignored as a major contributor to our *in vivo* phenotypes. That there was no difference in the migration of β3-WT ECs lacking NRP1's cytoplasmic tail compared to WT ECs with full-length NRP1 came in contrast to the previously reported slower rate of migration exhibited by NRP1Δcyto heart ECs [289]. However, this discrepancy is likely explained by differences between lung microvascular ECs and heart ECs, which may reflect the dispensable role of NRP1's cytoplasmic tail in angiogenesis and significant role of this portion of NRP1 in arteriogenesis, respectively [267,268]. Since the knock-down of NRP1

has consistently impaired EC migration in the past [133,272], it stands to reason that the extracellular portion of NRP1 plays an important part in migration. In contrast to β3-NULL animals, increased angiogenesis in β3-HET mice does not occur through overt changes in VEGFR2 expression or VEGFR2-NRP1 interactions. Moreover, although ERK1/2 phosphorylation in β3-HET ECs was slightly reduced without NRP1's cytoplasmic tail, and there may be subtle changes in VEGFR2 recycling between β3-WT and β3-HET ECs, the increased sensitivity of β3-HET EC migration to the loss of NRP1's cytoplasmic tail does not appear to be wholly related to differences in VEGFR2 signalling or trafficking, which have previously been reported to be regulated by NRP1 [68,80,272,273,275,284]. Rather, we have identified a novel function for β3-integrin whereby it regulates the retention of NRP1 within mature FAs upon VEGF-stimulation. NRP1's involvement in EC migration, at least in microvascular ECs, is thereupon regulated by β3. When β3 is expressed at normal levels, NRP1 is stabilised in PXN-positive mature FAs, even following VEGF stimulation, and its cytoplasmic tail is dispensable for EC migration. However, when β3 expression is reduced, NRP1 is mobilised from mature FAs upon VEGF stimulation, and instead, unless it is missing its cytoplasmic tail, preferentially localises to PXN-positive vesicles. Though likely not through a direct interaction, β3 regulates NRP1's molecular associations with proteins within the adhesome, including filamin a and IQGAP1, whose associations with NRP1 become decreased in VEGF-stimulated β3-HET ECs, thus concurring with NRP1's localisation away from mature FAs. β3 also regulates NRP1's role in FA turnover and PXN activation. Whilst the loss of NRP1's cytoplasmic tail slightly impairs FA turnover, it does not affect PXN phosphorylation, and therefore may not perturb Cdc42-dependent migration [290]. β3-HET ECs display fast FA turnover, but without NRP1's cytoplasmic tail both FA turnover and PXN phosphorylation are strongly impaired. Thus, EC migration in β3-HET ECs is dependent on NRP1 via its involvement in FA turnover and PXN activation.

Since αvβ3-integrin is known to immobilise in static FAs [224], we hypothesise a mechanism in microvascular ECs whereby, when adequately expressed, αvβ3-integrin prevents NRP1 from fully participating in FA dynamics by sequestering it at these mature FAs even after VEGF stimulation. When αvβ3 expression is

reduced, however, VEGF stimulation mobilises NRP1 from these sites, allowing NRP1 to regulate the rapid vesicular recycling of FA components and concomitant FA turnover and PXN activation. PXN activation and concomitant Cdc42 activation can be adequately mediated by either unaltered αvβ3 or NRP1, but not when both are perturbed. Though not yet proven, NRP1 may also contribute to an increase in VEGFR2 recycling when β3 expression is reduced, thus accounting for an increase in ERK1/2 phosphorylation that is sensitive to the loss of NRP1's cytoplasmic tail. As a result of all this, whilst the role of NRP1's cytoplasmic tail in WT tumour growth and angiogenesis, and EC migration, is redundant, these processes become dependent on it when αvβ3 levels are reduced (see **Figure 6.1**).

This mechanism may also explain why simultaneously targeting both αvβ3 and NRP1 in ECs blocks the growth and angiogenesis of already established tumours. Accordingly, our work provides proof-of-concept that a dual-combative αvβ3-integrin/NRP1 targeting approach offers a clinically beneficial way of treating advanced solid cancers. Indeed, since β3-integrin's regulation of NRP1 function is dependent on the presence of VEGF, even when NRP1's regulation of VEGFR2 is largely unchanged, this approach may improve upon the efficacy of current strategies that mainly focus on manipulating the VEGF-VEGFR2 pathway, which are linked with significant side-effects and prone to treatment resistance [120].

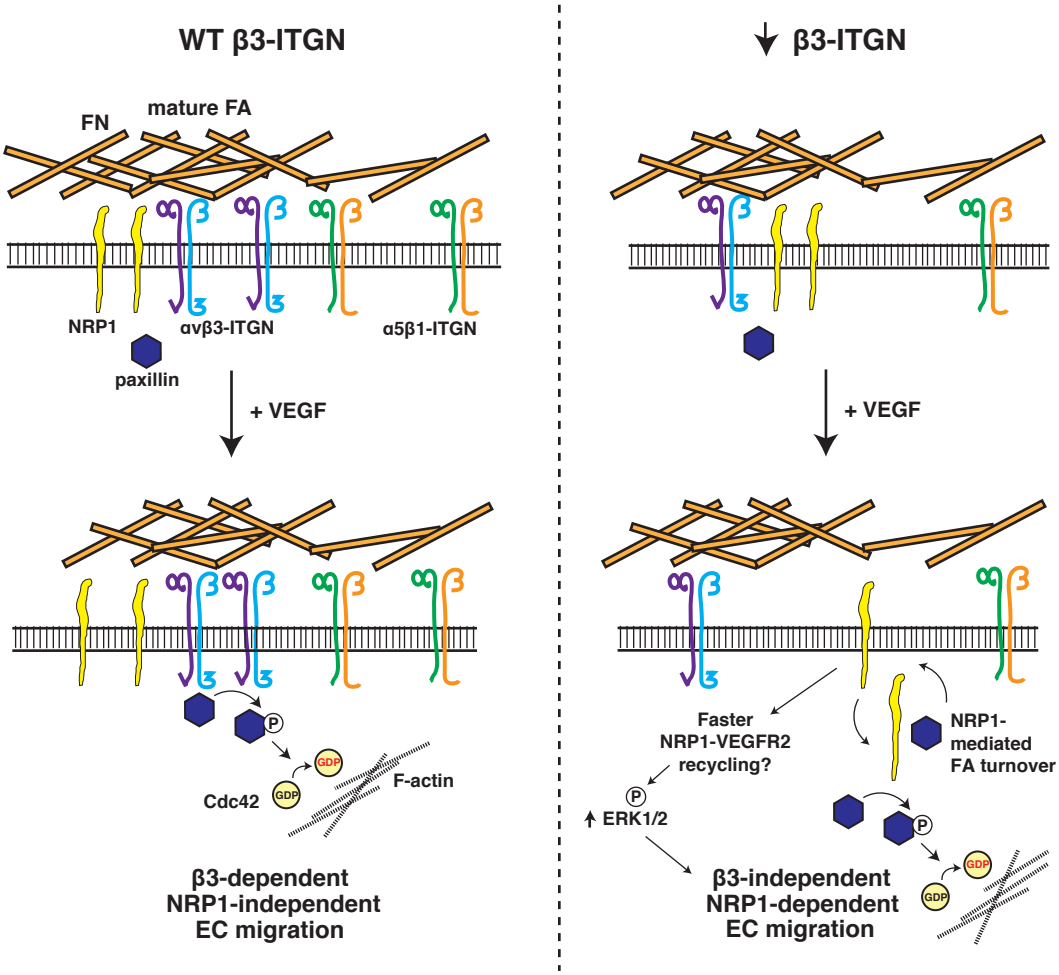

Figure 6.1: Model mechanism. Schematic representation of the hypothesised participation of neuropilin-1 (NRP1) in focal adhesion (FA) turnover and migration in β3-integrin-wild-type (β3-WT) (left) and β3-suppressed (right) endothelial cells (EC)s. See text for full details. ITGN, integrin. FN, fibronectin.

6.2 Future Work

Despite achieving the overall aims of this project, there are a number of areas that can be developed further in the future. Firstly, since our investigation into the effect of β3/NRP1 dual targeting on tumour metastasis was unsuccessful, this experiment remains a priority for us to better understand the longer-term implications of this type of intervention therapy. As our attempts using CMT19T cancer cells did not result in metastases, we propose to subcutaneously inject a different resectable cell-line, such as the Lewis lung carcinoma (LLC) cell-line, and carry on the experiment as before. Alternatively, we could also employ an orthotopic bone metastasis model that is currently being further developed in our laboratory. This model makes use of a C57BL/6 MMTV-PyMT-derived transplant cell-line (B6 LV-1) established by Prof Katherine Weilbaecher (Washington University, St Louis, USA), which selectively metastasises to bone following an orthotopic injection into mammary fat pads of mice. With this model, an adjuvant form of therapy can be simulated by administering OHT to induce endothelial depletion of β3 and/or NRP1 in our Cre-transgenic mice at the time of mastectomy. Subsequently, the formation of metastases in long bones can be monitored *in vivo* by bioluminescent/fluorescent imaging, as the B6 LV-1 cells are both GFP- and luciferase-tagged. If, like tumour growth, metastasis is reduced in the β3/NRP1 dual-targeted model, then the case for their joint targeting in the clinic is strengthened.

To expand on our proposed mechanism of αvβ3-regulated NRP1 function in FAs, a number of areas can be further clarified. As previously mentioned, to gain a clearer idea of potentially differential associations between NRP1 and particular FA proteins that were detected by mass spectrometry, but not reliably by co-IP, in our transgenic MLECs, we could use immunocytochemistry to co-localise NRP1 and these molecules, which include filamin a, IQGAP1, myosin 9, and α5β1-integrin, over a VEGF time course. Extending this further, to determine whether NRP1 does differentially recycle FA proteins in vesicles between EC genotypes, and thus explain NRP1-dependent differences in FA turnover, we would like to additionally co-localise these molecules with Rab4 or Rab11 markers of recycling vesicles. NRP1-PXN-Rab11 co-localisation in vesicles in β3-HET ECs, for example, which dynamically changes over a time course of VEGF stimulation,

may help prove that FA turnover is elevated in these cells as a result of faster NRP1-mediated PXN recycling. To further clarify whether there are subtle changes in NRP1-mediated VEGFR2 recycling between β3-WT and β3-HET ECs that explains their differential ERK1/2 activity, we could also monitor co-localisation between VEGFR2, Rab11 and NRP1 over time after stimulation in this way. As we wondered whether Cdc42 and Rac1 activation may be differentially activated via NRP1 in our ECs, we would to like to test this by using a PAK pull-down assay. If we detect differences in Cdc42 activation, it would also be worth looking at ABL1 activation to see if there is a β3/NRP1-regulated ABL1-mediated activation of PXN and Cdc42, as partly predicted by Raimondi et al. [271] and Fantin et al. [290]. Since these two previous studies were stimulating ECs by adhering them to FN, as opposed to VEGF-stimulating ECs already adhered to FN as we did, it might be interesting to try this alternative approach to seek potential differences. Moreover, we could also see if other growth factors besides VEGF have the same overall effect on NRP1 and its downstream effects in our ECs (or, indeed, on NRP1 localisation). If there are differences in Rac1 activation, we could initially determine whether NRP1 regulates this through filamin a and IQGAP1 by knocking down NRP1 and examining filamin a/IQGAP1 associations with Rac1.

Perhaps a more pertinent question regarding αvβ3's regulation of NRP1 is how does αvβ3-integrin control NRP1 localisation? To answer this we suggest transfecting different mutant β3 cDNA constructs into β3-NULL ECs in order to establish the particular functional properties of αvβ3 that exert control over NRP1's localisation to mature FAs. Specifically, we could make use of the DiYF β3 mutant developed by Phillips et al. [320], and previously used by Mahabeleshwar et al. [186], which contains mutations in the cytoplasmic tail residues Y747 and Y459, located in the NPxY and NxxY motifs, respectively, and thus is unable to be activated at these sites. Also available is the β3Δ722 mutant used by Robinson et al. [202], which lacks the end residues 723-787 of β3's cytoplasmic tail, and though still able to dimerise and engage ligands of the ECM, has impaired outside-in signalling. Another β3 mutant, β3Δ744, which is similar to β3Δ722 but less able to engage the ECM, could also be used. These constructs can be transfected into β3-NULL ECs alongside full-length β3 and an

empty vector as controls to compare NRP1 localisation between them by immunocytochemistry. This would additionally clarify whether the absence of β3 in β3-NULL ECs affects NRP1 localisation in the same way as in β3-HET ECs.

Having a clearer idea of the functionally relevant parts of the β3 and NRP1 molecules that contribute to our phenotypes should allow for the design of antagonists that are better suited to reducing tumour growth and angiogenesis in a dual-targeting strategy. Currently, small molecule inhibitors directed against NRP1 are under development [274,299,300], which target the VEGF-binding portion of NRP1. It would be interesting to initially determine whether these inhibitors have the same effect on EC migration in β3-HET ECs, or in ECs additionally targeted with existing αvβ3 antagonists, as the loss of NRP1's cytoplasmic tail has in β3-HET ECs. Similarly, we could examine EC migration in a reverse scenario, where αvβ3 is targeted with antagonists in β3-WT and β3-WT-NRP1Δcyto ECs, to determine whether the acute targeting of αvβ3, like long-term genetic targeting in the β3-HET model, also renders EC migration dependent on NRP1's cytoplasmic tail. One αvβ3 antagonist we would like to trial in particular is the RGDfV (EMD66203) cyclic peptide compound, which has greater specificity for αvβ3 compared to cilengitide, which more equally targets boh α5β1 and αvβ3. If these antagonists are similarly effective in inhibiting EC migration as our genetic approach, then this would pave the way for their joint use in clinically relevant tumour models, and ultimately in clinical trials. However, we suspect that inhibitors targeted against the cytoplasmic tail of NRP1 may meet with greater success than those currently under development, given the importance of this portion of NRP1 in regulating both FA proteins and VEGFR2. Moreover, until we have a better idea of what portion of the αvβ3 molecule regulates NRP1, we cannot decisively recommend an antagonist that would work most efficaciously alongside NRP1 inhibition. As both molecules are expressed by multiple cell types that contribute to tumour growth and angiogenesis, we must also carefully consider the off-target effects of antagonists on cell types other than ECs. Overall, a dual-targeted αvβ3/NRP1 pharmacological approach must be properly scutinised in the future in order to fulfil its potential for clinically beneficial and durable results.

German et al. [252] recently found that reducing PXN expression also reduced NRP2, thereby increasing HUVEC migration and angiogenesis. NRP2 has also separately been shown to regulate α6β1-integrin in the formation of FAs on laminin in breast cancer cells [321]. Another possible area for future research would therefore be to examine the relationship between αvβ3 and NRP2. Does β3 expression regulate NRP2 localisation in the same way as NRP1? Is NRP2 involved in directing FA turnover in ECs? Are tumour growth, angiogenesis, and EC migration sensitive to NRP2 targeting in β3-depleted models? These are some of the questions that would be interesting to attempt to answer in this regard.

Our findings that β3-integrin changes NRP1's associations within the adhesome, and that both molecules are implicated in directing FA dynamics and EC migration, warrant a wider investigation into how αvβ3 influences the endothelial adhesome. We would therefore like to conduct detailed further analyses of the adhesome by mass spectrometry with a view to observing how the composition of the adhesome changes following different αvβ3 targeting methods in ECs. FA proteins that change consistently between different approaches of targeting αvβ3 might offer themselves as novel candidates that contribute to differential adhesion dynamics, and thus could potentially be co-targeted with αvβ3 to manipulate angiogenic responses. We can additionally assess the role of myosin II-generated force and externally applied forces in changes in NRP1 and the adhesome, as well as examining changes following myosin II inhibition with blebbistatin.

Finally, results from this project have hinted at the possible involvement of α5β1-integrin in a β3/NRP1-related mechanism. We would therefore like to begin to decipher how these three molecules behave together in ECs, with a view to continue developing the search for a novel anti-angiogenic therapeutic approach.

Appendix

1. Supplementary Figures

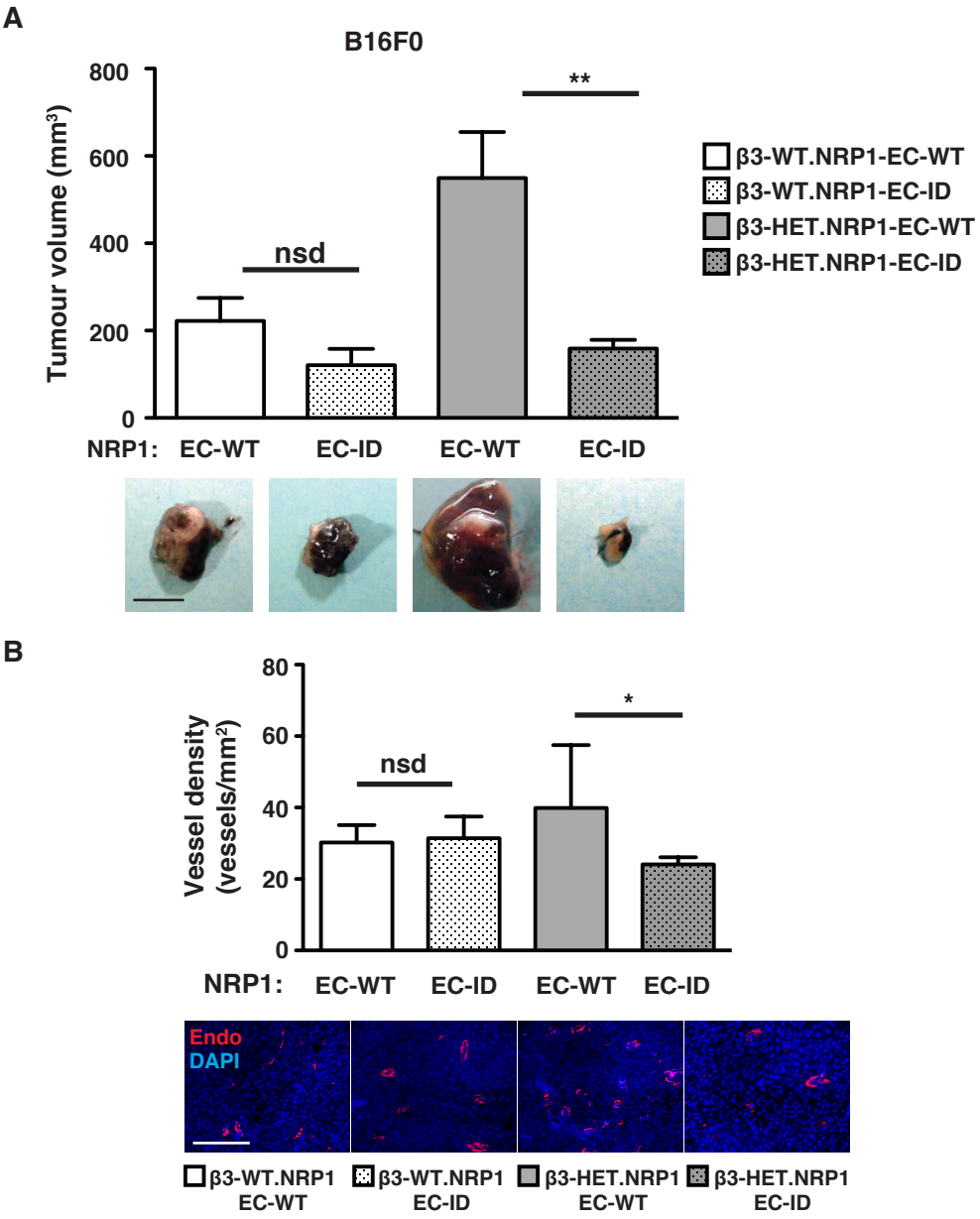

Appendix Figure 1: B16F0 Tumour growth and tumour angiogenesis in β3-integrin-heterozygous mice are sensitive to endothelial neuropilin-1 depletion. A Tumour growth was measured in animals of the indicated genotypes. Mice were given subcutaneous injections of B16F0 tumour cells. To induce depletion of endothelial NRP1 (NRP1-EC-ID), 21-day slow-release OHT pellets were administered 3-days prior to tumour cell injection. OHT-treated Cre-negative (NRP1-EC-WT) littermates served as controls. Tumour volumes were measured after 12 days of growth (mean +SEM of 3 independent experiments; n≥10 animals per genotype). Representative pictures of tumour macroscopic appearances are shown below. Scale bar = 10 mm. **B** Blood vessel density was assessed in tumours of the indicated genotypes by counting the total number of endomucin-positive vessels across tumour sections (mean +SEM; n≥10 sections per genotype). Representative micrographs of immunofluorescence staining for endomucin, an endothelial cell marker (Endo, red) in tumour sections from each genotype are shown below. DAPI (blue) was used as a nuclear counterstain. Scale bar = 100 µm. Asterisks indicate statistical significance: *, $P<0.05$; **, $P<0.01$; nsd = not significantly different. Unpaired two-tailed *t* test.

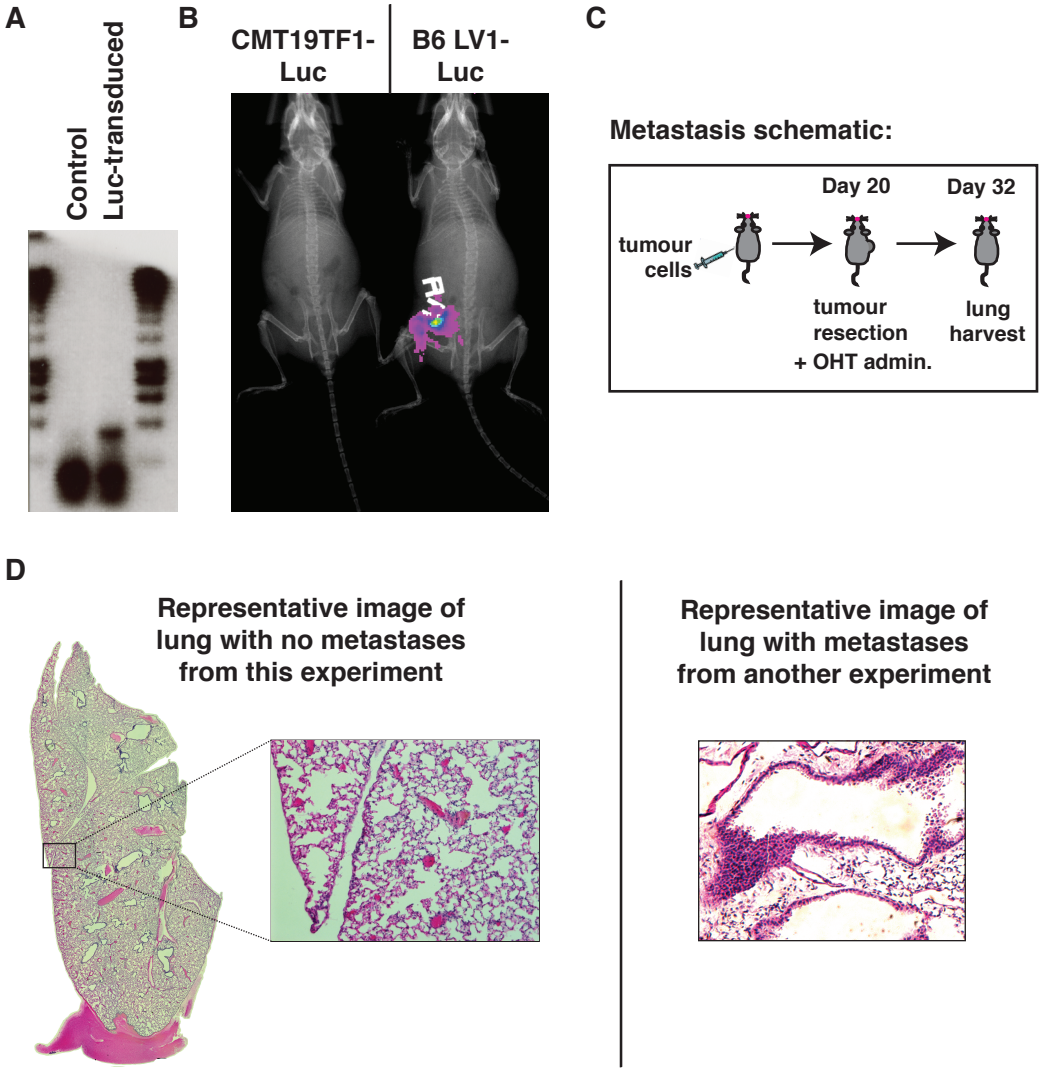

Appendix Figure 2: The investigation of the dual importance of β3-integrin and neuropilin-1 in metastasis was unsuccessful. A RT-PCR of the luciferase (Luc) gene from CMT19TF1 cells transduced with a lentiviral-luciferase construct and control cells that were not transduced. **B** Bioluminescence image of mice previously injected with the alleged CMT19TF1-Luc cells and another cell-line known to be tagged with Luc (B6 LV1-Luc). No bioluminescence was detected in the CMT19TF1-Luc-injected mice. **C** *Metastasis model schematic*: Mice were injected subcutaneously with CMT19TF1 cells and 20 days later tumours were resected and OHT was administered to induce depletion of endothelial β3 and/or NRP1 (EC-ID). After an additional 12 days (32 days in total) lungs were harvested and processed to detect metastases. **D** Representative H&E images of all lungs from this experiment showing no metastases (*left*) and of lungs from Cre-negative Tie.Cre/β3-floxed mice in another experiment from our laboratory that do display metastases (*right*).

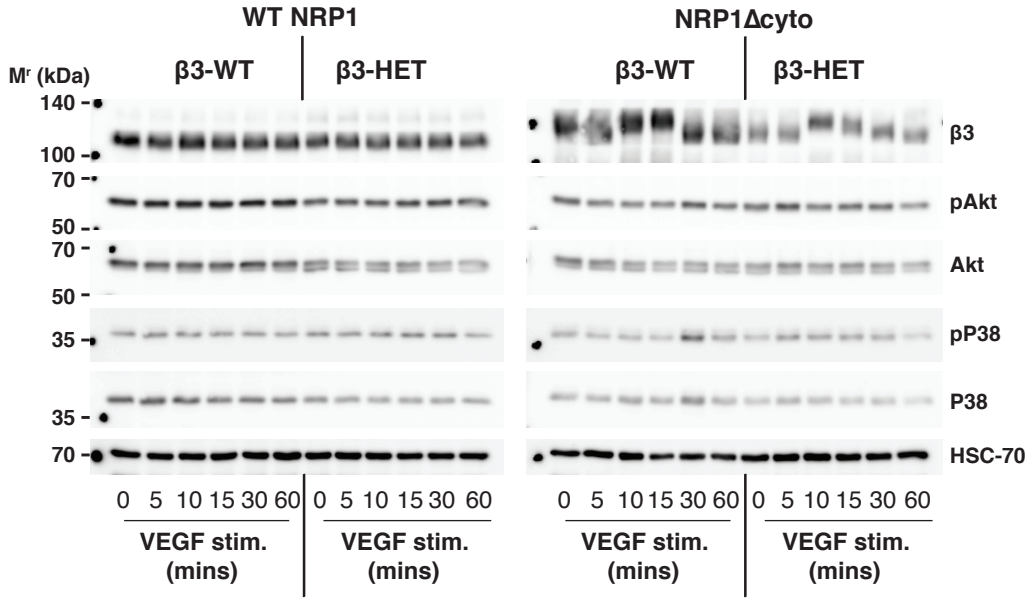

Appendix Figure 3: Neuropilin-1-regulated VEGFR2 signalling via Akt and p38MAPK is no different between wild-type and β3-integrin heterozygous endothelial cells with and without neuropilin-1's cytoplasmic tail. Lung microvascular endothelial cells (ECs) were isolated and immortalised (polyoma-middle-T-antigen) from β3-WT and β3-HET mice that were expressing either normal (WTNRP1) or cytoplasmic-tail deleted NRP1 (NRP1Δcyto). ECs were seeded overnight on a complex matrix containing gelatin, collagen, fibronectin and vitronectin, and were then stimulated with VEGF over an extended time course to examine signalling kinetics. ECs were lysed and blotted for levels of phosphorylated ('p'...) and total Akt, and phosphorylated p38MAPK and total p38MAPK. HSC-70 was used as a loading control. Data are representative of 3 independent experiments.

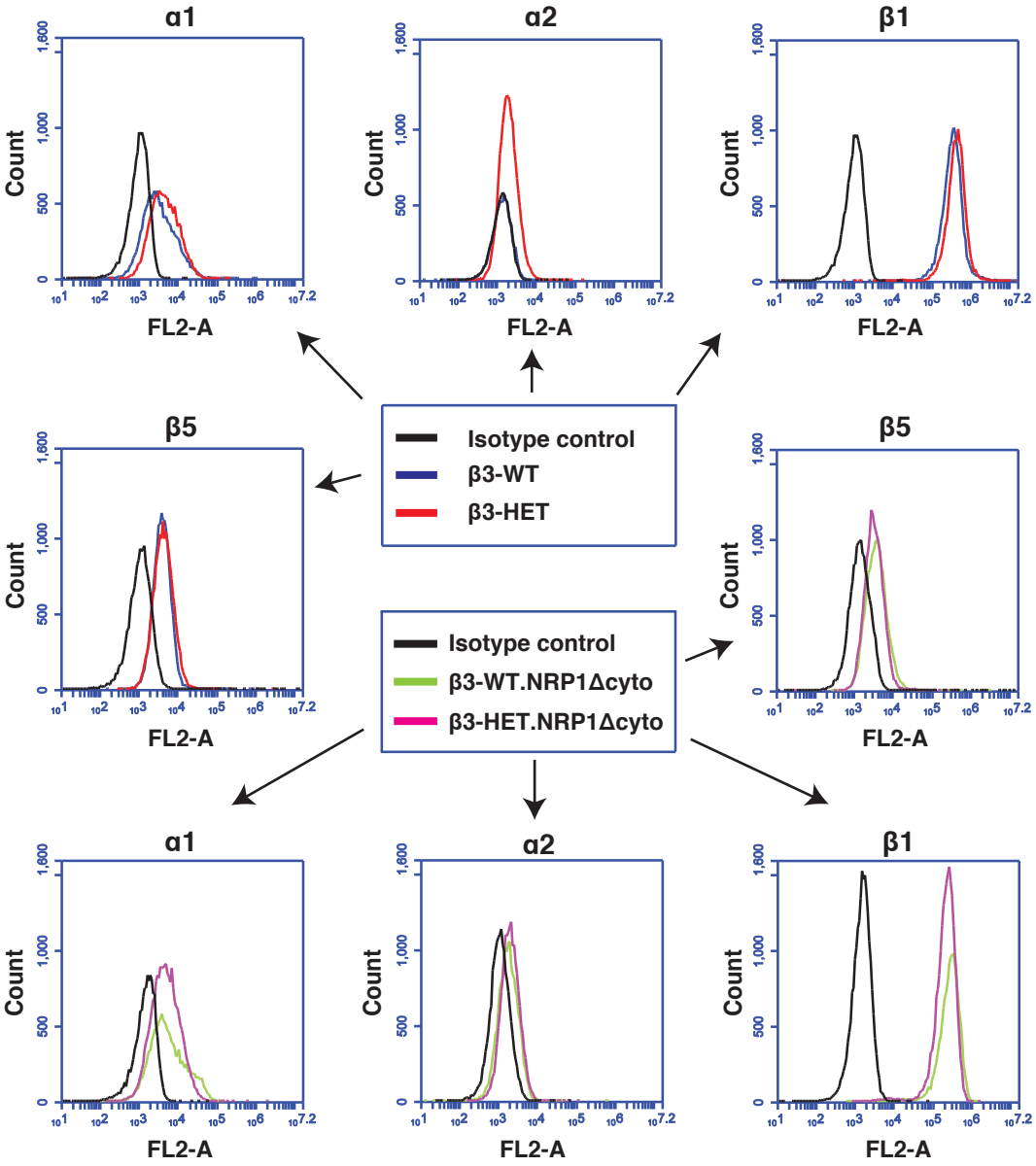

Appendix Figure 4: Examining surface levels of integrins in β3-integrin-wild-type and heterozygous endothelial cells with and without neuropilin-1's cytoplasmic tail. ECs of the indicated genotypes were measured for their surface expression of endothelial integrin subunits by flow-cytometry. Flow-cytometric histogram profiles were generated after forward versus side scatter data were tightly gated around, and normalised to, an isotype control. Representative profiles are shown from 3 independent experiments.

2. Publications

Ellison, TS, Atkinson, SJ, Steri, V, Kirkup, BM, Preedy, MEJ, Johnson, RT, Ruhrberg, C, Edwards, DR, Schneider, JG, Weilbaecher, K, Robinson SD. Suppression of β3-integrin in mice triggers a neuropilin-1- dependent change in focal adhesion remodelling that can be targeted to block pathological angiogenesis. *Dis Model Mech*. 2015; 8: 1105-1119. (**Attached below**)**.**

Atkinson SJ, Ellison TS, Steri V, Gould E, Robinson SD. Redefining the role(s) of endothelial alphavbeta3-integrin in angiogenesis. *Biochem Soc Trans*. 2014; 42: 1590-5. (**Attached below**).

Steri V, Ellison TS, Gontarczyk AM, Weilbaecher K, Schneider JG, Edwards D, Fruttiger M, Hodivala-Dilke KM, Robinson SD. Acute depletion of endothelial beta3-integrin transiently inhibits tumor growth and angiogenesis in mice. *Circ Res. 2014*; 114: 79-91.

© 2015. Published by The Company of Biologists Ltd | Disease Models & Mechanisms (2015) 8, 1105-1119 doi:10.1242/dmm.019927

RESEARCH ARTICLE

Suppression of β3-integrin in mice triggers a neuropilin-1-dependent change in focal adhesion remodelling that can be targeted to block pathological angiogenesis

Tim S. Ellison[1], Samuel J. Atkinson[1], Veronica Steri[1], Benjamin M. Kirkup[1], Michael E. J. Preedy[1], Robert T. Johnson[1], Christiana Ruhrberg[2], Dylan R. Edwards[1], Jochen G. Schneider[3], Katherine Weilbaecher[4] and Stephen D. Robinson[1,*]

ABSTRACT

Anti-angiogenic treatments against αvβ3-integrin fail to block tumour growth in the long term, which suggests that the tumour vasculature escapes from angiogenesis inhibition through αvβ3-integrin-independent mechanisms. Here, we show that suppression of β3-integrin in mice leads to the activation of a neuropilin-1 (NRP1)-dependent cell migration pathway in endothelial cells via a mechanism that depends on NRP1's mobilisation away from mature focal adhesions following VEGF-stimulation. The simultaneous genetic targeting of both molecules significantly impairs paxillin-1 activation and focal adhesion remodelling in endothelial cells, and therefore inhibits tumour angiogenesis and the growth of already established tumours. These findings provide a firm foundation for testing drugs against these molecules in combination to treat patients with advanced cancers.

KEY WORDS: Integrin, Neuropilin-1, Angiogenesis, Tumour, Focal adhesion

INTRODUCTION

Angiogenesis, the formation of new blood vessels from pre-existing vasculature, is essential to support both primary and metastatic tumour growth (Hanahan and Weinberg, 2011). It occurs when hypoxia causes tumour cells to release growth factors such as vascular endothelial growth factor (VEGF), which stimulate nearby endothelial cells (ECs) to activate appropriate growth factor receptors, e.g. VEGF-receptor-2 (VEGFR2). New blood-vessel formation ensues as ECs proliferate and migrate through the extracellular matrix (ECM) toward the tumour in an integrin-dependent fashion (Robinson and Hodivala-Dilke, 2011). This process of tumour angiogenesis frequently offers a route to metastasis by providing an increased density of highly permeable blood vessels. Thus, anti-angiogenic strategies form a key component of the current cancer-targeting arsenal. Because of its central role in the process, many of the existing anti-angiogenic strategies target the VEGF-VEGFR2 pathway, but these approaches are linked to a plethora of unwanted side effects and the development of treatment resistance (Ebos and Kerbel, 2011).

Integrins are the main ECM adhesion receptors. They sense, integrate and disseminate ECM and growth factor signals to co-ordinate EC responses during angiogenesis (Silva et al., 2008). αvβ3-integrin has emerged as a key anti-angiogenic therapeutic target because it is upregulated in the vasculature of solid tumours, but its expression is low in quiescent vasculature (Brooks et al., 1994). Unlike current FDA-approved anti-angiogenic drugs, αvβ3-integrin antagonists are well-tolerated, likely owing to the fact that αvβ3-integrin expression is restricted to neo-angiogenic vessels (Hariharan et al., 2007). However, the synthetic inhibitors directed against αvβ3-integrin have so far failed to improve overall survival in patients (Marelli et al., 2013). Moreover, although we have shown that suppressing endothelial αvβ3-integrin in the early stages of tumour growth has an inhibitory growth effect, its long-term suppression leads to 'treatment' resistance (Steri et al., 2014). We do not yet understand what the mechanisms of resistance are, or how to overcome them. In order to improve therapeutic outcomes when targeting this key molecule, we need to rethink how to best use anti-angiogenic strategies based on αvβ3-integrin antagonism.

A promising approach to overcome resistance to anti-angiogenic treatment is to identify pathways of resistance and to co-target them alongside the original target. Such approaches are emerging in a number of cancer types as viable therapeutic strategies to improve upon existing treatments (Sennino and McDonald, 2012). In 2009, an αvβ3-integrin co-target candidate emerged: the VEGF co-receptor, neuropilin-1 (NRP1) (Robinson et al., 2009). However, we do not yet fully understand how these two molecules cooperate mechanistically to regulate pathological angiogenesis, nor do we know whether their interaction can be manipulated to alter outcomes.

NRP1 is a single-pass transmembrane molecule found, for example, in neurons and ECs. Originally identified as an adhesion molecule (Takagi et al., 1995), attention shifted to its VEGF-dependent role in binding and regulating the signalling and trafficking of VEGFR2 in ECs (Ballmer-Hofer et al., 2011; Herzog et al., 2011). NRP1's short cytoplasmic tail is crucial for the regulation of VEGFR2 trafficking because its SEA motif binds the PDZ domain of synectin, linking the complex to the inward trafficking motor myosin VI (Ballmer-Hofer et al., 2011; Cai and Reed, 1999). Recent work has returned to its original role as an adhesion molecule. Valdembri et al. (2009) showed that NRP1 binds and regulates α5β1-integrin trafficking, again via its cytoplasmic tail, and thus promotes EC spreading on low

[1]School of Biological Sciences, University of East Anglia, Norwich Research Park, Norwich, NR4 7TJ, UK. [2]Institute of Ophthalmology, University College London, London, EC1V 9EL, UK. [3]Luxembourg Center for Systems Biomedicine (LCSB), University of Luxembourg, Luxembourg & Saarland University Medical Center, Internal Medicine II, L-4362 Homburg, Germany. [4]Department of Internal Medicine, Division of Molecular Oncology, Washington University in St Louis, St Louis, MO 63110, USA.

*Author for correspondence (stephen.robinson@uea.ac.uk)

This is an Open Access article distributed under the terms of the Creative Commons Attribution License (http://creativecommons.org/licenses/by/3.0), which permits unrestricted use, distribution and reproduction in any medium provided that the original work is properly attributed.

Received 13 January 2015; Accepted 7 July 2015

Disease Models & Mechanisms (2015) 8, 1105-1119 doi:10.1242/dmm.019927

TRANSLATIONAL IMPACT

Clinical issue

αvβ3-integrin has emerged as a key anti-angiogenic target in cancer therapy because it plays a pivotal role in endothelial cell migration and vascular endothelial growth factor (VEGF)-mediated signalling. However, innate and acquired treatment resistance occurs with its blockade, so treatment fails to block tumour growth in the long term. Understanding the molecular mechanisms that contribute to this resistance is necessary for developing new strategies that target αvβ3-integrin to inhibit tumour growth and progression. It is clear that alternative pro-angiogenic pathways become active in the absence of αvβ3-integrin expression, which suggests that these pathways offer routes to resistance to αvβ3-integrin blockade. This study seeks to understand the molecular basis behind how αvβ3-integrin-regulated pathways contribute to anti-angiogenic resistance and to test the hypothesis that blocking αvβ3-integrin in combination with these pathways will block tumour progression.

Results

Using heterozygous β3-integrin-deficient mice as a model of αvβ3-integrin blockade, the authors uncovered a neuropilin-1 (NRP1)-regulated endothelial-cell-migration pathway that only becomes active when αvβ3-integrin expression is suppressed. In β3-integrin heterozygous endothelial cells, but not in wild type, NRP1 regulated paxillin-1 phosphorylation, focal adhesion remodelling and cell migration. This newly found role for NRP1 correlates with its mobilisation away from mature focal adhesions in VEGF-induced β3-integrin-depleted cells; this shift in cellular localisation does not occur in wild-type cells. Finally, the authors show that suppressing the endothelial expression of both αvβ3-integrin and NRP1 blocks the progression of already-established tumours.

Implications and future directions

This study uncovered an NRP1-dependent migration pathway that only becomes active upon αvβ3-integrin depletion and it showed that this pathway can be targeted to block tumour progression. These results implicate endothelial NRP1 as a potential co-target during αvβ3-integrin-directed therapies to prevent anti-angiogenic treatment resistance.

concentrations of fibronectin (FN), whereas Raimondi et al. (2014) demonstrated an essential role for NRP1 in promoting FN-dependent signalling in ECs. In support of VEGF-independent roles for NRP1 in ECs, Fantin et al. (2014) found that mice with a mutant NRP1 defective in VEGF binding overcome the mid-gestation lethality of full NRP1-knockout mice (Kawasaki et al., 1999). Indeed, there is mounting evidence that links VEGF-independent roles for NRP1 to focal adhesion (FA) function (Raimondi et al., 2014; Seerapu et al., 2013). What we do not yet know is how and when, and in what cell types, NRP1 contributes to the assembly and maintenance of these large and dynamic macromolecular assemblies that link the ECM to the cytoskeleton and through which both mechanical force and regulatory signals are transmitted (Zamir and Geiger, 2001).

That NRP1 plays a crucial role in developmental angiogenesis and arteriogenesis is undeniable (Fantin et al., 2014, 2011; Gerhardt et al., 2004; Kawasaki et al., 1999; Lanahan et al., 2013), but its role in pathological angiogenesis is not clear. Although a number of papers allude to it having no role, Fantin et al. (2014) published findings suggesting that the VEGF-binding domain of NRP1 is important for pathological neovascularisation of the retina and angiogenesis-dependent tumour growth. Here, we conclusively show, however, that disrupting NRP1 function by deleting its cytoplasmic tail or by depleting its expression in wild-type mice has no effect on tumour growth or angiogenesis. However, we can sensitise angiogenic responses to NRP1 perturbations by reducing β3-integrin expression in heterozygous β3-integrin-deficient mice. We show that β3-integrin expression is essential for the efficient retention of NRP1 at FAs after VEGF-stimulation. NRP1 can influence paxillin-1 (PXN) activity and FA remodelling, but only if it is relieved from its retention within mature FAs by reducing β3-integrin expression. This sensitisation to NRP1 perturbations that occurs upon suppressing β3-integrin means that we can target both molecules simultaneously to significantly improve inhibition of growth and angiogenesis in both new and established tumours. This finding offers a potential solution to improve anti-angiogenic strategies.

RESULTS

Pathological angiogenesis is sensitive to NRP1 disruption in heterozygous β3-integrin-deficient mice

We previously showed that VEGF-mediated angiogenic responses become dependent on NRP1 in β3-integrin-knockout (β3-KO) mice (Robinson et al., 2009). In this model, angiogenesis was significantly blocked only by simultaneously inhibiting both β3-integrin and NRP1, a finding that we would like to translate to the clinic. In the β3-KO model, however, pathological angiogenesis is elevated over the wild type (Reynolds et al., 2002). It has been postulated that this phenotypic response occurs, in part, through the developmental upregulation of VEGFR2 (Reynolds et al., 2004), making it potentially difficult to interpret experimental outcomes that depend on molecular interactions with this growth-factor receptor. We therefore moved our analyses to β3-integrin-heterozygous (β3-HET) mice, hypothesising that this would circumvent developmental changes arising from the complete loss of the protein, whilst at the same time maintaining, at least to a degree, critical interactions between β3-integrin and VEGFR2 (Mahabeleshwar et al., 2007) and/or NRP1 (Robinson et al., 2009).

We crossed β3-integrin-wild-type (β3-WT) and β3-HET mice to tamoxifen (OHT)-inducible Pdgfb-iCreER^{T2}/NRP1-floxed mice (Claxton et al., 2008; Gu et al., 2003) and examined the effect of an acute EC-specific depletion of NRP1 (EC-NRP1-KO) on subcutaneous allograft tumour growth with both CMT19T cells (Fig. 1A) and B16F0 cells (supplementary material Fig. S1), as well as on aortic ring sprouting (Fig. 1B). Depleting EC-NRP1 expression in this way had no effect on β3-WT responses, but significantly inhibited tumour growth and VEGF-induced microvessel sprouting in β3-HET mice. Tumour angiogenesis was significantly inhibited in β3-HET mice by depleting EC-NRP1, although vessel morphology and pericyte coverage were normal (Fig. 1C). These studies are reminiscent of the changes observed in β3-KO mice, but, importantly, suggest that NRP1 function is already perturbed by subtle changes in β3-integrin expression levels.

To narrow our mechanistic focus further, we crossed β3-WT and β3-HET animals with mice carrying a global deletion of NRP1's cytoplasmic tail (NRP1Δcyto), which is essential for many of its functions (Fantin et al., 2011; Lanahan et al., 2013). CMT19T tumour growth (Fig. 1D) and microvessel sprouting (Fig. 1E) patterns were unaltered in β3-WT mice by the introduction of the NRP1Δcyto mutation, whereas both parameters were inhibited in β3-HET mice. Although the loss of NRP1's cytoplasmic tail had a small effect on tumour angiogenesis in β3-WT mice (Fig. 1F), this did not translate to an overall difference in tumour growth (Fig. 1D). As in EC-NRP1-KO tumours, pericyte coverage of tumour vasculature was not affected by an NRP1 cytoplasmic deletion (Fig. 1F). We conclude from these studies that NRP1's cytoplasmic tail is normally dispensable for pathological angiogenesis, but plays a significant role when insufficient β3-integrin is expressed.

Disease Models & Mechanisms (2015) 8, 1105-1119 doi:10.1242/dmm.019927

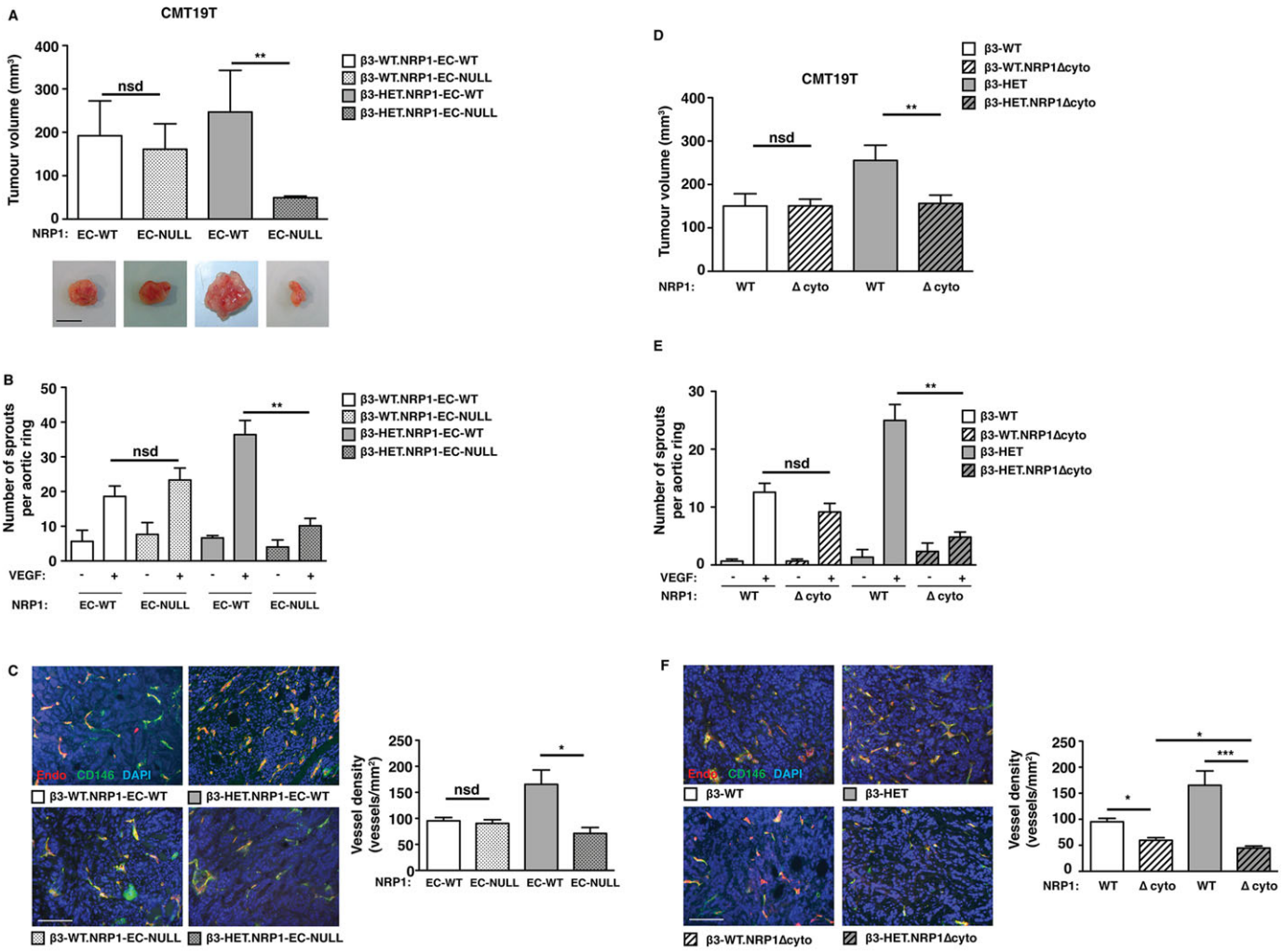

Fig. 1. Tumour growth, tumour angiogenesis and microvessel sprouting in β3-integrin-deficient heterozygous mice are sensitive to NRP1 perturbations. (A) Tumour growth was measured in animals of the indicated genotypes. Mice were given subcutaneous injections of CMT19T tumour cells. To generate NRP1-EC-KO (EC-null), 21-day slow-release OHT pellets were administered 3 days prior to tumour-cell injection. OHT-treated Cre-negative (NRP-EC-WT) littermates served as controls. Tumour volumes were measured after 12 days of growth (mean+s.e.m. of three independent experiments; $n \geq 10$ animals per genotype). Representative pictures of tumour macroscopic appearances are shown. Scale bar: 10 mm. (B) Microvessel sprouting of aortic ring explants of the indicated genotypes. NRP1-EC-KO was induced in culture with 1 μM OHT. OHT-treated Cre-negative (EC-NRP-WT) rings served as controls. The bar chart shows the total number of microvessel sprouts per aortic ring after 6 days of VEGF-stimulation (mean+s.e.m. from three independent experiments; $n \geq 40$ rings per genotype). (C) Blood-vessel density was assessed in tumours of the indicated genotypes by counting the total number of endomucin-positive vessels across tumour sections (mean+s.e.m.; $n \geq 10$ sections per genotype over three independent experiments). Representative micrographs of immunofluorescence staining for endomucin, an endothelial cell marker (Endo; red) and CD146, a pericyte marker (green) in tumour sections from each genotype are shown. DAPI (blue) was used as a nuclear counterstain. Scale bar: 100 μm. (D) CMT19T tumour growth and angiogenesis were measured in animals of the indicated genotypes. In addition to their β3-integrin genetic status, mice were negative (NRP1 WT) or positive (NRP1 Δcyto) for the loss of NRP1's cytoplasmic tail. Mice were given subcutaneous injections of CMT19T cells and tumour volumes were measured 12 days later. The bar chart shows tumour volumes (mean+s.e.m. of three independent experiments; $n \geq 10$ animals per genotype). (E) Microvessel sprouting of aortic ring explants of the indicated genotypes. The bar chart shows the total number of microvessel sprouts per aortic ring after 6 days of VEGF-stimulation (mean+s.e.m. from three independent experiments; $n \geq 40$ rings per genotype). (F) Blood-vessel density was assessed by endomucin (red) and CD146 (green) staining (mean+s.e.m.; $n \geq 10$ sections per genotype). DAPI was used as a nuclear counterstain (blue). Scale bar: 100 μm. Asterisks indicate statistical significance: *P<0.05; **P<0.01; ***P<0.001; nsd, not significantly different. Unpaired two-tailed t-test.

NRP1-dependent functions of VEGFR2 are normal in β3-integrin-heterozygous endothelial cells

Given that NRP1's cytoplasmic tail is important for the regulation of VEGFR2 signalling and trafficking (Ballmer-Hofer et al., 2011; Herzog et al., 2011), we wanted to investigate whether the NRP1Δcyto mutation differentially affects VEGFR2 function in β3-WT versus β3-HET lung microvascular ECs. We employed polyoma-middle-T-antigen immortalised ECs, isolated from the mutant mice described above, because we and others have shown that they present good models to study angiogenesis (Ni et al., 2014; Robinson et al., 2009; Steri et al., 2014; Tavora et al., 2014). We first compared total VEGFR2 levels in the four genotypes (β3-WT, β3-HET, β3-WT;NRP1Δcyto and β3-HET;NRP1Δcyto). Unlike β3-KO ECs, we noted only a small trend of increased VEGFR2 levels in β3-HET and β3-HET;NRP1Δcyto ECs (Fig. 2A).

To explore potential changes in VEGFR2-dependent signalling, we seeded ECs on a complex matrix containing gelatin, collagen I (COLI), FN and vitronectin (VN) to preserve the known VN-dependent β3-VEGFR2 interaction (Soldi et al., 1999), stimulated with VEGF, and immunoblotted for changes in total

Disease Models & Mechanisms (2015) 8, 1105-1119 doi:10.1242/dmm.019927

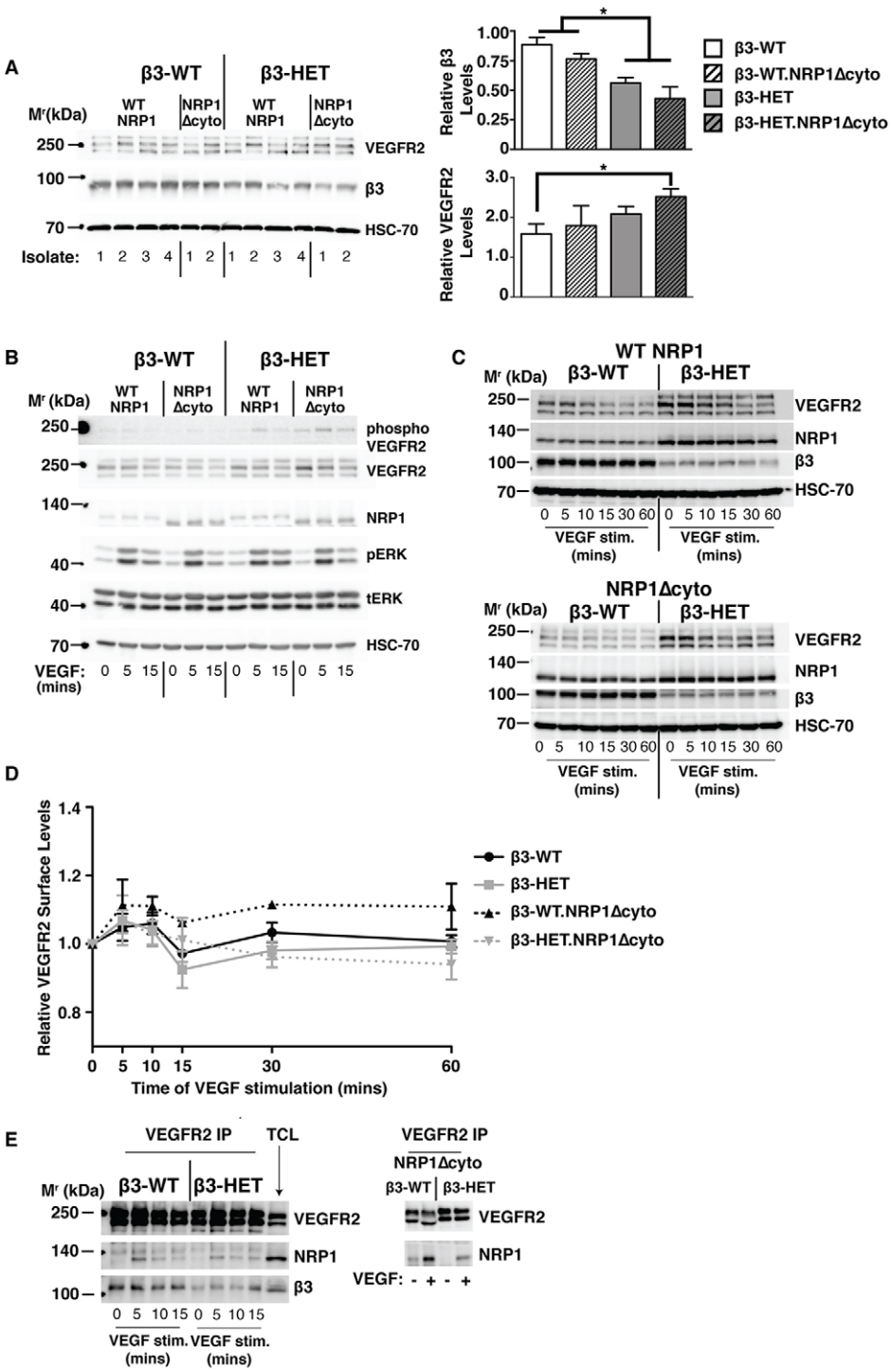

Fig. 2. NRP1-dependent functions of VEGFR-2 are normal in β3-integrin-heterozygous endothelial cells. (A) Lung microvascular endothelial cells (ECs) were isolated and immortalised (polyoma-middle-T-antigen) from β3-WT and β3-HET mice that were expressing either normal (WT NRP1) or cytoplasmic-tail-deleted (NRP1 Δcyto) NRP1. Multiple EC lysates of each genotype were western blotted (WB) to examine total cellular levels of VEGFR2 and β3-integrin. Bar charts of densitometric analysis of mean (+s.e.m.) changes between the four genotypes are shown to the right. Asterisks indicate statistical significance: *P<0.05. (B-E) Representative of ≥three independent experiments per blotted protein. ECs were seeded overnight on a complex matrix containing gelatin, collagen, fibronectin and vitronectin, and were then stimulated with VEGF over the indicated time courses. (B) ECs were lysed and blotted for levels of phosphorylated (phospho) and total VEGFR2, NRP1, and phospho (pERK) and total (tERK) ERK1/2. (C) To examine protein degradation, the VEGF time course was extended and EC lysates were blotted for levels of total VEGFR2, NRP1 and β3-integrin. (D) Following a VEGF time course, ECs were trypsinised and analysed by flow cytometry for surface levels of VEGFR2. Median fluorescence intensity was measured after forward versus side scatter data were tightly gated around, and normalised to, an isotype control. The graph shows the relative surface level of VEGFR2 (means±s.e.m.) relative to the 0 (non-stimulated) time point. (E) ECs were stimulated with VEGF for the indicated amounts of time and then lysed and immunoprecipitated for VEGFR2 (VEGFR2 IP), before being blotted for NRP1 association. A total cell lysate (TCL) is shown for comparison. (A-E) HSC-70 served as a loading control. Data are representative of three independent experiments.

Disease Models & Mechanisms (2015) 8, 1105-1119 doi:10.1242/dmm.019927

and phosphorylated levels of VEGFR2 and its downstream targets ERK1/2 (Koch et al., 2011) (Fig. 2B). Although VEGF-induced VEGFR2 phosphorylation was slightly elevated in β3-HET ECs, VEGFR2 phosphorylation was not significantly changed by the introduction of the NRP1Δcyto mutation in either β3-WT or β3-HET ECs, suggesting that VEGFR2 signalling is NRP1-independent in these microvascular ECs despite differences in β3-integrin expression. In contrast, VEGF-induced ERK1/2 phosphorylation was sensitive to an NRP1 cytoplasmic deletion in β3-HET ECs but not β3-WT ECs (Fig. 2B).

We observed no overt changes in the pattern of total cellular VEGFR2 expression over time after VEGF stimulation when comparing the four genotypes to one another (Fig. 2C). In each case, VEGFR2 expression levels dropped over the time course of stimulation. This is suggestive of the protein being degraded over time in all four genotypes and is congruent with prior reports (Ewan et al., 2006; Reynolds et al., 2009; Reynolds and Hodivala-Dilke, 2006).

Taken together, these signalling studies pointed to a VEGFR2-independent role for NRP1 in mediating VEGF-induced responses in β3-HET ECs. However, as previously mentioned, when compared to their β3-WT counterparts, total VEGFR2 levels were slightly elevated in both β3-HET and β3-HET;NRP1Δcyto ECs. Moreover, NRP1 expression was substantially increased in both β3-WT;NRP1Δcyto and β3-HET;NRP1Δcyto ECs (Fig. 2A,B). We therefore decided to examine VEGFR2 behaviour in greater detail, including its direct interactions with NRP1.

We measured VEGFR2 surface levels via flow-cytometry over a VEGF-stimulated time course (Fig. 2D). However, surface levels were similar between the four genotypes, and were as predicted from previously published studies (Lampugnani et al., 2006; Reynolds et al., 2009). Because VEGF-induced interactions between VEGFR2 and NRP1 are elevated in β3-KO ECs (Robinson et al., 2009), we next examined this interaction in β3-HET ECs by co-immunoprecipitation, but observed no alterations compared to β3-WT ECs (Fig. 2E). In contrast to previously published studies (Prahst et al., 2008), we saw that the VEGF-induced association between the two molecules was preserved in both β3-WT;NRP1Δcyto and β3-HET;NRP1Δcyto ECs (Fig. 2E). We also examined by immunoblotting other known NRP1-dependent signalling pathways, including the activation of focal adhesion kinase (FAK) (Herzog et al., 2011) and p130Cas (Evans et al., 2011), but saw no changes that might explain why β3-HET mice are sensitive to NRP1 perturbation, whereas β3-WT mice are not (supplementary material Fig. S2); both pathways were inhibited in both genotypes by the introduction of the NRP1Δcyto mutation.

Although these analyses did not rule out subtle differences between the four genotypes in VEGFR2 trafficking, they did allow us to draw an important conclusion: the differential sensitivity of β3-WT and β3-HET animals to NRP1 disruption does not seem to arise from overt changes in VEGFR2 function.

The VEGF-induced migration in β3-integrin-heterozygous microvascular endothelial cells depends on the cytoplasmic tail of NRP1

Prior to its description as a VEGF co-receptor, NRP1 was identified as a surface protein mediating cell adhesion (Takagi et al., 1995). Moreover, evidence has mounted to support a VEGFR2-independent role for NRP1 in regulating EC functions through an FA-dependent mechanism (Fantin et al., 2014; Raimondi et al., 2014; Seerapu et al., 2013). Because NRP1 is known to interact with a number of integrins (Fukasawa et al., 2007; Robinson et al., 2009; Valdembri et al., 2009), we first compared static cell adhesion between β3-WT, β3-HET, β3-WT;NRP1Δcyto and β3-HET; NRP1Δcyto ECs on saturating concentrations of various matrices. The only clear difference noted on saturating matrix concentrations in these assays was an expected reduced adhesion of β3-HET and β3-HET.NRP1Δcyto ECs to matrices containing VN, β3-integrin's canonical ligand (Fig. 3A). A more vigorous examination of adhesions (see Materials and Methods) over a range of matrix concentrations, however, uncovered subtle changes between the genotypes (Fig. 3B). Not surprisingly, compared to β3-WT and β3-WT;NRP1Δcyto ECs, β3-HET and β3-HET;NRP1Δcyto ECs showed reduced adhesion to VN over a range of concentrations tested. β3-WT;NRP1Δcyto EC adhesion to FN was, as expected (Valdembri et al., 2009), somewhat reduced compared to β3-WT ECs. Compared to their WT counterparts, β3-HET and β3-HET; NRP1Δcyto ECs exhibited reduced strength of adhesion to FN over the gradient of concentrations tested.

We therefore used flow-cytometry to examine the surface expression of various EC integrin subunits (Fig. 3C). Consistent with the adhesion data, αv- and β3-integrin levels were significantly higher in β3-WT and β3-WT;NRP1Δcyto ECs compared to their β3-HET counterparts. Whereas α1, β1 and β5 surface levels were unchanged, we noted a small increase in α2 surface expression in β3-HET ECs. Most notably, however, α5-integrin surface levels were lower in ECs expressing reduced levels of β3-integrin (Fig. 3C), which might partially account for their reduced adhesion to FN.

Our observations of VEGFR2-independent changes in ERK1/2 phosphorylation (a known regulator of integrin-mediated migration) that were nonetheless sensitive to alterations in NRP1 function in β3-HET but not β3-WT ECs prompted us to examine whether cell migration was differentially dependent on NRP1 upon reduced levels of β3-integrin expression. Because NRP1, α5β1-integrin and αvβ3-integrin all promote adhesion to FN (Hynes, 2002; Valdembri et al., 2009), we next set out to measure migration on this matrix component. In light of noted subtle differences in short-term adhesion to FN (and in surface expression of α5-integrin), we first tested long-term cell spreading of our four cell lines to 10 μg/ml FN, a saturating concentration which effectively promotes cell adhesion and migration (Clark et al., 1986; Sottile et al., 1998; Tvorogov et al., 2005). Cell spreading after 6 h was similar in all four genotypes (Fig. 3D). This, along with our static adhesion assays, which showed no differences between the genotypes on this concentration of the matrix, provided justification for examining random (Fig. 3E) and directed (Fig. 3F) migration in cells plated long-term (overnight) on this concentration of FN. Both types of migration assays revealed enhanced baseline and VEGF-induced migration in β3-HET ECs, compared to β3-WT ECs; unlike β3-WT ECs, β3-HET ECs were sensitive to NRP1 disruption.

NRP1's localisation to focal adhesions is altered in β3-integrin-heterozygous endothelial cells

The findings described above suggested that aberrant integrin-directed migration, essential for pathological angiogenesis, correlates with the phenotypic difference in sensitivity to NRP1 perturbations that we observed in β3-HET mice. NRP1 is known to colocalise with a number of FA-associated proteins (Seerapu et al., 2013) and is involved in FA turnover. We therefore took a closer look at the structural and functional characteristics of mature endothelial FAs, focal points of cellular migration. We first examined NRP1's distribution in subcellular compartments after cell fractionation and immunoblotting. Other than the previously noted trend toward overexpression of the protein in β3-HET ECs, we

Disease Models & Mechanisms (2015) 8, 1105-1119 doi:10.1242/dmm.019927

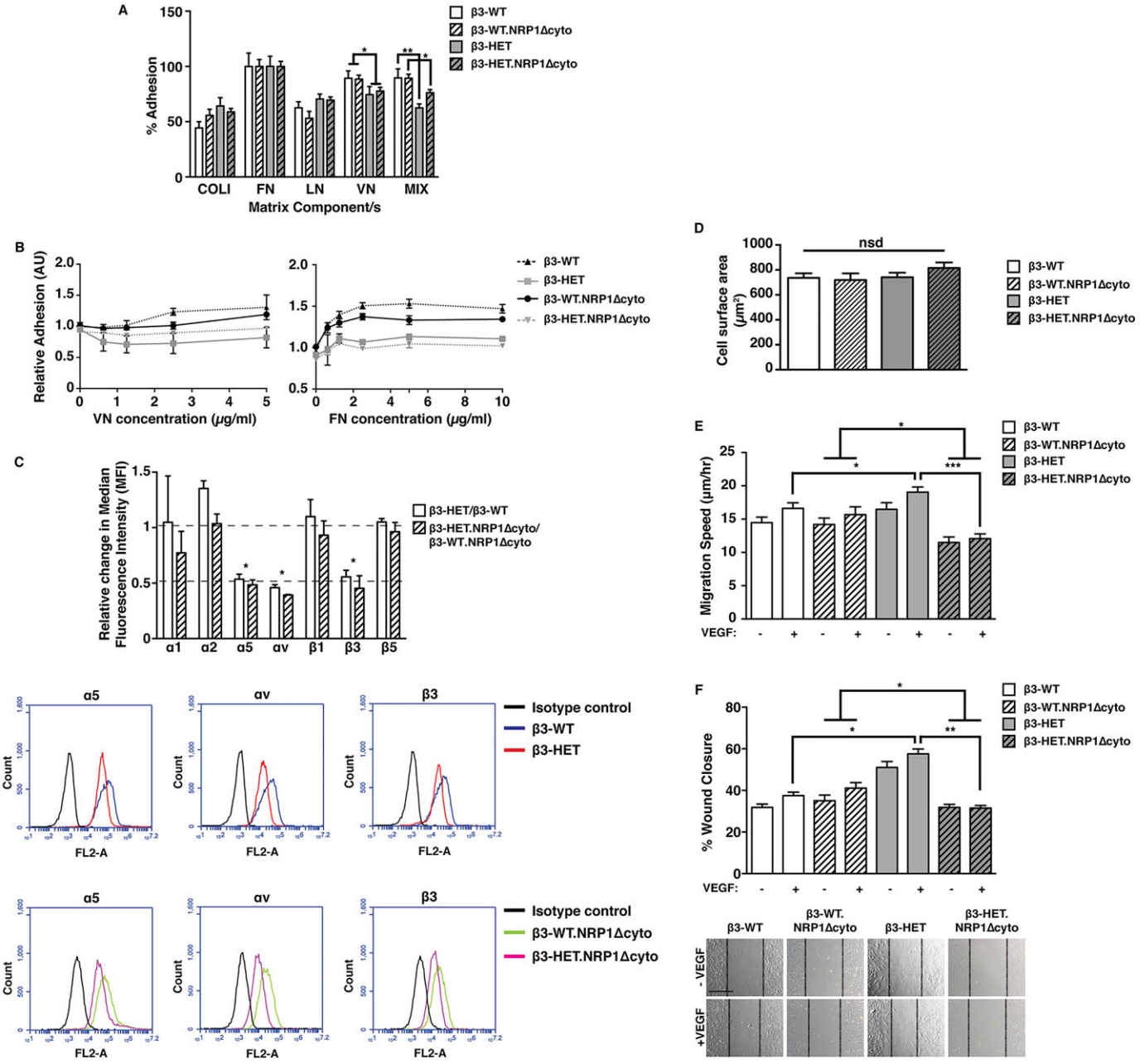

Fig. 3. VEGF-induced migration in β3-integrin-heterozygous endothelial cells is dependent on NRP1. (A) ECs isolated from animals of the four indicated genotypes were seeded on collagen type I (COLI), fibronectin (FN), laminin (LN), vitronectin (VN), or a complex mixture of COLI, FN, VN and gelatin (MIX) for 90 min. Unattached cells were gently washed off, and the remaining cells were fixed and stained. Dye was extracted and measured spectophotometrically. The bar chart shows the percentage of cell adhesion to each component relative to FN (means+s.e.m. from three independent experiments). (B) ECs of the indicated genotypes were plated on increasing concentrations of FN or VN. After 90 min, plates were vigorously washed and remaining cells were fixed and stained. Dye was extracted and measured spectophotometrically. The graph shows the mean (±s.e.m. from ≥two independent experiments) number of cells that remained attached to the plate after the procedure. (C) ECs of the indicated genotypes were measured for their surface expression of endothelial integrin subunits by flow cytometry. Median fluorescence intensity (MFI) was measured after forward versus side scatter data were tightly gated around, and normalised to, an isotype control. The bar chart shows the relative change in MFI of β3-HET compared to β3-WT ECs, or of β3-HET. NRP1Δcyto ECs compared to β3-WT.NRP1Δcyto ECs (means+s.e.m. from three independent experiments). Relative changes were deemed significant with a twofold change. Representative flow-cytometric histogram profiles are shown below for significantly changed integrins. (D) 70×10^5 cells of the indicated genotypes were plated for 6 h on 10 μg/ml FN in six-well plates. Phase-contrast photographs were taken and cell surface areas were measured using ImageJ™ software. The bar chart represents mean (+s.e.m.) surface area quantified from multiple images ($n\geq50$ cells per genotype). (E) ECs were firmly attached to FN-coated dishes and then imaged live for 15 h in low-serum medium ±VEGF. Individual cells were tracked every 10 min over this period using ImageJ™. The bar chart shows the EC migration speed of each of the indicated genotypes (mean+s.e.m. from three independent experiments; n=50 cells per condition). (F) ECs were plated onto FN-coated dishes overnight. After 3 h of starvation, a scratch wound was created and cells were incubated in low-serum medium ±VEGF for 24 h. The bar chart shows the percentage closure of the scratch 'wound' as a result of directed cell migration (means+s.e.m. from three independent experiments; n=27 for each condition). Representative images of scratch-wound closure at 24 h are shown below. Scale bar: 200 μm. Asterisks indicate statistical significance: *P<0.05; **P<0.01; ***P<0.001; nsd, not significantly different. Unpaired two-tailed t-test.

Disease Models & Mechanisms (2015) 8, 1105-1119 doi:10.1242/dmm.019927

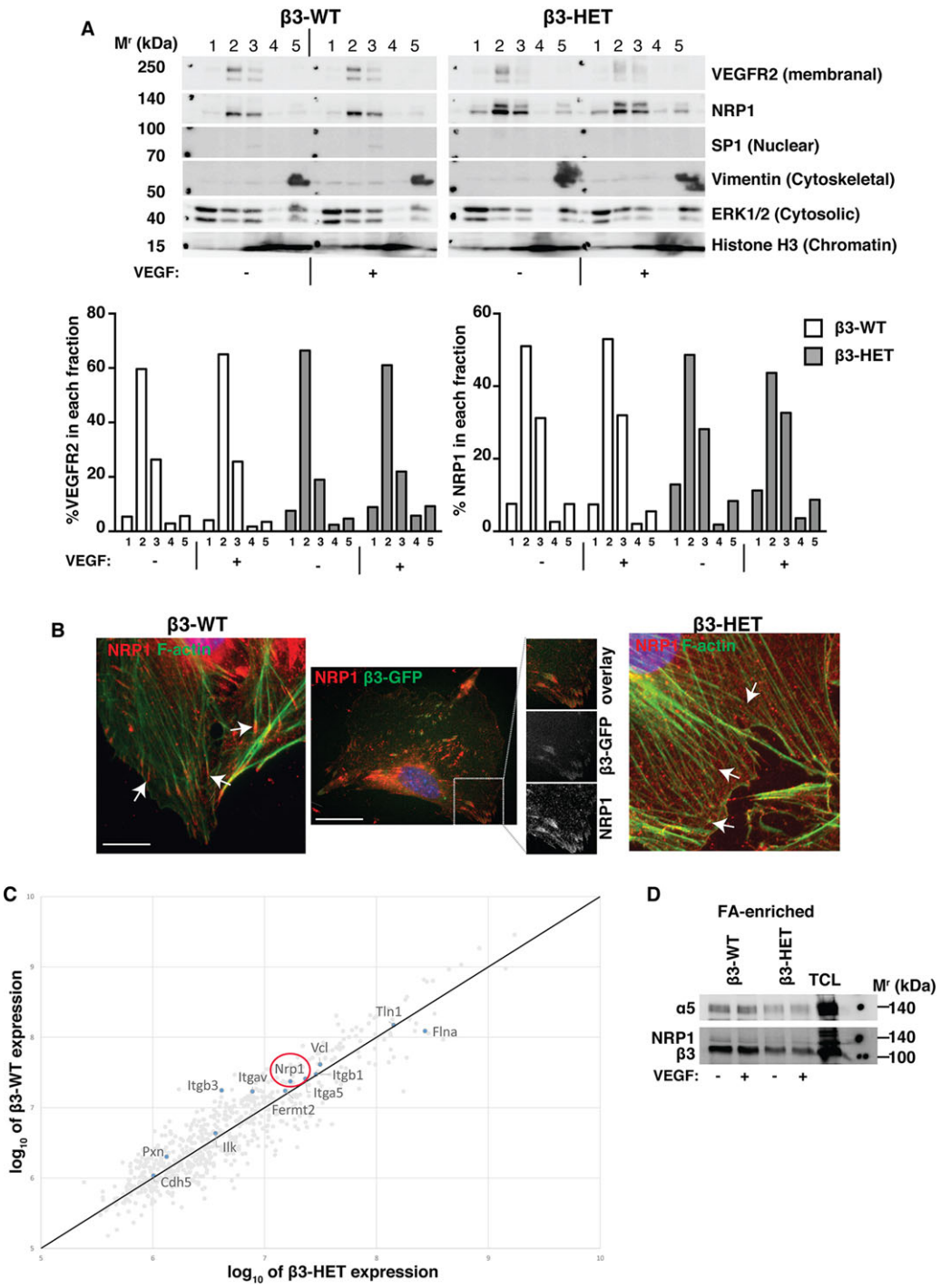

Fig. 4. NRP1's localisation in focal adhesions is altered in β3-integrin-heterozygous endothelial cells. (A) β3-WT and β3-HET ECs were subjected to a cell-fractionation experiment following ±VEGF treatment for 10 min. Fractionated samples were then analysed by western blot for the indicated proteins. 1=cytoplasmic extract; 2=membrane extract; 3=soluble nuclear extract; 4=chromatin-bound nuclear extract; 5=cytoskeletal extract. Protein markers for each subcellular compartment were included as controls. Data are representative of two independent experiments. The bar charts represent the relative proportion (%) of VEGFR2 or NRP1 present in each fraction determined by ImageJ™ densitometry. (B) Left and right panels: β3-WT and β3-HET ECs were seeded overnight onto FN-coated glass coverslips and then stimulated with VEGF for 10 min. Cells were fixed and stained with phalloidin for filamentous actin (F-actin; green), and immunostained for neuropilin-1 (NRP1; red). Arrows point to the ends of actin filaments. Middle panel: β3-WT ECs were transfected with a β3-integrin-GFP construct (green) and seeded on FN-coated coverslips. 48 h later, cells were fixed and immunostained for NRP1 (red). Split-channel close-ups are shown to depict β3-integrin/NRP1 colocalisation. Scale bars: 10 μm (middle), or 20 μm. (C) ECs were allowed to adhere to FN-coated dishes for 90 min to establish 'mature' integrin-dependent focal adhesions (FAs). FAs were chemically cross-linked to the plates and cells were lysed with RIPA buffer. Non-cross-linked proteins and other cellular components were rinsed away under high-sheer flow. FA-enriched complexes were eluted, subjected to SDS-PAGE and then analysed by label-free, quantitative mass spectometry. The graphs represent log ratio plots of the proteomic data comparing unstimulated β3-WT ECs (*y*-axis) and β3-HET ECs (*x*-axis). Proteins above the diagonal line are higher in β3-WT ECs, whereas those below the line are higher in β3-HET ECs (*n*=3 samples per genotype). NRP1 is present in both adhesomes (red circle). (D) FA-enriched EC samples were processed as in C and then analysed by western blot for the indicated proteins. A total cell lysate (TCL) is shown for comparison. Data are representative of three independent experiments.

Disease Models & Mechanisms (2015) 8, 1105-1119 doi:10.1242/dmm.019927

found no obvious differences (Fig. 4A). We next immunolocalised NRP1 in cells plated on FN overnight. Because of the VEGF-dependence of our phenotypic angiogenic responses, we initially concentrated on VEGF-stimulated cells. In β3-WT ECs, NRP1 localised to mature FAs, which were found at the ends of filamentous actin (F-actin) fibres (Fig. 4B, left); as expected from previous studies (Robinson et al., 2009), NRP1 also colocalised with GFP-tagged β3-integrin in cDNA-expression-construct-transfected β3-WT ECs (Fig. 4B, middle). However, in VEGF-stimulated β3-HET ECs, NRP1 no longer localised to these sites (Fig. 4B, right).

To explore more precisely whether β3-integrin was required for the initial recruitment of NRP1 to FAs, we plated cells on FN for 90 min, which allows mature, β3-integrin-rich, adhesions to form (Schiller et al., 2011, 2013), and performed quantitative mass spectrometry of the FA-enriched endothelial adhesome from β3-WT and β3-HET ECs (Schiller et al., 2011) (Fig. 4C). For the present study, we focused our attention on known adhesome proteins. β3- and αv-integrins were, as expected, enriched in β3-WT adhesomes. Although many differences were noted between the two genotypes, the stoichiometry of many classical adhesome-related proteins (such as β1-integrin, vinculin, talin and integrin-linked kinase) was unchanged in β3-HET ECs. Most importantly, NRP1, as previously reported by others (Kuo et al., 2011; Schiller et al., 2011), was present within the adhesome of both genotypes. Immunoblotting of FA-enriched cellular lysates confirmed this finding (Fig. 4D); although the western blot (WB) signal for NRP1 was relatively weak, it was present in both β3-WT and β3-HET ECs. Together, these results suggest that β3-integrin is not essential for the initial localisation of NRP1 to mature FAs, but, rather, regulates its retention within FAs upon VEGF-stimulation.

β3-integrin directs NRP1's control over FA remodelling

Given the noted changes in NRP1-dependent migration and retention within FAs following an angiogenic stimulus, we next investigated whether NRP1's association with FA proteins in general was altered in β3-HET ECs. We performed NRP1 immunoprecipitations on lysates from β3-WT and β3-HET ECs followed by label-free quantitative mass spectrometry, which highlighted a number of previously demonstrated NRP1 co-associations such as myosin-9, myosin-10 and filamin-A (Seerapu et al., 2013). Many VEGF-induced associations between NRP1 and FA-associated proteins were similar between the two genotypes, but β3-HET cells showed a number of significant changes in VEGF-induced interactions between NRP1 and cytoskeletal proteins involved with cell migration (Table 1), such as decreased interactions with filamin-A. These observations, coupled with changes in NRP1's mobilisation away from mature FAs upon VEGF-stimulation, suggested that NRP1-dependent changes in FA remodelling might be at the heart of phenotypic differences between β3-WT and β3-HET cells.

Therefore, as a marker of FAs, we turned our attention to examining interactions between NRP1 and PXN. As well as demarcating FAs, PXN plays an important role in EC motility and can be regulated by NRP1 (Raimondi et al., 2014). Immunocytochemistry of cells plated overnight on FN showed a predicted colocalisation of total PXN and NRP1 in non-VEGF-stimulated β3-WT ECs. This colocalisation was maintained after 10 min of VEGF-stimulation (Fig. 5A). NRP1/PXN colocalisation was also apparent in non-VEGF-stimulated β3-HET ECs, but it was lost upon VEGF-stimulation. A similar pattern was observed in β3-HET;NRP1Δcyto ECs, with β3-WT;NRP1Δcyto ECs showing only a small loss of NRP1/PXN colocalisation after VEGF-stimulation.

Table 1. Label-free quantitative mass-spectrometry analysis of NRP1-associated cytoskeletal-classed proteins

		LFQ values normalised to immunoprecipitated NRP1						
UNIPROT ID	Gene	WT –V	WT +V	HET –V	HET +V	Ratio WT+V/WT–V	Ratio HET+V/HET–V	Fold change HET/WT
Q6IRU2	*Tpm4*	0.54	0.21	0.11	0.13	0.38	1.12	2.94
P21107	*Tpm3*	1.82	1.33	0.34	0.58	0.73	1.73	2.37
P63260	*Actg1*	9.99	9.22	4.73	7.06	0.92	1.49	1.62
P58771	*Tpm1*	0.39	0.36	0.09	0.13	0.93	1.43	1.55
Q6URW6	*Myh14*	5.54	3.86	4.62	4.78	0.70	1.04	1.49
Q9QXS1	*Plec*	3.64	2.26	1.86	1.39	0.62	0.75	1.20
P47754	*Capza2*	0.64	0.56	0.38	0.37	0.88	0.97	1.10
Q9WTI7	*Myo1c*	0.78	0.71	0.38	0.37	0.90	0.99	1.09
Q61879	***Myh10***	**3.97**	**3.97**	**6.32**	**6.52**	**1.00**	**1.03**	**1.03**
E9QA15	*Cald1*	1.48	1.19	0.57	0.46	0.80	0.82	1.02
Q9JHJ0	*Tmod3*	0.29	0.31	0.18	0.19	1.07	1.08	1.01
P63260	*Actg1*	166.25	172.15	109.54	110.31	1.04	1.01	–1.03
Q5RKN9	*Capza1*	0.25	0.26	0.21	0.21	1.05	1.01	–1.04
Q9JJ28	*Flii*	0.22	0.18	0.15	0.12	0.81	0.77	–1.05
P68033	*Actc1*	2.37	3.72	0.65	0.96	1.57	1.47	–1.07
Q8BFZ3	*Actbl2*	38.52	41.16	21.77	20.61	1.07	0.95	–1.13
P47757	*Capzb*	0.30	0.33	0.22	0.21	1.10	0.94	–1.18
Q8VDD5	***Myh9***	**226.75**	**246.90**	**159.30**	**146.76**	**1.09**	**0.92**	**–1.18**
P46735	*Myo1b*	0.11	0.12	0.08	0.07	1.12	0.89	–1.26
E9Q634	*LOC100504972*	0.10	0.11	0.08	0.07	1.13	0.88	–1.28
Q8BTM8	***Flna***	**0.12**	**0.11**	**0.11**	**0.07**	**0.93**	**0.58**	**–1.59**
P16546	*Spna2*	0.22	0.23	0.21	0.14	1.07	0.64	–1.67
Q9JMH9	*Myo18a*	0.48	0.47	0.54	0.28	0.97	0.52	–1.88
P05213	*Tuba1b*	0.15	0.68	0.16	0.17	4.46	1.02	–4.36

The table shows a pared-down list of cytoskeletal-classed proteins that co-immunoprecipitated with NRP1 in β3-integrin wild-type (WT) and heterozygous β3-integrin-deficient (HET) ECs in the presence (+V) or absence (–V) of VEGF-stimulation. Although they might be biologically relevant, for the sake of confidence we have removed from the full list proteins that were only identified in one of the four samples or whose NRP1-normalised label-free quantification (LFQ) values fell below 0.1. Highlighted in bold are previously reported interactions (Seerapu et al., 2013).

Disease Models & Mechanisms (2015) 8, 1105-1119 doi:10.1242/dmm.019927

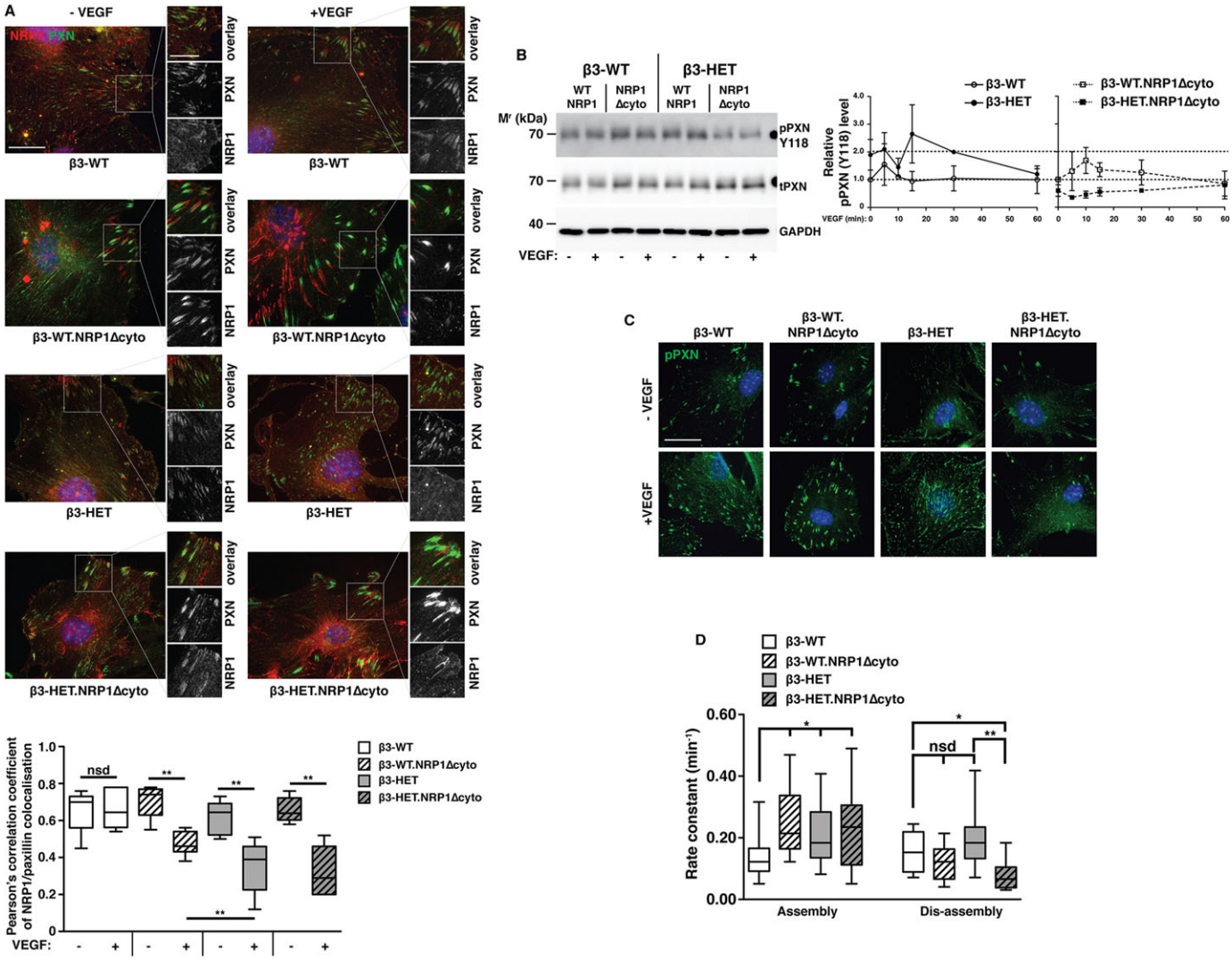

Fig. 5. Paxillin activation and focal adhesion disassembly are sensitive to NRP1 disruption in β3-integrin-heterozygous endothelial cells. (A) ECs of the indicated genotypes were seeded overnight on FN-coated glass coverslips. After 3 h of starvation, cells were treated ±VEGF for 10 min in serum-free medium, then fixed and immunostained for total paxillin (PXN; green) and neuropilin-1 (NRP1; red). Split-channel close-ups are shown to depict PXN/NRP1 colocalisation. Scale bar: 20 μm. The box and whisker plot shows Pearson's correlation coefficient of PXN/NRP1 colocalisation in each of the indicated genotypes in the indicated regions as determined using the ImageJ™ coloc2 plugin (means±interquartile ranges and extreme values; $n \geq 5$ cells per genotype, over ≥three independent experiments). (B) Left panel: ECs of the indicated genotype were seeded overnight on FN. They were then starved for 3 h and treated ±VEGF for 10 min in serum-free medium. Cells were lysed and western blotted (WB) for levels of phosphorylated (p) and total (t) PXN. GAPDH served as a loading control. Data are representative of three independent experiments. Right panel: the graph shows densitometry of pPXN relative to tPXN, as determined by WB, over an extended VEGF time course (means±s.e.m. from ≥three independent experiments). (C) ECs were seeded overnight onto FN-coated glass coverslips and stained for pPXN. ECs were starved for 3 h and treated ±VEGF for 10 min in serum-free medium. Cells were fixed and immunostained for pPXN (green). Scale bar: 10 μm. (D) ECs were transfected with a PXN-GFP construct and seeded at a low density on FN-coated coverslips. 72 h later, cells were starved and then treated with VEGF in reduced-serum medium. Representative cells were then imaged live (every 2 min) on an inverted fluorescence microscope for 1 h to monitor focal adhesion (FA) remodelling. The front and back ends of individual FAs were tracked over this period to measure FA assembly and disassembly, using the ImageJ™ MTrack2 plugin. The box and whisker plot shows the rate of FA assembly or disassembly for each of the indicated genotypes (means±interquartile ranges and extreme values; $n \geq 20$ FAs per genotype, from ≥two independent experiments). Asterisks indicate statistical significance: *$P<0.05$; **$P<0.01$; nsd, not significantly different. Unpaired two-tailed *t*-test.

To pursue a potential β3-integrin-regulated NRP1 link with PXN activation, we also analysed the phosphorylation of PXN through tyrosine 118 by immunoblotting (Fig. 5B) and immunocytochemistry (Fig. 5C), and found a substantial reduction in PXN phosphorylation in β3-HET;NRP1Δcyto ECs, but not β3-WT;NRP1Δcyto ECs, suggesting that PXN activation is only NRP1-dependent when β3-integrin levels are suppressed. Moreover, it seems that FA disassembly only becomes substantially NRP1-dependent with reduced levels of β3-integrin: through the live tracking of GFP-PXN in transfected cells (Fig. 5D), we discovered that FA-assembly was faster in β3-HET, β3-WT; NRP1Δcyto and β3-HET;NRP1Δcyto ECs compared to β3-WT cells. Additionally, there was a trend toward increased FA-disassembly rates in β3-HET ECs. However, although FA-disassembly rates in β3-WT;NRP1Δcyto ECs were slightly reduced compared to their β3-WT counterparts, FA-disassembly rates were markedly retarded in β3-HET;NRP1Δcyto ECs, illustrating the increased role for NRP1 in these cells.

Overall, our data suggest that, in the presence of β3-integrin, EC migration is NRP1-independent; β3-integrin maintains NRP1 in

Disease Models & Mechanisms (2015) 8, 1105-1119 doi:10.1242/dmm.019927

FAs, thus ensuring a controlled migratory response to VEGF-stimulation. Reduced levels of β3-integrin lead to changes in FA remodelling and cell migration that are NRP1-dependent.

Simultaneous depletion of both endothelial β3-integrin and NRP1 effectively inhibits already-established tumour growth and angiogenesis

The identification of the mechanisms underlying increased sensitivity to NRP1 disruption in ECs with reduced β3-integrin expression should enable the rational design of intervention strategies to improve anti-angiogenic outcomes in patients with advanced cancers. To provide evidence in support of this idea, we performed proof-of-concept studies in β3-integrin/NRP1-double-floxed mice crossed to OHT-inducible-Pdgfb-iCreER^{T2} transgenics. First, though, we confirmed the same mechanistic principle described above in primary lung ECs acutely depleted of β3-integrin (Fig. 6A). We observed NRP1 expression at the ends of F-actin in OHT-treated β3-WT cells with and without VEGF-stimulation, but not in the majority of OHT-treated β3-KO ECs after VEGF treatment. We then initiated VEGF-induced microvessel sprouting in aortic rings isolated from: (1) β3-floxed mice with and without Pdgfb-iCreER^{T2}; (2) NRP1-floxed mice with and without Pdgfb-iCreER^{T2}; or (3) double-floxed mice with and without Pdgfb-iCreER^{T2}. OHT was administered to all rings after 4 days of sprouting, and microvessels were enumerated 4 days later. Only in rings from double-floxed Pdgfb-iCreER^{T2}-positive animals was further sprouting significantly inhibited (Fig. 6B). Finally, we performed intervention CMT19T allograft studies by establishing vascularised tumours in these same animals. After 10 days of growth, all animals were administered OHT and tumours were allowed to grow for another 10 days. In concordance with the intervention aortic ring studies, further tumour growth and angiogenesis were significantly inhibited in double-floxed Pdgfb-iCreER^{T2}-positive animals, but not in any of the other genotypes (Fig. 6C).

DISCUSSION

We previously showed that the total loss of β3-integrin expression sensitises angiogenesis to NRP1 inhibition by siRNA or small peptides (Robinson et al., 2009). This finding suggested to us, even at the time, that an anti-angiogenic approach that simultaneously targeted both molecules might offer therapeutic benefit to patients with advanced cancers where traditional mono-target strategies were largely failing; a concept strengthened further by our recent findings demonstrating only transient inhibition of tumour growth and angiogenesis after long-term depletion of endothelial β3-integrin expression (Steri et al., 2014). Testing this notion, however, requires that we have a deeper mechanistic understanding of, at the very least, how the dual targeting affects its outcome. Achieving this understanding necessitated moving away from β3-KO animals, which are often criticised for sustaining angiogenesis through developmental upregulation of VEGFR2, to a more subtle, albeit global, alteration in β3-integrin expression – β3 heterozygosity.

Like their knockout counterparts (Robinson et al., 2009), β3-HET mice display increased sensitivity to perturbations in NRP1 expression and we extend this finding to include NRP1 function, as assayed through the deletion of its cytoplasmic tail. In marked contrast to β3-KO animals, however, this phenomenon does not occur through increased interactions in ECs between VEGFR2 and NRP1 (Fig. 2). Rather, the work we present here guides us toward a newly identified mechanism for β3-integrin function whereby it regulates the retention of NRP1 within mature FAs upon VEGF-stimulation (Fig. 5).

A VEGFR2-independent role for NRP1 in regulating EC migration is gaining ground. NRP1's cytoplasmic domain is known to promote FN fibrillogenesis in arterial ECs by regulating the trafficking of activated α5β1-integrin (Valdembri et al., 2009), and NRP1 is involved in ABL1-mediated PXN activity in human dermal ECs (Raimondi et al., 2014) on FN. Crucially, however, here we report that NRP1's involvement in EC migration, at least in microvascular ECs, is regulated by β3-integrin. Endothelial NRP1 seems to play no role in pathological angiogenesis in β3-WT mice (Figs 1 and 6). Although this idea has been alluded to in a number of studies (Fantin et al., 2011, 2013; Lanahan et al., 2013; Robinson et al., 2009), we fully extend this conclusion to primary tumour growth and angiogenesis. In the models that we have employed, we demonstrate, categorically, that NRP1 perturbations alone do not disrupt pathological angiogenesis. When coupled to reductions in β3-integrin levels, however, NRP1's participation in angiogenesis becomes essential. Equally, reductions in β3-integrin expression without concomitant changes in NRP1 do not drastically alter tumour angiogenesis (particularly in already-established tumours). This suggests that there is redundancy built into the system such that the presence of either molecule in mature FAs is sufficient to mediate adequate PXN activity.

We hypothesise a default system in wild-type microvascular ECs in which αvβ3-integrin's molecular associations at mature FAs predominate and prevent NRP1 from fully participating in FA dynamics. αvβ3-integrins are known to immobilise in static FAs (Zamir et al., 2000) and it seems that they help to sequester NRP1 at these sites, even after VEGF-stimulation, which prevents it from activating PXN. In contrast, the long-term suppression of β3-integrin triggers an escape pathway whereby PXN activation and EC migration become dependent on NRP1 function; mobilisation of NRP1 away from mature/static FAs allows it to direct PXN activity (Fig. 6D). The idea of differential FA dynamics dependent on which integrin subclasses are engaged with an FN-rich ECM is not a new concept (see Truong and Danen, 2009, for example). However, this is the first time that differential NRP1 localisation and function have been linked to these changes.

The role that NRP1 plays in mediating VEGF-induced ERK phosphorylation seems to be controversial and dependent on the EC source and method employed to elicit NRP1 inhibition. Although Pan et al. (2007) found that anti-NRP1 monoclonal antibodies (mAbs) had no effect on VEGF-dependent ERK phosphorylation in human umbilical vein endothelial cells (HUVECs), Murga et al. (2005) demonstrated reduced VEGF-induced ERK phosphorylation in these cells after *NRP1* siRNA knockdown. Lanahan et al. (2013) found that the loss of NRP1's cytoplasmic tail reduced VEGF-dependent ERK phosphorylation in both heart and arterial ECs. Raimondi et al. (2014) report that *NRP1* siRNA knockdown impairs ERK phosphorylation in human dermal microvascular endothelial cells (HDMECs). We report here that the deletion of NRP1's cytoplasmic tail does not affect VEGF-induced ERK phosphorylation in WT microvascular ECs (Fig. 2). These apparent discrepancies need addressing and are the focus of ongoing research in our laboratory.

It is particularly important to address these discrepancies given our finding that β3-integrin's regulation of NRP1 function is dependent on the presence of VEGF, even when NRP1's regulation of VEGFR2 is unchanged. This is important clinically because it provides a therapeutic opportunity to enhance the efficacy of current strategies that largely focus on manipulating the VEGF-VEGFR2 pathway, which is linked with significant side-effects and prone to treatment resistance (Ebos and Kerbel, 2011). We now have the chance to affect VEGF-dependent angiogenesis in an apparently VEGFR2-independent manner.

Disease Models & Mechanisms (2015) 8, 1105-1119 doi:10.1242/dmm.019927

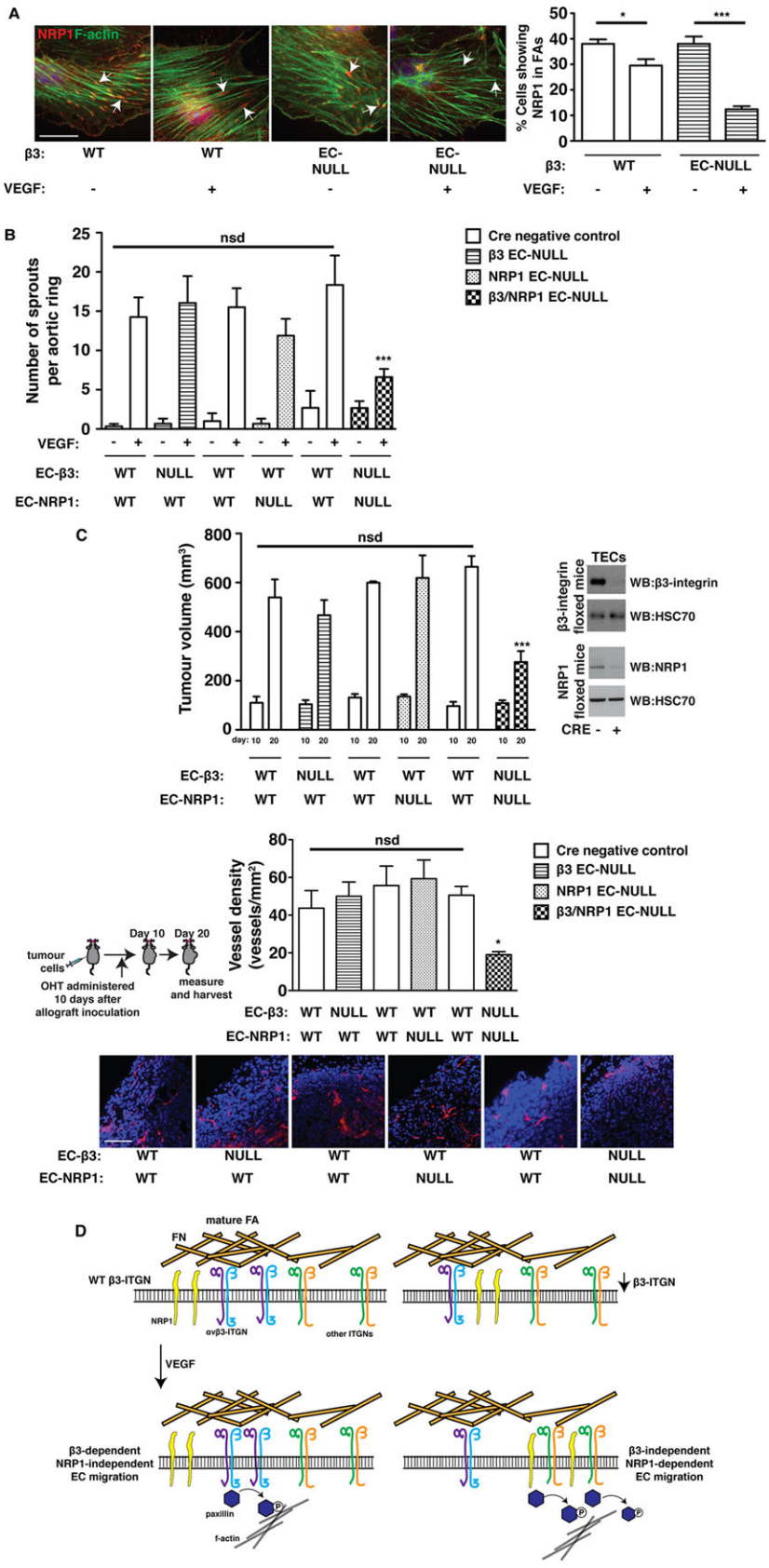

Fig. 6. Simultaneously depleting both β3-integrin and NRP1 blocks growth and angiogenesis in already-established tumours. (A) Primary lung microvascular ECs were isolated from β3-floxed-Pdgfb-iCreER^{T2}-negative and -positive animals. Tamoxifen (OHT) was administered after pure EC populations were achieved. Cells were then plated overnight on FN-coated glass coverslips. Cells were starved for 3 h and then treated ±VEGF for 10 min in serum-free medium. Cells were fixed and stained with phalloidin for F-actin (green), and immunostained for NRP1 (red). White arrows point to the ends of actin filaments. Scale bar: 20 μm. The bar chart shows the percentage of cells within the population showing NRP1 staining at the end of actin filaments (mean+s.e.m.; $n \geq 50$ cells per condition). (B) Microvessel sprouting of aortic ring explants of the indicated genotypes. Protein knockout in ECs was induced in culture with 1 μM OHT 4 days after VEGF-induced sprouting had been established. The bar chart shows the total number of microvessel sprouts per aortic ring after an additional 4 days of VEGF-stimulation (mean+s.e.m. from three independent experiments; $n \geq 40$ rings per genotype). (C) Tumour growth and angiogenesis were measured in animals of the indicated genotypes. Mice were injected subcutaneously with CMT19T cells and 10 days later OHT was administered. After an additional 10 days (20 days in total) tumours were harvested. Upper panel: the bar chart shows mean tumour volumes measured at days 10 and 20 (+s.e.m. of two or more independent experiments; $n \geq 10$ animals per genotype). The western blot to the right shows representative depletion of β3-integrin and NRP1 in tumour endothelial cells (TECs) isolated from Cre-positive animals, compared to Cre-negative littermate controls. Bottom panel: blood-vessel density in 20-day tumours was assessed by counting the total number of endomucin-positive vessels around the periphery (within 150 μm of the edge of the tumour) of midline bisected tumour sections. The bar chart shows mean vessel number per mm^2 (+s.e.m.). Representative micrographs of endomucin staining (red) are shown below. Scale bar: 50 μm. Asterisks indicate statistical significance: *P<0.05; ***P<0.001; nsd, not significantly different. Unpaired two-tailed t-test. (D) Schematic representation of the hypothesised participation of NRP1 in focal adhesion (FA) remodelling and migration in β3-WT (left) and β3-suppressed (right) ECs. ITGN, integrin.

Disease Models & Mechanisms (2015) 8, 1105-1119 doi:10.1242/dmm.019927

This study provides proof-of-concept that a dual-combative αvβ3-integrin/NRP1 targeting approach offers a clinically beneficial way of treating advanced solid cancers. Small-molecule inhibitors directed against NRP1 are currently under development and we hope that these can soon be tested alongside existing or new αvβ3-integrin antagonists, with the caveat that both molecules are expressed by multiple cell types that contribute to tumour growth and angiogenesis, including platelets, and off-target (i.e. non-EC) effects will have to be examined carefully; although we can rule out their contribution to the EC-double-KO intervention studies (Fig. 6), these other cells types might be contributing to β3-HET angiogenic responses. Nonetheless, we provide a strong mechanistic foundation for understanding the molecular basis of how a dual-targeted approach against these two endothelial molecules might meet with success. This will allow us, in the meantime, to more fully explore the long-term durability of such an approach when applied to additional clinically relevant scenarios. Moreover, detailed further analysis and extension of our mass spectrometric studies in ECs will allow us to fully explore how differential adhesion dynamics, mediated by distinct integrin-ECM interactions, result in the formation of unique signalling platforms that can be exploited to manipulate angiogenic responses.

MATERIALS AND METHODS

Reagents

VEGF-A^{164} was made in-house according to the method published by Krilleke et al. (2007). All chemicals were from Sigma-Aldrich (Poole, UK) unless otherwise indicated.

Animals

All animals were on a mixed C57BL6/129 background. Littermate controls were used for all *in vivo* experiments. All animal experiments were performed in accordance with UK Home Office regulations and the European Legal Framework for the Protection of Animals used for Scientific Purposes (European Directive 86/609/EEC).

In vivo tumour growth assays

Mouse melanoma (B16F0, ATCC; mycoplasma free) or mouse lung carcinoma (CMT19T, CR-UK Cell Production; mycoplasma free) cells (1×10^6) were injected subcutaneously in the flank of experimental and littermate-control mice. 12-20 days after injection, mice were killed, tumour sizes measured and tumour samples were fixed in 4% paraformaldehyde for histological analysis. For prevention studies in Pdgfb-iCreER^{T2} mice (Fig. 1, supplementary material Fig. S1), slow release (5 mg, 21-day release) tamoxifen pellets (Innovative Research of America, Sarasota, FL) were implanted subcutaneously into the scruff of the neck 3 days prior to tumour cell injection. For intervention studies (Fig. 6), pellets were implanted after 10 days of initial tumour growth. Tumour volumes were calculated according to the formula: length×width^2×0.52.

Immunohistochemical analysis of tumour sections

At 24-h post-fixation, tumours were bisected at the midline and embedded in paraffin (cut face toward blade) and 5-µm sections were prepared. Immunostaining was then performed with sodium-citrate antigen retrieval as described previously (Reynolds et al., 2002). Images were acquired on an Axioplan (Zeiss, Cambridge, UK) epifluorescent microscope and tissue area was quantified using ImageJ™ software available at the National Institutes of Health website. Primary antibodies were: rat anti-endomucin (clone V.7C7, used at 1:500, Santa Cruz Biotechnology, Santa Cruz, CA); rabbit anti-CD146 (clone EPR3208, used at 1:500, Abcam, Cambridge, UK). Secondary antibodies were: donkey anti-rat Alexa-Fluor®-594 and donkey anti-rabbit Alexa-Fluor®-488 conjugates (Invitrogen, Paisley, UK), both used at 1:500.

Blood-vessel density was assessed by counting the total number of endomucin-positive vessels per mm^2 across entire midline tumour sections from age-matched, size-matched tumours. For tumour sections from the intervention studies (Fig. 6), vessels around the perimeter of the sections were counted in order to avoid the necrotic centres of tumours.

Mouse tumour endothelial cell isolation

Tumour ECs were isolated and analysed by western blot as previously described by Steri et al. (2014).

Ex vivo aortic ring assay

Thoracic aortae were isolated from 6- to 9-week-old adult mice and prepared for culture as described extensively by Baker et al. (2012). Protein knockout in ECs was induced in culture with 1 µM 4-hydroxytamoxifen (OHT). Where indicated, VEGF was added at 30 ng/ml. Microvessel growth of aortic rings was quantified after 6-10 days. For the intervention study, protein knockout in ECs was induced in culture with 1 µM OHT 4 days after VEGF-induced sprouting had been established, and the microvessel sprouts were quantified after an additional 4 days of VEGF-stimulation.

Mouse lung microvascular endothelial cell isolation and culture

Primary mouse lung ECs were isolated from adult mice as described previously by Reynolds and Hodivala-Dilke (2006). To induce target gene deletion in Pdgfb-iCreER^{T2}-floxed cell lines, cells were grown for 48 h in medium supplemented with 500 nM OHT.

For immortalisation, cells were treated with polyoma-middle-T-antigen (PyMT) retroviral transfection as described previously by Robinson et al. (2009). Briefly, PyMT conditioned medium was collected, filter sterilised using a 0.45 µm filter, and stored at −80°C until use. Following two rounds of CD102-positive selection, primary ECs in six-well plates were treated with the preserved PyMT conditioned medium supplemented with 8 µg/ml polybrene for 6 h at 37°C. PyMT conditioned medium was removed and replaced with complete growth medium. This same procedure was repeated the following day. Cells were observed and passaged for 4 weeks to ensure their immortalisation. Subsequently, they were maintained in a 1:1 mixture of DMEM low glucose:Ham's F12 nutrient mixture (Invitrogen) supplemented with 0.1 mg/ml heparin and 10% FBS, and used between passages 5-20. Cells were routinely checked by flow cytometry for surface expression of ICAM2, CD31 and VECAD (see supplementary material Fig. S3) to ensure that they retained their normal EC characteristics. Cells were also routinely checked for their ability to survive extended periods of confluency, which indicates absence of transformation (May et al., 2005).

For experimental analyses, tissue culture plates and flasks were coated overnight at 4°C with one or more of the following, as specified below: 0.1% gelatin (type A from porcine skin, ~300 g bloom), Purecol (COLI) (Nutacon B.V., The Netherlands), human plasma fibronectin (FN) (Millipore, Watford, UK) and mouse multimeric vitronectin (VN) (Patriecell Ltd, Nottingham, UK).

Western blot analysis

For the analysis of VEGFR2, NRP1, β3-integrin, ERK1/2, p130cas and FAK, ECs were seeded at 2×10^5 cells per well in six-well plates coated with 0.1% gelatin, 10 µg/ml FN, 10 µg/ml COLI and 2 µg/ml VN. For paxillin analysis, ECs were seeded at the same density, but on plates coated with only 10 µg/ml FN in PBS. 24 h later, cells were starved for 3 h in serum-free medium (OptiMEM®; Invitrogen). VEGF was then added to a final concentration of 30 ng/ml and cells were lysed at the indicated times (see main text) in EB (3% SDS, 60 mM sucrose, 65 mM Tris-HCl pH 6.8). 15-30 µg of protein from each sample was loaded onto 8-10% polyacrylamide gels. For paxillin analysis, samples were loaded onto a 4-12% gradient gel for better resolution. The protein was transferred to a nitrocellulose membrane and incubated for 1 h in 5% milk powder/PBS plus 0.1% Tween-20 (PBSTw), followed by an overnight incubation in primary antibody diluted 1:1000 in 5% bovine serum albumin (BSA)/PBSTw at 4°C. The blots were then washed 3× with PBSTw and incubated with the relevant horseradish peroxidase (HRP)-conjugated secondary antibody (Dako) diluted 1:2000 in 5% milk/PBSTw, for 1 h at room temperature. Chemiluminescence was detected on a Fujifilm LAS-3000 darkroom (Fujifilm UK Ltd, Bedford, UK). Antibodies (all used at 1:1000

and purchased from Cell Signaling Technology, unless noted otherwise) were: anti-phospho (Y1175) VEGFR2 (clone 19A10); anti-VEGFR-2 (clone 55B11); anti-Neuropilin-1 (cat. no. 3725); anti-β3-integrin (cat. no. 4702); anti-phospho (Thr202/Tyr204) p44/42 MAPK Erk1/2 (clone D13.14.4E); anti-total p44/42 MAPK Erk1/2 (clone 137F5); anti-phospho (Y410) p130cas (cat. no. 4011); anti-p130cas (cat. no. 610271, BD Biosciences, Oxford); anti-phospho (Y407) FAK (#OPA1-03887, ThermoScientific); anti-FAK (cat. no. 3285); anti-HSC70 (clone B-6, Santa Cruz Biotechnology); anti-phospho (Y118) paxillin (cat. no. 2541); anti-paxillin (ab32084; Abcam); anti-GAPDH (14C10, cat. no. 2118); anti-SP1 (cat. no. 5931); anti-histone H3 (D1H2, cat. no. 4499); anti-vimentin (D21H3, cat. no. 5741).

Flow cytometry

For flow-cytometric analysis, cells were trypsinised, resuspended in FACS buffer (1% FBS in PBS+1 mM $CaCl_2$+1 mM $MgCl_2$) and labelled with one of the following antibodies (all used at 1:200 and, unless stated otherwise, purchased from eBioscience, Hatfield, UK): PE-anti-mouse Flk1, PE-anti-mouse CD49a (Cambridge Bioscience, Cambridge, UK); PE-anti-mouse CD49b; PE-anti-mouse CD49e; PE-anti-mouse CD51; PE-anti-mouse CD29; PE-anti-mouse CD61; PE-anti-mouse integrin beta 5; PE-anti-mouse CD31; FITC-anti-mouse ICAM2; PE-anti-mouse VECAD; appropriate PE/FITC-labelled isotype-matched controls were from eBioscience. In the case of Flk1 analysis, cells were stimulated with 30 ng/ml VEGF at 37°C over a 60-min time course before trypsinisation.

Immunoprecipitation assay

Cells were grown to 80-90% confluency in 15-cm dishes coated with 10 µg/ml FN in PBS. After starvation in OptiMEM® for 3 h, cells were stimulated with 30 ng/ml VEGF for 10 min (+VEGF), or for the indicated times, at 37°C. Cells were then placed on ice, washed two times with PBS, and lysed in 0.5 ml/plate of RIPA buffer (20 mM Tris pH 7.4, 50 mM NaCl, 0.1% SDS, 1% Triton, 1% Deoxycholate, 1% NP40) containing PMSF (~1 mM) and Halt® Protease and Phosphatase inhibitor (1:100). Lysates were centrifuged at 12,000 ***g*** for 10 min at 4°C. 400 µg of total protein from each sample was immunoprecipitated by incubating them with protein-G Dynabeads® (Invitrogen) coupled to a rabbit-anti-mouse-VEGFR2 antibody (clone 55B11, Cell Signaling Technology) for the VEGFR2 immunoprecipitation (IP), or a goat anti-mouse Neuropilin-1 antibody (AF566, R&D Systems) for the NRP1 IP, on a rotator overnight at 4°C. Immunoprecipitated complexes were washed three times with 0.2 ml of RIPA buffer, and once in PBS, before being added to, and boiled in, 1× NuPAGE® sample reducing agent (Life Technologies), ready for western blotting or mass spectrometry analysis.

Adhesion assays

Static adhesion

96-well plates were coated overnight at 4°C with 10 µg/ml COLI, 10 µg/ml FN, 10 µg/ml laminin-I (LN) or 2 µg/ml VN in PBS, or a mixture (MIX) containing 10 µg/ml COLI, 10 µg/ml FN and 2 µg/ml VN in 0.1% gelatin was also used. The wells were then washed with PBS, and blocked for 1 h at room temperature (RT) with 1% BSA in PBS, before a final wash in PBS. Prior to seeding, cells were starved for 3 h in Opti-MEM®, trypsinised and resuspended in serum-free OptiMEM®. They were then seeded in serum-free OptiMEM® at a concentration of 1×10^4 cells/well for 90 min at 37°C. Plates were washed three times gently by immersion in a bucket of PBS, and any excess volume was removed. Wells were stained with methylene blue for 30 min, washed for 15 min under running water and air-dried. Dye was extracted with 50% ethanol:50% 0.1 N HCl and the absorbance of each well was measured at 610 nm.

Adhesion on various matrix concentrations

96-well plates were coated overnight at 4°C with serial dilutions of VN or FN. The wells were then washed with PBS, and blocked for 1 h at RT with 1% BSA in PBS. Prior to seeding, cells were starved for 3 h in Opti-MEM®, trypsinised and resuspended in serum-free OptiMEM®. They were then seeded in serum-free Opti-MEM® at a concentration of 3×10^4 cells/well for 90 min at 37°C. Plates were tapped vigorously on the bench top and wells were washed thoroughly using a multi-channel pipette. Wells were stained with methylene blue for 30 min, washed for 15 min under running water and air-dried. Dye was extracted with 50% ethanol:50% 0.1 N HCl and the absorbance of each well was measured at 610 nm.

Random-migration assay

ECs were starved in OptiMEM® for 3 h, trypsinised and seeded at 1.5×10^4 cells/well in 24-well plates coated with 10 µg/ml FN in PBS, and allowed to adhere for 3 h. The media was then replaced with OptiMEM®+2% FBS, and half of the wells were supplemented with 30 ng/ml VEGF. One phase-contrast image/well was taken live every 10 min in a fixed field of view using an inverted Axiovert (Zeiss) microscope for 15 h at 37°C and 4% CO_2. Individual cells were then manually tracked using the ImageJ™ cell tracking plugin, and the speed of random migration was calculated in µm moved/hour.

Wound-closure assay

ECs were seeded at 4×10^5 cells/well in six-well plates coated with 10 µg/ml FN in PBS, and cultured until the next day, by which time they had reached confluency. Cells were serum starved for 3 h in OptiMEM® before scratching the confluent monolayer with a P200 pipette tip. Phase-contrast images of scratches were then captured and the media was changed to OptiMEM® containing 30 ng/ml VEGF. After 24 h, cells were fixed for 10 min with 4% formaldehyde and scratches were imaged again. The degree of scratch-wound closure was quantified by measuring the gap between cells in three areas per field using Axiovision (Zeiss) software, taking an average, and calculating the length of change between time points.

Immunocytochemistry

Either primary or immortalised ECs were seeded at 1.5×10^5 cells/well in six-well plates on acid-washed and oven-sterilised glass coverslips, coated with 10 µg/ml FN in PBS and cultured until the next day. Cells were starved for 3 h in serum-free OptiMEM®, and either stimulated with 30 ng/ml VEGF at 37°C for 10 min (+VEGF), or not at all (−VEGF). Cells were then fixed in 4% formaldehyde for 10 min, washed in PBS, permeabilised with 0.5% NP40 in PBS, blocked in 0.1% BSA+0.2% Triton in PBS, and incubated with primary antibody diluted 1:100 in PBS for 1 h at RT. After further PBS washes, cells were incubated with the relevant Alexa-Fluor®-conjugated secondary antibody (Invitrogen) diluted 1:500 in PBS for 45 min at RT. Coverslips were washed in PBS again before they were mounted on slides with Prolong® Gold containing DAPI (Invitrogen). To stain for filamentous-(F) actin, Alexa-Fluor®-568–phalloidin (Invitrogen) was used 1:300 in PBS at the secondary-antibody incubation stage. To look at β3-integrin fluorescently, 1×10^6 ECs were transfected with a GFP-tagged β3-integrin cDNA expression construct (provided by Dr Maddy Parsons, King's College London, London, UK) by nucleofection prior to seeding on coverslips at 1.5×10^5 cells/well. Antibodies (all used at 1:100) were: anti-phospho (Y118) paxillin (Cell Signaling Technology, cat. no. 2541); anti-paxillin (ab32084, Abcam); anti-neuropilin-1 (AF566, R&D Systems). NRP1-PXN colocalisation was quantified using the Coloc2 ImageJ™ plugin to determine the Pearson's correlation coefficient.

Cell fractionation assay

ECs were seeded in plates coated with 0.1% gelatin, 10 µg/ml FN, 10 µg/ml COLI and 2 µg/ml VN. 24 h later, cells were starved for 3 h in serum-free OptiMEM®, and either stimulated with 30 ng/ml VEGF or not. Cells were then trypsinised and centrifuged at 500 ***g***. Cell fractionation was carried out following the 'Subcellular protein fractionation kit for cultured cells' (ThermoScientific) protocol exactly, and samples were prepared for western blotting.

Focal-adhesion enrichment

ECs were starved in serum-free OptiMEM® for 3 h and seeded at 6×10^6 cells/plate in 10-cm plates that were previously coated with 10 µg/ml FN in PBS overnight at 4°C and blocked in 1% BSA in PBS for 1 h at RT. Cells were allowed to adhere for 90 min to allow for mature FAs to form and either

stimulated with 30 ng/ml VEGF at 37°C for 10 min (+VEGF) or not at all (−VEGF). Cells were washed in PBS+1 mM $CaCl_2$+1 mM $MgCl_2$ (PBS^{++}) and incubated with 0.5 mM Dithiobis(succinimidyl propionate) (DSP) and 0.05 mM 1,4-di-[30-(20-pyridyldithio)-propionamido] butane (DPP) diluted in PBS^{++} for 5 min to cross-link FAs to the plate. This reaction was quenched with 1 M Tris-HCl pH 7.5 before cells were lysed in RIPA for 30 min on ice with occasional agitation. RIPA was collected without scraping, and the plates were blasted with a high-sheer flow jet of distilled water to remove cell debris. Cross-linked proteins were eluted with 2 ml dithiothereitol (DTT) buffer (25 mM Tris-HCl pH 7.5, 10 mM NaCl, 0.1% SDS, 100 mM DTT) for 1 h at 60°C in a sealed and humidified chamber. 8 ml of acetone was added to this solution and left overnight at −20°C to allow the proteins to precipitate. Samples were then centrifuged at 13,000 ***g*** for 40 min, and the acetone layer removed. The pellet was resuspended in EB (see above) ready for western-blot or mass-spectrometry analysis.

Focal-adhesion tracking

1×10^6 ECs were transfected with a GFP-tagged paxillin cDNA expression construct (kindly provided by Dr Maddy Parsons, King's College London, London, UK) and a fraction of these were seeded on acid-washed and oven-sterilised glass coverslips, coated with 10 µg/ml FN in PBS, in wells of a six-well plate. Cells were cultured for ∼48 h before they were starved in serum-free OptiMEM® for 3 h. In turn, individual coverslips were separately transferred to OptiMEM®+2% FBS and 30 ng/ml VEGF was added. An Axiovert (Zeiss) inverted microscope was then used to take live images of the GFP-paxillin-positive focal adhesions in a selected field of view every 2 min for 1 h at 37°C+4% CO_2. Assembly and disassembly was quantified by manually tracking leading and trailing edges of FAs using the MTrackJ plugin for ImageJ™.

Mass-spectrometry analysis

Mass spectrometry was carried out by the Fingerprints Proteomics Facility, Dundee University, Dundee, UK as per Schiller et al. (2011). Peptides were identified and quantified using MaxQuant software using the Andromeda peptide database. To achieve label-free quantitative results, three biological repeats were pooled and each of these pooled samples was analysed via three technical repeats through the spectrometer.

Statistical analysis

Significant differences between means were evaluated by Student's *t*-test. $P<0.05$ was considered statistically significant. For flow cytometric analysis of integrins, relative differences were deemed significant if they were greater than twofold.

Acknowledgements

We thank Dr Maddy Parsons (Kings College London, London, UK) for her gift of the paxillin-GFP and β3-integrin-GFP constructs. A special thanks to Dr Sophie Akbareian for her undying enthusiastic and crucial support of this project.

Competing interests

The authors declare no competing or financial interests.

Author contributions

T.S.E. designed and performed experiments, analysed data, and helped write and edit the manuscript. S.J.A. designed and performed experiments, analysed data and helped edit the manuscript. V.S. performed experiments, analysed data and helped edit the manuscript. B.M.K. performed experiments and analysed data. M.E.J.P. and R.T.J. performed experiments. C.R. provided NRP1Δcyto mice and helped edit the manuscript. J.G.S. and K.W. generated β3-floxed mice and helped edit the manuscript. D.R.E. analysed data and helped edit the manuscript. S.D.R. designed experiments, performed experiments, analysed data and wrote the manuscript.

Funding

This work was part-funded by a BigC PhD studentship to T.S.E. (11-27R), by BBSRC DTP PhD studentship to both S.J.A. and B.M.K., and by a UEA Dean's PhD studentship to V.S. The work has also been supported by a start-up grant from UEA's School of Biological Sciences, and by funding from the John and Pamela Salter Trust (S.D.R.), DFG SCH682/3-1 and FNR Core ITGB3 VascIn funding (J.G.S.), and European Union Framework Programme 7 (SaveMe) funding (D.R.E.).

Supplementary material

Supplementary material available online at
http://dmm.biologists.org/lookup/suppl/doi:10.1242/dmm.019927/-/DC1

References

Baker, M., Robinson, S. D., Lechertier, T., Barber, P. R., Tavora, B., D'Amico, G., Jones, D. T., Vojnovic, B. and Hodivala-Dilke, K. (2012). Use of the mouse aortic ring assay to study angiogenesis. *Nat. Protoc.* **7**, 89-104.

Ballmer-Hofer, K., Andersson, A. E., Ratcliffe, L. E. and Berger, P. (2011). Neuropilin-1 promotes VEGFR-2 trafficking through Rab11 vesicles thereby specifying signal output. *Blood* **118**, 816-826.

Brooks, P. C., Montgomery, A. M. P., Rosenfeld, M., Reisfeld, R. A., Hu, T., Klier, G. and Cheresh, D. A. (1994). Integrin alpha v beta 3 antagonists promote tumor regression by inducing apoptosis of angiogenic blood vessels. *Cell* **79**, 1157-1164.

Cai, H. and Reed, R. R. (1999). Cloning and characterization of neuropilin-1-interacting protein: a PSD-95/Dlg/ZO-1 domain-containing protein that interacts with the cytoplasmic domain of neuropilin-1. *J. Neurosci.* **19**, 6519-6527.

Clark, R. A., Mason, R. J., Folkvord, J. M. and McDonald, J. A. (1986). Fibronectin mediates adherence of rat alveolar type II epithelial cells via the fibroblastic cell-attachment domain. *J. Clin. Invest.* **77**, 1831-1840.

Claxton, S., Kostourou, V., Jadeja, S., Chambon, P., Hodivala-Dilke, K. and Fruttiger, M. (2008). Efficient, inducible Cre-recombinase activation in vascular endothelium. *Genesis* **46**, 74-80.

Ebos, J. M. L. and Kerbel, R. S. (2011). Antiangiogenic therapy: impact on invasion, disease progression, and metastasis. *Nat. Rev. Clin. Oncol.* **8**, 210-221.

Evans, I. M., Yamaji, M., Britton, G., Pellet-Many, C., Lockie, C., Zachary, I. C. and Frankel, P. (2011). Neuropilin-1 signaling through p130Cas tyrosine phosphorylation is essential for growth factor-dependent migration of glioma and endothelial cells. *Mol. Cell. Biol.* **31**, 1174-1185.

Ewan, L. C., Jopling, H. M., Jia, H., Mittar, S., Bagherzadeh, A., Howell, G. J., Walker, J. H., Zachary, I. C. and Ponnambalam, S. (2006). Intrinsic tyrosine kinase activity is required for vascular endothelial growth factor receptor 2 ubiquitination, sorting and degradation in endothelial cells. *Traffic* **7**, 1270-1282.

Fantin, A., Schwarz, Q., Davidson, K., Normando, E. M., Denti, L. and Ruhrberg, C. (2011). The cytoplasmic domain of neuropilin 1 is dispensable for angiogenesis, but promotes the spatial separation of retinal arteries and veins. *Development* **138**, 4185-4191.

Fantin, A., Vieira, J. M., Plein, A., Denti, L., Fruttiger, M., Pollard, J. W. and Ruhrberg, C. (2013). NRP1 acts cell autonomously in endothelium to promote tip cell function during sprouting angiogenesis. *Blood* **121**, 2352-2362.

Fantin, A., Herzog, B., Mahmoud, M., Yamaji, M., Plein, A., Denti, L., Ruhrberg, C. and Zachary, I. (2014). Neuropilin 1 (NRP1) hypomorphism combined with defective VEGF-A binding reveals novel roles for NRP1 in developmental and pathological angiogenesis. *Development* **141**, 556-562.

Fukasawa, M., Matsushita, A. and Korc, M. (2007). Neuropilin-1 interacts with integrin beta1 and modulates pancreatic cancer cell growth, survival and invasion. *Cancer Biol. Ther.* **6**, 1184-1191.

Gerhardt, H., Ruhrberg, C., Abramsson, A., Fujisawa, H., Shima, D. and Betsholtz, C. (2004). Neuropilin-1 is required for endothelial tip cell guidance in the developing central nervous system. *Dev. Dyn.* **231**, 503-509.

Gu, C., Rodriguez, E. R., Reimert, D. V., Shu, T., Fritzsch, B., Richards, L. J., Kolodkin, A. L. and Ginty, D. D. (2003). Neuropilin-1 conveys semaphorin and VEGF signaling during neural and cardiovascular development. *Dev. Cell* **5**, 45-57.

Hanahan, D. and Weinberg, R. A. (2011). Hallmarks of cancer: the next generation. *Cell* **144**, 646-674.

Hariharan, S., Gustafson, D., Holden, S., McConkey, D., Davis, D., Morrow, M., Basche, M., Gore, L., Zang, C., O'Bryant, C. L. et al. (2007). Assessment of the biological and pharmacological effects of the alpha nu beta3 and alpha nu beta5 integrin receptor antagonist, cilengitide (EMD 121974), in patients with advanced solid tumors. *Ann. Oncol.* **18**, 1400-1407.

Herzog, B., Pellet-Many, C., Britton, G., Hartzoulakis, B. and Zachary, I. C. (2011). VEGF binding to Neuropilin-1 (NRP1) is essential for VEGF stimulation of endothelial cell migration, complex formation between NRP1 and VEGFR2, and signaling via FAK Tyr407 phosphorylation. *Mol. Biol. Cell* **22**, 2766-2776.

Hynes, R. O. (2002). Integrins: bidirectional, allosteric signaling machines. *Cell* **110**, 673-687.

Kawasaki, T., Kitsukawa, T., Bekku, Y., Matsuda, Y., Sanbo, M., Yagi, T. and Fujisawa, H. (1999). A requirement for neuropilin-1 in embryonic vessel formation. *Development* **126**, 4895-4902.

Koch, S., Tugues, S., Li, X., Gualandi, L. and Claesson-Welsh, L. (2011). Signal transduction by vascular endothelial growth factor receptors. *Biochem. J.* **437**, 169-183.

Krilleke, D., DeErkenez, A., Schubert, W., Giri, I., Robinson, G. S., Ng, Y.-S. and Shima, D. T. (2007). Molecular mapping and functional characterization of the VEGF164 heparin-binding domain. *J. Biol. Chem.* **282**, 28045-28056.

Kuo, J.-C., Han, X., Hsiao, C.-T., Yates, J. R., III and Waterman, C. M. (2011). Analysis of the myosin-II-responsive focal adhesion proteome reveals a role for

beta-Pix in negative regulation of focal adhesion maturation. *Nat. Cell Biol.* **13**, 383-393.

Lampugnani, M. G., Orsenigo, F., Gagliani, M. C., Tacchetti, C. and Dejana, E. (2006). Vascular endothelial cadherin controls VEGFR-2 internalization and signaling from intracellular compartments. *J. Cell Biol.* **174**, 593-604.

Lanahan, A., Zhang, X., Fantin, A., Zhuang, Z., Rivera-Molina, F., Speichinger, K., Prahst, C., Zhang, J., Wang, Y., Davis, G. et al. (2013). The neuropilin 1 cytoplasmic domain is required for VEGF-A-dependent arteriogenesis. *Dev. Cell* **25**, 156-168.

Mahabeleshwar, G. H., Feng, W., Reddy, K., Plow, E. F. and Byzova, T. V. (2007). Mechanisms of integrin vascular endothelial growth factor receptor cross-activation in angiogenesis. *Circ. Res.* **101**, 570-580.

Marelli, U. K., Rechenmacher, F., Sobahi, T. R. A., Mas-Moruno, C. and Kessler, H. (2013). Tumor targeting via integrin ligands. *Front. Oncol.* **3**, 222.

May, T., Mueller, P. P., Weich, H., Froese, N., Deutsch, U., Wirth, D., Kröger, A. and Hauser, H. (2005). Establishment of murine cell lines by constitutive and conditional immortalization. *J. Biotechnol.* **120**, 99-110.

Murga, M., Fernandez-Capetillo, O. and Tosato, G. (2005). Neuropilin-1 regulates attachment in human endothelial cells independently of vascular endothelial growth factor receptor-2. *Blood* **105**, 1992-1999.

Ni, C.-W., Kumar, S., Ankeny, C. J. and Jo, H. (2014). Development of immortalized mouse aortic endothelial cell lines. *Vasc. Cell* **6**, 7.

Pan, Q., Chanthery, Y., Liang, W.-C., Stawicki, S., Mak, J., Rathore, N., Tong, R. K., Kowalski, J., Yee, S. F., Pacheco, G. et al. (2007). Blocking neuropilin-1 function has an additive effect with anti-VEGF to inhibit tumor growth. *Cancer Cell* **11**, 53-67.

Prahst, C., Heroult, M., Lanahan, A. A., Uziel, N., Kessler, O., Shraga-Heled, N., Simons, M., Neufeld, G. and Augustin, H. G. (2008). Neuropilin-1-VEGFR-2 complexing requires the PDZ-binding domain of neuropilin-1. *J. Biol. Chem.* **283**, 25110-25114.

Raimondi, C., Fantin, A., Lampropoulou, A., Denti, L., Chikh, A. and Ruhrberg, C. (2014). Imatinib inhibits VEGF-independent angiogenesis by targeting neuropilin 1-dependent ABL1 activation in endothelial cells. *J. Exp. Med.* **211**, 1167-1183.

Reynolds, L. E. and Hodivala-Dilke, K. M. (2006). Primary mouse endothelial cell culture for assays of angiogenesis. *Methods Mol. Med.* **120**, 503-509.

Reynolds, L. E., Wyder, L., Lively, J. C., Taverna, D., Robinson, S. D., Huang, X., Sheppard, D., Hynes, R. O. and Hodivala-Dilke, K. M. (2002). Enhanced pathological angiogenesis in mice lacking beta3 integrin or beta3 and beta5 integrins. *Nat. Med.* **8**, 27-34.

Reynolds, A. R., Reynolds, L. E., Nagel, T. E., Lively, J. C., Robinson, S. D., Hicklin, D. J., Bodary, S. C. and Hodivala-Dilke, K. M. (2004). Elevated Flk1 (vascular endothelial growth factor receptor 2) signaling mediates enhanced angiogenesis in beta3-integrin-deficient mice. *Cancer Res.* **64**, 8643-8650.

Reynolds, A. R., Hart, I. R., Watson, A. R., Welti, J. C., Silva, R. G., Robinson, S. D., Da Violante, G., Gourlaouen, M., Salih, M., Jones, M. C. et al. (2009). Stimulation of tumor growth and angiogenesis by low concentrations of RGD-mimetic integrin inhibitors. *Nat. Med.* **15**, 392-400.

Robinson, S. D. and Hodivala-Dilke, K. M. (2011). The role of beta3-integrins in tumor angiogenesis: context is everything. *Curr. Opin. Cell Biol.* **23**, 630-637.

Robinson, S. D., Reynolds, L. E., Kostourou, V., Reynolds, A. R., da Silva, R. G., Tavora, B., Baker, M., Marshall, J. F. and Hodivala-Dilke, K. M. (2009). Alphav beta3 integrin limits the contribution of neuropilin-1 to vascular endothelial growth factor-induced angiogenesis. *J. Biol. Chem.* **284**, 33966-33981.

Schiller, H. B., Friedel, C. C., Boulegue, C. and Fässler, R. (2011). Quantitative proteomics of the integrin adhesome show a myosin II-dependent recruitment of LIM domain proteins. *EMBO Rep.* **12**, 259-266.

Schiller, H. B., Hermann, M.-R., Polleux, J., Vignaud, T., Zanivan, S., Friedel, C. C., Sun, Z., Raducanu, A., Gottschalk, K.-E., Théry, M. et al. (2013). beta1- and alphav-class integrins cooperate to regulate myosin II during rigidity sensing of fibronectin-based microenvironments. *Nat. Cell Biol.* **15**, 625-636.

Seerapu, H. R., Borthakur, S., Kong, N., Agrawal, S., Drazba, J., Vasanji, A., Fantin, A., Ruhrberg, C., Buck, M. and Horowitz, A. (2013). The cytoplasmic domain of neuropilin-1 regulates focal adhesion turnover. *FEBS Lett.* **587**, 3392-3399.

Sennino, B. and McDonald, D. M. (2012). Controlling escape from angiogenesis inhibitors. *Nat. Rev. Cancer* **12**, 699-709.

Silva, R., D'Amico, G., Hodivala-Dilke, K. M. and Reynolds, L. E. (2008). Integrins: the keys to unlocking angiogenesis. *Arterioscler. Thromb. Vasc. Biol.* **28**, 1703-1713.

Soldi, R., Mitola, S., Strasly, M., Defilippi, P., Tarone, G. and Bussolino, F. (1999). Role of alphavbeta3 integrin in the activation of vascular endothelial growth factor receptor-2. *EMBO J.* **18**, 882-892.

Sottile, J., Hocking, D. C. and Swiatek, P. J. (1998). Fibronectin matrix assembly enhances adhesion-dependent cell growth. *J. Cell Sci.* **111**, 2933-2943.

Steri, V., Ellison, T. S., Gontarczyk, A. M., Weilbaecher, K., Schneider, J. G., Edwards, D., Fruttiger, M., Hodivala-Dilke, K. M. and Robinson, S. D. (2014). Acute depletion of endothelial beta3-integrin transiently inhibits tumor growth and angiogenesis in mice. *Circ. Res.* **114**, 79-91.

Takagi, S., Kasuya, Y., Shimizu, M., Matsuura, T., Tsuboi, M., Kawakami, A. and Fujisawa, H. (1995). Expression of a cell adhesion molecule, neuropilin, in the developing chick nervous system. *Dev. Biol.* **170**, 207-222.

Tavora, B., Reynolds, L. E., Batista, S., Demircioglu, F., Fernandez, I., Lechertier, T., Lees, D. M., Wong, P.-P., Alexopoulou, A., Elia, G. et al. (2014). Endothelial-cell FAK targeting sensitizes tumours to DNA-damaging therapy. *Nature* **514**, 112-116.

Truong, H. and Danen, E. H. J. (2009). Integrin switching modulates adhesion dynamics and cell migration. *Cell Adh. Migr.* **3**, 179-181.

Tvorogov, D., Wang, X.-J., Zent, R. and Carpenter, G. (2005). Integrin-dependent PLC-gamma1 phosphorylation mediates fibronectin-dependent adhesion. *J. Cell Sci.* **118**, 601-610.

Valdembri, D., Caswell, P. T., Anderson, K. I., Schwarz, J. P., König, I., Astanina, E., Caccavari, F., Norman, J. C., Humphries, M. J., Bussolino, F. et al. (2009). Neuropilin-1/GIPC1 signaling regulates alpha5beta1 integrin traffic and function in endothelial cells. *PLoS Biol.* **7**, e25.

Zamir, E. and Geiger, B. (2001). Molecular complexity and dynamics of cell-matrix adhesions. *J. Cell Sci.* **114**, 3583-3590.

Zamir, E., Katz, M., Posen, Y., Erez, N., Yamada, K. M., Katz, B. Z., Lin, S., Lin, D. C., Bershadsky, A., Kam, Z. et al. (2000). Dynamics and segregation of cell-matrix adhesions in cultured fibroblasts. *Nat. Cell Biol.* **2**, 191-196.

Supplementary Figures

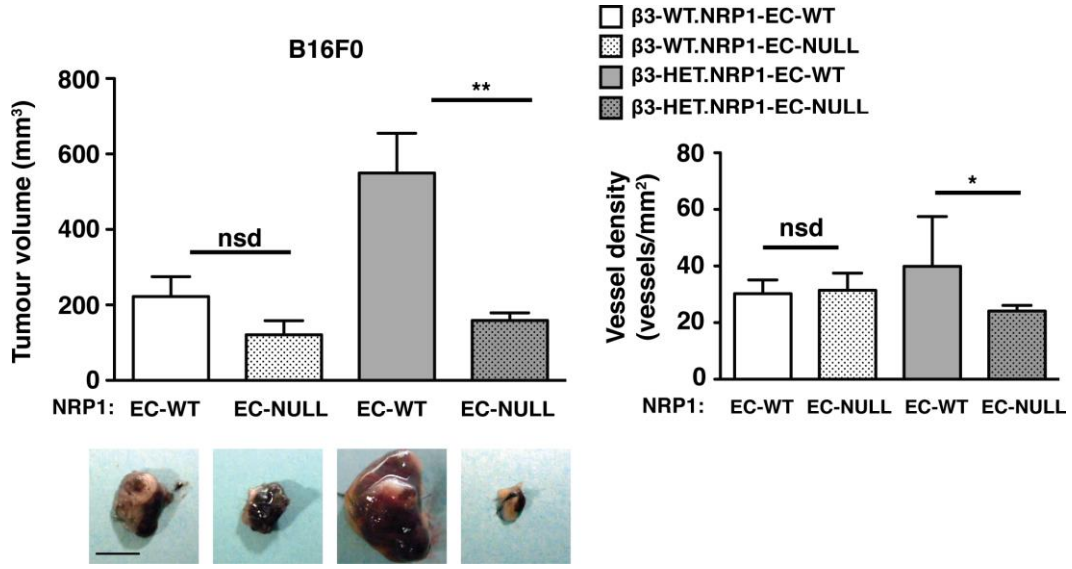

Supplementary Figure 1: B16F0 tumour growth and angiogenesis in β3-integrin-heterozygous mice are sensitive to NRP1 perturbations. Tumour growth and angiogenesis were measured in animals of the indicated genotypes. **Left panels**. Mice were given subcutaneous injections of B16F0 tumour cell lines. To generate NRP1-EC-KO (EC-Null), 21-day slow-release OHT pellets were administered 3-days prior to tumour cell injection. OHT-treated Cre-negative (EC-NRP-WT) littermates served as controls. Tumour volumes were measured after 12 days of growth (mean +SEM of 3 independent experiments; n≥10 animals per genotype). Representative pictures of tumour macroscopic appearances are shown. Scale bar = 10mm. **Right panels**. Blood vessel density was assessed by counting the total number of endomucin-positive vessels across tumour sections (mean +SEM; n≥10 sections per genotype).

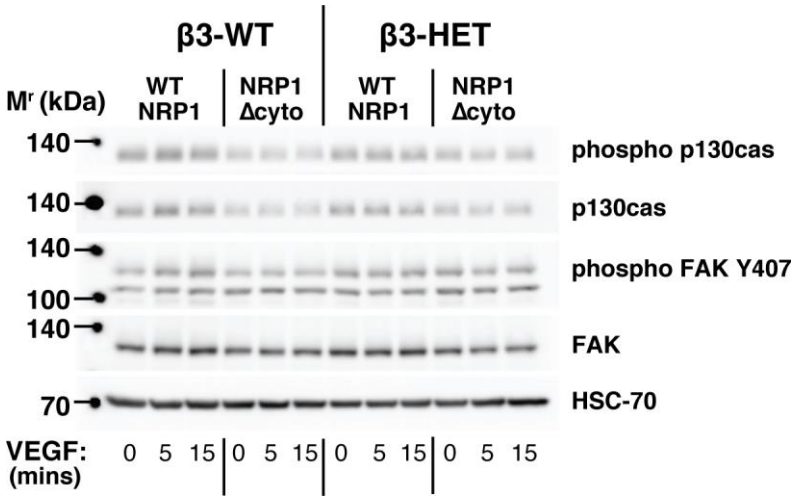

Supplementary Figure 2: No changes in the expression/activity of proteins involved in NRP1-regulated VEGF signalling. ECs were seeded on a complex matrix containing gelatin, collagen, fibronectin and vitronectin to preserve β3-VEGFR2 interactions, and were stimulated with 30 ng/ml VEGF at 37°C over a time course. ECs were lysed and analysed by Western blot (WB) for protein levels of phosphorylated (phospho) and total p130cas and FAK. HSC-70 served as a loading control. Data are representative of 3 independent experiments.

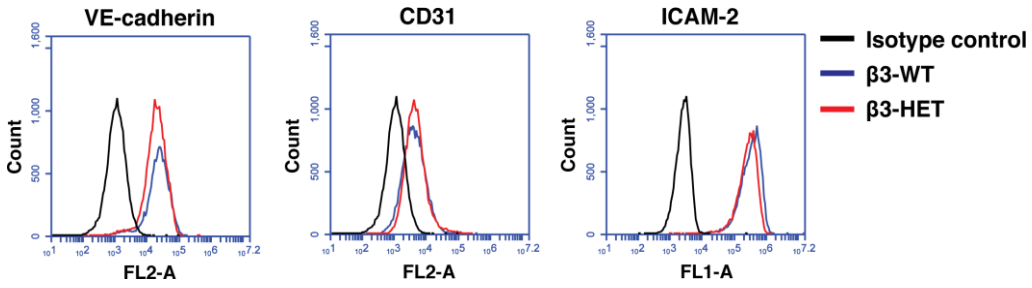

Supplementary Figure 3: Polyoma-middle-T-antigen immortialised endothelial cells maintain the endothelial identity. ECs were trypsinised and analysed by flow cytometry for surface levels of the EC markers VE-Cadherin, CD31, and ICAM-2. Median fluorescence intensity was measured after forward versus side scatter data were tightly gated around, and normalised to, an isotype control. Representative flow-cytometric histogram profiles of β3-WT and β3-HET ECs are shown.

Biochemical Society TRANSACTIONS
www.biochemsoctrans.org
Biochemical Society Transactions

Redefining the role(s) of endothelial αvβ3-integrin in angiogenesis

Samuel J. Atkinson*[1], Tim S. Ellison*[1], Veronica Steri*[1], Emma Gould† and Stephen D. Robinson*[2]

*School of Biological Sciences, University of East Anglia, Norwich Research Park, Norwich NR4 7TJ, U.K.

†School of Pharmacy, University of East Anglia, Norwich Research Park, Norwich NR4 7TJ, U.K.

Abstract

For nearly two decades now, the RGD (Arg-Gly-Asp)-binding αvβ3-integrin has been a focus of anti-angiogenic drug design. These inhibitors are well-tolerated, but have shown only limited success in patients. Over the years, studies in β3-integrin-knockout mice have shed some light on possible explanations for disappointing clinical outcomes. However, studying angiogenesis in β3-integrin-knockout mice is a blunt tool to investigate β3-integrin's role in pathological angiogenesis. Since establishing our laboratory at University of East Anglia (UEA), we have adopted more refined models of genetically manipulating the expression of the β3-integrin subunit. The present review will highlight some of our findings from these models and describe how data from them have forced us to rethink how targeting αvβ3-integrin expression affects tumour angiogenesis and cancer progression. Revisiting the fundamental biology behind how this integrin regulates tumour growth and angiogenesis, we believe, is the key not only to understanding how angiogenesis is normally co-ordinated, but also in success with drugs directed against it.

Introduction

In 1994, Brooks et al. [1,2] published two studies which reported αvβ3-integrin as a marker of angiogenic vasculature and, importantly, that it could be targeted to induce apoptosis of proliferative angiogenic vascular cells while leaving quiescent vasculature untouched. Here, it seemed, was an ideal therapeutic target to treat diseases characterized by too much neovascularization (such as cancer). These seminal findings sparked the development of inhibitors directed against αvβ3-integrin which, in a number of *in vivo* studies, demonstrated effective inhibition of tumour growth and angiogenesis [3]

However, with the generation of β3-integrin knockout mice [4], which display enhanced tumour growth [5], the angiogenesis field was seemingly divided into two camps, split across a dividing line defined by whether the molecule was viewed as pro- or anti-angiogenic. Those in the 'pro' camp dismissed the knockout findings as simply reflecting a developmental up-regulation of vascular endothelial growth factor receptor type 2 (VEGFR2) that occurs in this model [6]. Those in the 'anti' camp argued the lack of significant results in humans [3,7] could be interpreted through the knockout studies. The camps were further divided by findings indicating that the pharmacological agents being developed could stimulate tumour growth and angiogenesis, if not used optimally [8,9].

On the surface, the two approaches are quite different. Certainly a systemically-administered drug directed against αvβ3-integrin is going to operate differently from a genetic alteration that removes the expression of the β3-integrin subunit. In practice, though, both are blunt tools to dissect the innumerable cellular and molecular pathways regulated by the molecule; pathways that must be tightly-controlled to maintain vascular homoeostasis, but are skewed toward chaotic growth during cancer and other diseases. Since establishing ourselves at the University of East Anglia (UEA), my group has been fine-tuning our models for exploring the fundamental biology behind the roles played by αvβ3-integrin during tumour growth and angiogenesis. We are trying to bring together the two camps. We believe there remains great promise in targeting αvβ3-integrin to limit tumour growth and progression; by returning to basic biology we should be able to translate encouraging pre-clinical findings with αvβ3-integrin antagonists into real treatments in patients.

In the present mini-review, each of the current members of my group has contributed their opinion on an area of αvβ3-integrin biology that, they feel, holds promise and/or needs further exploration in order to understand why, for example, cilengitide, the furthest progressed RGD (Arg-Gly-Asp)-mimetic, has recently failed its first Phase III clinical trial [10] (Figure 1). Although the reasons for its failure are as yet unknown, some of our current studies, as outlined below, are aimed at finding out how, when and where it might be best to employ inhibitors directed against αvβ3-integrin to achieve maximum benefit.

Understanding the *in vivo* role of endothelial β3-integrin

Ten years after the Food and Drug Administration's (FDA's) approval of the first anti-angiogenic therapy (Bevacizumab),

Key words: angiogenesis, antagonist, cancer, endothelial cell, β3-integrin, tumour.

Abbreviations: EC, endothelial cell; ECM, extracellular matrix; FA, focal adhesion; FN, fibronectin; NRP1, neuropilin-1; TNFα, tumour necrosis factor α; VEGFR2, vascular endothelial growth factor receptor type 2.

[1]These authors contributed equally to this article.

[2]To whom correspondence should be addressed (email stephen.robinson@uea.ac.uk).

©The Authors Journal compilation ©2014 Biochemical Society

Figure 1 | An artistic representation of tumour vasculature which highlights the three main themes relating to β3-integrin biology discussed

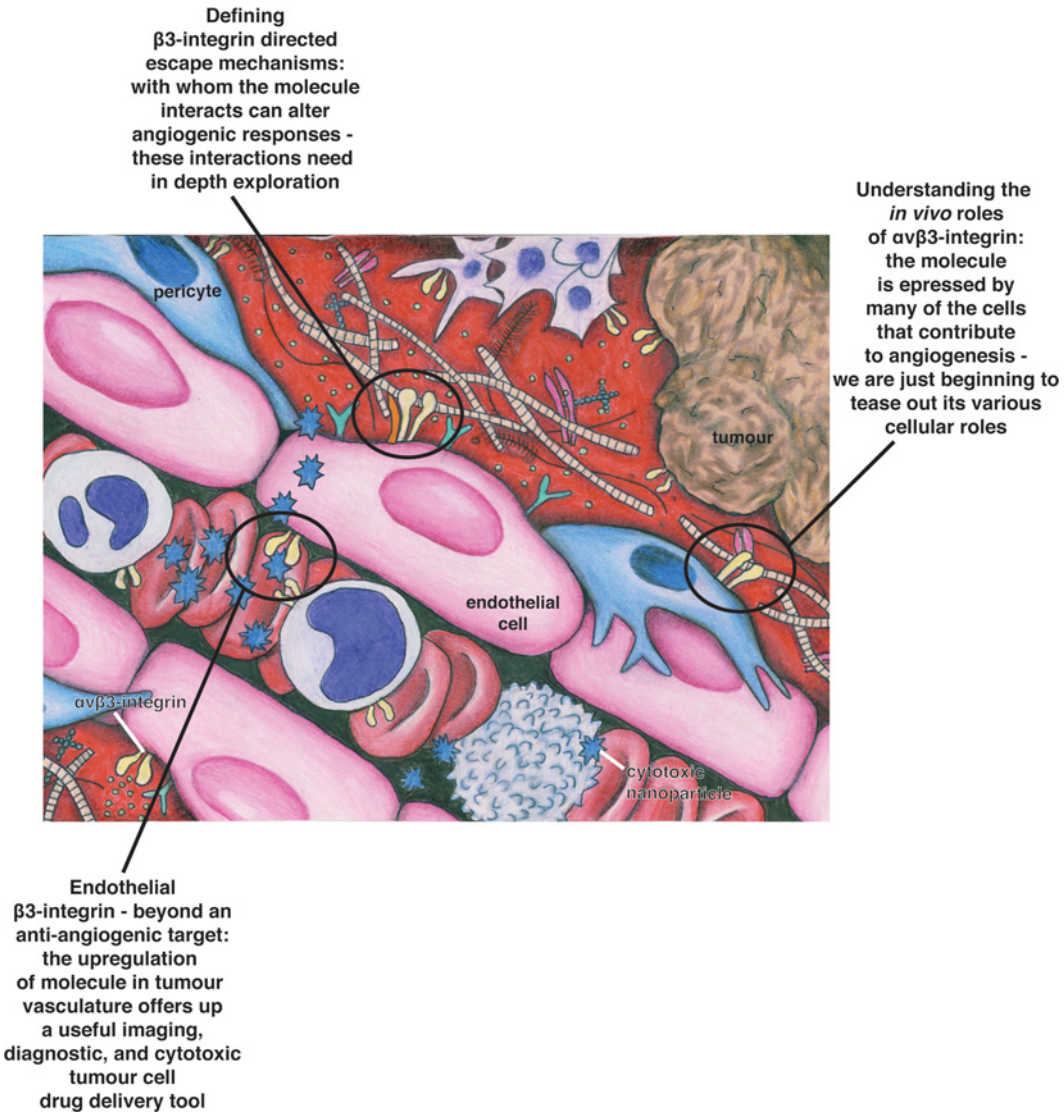

our strategies need to be rethought. Endothelial cell (EC) heterogeneity along with the complexity of tumour vasculature represents a gap in our fundamental knowledge of tumour biology that needs to be re-evaluated in order to effectively translate theories into clinical therapies. Integrins may hold the key to this unmet challenge. They are a large and diverse family of cell adhesion receptors which transduce signals bidirectionally across the plasma membrane [11]. Nine vertebrate integrin heterodimers are implicated in angiogenesis, with the RGD tripeptide-binding integrins $\alpha5\beta1$, $\alpha v\beta3$, $\alpha v\beta5$, and $\alpha v\beta8$ playing major roles [12,13]. As mentioned above, $\alpha v\beta3$-integrin, in particular, has garnered therapeutic attention because its expression is up-regulated in vasculature associated with solid tumours [14] but is contrastingly low in quiescent vasculature [2,15], thereby reducing the potential for side effects from its blockade.

Although this suggests that the EC expression of $\beta3$-integrin is an ideal anti-cancer target, it is easy to forget that the molecule is expressed by a myriad of cells, each contributing in their own way to angiogenesis. Moreover, $\beta3$-integrin expression on tumour cells has been shown to contribute towards tumour progression and metastasis, as well as correlating with poor patient survival. However, in some human tumours (e.g. angiosarcomas), vascular $\alpha v\beta3$-integrin levels are found to diminish in the course of malignant transformation and to be lower in lung metastases in comparison with its levels in the originating primary colorectal carcinomas [13]. These observations additionally substantiate the idea that $\alpha v\beta3$-integrin can play either a pro- or anti-tumourigenic role in a way which is not quite fully understood.

Global genetic studies have given us many clues into $\alpha v\beta3$-integrin biology, but still have not answered the

©The Authors Journal compilation ©2014 Biochemical Society

question. Knockin mice that express a mutant αvβ3-integrin, which is unable to undergo cytoplasmic tyrosine phosphorylation, show reduced tumour vascularization [16], suggesting downstream signalling through the molecule promotes angiogenesis. β3-integrin knockout mice exibit enhanced tumour growth and vascularization [5] indicating expression of the molecule negatively regulates angiogenesis. What then is going on? It is clear in both studies that more than one cell-type contributes to the ultimate phenotype. In both cases, the mutant phenotype can be partially abrogated by restoring wild-type expression of β3-integrin in bone marrow derived cells (BMDCs) through adoptive transfer [17,18].

Thanks to the Weilbaecher laboratory in St. Louis, we are now finally beginning to dissect the role of β3-integrins, as expressed by individual cell-types, in pathological conditions. Although platelet β3-knockout has no effect on tumour growth or angiogenesis, the myeloid β3-knockout displays enhanced tumour burden [19] (although tumour angiogenesis appears unaffected), a finding consistent with the bone marrow transplant studies described above.

Although these two cell types are certainly important, the original intended target of αvβ3-integrin antagonists are ECs; elucidating the role of αvβ3-integrin expression here is probably the key to developing more effective anti-angiogenic therapies directed against it. We have recently described the role played by EC β3-integrin in mice [20]. We show that αvβ3-integrin plays a crucial role in the very early steps of tumour angiogenesis, whereas its EC expression is dispensable once tumour vasculature has been established and prolonged EC-depletion of the molecule is eventually overcome (escape occurs). It appears that over the long term, the plasticity of ECs leads to their cellular rewiring such that alternative means of executing/maintaining angiogenesis are utilized. Furthermore, our findings, in combination with the other genetic studies described in the present paper, reinforce the concept that there are multiple levels of cellular complexity to angiogenic regulation, all of which will matter when it comes to pharmacological inhibition of αvβ3-integrin. We are just at the beginning of understanding its EC-role, let alone its role when expressed by pericytes, stromal fibroablasts and macrophages.

Defining β3-integrin-directed escape mechanisms

The discrepant angiogenic results garnered from targeting αvβ3-integrin in different ways have highlighted the sheer complexity of this molecule's role in angiogenesis. Our discovery that the acute depletion of endothelial αvβ3-integin can reduce tumour angiogenesis, albeit transiently and in a preventive manner, has suggested that we can still think of using it as a target, but only if we discover the right conditions that render it therapeutically useful. It is our hope that we can use the models we have generated (the EC-specific knockouts described above, as well as β3-integrin-heterozygous animals) to understand EC plasticity and determine whether there are escape pathways common to pharmacological and genetic inhibition of αvβ3-integrin; pathways that might be targeted alongside the molecule to sustain, or at least extend, inhibition.

It is therefore extremely important to carefully consider the ways in which targeting αvβ3-integrin can effectuate resistance mechanisms in ECs. First and foremost, we need to study the interactions that αvβ3 makes in ECs, as targeting αvβ3-integrin genetically or with inhibitors could affect interacting molecules and potentially enhance or change their roles.

One αvβ3-integrin interaction that has not been lacking in attention in the field has been with the main receptor mediator of angiogenesis, VEGFR2. This interaction, dependent on the presence of αvβ3-integrin's natural extracellular matrix (ECM) ligand vitronectin, and VEGF, has now been shown to be a direct one between the two cytoplasmic tails and enhanced through Tyr^{747} phosphorylation of the β3-integrin subunit. The cross-talk between αvβ3-integrin and VEGFR2 enhances the activity of each and has been found to increase VEGF-induced signalling and angiogenesis [16,21]. However, the enhanced tumour growth and angiogenesis observed in β3-knockout mice clearly shows that this interaction is non-essential to angiogenesis [5]. Indeed, the global loss of β3-integrin in this model is actually associated with a vast up-regulation of VEGFR2 expression and treatment with a VEGFR2 inhibitor reverses the phenotype [6].

αvβ3-Integrin has also been found to associate with the VEGF co-receptor neuropilin-1 (NRP1), which is known to form a complex with VEGFR2 and regulate its trafficking and signalling [22–25]. Interestingly, αvβ3-integrin can limit this VEGF-induced association as the interaction is enhanced in β3-knockout ECs [26], suggesting that αvβ3-integrin can regulate NRP1's role in angiogenesis. It may be important to note that NRP1's role in angiogenesis is not limited to the confines of VEGFR2 [27]; recent evidence has highlighted a role for NRP1 in regulating focal adhesion (FA) turnover [28] and in promoting fibronectin (FN)-dependent paxillin activation and actin remodelling [29]. We also know that NRP1 can bind and regulate α5β1-integrin and, thus, promote EC spreading on FN [30]. This duplicity in NRP1 binding two subclasses of FN-binding RGD-integrins, αvβ3 and α5β1, in ECs has led us to the present work exploring the role of ECs for the latter in tumour growth and angiogenesis.

The dynamic adhesion properties of ECs are crucial for their motility and migration and therefore crucial for angiogenesis. Integrins, as bidirectional signalling intermediaries between the ECM and the cell-interior and key regulators of EC migration, are key components of FAs, the cluster of scaffolding and enzymatic proteins that mediate cell movement through linking the force-generating actin machinery with the outside environment. Integrins therefore interact with many of these so-called adhesome components and so it would be interesting to see how targeting αvβ3-integrin might affect FA composition and stoichiometry.

©The Authors Journal compilation ©2014 Biochemical Society

Indeed, with NRP1's prominence in EC adhesion function, the interplay between $\alpha v\beta 3$-integrin and NRP1 may have an added dimension. Of note, Schiller et al. [31,32] recently profiled the integrin adhesome in fibroblasts and found that αv-integrins are more associated with mature FAs, whereas $\beta 1$-integrins play a more prominent role in nascent adhesions. The present work has recently led us to profile the endothelial adhesome, the results of which we are preparing for publication and further analysis.

EC $\beta 3$-integrin: beyond an anti-angiogenic target

$\alpha v\beta 3$-Integrin's up-regulation in angiogenic vasculature [1,2] in multiple cancers (breast, renal, ovarian, glioma, myeloma, melanoma and more) [33] and in osteoclasts [34] provides a useful marker of particular interest to cancer therapy/diagnostics. This expression may potentially allow the selective delivery of compounds to these sites to impede tumour vasculature formation, inhibit tumour cell-growth or halt the expansion of osteolytic lesions that are common place in bone metastases, thus overcoming dose limiting toxicity from systemic effects.

Integrin targeting strategies have been revolutionized by the development of selective cyclic peptides – most notably RGD-mimetics such as cilgengitide. Several simple strategies, such as conjugating RGD-targeting peptides to traditional chemotherapeutics (e.g. paclitaxel and doxorubicin), have proved successful *in vivo*. These approaches provide increased chemotherapeutic dose at the tumour as well as increased duration of effect compared with non-RGD targeted controls [35,36]. For a comprehensive review on integrin-targeted chemotherapeutics, see Chen and Chen [37]. More recent strategies have included using silica nanoparticles as platforms for assembly of a targeted therapy. Their inherent low toxicity, innate fluorescence and high loading ability make them ideal carriers for compounds such as doxorubicin, camptothecin, etc. and they can be surface-coated in integrin targeting molecules, antibodies or RGD peptides [38]. The next generation of RGD-mimetics that induce internalization of the 'payload' are also under intense study [39].

Radiotherapy can also be focused like chemotherapy. Radioisotopes have been conjugated to RGD-targeting peptides such as ^{111}In, ^{99m}Tc and ^{90}Y [40], where all three radio-conjugates showed selective tumour uptake and a significant decrease in tumour growth was exhibited by ^{90}Y. It has been suggested that, with radiotherapy, RGD peptides do not persist long enough before excretion to allow for a sustained dose in most cases [41]. Hence, antibody directed radiotherapies may be a better alternative. Veeravagu et al. [42] have shown that a novel ^{90}Y-labelled Abegrin (a humanized anti-$\alpha v\beta 3$-integrin antibody) radioimmunotherapeutic agent is effective against glioblastoma in mouse xenograft models and can also be used to image the tumour.

Biologics, such as tumour necrosis factor α (TNFα), are currently being used/evaluated for several cancers as monotherapies or in combination with chemo/radiotherapy [43]. Several have also been conjugated to RGD peptides. Wang et al. [44] showed that an RGD-TNFα fusion protein was effective at reducing tumour volume by 72 % compared with TNFα at doses low enough to have no toxicity effects. Another promising example is the chemical synthesis of a pro-apoptotic SMAC mimetic conjugated to an RGD-mimetic [45]. Integrin $\alpha v\beta 3$ is also being used to direct nucleic acid delivery, most notably siRNAs. A sophisticated liposomal delivery system for siRNA targeting VEGFR2 (present on more than just tumour vasculature), targeted using RGD-peptides, produced a sustained reduction in tumour growth with no systemic toxicity [46]. It is easy to imagine that an extension of this strategy might be used to overcome anti-angiogenic escape mechanisms by incorporating multiple siRNAs into the system once appropriate targets are identified.

The majority of data clearly indicate that even in the unlikely event that we eventually abandon $\alpha v\beta 3$-integrin as a direct anti-angiogenic target, its up-regulated expression in angiogenic vasculature will certainly prove useful. Aside from the aforementioned therapeutic uses, the molecule has great potential for imaging, by using the selectivity of its targeting motifs. For example, when ^{64}Cu is added to the RGD–TNFα conjugate by Wang et al. [44], it allows specific imaging of tumours by micro positron emission tomography (μPET). Other RGD targets can be modified similarly by the incorporation of radioactive markers such as ^{18}F [47,48]. A more detailed review of $\alpha v\beta 3$-integrin-based diagnostics has been produced by Danhier et al. [49].

Concluding remarks

We hope we have convinced the reader of the present review that, in spite of, to date, lacklustre results in the clinic, it would be premature to give up on $\alpha v\beta 3$-integrin as a cancer target. Aside from its unique angiogenic expression profile, which reduces the likely side effects from its blockade, inhibiting the molecule has potential benefits we have not had space to comment on in depth: (i) inhibiting its function simultaneously hampers and normalizes the formation of tumour blood vessels [50], thereby possibly increasing effective delivery of chemotherapeutic agents; and (ii) $\alpha v\beta 3$-integrin augments signalling through multiple pro-angiogenic-growth-factor pathways [51], therefore inhibiting its function may block multiple pro-angiogenic pathways at the same time.

So, how do we move forward? Our published findings [20,26] suggest that disappointing clinical outcomes achieved with the existing pharmaceutical agents directed against $\alpha v\beta 3$-integrin (http://www.pharmatimes.com/article/13-02-26/Merck_KGaA_s_cilengitide_fails_in_Phase_III.aspx) [52] arise, at least in part, from treatment escape associated with long-term $\alpha v\beta 3$-integrin targeting. However, until we fully understand how these antagonists function, we cannot rule out the possibility that poor outcomes are the result of reported mechanistic [8,53] and dosing [9] problems

©The Authors Journal compilation ©2014 Biochemical Society

associated with these antagonists. If we wish to mirror the successes that have been achieved with other targeted therapies, we too must return to fundamental biology in order to move forward with this promising target. The models we have generated have already gone some way towards a deeper mechanistic understanding of how EC $\alpha v\beta 3$-integrin regulates the initial stages of tumour growth and angiogenesis. By extending these models into more clinically relevant scenarios, where there is frequently a gap between pre-clinical and clinical studies that may contribute to eventual strategy failure, we may be able to re-direct the use of current drugs in combination and/or spur the development of new inhibitors, building towards directed therapies that integrate multiple angiogenic pathways.

Acknowledgements

We thank Professor Dylan Edwards and Professor Ulrike Mayer for their wonderful mentoring of S.D.R. during the early stages of his independent career. We also thank Dr Sophia Akbareian for her unquenchable spirit and her day-to-day intellectual input into all goings-on in the laboratory.

Funding

This work was supported by the Norwich Research Park Biotechnology and Biological Sciences Research Council Doctoral Training Partnership (DTP) studentship (to S.A.); BigC Ph.D. studentship (to T.S.E.); the University of East Anglia Dean's Ph.D. studentship; and the John and Pamela Salter Charitable Trust.

References

1 Brooks, P.C., Clark, R.A. and Cheresh, D.A. (1994) Requirement of vascular integrin $\alpha v\beta 3$ for angiogenesis. Science **264**, 569–571 CrossRef PubMed
2 Brooks, P.C., Montgomery, A.M., Rosenfeld, M., Reisfeld, R.A., Hu, T., Klier, G. and Cheresh, D.A. (1994) Integrin $\alpha v\beta 3$ antagonists promote tumor regression by inducing apoptosis of angiogenic blood vessels. Cell **79**, 1157–1164 CrossRef PubMed
3 Tucker, G.C. (2006) Integrins: molecular targets in cancer therapy. Curr. Oncol. Rep. **8**, 96–103 CrossRef PubMed
4 Hodivala-Dilke, K.M., McHugh, K.P., Tsakiris, D.A., Rayburn, H., Crowley, D., Ullman-Culleré, M., Ross, F.P., Coller, B.S., Teitelbaum, S. and Hynes, R.O. (1999) $\beta 3$-integrin-deficient mice are a model for Glanzmann thrombasthenia showing placental defects and reduced survival. J. Clin. Invest. **103**, 229–238 CrossRef PubMed
5 Reynolds, L.E., Wyder, L., Lively, J.C., Taverna, D., Robinson, S.D., Huang, X., Sheppard, D., Hynes, R.O. and Hodivala-Dilke, K.M. (2002) Enhanced pathological angiogenesis in mice lacking $\beta 3$ integrin or $\beta 3$ and $\beta 5$ integrins. Nat. Med. **8**, 27–34 CrossRef PubMed
6 Reynolds, A.R., Reynolds, L.E., Nagel, T.E., Lively, J.C., Robinson, S.D., Hicklin, D.J., Bodary, S.C. and Hodivala-Dilke, K.M. (2004) Elevated Flk1 (vascular endothelial growth factor receptor 2) signaling mediates enhanced angiogenesis in $\beta 3$-integrin-deficient mice. Cancer Res. **64**, 8643–8650 CrossRef PubMed
7 Stupp, R. and Ruegg, C. (2007) Integrin inhibitors reaching the clinic. J. Clin. Oncol. **25**, 1637–1638 CrossRef PubMed
8 Alghisi, G.C., Ponsonnet, L. and Ruegg, C. (2009) The integrin antagonist cilengitide activates $\alpha V\beta 3$, disrupts VE-cadherin localization at cell junctions and enhances permeability in endothelial cells. PLoS ONE **4**, e4449 CrossRef PubMed
9 Reynolds, A.R., Hart, I.R., Watson, A.R., Welti, J.C., Silva, R.G., Robinson, S.D., Da Violante, G., Gourlaouen, M., Salih, M., Jones, M.C. et al. (2009) Stimulation of tumor growth and angiogenesis by low concentrations of RGD-mimetic integrin inhibitors. Nat. Med. **15**, 392–400 CrossRef PubMed
10 Grogan, K. (2013), Merck KGaA's cilengitide fails in Phase III. PharmaTimes online (http://www.pharmatimes.com/article/13-02-26/Merck_KGaA_s_cilengitide_fails_in_Phase_III.aspx)
11 Hynes, R.O. (2002) Integrins: bidirectional, allosteric signaling machines. Cell **110**, 673–687 CrossRef PubMed
12 van der Flier, A., Badu-Nkansah, K., Whittaker, C.A., Crowley, D., Bronson, R.T., Lacy-Hulbert, A. and Hynes, R.O. (2010) Endothelial $\alpha 5$ and αv integrins cooperate in remodeling of the vasculature during development. Development **137**, 2439–2449 CrossRef PubMed
13 Robinson, S.D. and Hodivala-Dilke, K.M. (2011) The role of $\beta 3$-integrins in tumor angiogenesis: context is everything. Curr. Opin. Cell Biol. **23**, 630–637 CrossRef PubMed
14 Brooks, P.C., Strömblad, S., Klemke, R., Visscher, D., Sarkar, F.H. and Cheresh, D.A. (1995) Antiintegrin $\alpha v\beta 3$ blocks human breast cancer growth and angiogenesis in human skin. J. Clin. Invest. **96**, 1815–1822 CrossRef PubMed
15 Cai, W. and Chen, X. (2006) Anti-angiogenic cancer therapy based on integrin $\alpha v\beta 3$ antagonism. Anticancer Agents Med. Chem. **6**, 407–428 CrossRef PubMed
16 Mahabeleshwar, G.H., Feng, W., Phillips, D.R. and Byzova, T.V. (2006) Integrin signaling is critical for pathological angiogenesis. J. Exp. Med. **203**, 2495–2507 CrossRef PubMed
17 Feng, W., McCabe, N.P., Mahabeleshwar, G.H., Somanath, P.R., Phillips, D.R. and Byzova, T.V. (2008) The angiogenic response is dictated by $\beta 3$ integrin on bone marrow-derived cells. J. Cell Biol. **183**, 1145–1157 CrossRef PubMed
18 Watson, A.R., Pitchford, S.C., Reynolds, L.E., Direkze, N., Brittan, M., Alison, M.R., Rankin, S., Wright, N.A. and Hodivala-Dilke, K.M. (2010) Deficiency of bone marrow $\beta 3$-integrin enhances non-functional neovascularization. J. Pathol. **220**, 435–445 PubMed
19 Morgan, E.A., Schneider, J.G., Baroni, T.E., Uluçkan, O., Heller, E., Hurchla, M.A., Deng, H., Floyd, D., Berdy, A., Prior, J.L. et al. (2010) Dissection of platelet and myeloid cell defects by conditional targeting of the $\beta 3$-integrin subunit. FASEB J. **24**, 1117–1127 CrossRef PubMed
20 Steri, V., Ellison, T.S., Gontarczyk, A.M., Weilbaecher, K., Schneider, J.G., Edwards, D., Fruttiger, M., Hodivala-Dilke, K.M. and Robinson, S.D. (2014) Acute depletion of endothelial $\beta 3$-integrin transiently inhibits tumor growth and angiogenesis in mice. Circ. Res. **114**, 79–91 CrossRef PubMed
21 West, X.Z., Meller, N., Malinin, N.L., Deshmukh, L., Meller, J., Mahabeleshwar, G.H., Weber, M.E., Kerr, B.A., Vinogradova, O. and Byzova, T.V. (2012) Integrin $\beta 3$ crosstalk with VEGFR accommodating tyrosine phosphorylation as a regulatory switch. PLoS ONE **7**, e31071 CrossRef PubMed
22 Whitaker, G.B., Limberg, B.J. and Rosenbaum, J.S. (2001) Vascular endothelial growth factor receptor-2 and neuropilin-1 form a receptor complex that is responsible for the differential signaling potency of $VEGF_{165}$ and $VEGF_{121}$. J. Biol. Chem. **276**, 25520–25531 CrossRef PubMed
23 Soker, S., Miao, H.Q., Nomi, M., Takashima, S. and Klagsbrun, M. (2002) $VEGF_{165}$ mediates formation of complexes containing VEGFR-2 and neuropilin-1 that enhance $VEGF_{165}$-receptor binding. J. Cell. Biochem. **85**, 357–368 CrossRef PubMed
24 Herzog, B., Pellet-Many, C., Britton, G., Hartzoulakis, B. and Zachary, I.C. (2011) VEGF binding to NRP1 is essential for VEGF stimulation of endothelial cell migration, complex formation between NRP1 and VEGFR2, and signalling via FAK Tyr^{407} phosphorylation. Mol. Biol. Cell **22**, 2766–2776 CrossRef PubMed
25 Ballmer-Hofer, K., Andersson, A.E., Ratcliffe, L.E. and Berger, P. (2011) Neuropilin-1 promotes VEGFR-2 trafficking through Rab11 vesicles thereby specifying signal output. Blood **118**, 816–826 CrossRef PubMed
26 Robinson, S.D., Reynolds, L.E., Kostourou, V., Reynolds, A.R., da Silva, R.G., Tavora, B., Baker, M., Marshall, J.F. and Hodivala-Dilke, K.M. (2009) $\alpha v\beta 3$ integrin limits the contribution of neuropilin-1 to vascular endothelial growth factor-induced angiogenesis. J. Biol. Chem. **284**, 33966–33981 CrossRef PubMed
27 Fantin, A., Herzog, B., Mahmoud, M., Yamaji, M., Plein, A., Denti, L., Ruhrberg, C. and Zachary, I. (2014) Neuropilin 1 (NRP1) hypomorphism combined with defective VEGF-A binding reveals novel roles for NRP1 in developmental and pathological angiogenesis. Development **141**, 556–562 CrossRef PubMed

©The Authors Journal compilation ©2014 Biochemical Society

28 Seerapu, H.R., Borthakur, S., Kong, N., Agrawal, S., Drazba, J., Vasanji, A., Fantin, A., Ruhrberg, C., Buck, M. and Horowitz, A. (2013) The cytoplasmic domain of neuropilin-1 regulates focal adhesion turnover. FEBS Lett. **587**, 3392–3399 CrossRef PubMed

29 Raimondi, C., Fantin, A., Lampropoulou, A., Denti, L., Chikh, A. and Ruhrberg, C. (2014) Imatinib inhibits VEGF-independent angiogenesis by targeting neuropilin 1-dependent ABL1 activation in endothelial cells. J. Exp. Med. **211**, 1167–1183 CrossRef PubMed

30 Valdembri, D., Caswell, P.T., Anderson, K.I., Schwarz, J.P., König, I., Astanina, E., Caccavari, F., Norman, J.C., Humphries, M.J., Bussolino, F. and Serini, G. (2009) Neuropilin-1/GIPC1 signaling regulates $\alpha 5\beta 1$ integrin traffic and function in endothelial cells. PLoS Biol. **7**, e25 CrossRef PubMed

31 Schiller, H.B., Friedel, C.C., Boulegue, C. and Fassler, R. (2011) Quantitative proteomics of the integrin adhesome show a myosin II-dependent recruitment of LIM domain proteins. EMBO Rep. **12**, 259–266 CrossRef PubMed

32 Schiller, H.B., Hermann, M.R., Polleux, J., Vignaud, T., Zanivan, S., Friedel, C.C., Sun, Z., Raducanu, A., Gottschalk, K.E., Théry, M. et al. (2013) $\beta 1$- and αv-class integrins cooperate to regulate myosin II during rigidity sensing of fibronectin-based microenvironments. Nat. Cell Biol. **15**, 625–636 CrossRef PubMed

33 Mulgrew, K., Kinneer, K., Yao, X.T., Ward, B.K., Damschroder, M.M., Walsh, B., Mao, S.Y., Gao, C., Kiener, P.A., Coats, S. et al. (2006) Direct targeting of αv$\beta 3$ integrin on tumor cells with a monoclonal antibody, abegrin. Mol. Cancer Ther. **5**, 3122–3129 CrossRef PubMed

34 Teti, A., Migliaccio, S. and Baron, R. (2002) The role of the αV$\beta 3$ integrin in the development of osteolytic bone metastases: a pharmacological target for alternative therapy? Calcif. Tissue Int. **71**, 293–299 CrossRef

35 Burkhart, D.J., Kalet, B.T., Coleman, M.P., Post, G.C. and Koch, T.H. (2004) Doxorubicin-formaldehyde conjugates targeting αv$\beta 3$ integrin. Mol. Cancer Ther. **3**, 1593–1604 PubMed

36 Cao, Q., Li, Z.B., Chen, K., Wu, Z., He, L., Neamati, N. and Chen, X. (2008) Evaluation of biodistribution and anti-tumor effect of a dimeric RGD peptide–paclitaxel conjugate in mice with breast cancer. Eur. J. Nucl. Med. Mol. Imaging **35**, 1489–1498 CrossRef PubMed

37 Chen, K. and Chen, X. (2011) Integrin targeted delivery of chemotherapeutics. Theranostics **1**, 189–200 CrossRef PubMed

38 Chen, H., Zhen, Z., Tang, W., Todd, T., Chuang, Y.J., Wang, L., Pan, Z. and Xie, J. (2013) Label-free luminescent mesoporous silica nanoparticles for imaging and drug delivery. Theranostics **3**, 650–657 CrossRef PubMed

39 Wang, K., Zhang, X., Liu, Y., Liu, C., Jiang, B. and Jiang, Y. (2014) Tumor penetrability and anti-angiogenesis using iRGD-mediated delivery of doxorubicin–polymer conjugates. Biomaterials **35**, 8735–8747 CrossRef PubMed

40 Janssen, M.L., Oyen, W.J., Dijkgraaf, I., Massuger, L.F., Frielink, C., Edwards, D.S., Rajopadhye, M., Boonstra, H., Corstens, F.H. and Boerman, O.C. (2002) Tumor targeting with radiolabeled αv$\beta 3$ integrin binding peptides in a nude mouse model. Cancer Res. **62**, 6146–6151 PubMed

41 Liu, Z., Wang, F. and Chen, X. (2008) Integrin αv$\beta 3$-targeted cancer therapy. Drug Dev. Res. **69**, 329–339 CrossRef PubMed

42 Veeravagu, A., Liu, Z., Niu, G., Chen, K., Jia, B., Cai, W., Jin, C., Hsu, A.R., Connolly, A.J., Tse, V. et al. (2008) Integrin αv$\beta 3$-targeted radioimmunotherapy of glioblastoma multiforme. Clin. Cancer Res. **14**, 7330–7339 CrossRef PubMed

43 van Horssen, R., Ten Hagen, T.L. and Eggermont, A.M. (2006) TNF-α in cancer treatment: molecular insights, antitumor effects, and clinical utility. Oncologist **11**, 397–408 CrossRef PubMed

44 Wang, H., Chen, K., Cai, W., Li, Z., He, L., Kashefi, A. and Chen, X. (2008) Integrin-targeted imaging and therapy with RGD4C–TNF fusion protein. Mol. Cancer Ther. **7**, 1044–1053 CrossRef PubMed

45 Mingozzi, M., Manzoni, L., Arosio, D., Dal Corso, A., Manzotti, M., Innamorati, F., Pignataro, L., Lecis, D., Delia, D., Seneci, P. and Gennari, C. (2014) Synthesis and biological evaluation of dual action cyclo-RGD/SMAC mimetic conjugates targeting αv$\beta 3$/αv$\beta 5$ integrins and IAP proteins. Org. Biomol. Chem. **12**, 3288–3302 CrossRef PubMed

46 Sakurai, Y., Hatakeyama, H., Sato, Y., Hyodo, M., Akita, H., Ohga, N., Hida, K. and Harashima, H. (2014) RNAi-mediated gene knockdown and anti-angiogenic therapy of RCCs using a cyclic RGD-modified liposomal–siRNA system. J. Control. Release **173**, 110–118 CrossRef PubMed

47 Morrison, M.S., Ricketts, S.A., Barnett, J., Cuthbertson, A., Tessier, J. and Wedge, S.R. (2009) Use of a novel Arg-Gly-Asp radioligand, ^{18}F-AH111585, to determine changes in tumor vascularity after antitumor therapy. J Nucl. Med. **50**, 116–122 CrossRef PubMed

48 Durkan, K., Jiang, Z., Rold, T.L., Sieckman, G.L., Hoffman, T.J., Bandari, R.P., Szczodroski, A.F., Liu, L., Miao, Y., Reynolds, T.S. and Smith, C.J. (2014) A heterodimeric [RGD-Glu-[^{64}Cu-NO2A]-6-Ahx-RM2] αv$\beta 3$/GRPr-targeting antagonist radiotracer for PET imaging of prostate tumors. Nucl. Med. Biol. **41**, 133–139 CrossRef PubMed

49 Danhier, F., Le Breton, A. and Préat, V. (2012) RGD-based strategies to target αv$\beta 3$ integrin in cancer therapy and diagnosis. Mol. Pharm. **9**, 2961–2973 CrossRef PubMed

50 Bouzin, C. and Feron, O. (2007) Targeting tumor stroma and exploiting mature tumor vasculature to improve anti-cancer drug delivery. Drug Resist. Updat. **10**, 109–120 CrossRef PubMed

51 Switala-Jelen, K., Dabrowska, K., Opolski, A., Lipinska, L., Nowaczyk, M. and Gorski, A. (2004) The biological functions of $\beta 3$ integrins. Folia Biol. **50**, 143–152 PubMed

52 Smith, J.W. (2003) Cilengitide Merck. Curr. Opin. Invest. Drugs **4**, 741–745 PubMed

53 Ghitti, M., Spitaleri, A., Valentinis, B., Mari, S., Asperti, C., Traversari, C., Rizzardi, G.P. and Musco, G. (2012) Molecular dynamics reveal that isoDGR-containing cyclopeptides are true αv$\beta 3$ antagonists unable to promote integrin allostery and activation. Angew. Chem. Int. Ed. Engl. **51**, 7702–7705 CrossRef PubMed

Received 30 July 2014
doi:10.1042/BST20140206

©The Authors Journal compilation ©2014 Biochemical Society

Abbreviations

1D nLC-MS/MS – 1D nano liquid chromatography tandem mass spectrometry

αvβ3 – alpha-v-beta-3-integrin

α5β1 – alpha-5-beta-1-integrin

β3 – beta-3-integrin

β3Δ722– Mutant β3-integrin lacking the residues (723-787) of its cytoplasmic tail

β3Δ744– Mutant β3-integrin lacking the residues (745-787) of its cytoplasmic tail

β3-EC-NULL – Constitutive knockout of β3-integrin from endothelial cells

β3-EC-ID – Inducible depletion of β3-integrin in endothelial cells

β3-HET – beta-3-integrin-heterozygous

β3-NULL – beta-3-integrin-knockout

Ab – Antibody

ABP – Actin-binding protein

ADAM – A disintegrin and metalloproteinase

ANG1/2 – Angiopoietin 1/2

B16F0 – a Mouse melanoma cell line

BM – Basement membrane

BMDC – Bone-marrow-derived cell

bp – Base pairs

BSA – Bovine serum albumin

C-terminal – Carboxy-terminal

CDK – Cyclin dependent kinase

CMT19T – a Mouse lung carcinoma cell line

Co-IP – Co-immunoprecipitation

COL – Collagen

CSC – Cancer stem cell

DAPI – 4',6-diamidino-2-phenylindole

DLL4 – Delta-like-ligand 4

DMEM – Dulbecco's modified eagle medium

DPP – 1,4-di-[30-(20-pyridyldithio)-propionamido] butane

DSP – Dithiobis(succinimidyl propionate)

DTT – Dithiothereitol

E – Embryonic day

EC – Endothelial cell

ECM – Extracellular matrix

ECS – EC sorting

EDTA – Ethylenediaminetetraacetic acid

EGF – Epidermal growth factor

EMT – Epithelial-to-mesenchymal transition

EPC – Endothelial progenitor cell

ERK – Extracellular signal-regulated protein kinase

ESB – Electrophoresis sample buffer

f-actin – filamentous actin

FA – Focal adhesion

FAK – Focal adhesion kinase

FBS – Fetal bovine serum

FGF – Fibroblast growth factor

FilGAP – Filamin A-associated Rho GAP

Flk1 – Fetal liver kinase-1 (mouse isoform of VEGFR2)

Flt1 – FMS-like tyrosine kinase (pseudonym for VEGFR1)

FN – Fibronectin

GAP – GTPase activating protein

GEF – Guanine nucleotide exchange factor

GIPC1 – GAIP-interacting protein (synectin)

GN – Gelatin

H&E – Hematoxylin and eosin

HBSS – Hank's Balanced Salt Solution

HDMEC – Human dermal microvascular endothelial cell

HPSG – Heparan sulfate proteoglycan

HIF – Hypoxia-inducible factor

HRP – Horse-radish peroxidise

HUAEC – Human umbilical arterial endothelial cell

HUVEC – Human umbilical vein endothelial cell

ICAM – Intercellular adhesion molecule

ICC – Immunocytochemistry

Ig – Immunoglobulin

IGF – Insulin growth factor

IHC – Immunohistochemistry

ILK – Integrin-linked kinase

IMD – Integrin-mediated death

IP – Immunoprecipitation

KDR – Kinase domain receptor (VEGFR2)

LFQ – Label-free quantification

LIM – LIN-11, Isl1, and MEC- 3

LLC – Lewis lung carcinoma

LN – Laminin

MACS – Magnetic activated cell sorting

MAPK – Mitogen activated protein kinase

MMP – Matrix metalloproteinase

mTOR – Mammalian target of rapamycin

neo – Neomycin

NM-II – Non-muscle myosin II

(e)NOS – (endothelial) Nitric oxide synthase

NRP1/2 – Neuropilin-1/2

NRP1-EC-ID – Inducible depletion of neuropilin-1 in endothelial cells

NRP1Δcyto – Neuropilin-1 lacking its C-terminal domain

o/n – overnight

OHT – 4-hydroxy-tamoxifen

p – phosphorylated

p130Cas – p130 CRK-associated substrate

PAE – Porcine aortic endothelial cell

PAI – Plasminogen activator inhibitor

PBS – Phosphate buffered saline

PBSTw – Phosphate buffered saline supplemented with Tween-20

PDGF – Platelet-derived growth factor

PDGFR – Platelet-derived growth factor receptor

PDZ – PSD-95/Dlg/ZO-1

PFA – Paraformaldehyde

PH – Pleckstrin homology

PHD – Prolyl hydroxylase domain

$PIP_{2/3}$ – Phosphatidylinositol bis/trisphosphate

PLCγ – Phospholipase C-gamma

PlGF – Placental growth factor

PMSF – Phenylmethanesulfonylfluoride

pMT – Polyoma middle T-antigen

PXN – Paxillin

RIAM – Rap1-interacting adapter molecule

RT – Room temperature

s – soluble

S1P – Sphingosine-1-phosphate

SBS – Soerensen's buffer

SDF-1 – Stromal cell-derived factor 1 (CXCL12)

SDS – Sodium dodecyl sulphate

SDS-PAGE – Sodium dodecyl sulphate polyacrylamide gel electrophoresis

SFKs – SRC family kinases

SH2/3 – SRC homology domain 2/3

SPK – Sphingosine kinase

TAE – Buffer containing Tris base, acetic acid, and EDTA

TAF – Tumour-associated fibroblast

TAM – Tumour-associated macrophage

TE – Tris-EDTA

TCEP – Tris-(2-carboxyethyl)phosphine

TGFβ – Transforming growth factor-beta

TIMP – Tissue inhibitor of metalloproteinases

TM – Transmembrane

VCAM – Vascular cell adhesion molecule

VEGF – Vascular endothelial growth factor (-A unless otherwise stated)

VEGFs – vascular endothelial growth factors

VEGFR1/2/3 – Vascular Endothelial Growth Factor Receptor 1/2/3

VN – Vitronectin

vSMC – Vascular Smooth muscle cell

vWF – von Willebrand factor

WB – Western blot

WT – Wild-type

Y – Tyrosine

References

1. **Pugsley MK, Tabrizchi R.** The vascular system. An overview of structure and function. *J Pharmacol Toxicol Methods*. 2000; 44: 333-40.
2. **Cleaver O, Melton DA.** Endothelial signaling during development. *Nat Med*. 2003; 9: 661-8.
3. **Young B, O'Dowd G, Woodford P.** Wheater's Functional Histology 6e. *Churchill Livingstone, Elsevir Ltd*. 2013.
4. **Garlanda C, Dejana E.** Heterogeneity of endothelial cells. Specific markers. *Arterioscler Thromb Vasc Biol*. 1997; 17: 1193-202.
5. **Aird WC.** Phenotypic heterogeneity of the endothelium: II. Representative vascular beds. *Circ Res*. 2007; 100: 174-90.
6. **Aird WC.** Phenotypic heterogeneity of the endothelium: I. Structure, function, and mechanisms. *Circ Res*. 2007; 100: 158-73.
7. **Aird WC.** Endothelial cell heterogeneity. *Cold Spring Harb Perspect Med*. 2012; 2: a006429.
8. **Favero G, Paganelli C, Buffoli B, Rodella LF, Rezzani R.** Endothelium and its alterations in cardiovascular diseases: life style intervention. *Biomed Res Int*. 2014; 2014: 801896.
9. **Thorin E, Shreeve SM.** Heterogeneity of vascular endothelial cells in normal and disease states. *Pharmacol Ther*. 1998; 78: 155-66.
10. **Carmeliet P, Jain RK.** Principles and mechanisms of vessel normalization for cancer and other angiogenic diseases. *Nat Rev Drug Discov*. 2011; 10: 417-27.
11. **Bazzoni G, Dejana E.** Endothelial cell-to-cell junctions: molecular organization and role in vascular homeostasis. *Physiol Rev*. 2004; 84: 869-901.
12. **Dejana E.** Endothelial cell-cell junctions: happy together. *Nat Rev Mol Cell Biol*. 2004; 5: 261-70.
13. **Rajendran P, Rengarajan T, Thangavel J, Nishigaki Y, Sakthisekaran D, Sethi G, Nishigaki I.** The vascular endothelium and human diseases. *Int J Biol Sci*. 2013; 9: 1057-69.
14. **Iivanainen E, Kahari VM, Heino J, Elenius K.** Endothelial cell-matrix interactions. *Microsc Res Tech*. 2003; 60: 13-22.
15. **Stratman AN, Davis GE.** Endothelial cell-pericyte interactions stimulate basement membrane matrix assembly: influence on vascular tube remodeling, maturation, and stabilization. *Microsc Microanal*. 2012; 18: 68-80.
16. **Senger DR, Davis GE.** Angiogenesis. *Cold Spring Harb Perspect Biol*. 2011; 3: a005090.
17. **Carmeliet P.** Angiogenesis in health and disease. *Nat Med*. 2003; 9: 653-60.
18. **Geevarghese A, Herman IM.** Pericyte-endothelial crosstalk: implications and opportunities for advanced cellular therapies. *Transl Res*. 2014; 163: 296-306.
19. **Gerhardt H, Betsholtz C.** Endothelial-pericyte interactions in angiogenesis. *Cell Tissue Res*. 2003; 314: 15-23.
20. **Sims DE.** The pericyte--a review. *Tissue Cell*. 1986; 18: 153-74.
21. **Armulik A, Abramsson A, Betsholtz C.** Endothelial/pericyte interactions. *Circ Res*. 2005; 97: 512-23.
22. **Chung AS, Ferrara N.** Developmental and pathological angiogenesis. *Annu Rev Cell Dev Biol*. 2011; 27: 563-84.
23. **Carmeliet P, Jain RK.** Angiogenesis in cancer and other diseases. *Nature*. 2000; 407: 249-57.
24. **Carmeliet P, Jain RK.** Molecular mechanisms and clinical applications of angiogenesis. *Nature*. 2011; 473: 298-307.
25. **Carmeliet P.** Mechanisms of angiogenesis and arteriogenesis. *Nat Med*. 2000; 6: 389-95.
26. **Jain RK.** Molecular regulation of vessel maturation. *Nat Med*. 2003; 9: 685-93.
27. **Plein A, Fantin A, Ruhrberg C.** Neuropilin regulation of angiogenesis, arteriogenesis, and vascular permeability. *Microcirculation*. 2014; 21: 315-23.
28. **Nussenbaum F, Herman IM.** Tumor angiogenesis: insights and innovations. *J Oncol*. 2010; 2010: 132641.
29. **Potente M, Gerhardt H, Carmeliet P.** Basic and therapeutic aspects of angiogenesis. *Cell*. 2011; 146: 873-87.
30. **Pugh CW, Ratcliffe PJ.** Regulation of angiogenesis by hypoxia: role of the HIF system. *Nat Med*. 2003; 9: 677-84.
31. **Eilken HM, Adams RH.** Dynamics of endothelial cell behavior in sprouting angiogenesis. *Curr Opin Cell Biol*. 2010; 22: 617-25.

32. **Gavard J, Gutkind JS.** VEGF controls endothelial-cell permeability by promoting the beta-arrestin-dependent endocytosis of VE-cadherin. *Nat Cell Biol*. 2006; 8: 1223-34.
33. **Dejana E, Tournier-Lasserve E, Weinstein BM.** The control of vascular integrity by endothelial cell junctions: molecular basis and pathological implications. *Dev Cell*. 2009; 16: 209-21.
34. **Vestweber D.** VE-cadherin: the major endothelial adhesion molecule controlling cellular junctions and blood vessel formation. *Arterioscler Thromb Vasc Biol*. 2008; 28: 223-32.
35. **Gerhardt H, Golding M, Fruttiger M, Ruhrberg C, Lundkvist A, Abramsson A, Jeltsch M, Mitchell C, Alitalo K, Shima D, Betsholtz C.** VEGF guides angiogenic sprouting utilizing endothelial tip cell filopodia. *J Cell Biol*. 2003; 161: 1163-77.
36. **Geudens I, Gerhardt H.** Coordinating cell behaviour during blood vessel formation. *Development*. 2011; 138: 4569-83.
37. **Phng LK, Gerhardt H.** Angiogenesis: a team effort coordinated by notch. *Dev Cell*. 2009; 16: 196-208.
38. **Welti J, Loges S, Dimmeler S, Carmeliet P.** Recent molecular discoveries in angiogenesis and antiangiogenic therapies in cancer. *J Clin Invest*. 2013; 123: 3190-200.
39. **Benedito R, Rocha SF, Woeste M, Zamykal M, Radtke F, Casanovas O, Duarte A, Pytowski B, Adams RH.** Notch-dependent VEGFR3 upregulation allows angiogenesis without VEGF-VEGFR2 signalling. *Nature*. 2012; 484: 110-4.
40. **Jakobsson L, Franco CA, Bentley K, Collins RT, Ponsioen B, Aspalter IM, Rosewell I, Busse M, Thurston G, Medvinsky A, Schulte-Merker S, Gerhardt H.** Endothelial cells dynamically compete for the tip cell position during angiogenic sprouting. *Nat Cell Biol*. 2010; 12: 943-53.
41. **Benedito R, Roca C, Sorensen I, Adams S, Gossler A, Fruttiger M, Adams RH.** The notch ligands Dll4 and Jagged1 have opposing effects on angiogenesis. *Cell*. 2009; 137: 1124-35.
42. **Fantin A, Vieira JM, Gestri G, Denti L, Schwarz Q, Prykhozhij S, Peri F, Wilson SW, Ruhrberg C.** Tissue macrophages act as cellular chaperones for vascular anastomosis downstream of VEGF-mediated endothelial tip cell induction. *Blood*. 2010; 116: 829-40.
43. **Holderfield MT, Hughes CC.** Crosstalk between vascular endothelial growth factor, notch, and transforming growth factor-beta in vascular morphogenesis. *Circ Res*. 2008; 102: 637-52.
44. **Goumans MJ, Valdimarsdottir G, Itoh S, Rosendahl A, Sideras P, ten Dijke P.** Balancing the activation state of the endothelium via two distinct TGF-beta type I receptors. *EMBO J*. 2002; 21: 1743-53.
45. **Gaengel K, Genove G, Armulik A, Betsholtz C.** Endothelial-mural cell signaling in vascular development and angiogenesis. *Arterioscler Thromb Vasc Biol*. 2009; 29: 630-8.
46. **Hellberg C, Ostman A, Heldin CH.** PDGF and vessel maturation. *Recent Results Cancer Res*. 2010; 180: 103-14.
47. **Augustin HG, Koh GY, Thurston G, Alitalo K.** Control of vascular morphogenesis and homeostasis through the angiopoietin-Tie system. *Nat Rev Mol Cell Biol*. 2009; 10: 165-77.
48. **McGuire PG, Rangasamy S, Maestas J, Das A.** Pericyte-derived sphingosine 1-phosphate induces the expression of adhesion proteins and modulates the retinal endothelial cell barrier. *Arterioscler Thromb Vasc Biol*. 2011; 31: e107-15.
49. **Gaengel K, Niaudet C, Hagikura K, Lavina B, Muhl L, Hofmann JJ, Ebarasi L, Nystrom S, Rymo S, Chen LL, Pang MF, Jin Y, Raschperger E, Roswall P, Schulte D, Benedito R, Larsson J, Hellstrom M, Fuxe J, Uhlen P, Adams R, Jakobsson L, Majumdar A, Vestweber D, Uv A, Betsholtz C.** The sphingosine-1-phosphate receptor S1PR1 restricts sprouting angiogenesis by regulating the interplay between VE-cadherin and VEGFR2. *Dev Cell*. 2012; 23: 587-99.
50. **Mosch B, Reissenweber B, Neuber C, Pietzsch J.** Eph receptors and ephrin ligands: important players in angiogenesis and tumor angiogenesis. *J Oncol*. 2010; 2010: 135285.
51. **Birdsey GM, Shah AV, Dufton N, Reynolds LE, Osuna Almagro L, Yang Y, Aspalter IM, Khan ST, Mason JC, Dejana E, Gottgens B, Hodivala-Dilke K, Gerhardt H, Adams RH, Randi AM.** The endothelial transcription factor ERG promotes vascular stability and growth through Wnt/beta-catenin signaling. *Dev Cell*. 2015; 32: 82-96.
52. **Yamamoto H, Ehling M, Kato K, Kanai K, van Lessen M, Frye M, Zeuschner D, Nakayama M, Vestweber D, Adams RH.** Integrin beta1 controls VE-cadherin localization and blood vessel stability. *Nat Commun*. 2015; 6: 6429.
53. **Roy H, Bhardwaj S, Yla-Herttuala S.** Biology of vascular endothelial growth factors. *FEBS Lett*. 2006; 580: 2879-87.

54. **Shibuya M.** Vascular endothelial growth factor and its receptor system: physiological functions in angiogenesis and pathological roles in various diseases. *J Biochem*. 2013; 153: 13-9.
55. **Cebe-Suarez S, Zehnder-Fjallman A, Ballmer-Hofer K.** The role of VEGF receptors in angiogenesis; complex partnerships. *Cell Mol Life Sci*. 2006; 63: 601-15.
56. **Tammela T, Enholm B, Alitalo K, Paavonen K.** The biology of vascular endothelial growth factors. *Cardiovasc Res*. 2005; 65: 550-63.
57. **Kerbel RS.** Tumor angiogenesis. *N Engl J Med*. 2008; 358: 2039-49.
58. **Moens S, Goveia J, Stapor PC, Cantelmo AR, Carmeliet P.** The multifaceted activity of VEGF in angiogenesis - Implications for therapy responses. *Cytokine Growth Factor Rev*. 2014; 25: 473-82.
59. **Carmeliet P, Ferreira V, Breier G, Pollefeyt S, Kieckens L, Gertsenstein M, Fahrig M, Vandenhoeck A, Harpal K, Eberhardt C, Declercq C, Pawling J, Moons L, Collen D, Risau W, Nagy A.** Abnormal blood vessel development and lethality in embryos lacking a single VEGF allele. *Nature*. 1996; 380: 435-9.
60. **Ferrara N, Carver-Moore K, Chen H, Dowd M, Lu L, O'Shea KS, Powell-Braxton L, Hillan KJ, Moore MW.** Heterozygous embryonic lethality induced by targeted inactivation of the VEGF gene. *Nature*. 1996; 380: 439-42.
61. **Ferrara N, Gerber HP, LeCouter J.** The biology of VEGF and its receptors. *Nat Med*. 2003; 9: 669-76.
62. **Gerber HP, Dixit V, Ferrara N.** Vascular endothelial growth factor induces expression of the antiapoptotic proteins Bcl-2 and A1 in vascular endothelial cells. *J Biol Chem*. 1998; 273: 13313-6.
63. **Kroll J, Waltenberger J.** A novel function of VEGF receptor-2 (KDR): rapid release of nitric oxide in response to VEGF-A stimulation in endothelial cells. *Biochem Biophys Res Commun*. 1999; 265: 636-9.
64. **Chen TT, Luque A, Lee S, Anderson SM, Segura T, Iruela-Arispe ML.** Anchorage of VEGF to the extracellular matrix conveys differential signaling responses to endothelial cells. *J Cell Biol*. 2010; 188: 595-609.
65. **Koch S, Claesson-Welsh L.** Signal transduction by vascular endothelial growth factor receptors. *Cold Spring Harb Perspect Med*. 2012; 2: a006502.
66. **Ruhrberg C, Gerhardt H, Golding M, Watson R, Ioannidou S, Fujisawa H, Betsholtz C, Shima DT.** Spatially restricted patterning cues provided by heparin-binding VEGF-A control blood vessel branching morphogenesis. *Genes Dev*. 2002; 16: 2684-98.
67. **Keyt BA, Berleau LT, Nguyen HV, Chen H, Heinsohn H, Vandlen R, Ferrara N.** The carboxyl-terminal domain (111-165) of vascular endothelial growth factor is critical for its mitogenic potency. *J Biol Chem*. 1996; 271: 7788-95.
68. **Whitaker GB, Limberg BJ, Rosenbaum JS.** Vascular endothelial growth factor receptor-2 and neuropilin-1 form a receptor complex that is responsible for the differential signaling potency of VEGF(165) and VEGF(121). *J Biol Chem*. 2001; 276: 25520-31.
69. **Zachary I.** Neuropilins: role in signalling, angiogenesis and disease. *Chem Immunol Allergy*. 2014; 99: 37-70.
70. **Harper SJ, Bates DO.** VEGF-A splicing: the key to anti-angiogenic therapeutics? *Nat Rev Cancer*. 2008; 8: 880-7.
71. **Lee S, Chen TT, Barber CL, Jordan MC, Murdock J, Desai S, Ferrara N, Nagy A, Roos KP, Iruela-Arispe ML.** Autocrine VEGF signaling is required for vascular homeostasis. *Cell*. 2007; 130: 691-703.
72. **Meadows KN, Bryant P, Pumiglia K.** Vascular endothelial growth factor induction of the angiogenic phenotype requires Ras activation. *J Biol Chem*. 2001; 276: 49289-98.
73. **Shu X, Wu W, Mosteller RD, Broek D.** Sphingosine kinase mediates vascular endothelial growth factor-induced activation of ras and mitogen-activated protein kinases. *Mol Cell Biol*. 2002; 22: 7758-68.
74. **Takahashi T, Ueno H, Shibuya M.** VEGF activates protein kinase C-dependent, but Ras-independent Raf-MEK-MAP kinase pathway for DNA synthesis in primary endothelial cells. *Oncogene*. 1999; 18: 2221-30.
75. **Holmqvist K, Cross MJ, Rolny C, Hagerkvist R, Rahimi N, Matsumoto T, Claesson-Welsh L, Welsh M.** The adaptor protein shb binds to tyrosine 1175 in vascular endothelial growth factor (VEGF) receptor-2 and regulates VEGF-dependent cellular migration. *J Biol Chem*. 2004; 279: 22267-75.
76. **Holmqvist K, Cross M, Riley D, Welsh M.** The Shb adaptor protein causes Src-dependent cell spreading and activation of focal adhesion kinase in murine brain endothelial cells. *Cell Signal*. 2003; 15: 171-9.

77. **Laramee M, Chabot C, Cloutier M, Stenne R, Holgado-Madruga M, Wong AJ, Royal I.** The scaffolding adapter Gab1 mediates vascular endothelial growth factor signaling and is required for endothelial cell migration and capillary formation. *J Biol Chem*. 2007; 282: 7758-69.
78. **Lamalice L, Houle F, Huot J.** Phosphorylation of Tyr1214 within VEGFR-2 triggers the recruitment of Nck and activation of Fyn leading to SAPK2/p38 activation and endothelial cell migration in response to VEGF. *J Biol Chem*. 2006; 281: 34009-20.
79. **Wallez Y, Cand F, Cruzalegui F, Wernstedt C, Souchelnytskyi S, Vilgrain I, Huber P.** Src kinase phosphorylates vascular endothelial-cadherin in response to vascular endothelial growth factor: identification of tyrosine 685 as the unique target site. *Oncogene*. 2007; 26: 1067-77.
80. **Ballmer-Hofer K, Andersson AE, Ratcliffe LE, Berger P.** Neuropilin-1 promotes VEGFR-2 trafficking through Rab11 vesicles thereby specifying signal output. *Blood*. 2011; 118: 816-26.
81. **Jopling HM, Odell AF, Hooper NM, Zachary IC, Walker JH, Ponnambalam S.** Rab GTPase regulation of VEGFR2 trafficking and signaling in endothelial cells. *Arterioscler Thromb Vasc Biol*. 2009; 29: 1119-24.
82. **Lanahan AA, Hermans K, Claes F, Kerley-Hamilton JS, Zhuang ZW, Giordano FJ, Carmeliet P, Simons M.** VEGF receptor 2 endocytic trafficking regulates arterial morphogenesis. *Dev Cell*. 2010; 18: 713-24.
83. **Berger P, Ballmer-Hofer K.** The reception and the party after: how vascular endothelial growth factor receptor 2 explores cytoplasmic space. *Swiss Med Wkly*. 2011; 141: w13318.
84. **Horowitz A, Seerapu HR.** Regulation of VEGF signaling by membrane traffic. *Cell Signal*. 2012; 24: 1810-20.
85. **Eichmann A, Simons M.** VEGF signaling inside vascular endothelial cells and beyond. *Curr Opin Cell Biol*. 2012; 24: 188-93.
86. **Gourlaouen M, Welti JC, Vasudev NS, Reynolds AR.** Essential Role for Endocytosis in the Growth Factor-stimulated Activation of ERK1/2 in Endothelial Cells. *J Biol Chem*. 2013; 288: 7467-80.
87. **Nakayama M, Nakayama A, van Lessen M, Yamamoto H, Hoffmann S, Drexler HC, Itoh N, Hirose T, Breier G, Vestweber D, Cooper JA, Ohno S, Kaibuchi K, Adams RH.** Spatial regulation of VEGF receptor endocytosis in angiogenesis. *Nat Cell Biol*. 2013; 15: 249-60.
88. **Gampel A, Moss L, Jones MC, Brunton V, Norman JC, Mellor H.** VEGF regulates the mobilization of VEGFR2/KDR from an intracellular endothelial storage compartment. *Blood*. 2006; 108: 2624-31.
89. **Lampugnani MG, Orsenigo F, Gagliani MC, Tacchetti C, Dejana E.** Vascular endothelial cadherin controls VEGFR-2 internalization and signaling from intracellular compartments. *J Cell Biol*. 2006; 174: 593-604.
90. **Sawamiphak S, Seidel S, Essmann CL, Wilkinson GA, Pitulescu ME, Acker T, Acker-Palmer A.** Ephrin-B2 regulates VEGFR2 function in developmental and tumour angiogenesis. *Nature*. 2010; 465: 487-91.
91. **Nakayama M, Berger P.** Coordination of VEGF receptor trafficking and signaling by coreceptors. *Exp Cell Res*. 2013; 319: 1340-7.
92. **Hanahan D, Weinberg RA.** The hallmarks of cancer. *Cell*. 2000; 100: 57-70.
93. **Hanahan D, Weinberg RA.** Hallmarks of cancer: the next generation. *Cell*. 2011; 144: 646-74.
94. **Folkman J.** Role of angiogenesis in tumor growth and metastasis. *Semin Oncol*. 2002; 29: 15-8.
95. **Folkman J.** Tumor angiogenesis: therapeutic implications. *N Engl J Med*. 1971; 285: 1182-6.
96. **Folkman J, Hanahan D.** Switch to the angiogenic phenotype during tumorigenesis. *Princess Takamatsu Symp*. 1991; 22: 339-47.
97. **Weis SM, Cheresh DA.** Tumor angiogenesis: molecular pathways and therapeutic targets. *Nat Med*. 2011; 17: 1359-70.
98. **Weis SM, Cheresh DA.** Pathophysiological consequences of VEGF-induced vascular permeability. *Nature*. 2005; 437: 497-504.
99. **Franco OE, Shaw AK, Strand DW, Hayward SW.** Cancer associated fibroblasts in cancer pathogenesis. *Semin Cell Dev Biol*. 2010; 21: 33-9.
100. **Maniotis AJ, Folberg R, Hess A, Seftor EA, Gardner LM, Pe'er J, Trent JM, Meltzer PS, Hendrix MJ.** Vascular channel formation by human melanoma cells in vivo and in vitro: vasculogenic mimicry. *Am J Pathol*. 1999; 155: 739-52.
101. **Claesson-Welsh L, Welsh M.** VEGFA and tumour angiogenesis. *J Intern Med*. 2013; 273: 114-27.

102. **Bentley K, Franco CA, Philippides A, Blanco R, Dierkes M, Gebala V, Stanchi F, Jones M, Aspalter IM, Cagna G, Westrom S, Claesson-Welsh L, Vestweber D, Gerhardt H.** The role of differential VE-cadherin dynamics in cell rearrangement during angiogenesis. *Nat Cell Biol*. 2014; 16: 309-21.
103. **De Bock K, Georgiadou M, Schoors S, Kuchnio A, Wong BW, Cantelmo AR, Quaegebeur A, Ghesquiere B, Cauwenberghs S, Eelen G, Phng LK, Betz I, Tembuyser B, Brepoels K, Welti J, Geudens I, Segura I, Cruys B, Bifari F, Decimo I, Blanco R, Wyns S, Vangindertael J, Rocha S, Collins RT, Munck S, Daelemans D, Imamura H, Devlieger R, Rider M, Van Veldhoven PP, Schuit F, Bartrons R, Hofkens J, Fraisl P, Telang S, Deberardinis RJ, Schoonjans L, Vinckier S, Chesney J, Gerhardt H, Dewerchin M, Carmeliet P.** Role of PFKFB3-driven glycolysis in vessel sprouting. *Cell*. 2013; 154: 651-63.
104. **Goveia J, Stapor P, Carmeliet P.** Principles of targeting endothelial cell metabolism to treat angiogenesis and endothelial cell dysfunction in disease. *EMBO Mol Med*. 2014; 6: 1105-20.
105. **Xu Y, An X, Guo X, Habtetsion TG, Wang Y, Xu X, Kandala S, Li Q, Li H, Zhang C, Caldwell RB, Fulton DJ, Su Y, Hoda MN, Zhou G, Wu C, Huo Y.** Endothelial PFKFB3 plays a critical role in angiogenesis. *Arterioscler Thromb Vasc Biol*. 2014; 34: 1231-9.
106. **Armulik A, Genove G, Betsholtz C.** Pericytes: developmental, physiological, and pathological perspectives, problems, and promises. *Dev Cell*. 2011; 21: 193-215.
107. **Nasarre P, Thomas M, Kruse K, Helfrich I, Wolter V, Deppermann C, Schadendorf D, Thurston G, Fiedler U, Augustin HG.** Host-derived angiopoietin-2 affects early stages of tumor development and vessel maturation but is dispensable for later stages of tumor growth. *Cancer Res*. 2009; 69: 1324-33.
108. **Banerjee S, Mehta S, Haque I, Sengupta K, Dhar K, Kambhampati S, Van Veldhuizen PJ, Banerjee SK.** VEGF-A165 induces human aortic smooth muscle cell migration by activating neuropilin-1-VEGFR1-PI3K axis. *Biochemistry*. 2008; 47: 3345-51.
109. **Gerhardt H, Semb H.** Pericytes: gatekeepers in tumour cell metastasis? *J Mol Med (Berl)*. 2008; 86: 135-44.
110. **Ziyad S, Iruela-Arispe ML.** Molecular mechanisms of tumor angiogenesis. *Genes Cancer*. 2011; 2: 1085-96.
111. **Orimo A, Gupta PB, Sgroi DC, Arenzana-Seisdedos F, Delaunay T, Naeem R, Carey VJ, Richardson AL, Weinberg RA.** Stromal fibroblasts present in invasive human breast carcinomas promote tumor growth and angiogenesis through elevated SDF-1/CXCL12 secretion. *Cell*. 2005; 121: 335-48.
112. **Grunewald M, Avraham I, Dor Y, Bachar-Lustig E, Itin A, Jung S, Chimenti S, Landsman L, Abramovitch R, Keshet E.** VEGF-induced adult neovascularization: recruitment, retention, and role of accessory cells. *Cell*. 2006; 124: 175-89.
113. **Lyden D, Hattori K, Dias S, Costa C, Blaikie P, Butros L, Chadburn A, Heissig B, Marks W, Witte L, Wu Y, Hicklin D, Zhu Z, Hackett NR, Crystal RG, Moore MA, Hajjar KA, Manova K, Benezra R, Rafii S.** Impaired recruitment of bone-marrow-derived endothelial and hematopoietic precursor cells blocks tumor angiogenesis and growth. *Nat Med*. 2001; 7: 1194-201.
114. **Rolny C, Mazzone M, Tugues S, Laoui D, Johansson I, Coulon C, Squadrito ML, Segura I, Li X, Knevels E, Costa S, Vinckier S, Dresselaer T, Akerud P, De Mol M, Salomaki H, Phillipson M, Wyns S, Larsson E, Buysschaert I, Botling J, Himmelreich U, Van Ginderachter JA, De Palma M, Dewerchin M, Claesson-Welsh L, Carmeliet P.** HRG inhibits tumor growth and metastasis by inducing macrophage polarization and vessel normalization through downregulation of PlGF. *Cancer Cell*. 2011; 19: 31-44.
115. **Dvorak HF.** Tumors: wounds that do not heal. Similarities between tumor stroma generation and wound healing. *N Engl J Med*. 1986; 315: 1650-9.
116. **Steeg PS.** Tumor metastasis: mechanistic insights and clinical challenges. *Nat Med*. 2006; 12: 895-904.
117. **S. P.** The distribution of secondary growths in cancer of the breast. *Lancet*. 1889; 1: 571–3.
118. **Santamaria-Martinez A, Huelsken J.** The niche under siege: novel targets for metastasis therapy. *J Intern Med*. 2013; 274: 127-36.
119. **Kaplan RN, Riba RD, Zacharoulis S, Bramley AH, Vincent L, Costa C, MacDonald DD, Jin DK, Shido K, Kerns SA, Zhu Z, Hicklin D, Wu Y, Port JL, Altorki N, Port ER, Ruggero D, Shmelkov SV, Jensen KK, Rafii S, Lyden D.** VEGFR1-positive haematopoietic bone marrow progenitors initiate the pre-metastatic niche. *Nature*. 2005; 438: 820-7.
120. **Ebos JM, Kerbel RS.** Antiangiogenic therapy: impact on invasion, disease progression, and metastasis. *Nat Rev Clin Oncol*. 2011; 8: 210-21.

121. **Sennino B, McDonald DM.** Controlling escape from angiogenesis inhibitors. *Nat Rev Cancer*. 2012; 12: 699-709.
122. **Vasudev NS, Reynolds AR.** Anti-angiogenic therapy for cancer: current progress, unresolved questions and future directions. *Angiogenesis*. 2014; 17: 471-94.
123. **De Falco S.** Antiangiogenesis therapy: an update after the first decade. *Korean J Intern Med*. 2014; 29: 1-11.
124. **Tugues S, Koch S, Gualandi L, Li X, Claesson-Welsh L.** Vascular endothelial growth factors and receptors: anti-angiogenic therapy in the treatment of cancer. *Mol Aspects Med*. 2011; 32: 88-111.
125. **Bergers G, Hanahan D.** Modes of resistance to anti-angiogenic therapy. *Nat Rev Cancer*. 2008; 8: 592-603.
126. **Sitohy B, Nagy JA, Dvorak HF.** Anti-VEGF/VEGFR therapy for cancer: reassessing the target. *Cancer Res*. 2012; 72: 1909-14.
127. **Kadenhe-Chiweshe A, Papa J, McCrudden KW, Frischer J, Bae JO, Huang J, Fisher J, Lefkowitch JH, Feirt N, Rudge J, Holash J, Yancopoulos GD, Kandel JJ, Yamashiro DJ.** Sustained VEGF blockade results in microenvironmental sequestration of VEGF by tumors and persistent VEGF receptor-2 activation. *Mol Cancer Res*. 2008; 6: 1-9.
128. **Van Cutsem E, de Haas S, Kang YK, Ohtsu A, Tebbutt NC, Ming Xu J, Peng Yong W, Langer B, Delmar P, Scherer SJ, Shah MA.** Bevacizumab in combination with chemotherapy as first-line therapy in advanced gastric cancer: a biomarker evaluation from the AVAGAST randomized phase III trial. *J Clin Oncol*. 2012; 30: 2119-27.
129. **Allen E, Walters IB, Hanahan D.** Brivanib, a dual FGF/VEGF inhibitor, is active both first and second line against mouse pancreatic neuroendocrine tumors developing adaptive/evasive resistance to VEGF inhibition. *Clin Cancer Res*. 2011; 17: 5299-310.
130. **Bergers G, Song S, Meyer-Morse N, Bergsland E, Hanahan D.** Benefits of targeting both pericytes and endothelial cells in the tumor vasculature with kinase inhibitors. *J Clin Invest*. 2003; 111: 1287-95.
131. **Casanovas O, Hicklin DJ, Bergers G, Hanahan D.** Drug resistance by evasion of antiangiogenic targeting of VEGF signaling in late-stage pancreatic islet tumors. *Cancer Cell*. 2005; 8: 299-309.
132. **Li JL, Sainson RC, Oon CE, Turley H, Leek R, Sheldon H, Bridges E, Shi W, Snell C, Bowden ET, Wu H, Chowdhury PS, Russell AJ, Montgomery CP, Poulsom R, Harris AL.** DLL4-Notch signaling mediates tumor resistance to anti-VEGF therapy in vivo. *Cancer Res*. 2011; 71: 6073-83.
133. **Pan Q, Chanthery Y, Liang WC, Stawicki S, Mak J, Rathore N, Tong RK, Kowalski J, Yee SF, Pacheco G, Ross S, Cheng Z, Le Couter J, Plowman G, Peale F, Koch AW, Wu Y, Bagri A, Tessier-Lavigne M, Watts RJ.** Blocking neuropilin-1 function has an additive effect with anti-VEGF to inhibit tumor growth. *Cancer Cell*. 2007; 11: 53-67.
134. **Reynolds AR, Reynolds LE, Nagel TE, Lively JC, Robinson SD, Hicklin DJ, Bodary SC, Hodivala-Dilke KM.** Elevated Flk1 (vascular endothelial growth factor receptor 2) signaling mediates enhanced angiogenesis in beta3-integrin-deficient mice. *Cancer Res*. 2004; 64: 8643-50.
135. **Rigamonti N, Kadioglu E, Keklikoglou I, Wyser Rmili C, Leow CC, De Palma M.** Role of angiopoietin-2 in adaptive tumor resistance to VEGF signaling blockade. *Cell Rep*. 2014; 8: 696-706.
136. **Jain RK.** Normalizing tumor vasculature with anti-angiogenic therapy: a new paradigm for combination therapy. *Nat Med*. 2001; 7: 987-9.
137. **Avraamides CJ, Garmy-Susini B, Varner JA.** Integrins in angiogenesis and lymphangiogenesis. *Nat Rev Cancer*. 2008; 8: 604-17.
138. **Plow EF, Meller J, Byzova TV.** Integrin function in vascular biology: a view from 2013. *Curr Opin Hematol*. 2014; 21: 241-7.
139. **Desgrosellier JS, Cheresh DA.** Integrins in cancer: biological implications and therapeutic opportunities. *Nat Rev Cancer*. 2010; 10: 9-22.
140. **Humphries JD, Byron A, Humphries MJ.** Integrin ligands at a glance. *J Cell Sci*. 2006; 119: 3901-3.
141. **Hynes RO.** Integrins: bidirectional, allosteric signaling machines. *Cell*. 2002; 110: 673-87.
142. **Plow EF, Haas TA, Zhang L, Loftus J, Smith JW.** Ligand binding to integrins. *J Biol Chem*. 2000; 275: 21785-8.
143. **Seguin L, Desgrosellier JS, Weis SM, Cheresh DA.** Integrins and cancer: regulators of cancer stemness, metastasis, and drug resistance. *Trends Cell Biol*. 2015; 25: 234-40.
144. **Stupack DG, Puente XS, Boutsaboualoy S, Storgard CM, Cheresh DA.** Apoptosis of adherent cells by recruitment of caspase-8 to unligated integrins. *J Cell Biol*. 2001; 155: 459-70.

145. **Schiller HB, Fassler R.** Mechanosensitivity and compositional dynamics of cell-matrix adhesions. *EMBO Rep*. 2013; 14: 509-19.
146. **Weis SM, Cheresh DA.** alphaV integrins in angiogenesis and cancer. *Cold Spring Harb Perspect Med*. 2011; 1: a006478.
147. **Desgrosellier JS, Barnes LA, Shields DJ, Huang M, Lau SK, Prevost N, Tarin D, Shattil SJ, Cheresh DA.** An integrin alpha(v)beta(3)-c-Src oncogenic unit promotes anchorage-independence and tumor progression. *Nat Med*. 2009; 15: 1163-9.
148. **Stupack DG, Teitz T, Potter MD, Mikolon D, Houghton PJ, Kidd VJ, Lahti JM, Cheresh DA.** Potentiation of neuroblastoma metastasis by loss of caspase-8. *Nature*. 2006; 439: 95-9.
149. **Fournier AK, Campbell LE, Castagnino P, Liu WF, Chung BM, Weaver VM, Chen CS, Assoian RK.** Rac-dependent cyclin D1 gene expression regulated by cadherin- and integrin-mediated adhesion. *J Cell Sci*. 2008; 121: 226-33.
150. **Vellon L, Menendez JA, Lupu R.** AlphaVbeta3 integrin regulates heregulin (HRG)-induced cell proliferation and survival in breast cancer. *Oncogene*. 2005; 24: 3759-73.
151. **Wang W, Luo BH.** Structural basis of integrin transmembrane activation. *J Cell Biochem*. 2010; 109: 447-52.
152. **Campbell ID, Humphries MJ.** Integrin structure, activation, and interactions. *Cold Spring Harb Perspect Biol*. 2011; 3.
153. **Hu P, Luo BH.** Integrin bi-directional signaling across the plasma membrane. *J Cell Physiol*. 2013; 228: 306-12.
154. **Harburger DS, Bouaouina M, Calderwood DA.** Kindlin-1 and -2 directly bind the C-terminal region of beta integrin cytoplasmic tails and exert integrin-specific activation effects. *J Biol Chem*. 2009; 284: 11485-97.
155. **Byzova TV, Goldman CK, Pampori N, Thomas KA, Bett A, Shattil SJ, Plow EF.** A mechanism for modulation of cellular responses to VEGF: activation of the integrins. *Mol Cell*. 2000; 6: 851-60.
156. **Scales TM, Parsons M.** Spatial and temporal regulation of integrin signalling during cell migration. *Curr Opin Cell Biol*. 2011; 23: 562-8.
157. **Wolfenson H, Lavelin I, Geiger B.** Dynamic regulation of the structure and functions of integrin adhesions. *Dev Cell*. 2013; 24: 447-58.
158. **Zaidel-Bar R, Itzkovitz S, Ma'ayan A, Iyengar R, Geiger B.** Functional atlas of the integrin adhesome. *Nat Cell Biol*. 2007; 9: 858-67.
159. **Morse EM, Brahme NN, Calderwood DA.** Integrin cytoplasmic tail interactions. *Biochemistry*. 2014; 53: 810-20.
160. **Winograd-Katz SE, Fassler R, Geiger B, Legate KR.** The integrin adhesome: from genes and proteins to human disease. *Nat Rev Mol Cell Biol*. 2014; 15: 273-88.
161. **Kim SH, Turnbull J, Guimond S.** Extracellular matrix and cell signalling: the dynamic cooperation of integrin, proteoglycan and growth factor receptor. *J Endocrinol*. 2011; 209: 139-51.
162. **Sadok A, Marshall CJ.** Rho GTPases: masters of cell migration. *Small GTPases*. 2014; 5: e29710.
163. **Lawson CD, Burridge K.** The on-off relationship of Rho and Rac during integrin-mediated adhesion and cell migration. *Small GTPases*. 2014; 5: e27958.
164. **Humphries JD, Paul NR, Humphries MJ, Morgan MR.** Emerging properties of adhesion complexes: what are they and what do they do? *Trends Cell Biol*. 2015; 25: 388-97.
165. **De Franceschi N, Hamidi H, Alanko J, Sahgal P, Ivaska J.** Integrin traffic - the update. *J Cell Sci*. 2015; 128: 839-52.
166. **Contois L, Akalu A, Brooks PC.** Integrins as "functional hubs" in the regulation of pathological angiogenesis. *Semin Cancer Biol*. 2009; 19: 318-28.
167. **Hodivala-Dilke KM, Reynolds AR, Reynolds LE.** Integrins in angiogenesis: multitalented molecules in a balancing act. *Cell Tissue Res*. 2003; 314: 131-44.
168. **Brooks PC, Clark RA, Cheresh DA.** Requirement of vascular integrin alpha v beta 3 for angiogenesis. *Science*. 1994; 264: 569-71.
169. **Brooks PC, Stromblad S, Klemke R, Visscher D, Sarkar FH, Cheresh DA.** Antiintegrin alpha v beta 3 blocks human breast cancer growth and angiogenesis in human skin. *J Clin Invest*. 1995; 96: 1815-22.
170. **Drake CJ, Cheresh DA, Little CD.** An antagonist of integrin alpha v beta 3 prevents maturation of blood vessels during embryonic neovascularization. *J Cell Sci*. 1995; 108 (Pt 7): 2655-61.
171. **Friedlander M, Brooks PC, Shaffer RW, Kincaid CM, Varner JA, Cheresh DA.** Definition of two angiogenic pathways by distinct alpha v integrins. *Science*. 1995; 270: 1500-2.

172. **Friedlander M, Theesfeld CL, Sugita M, Fruttiger M, Thomas MA, Chang S, Cheresh DA.** Involvement of integrins alpha v beta 3 and alpha v beta 5 in ocular neovascular diseases. *Proc Natl Acad Sci U S A*. 1996; 93: 9764-9.
173. **Loges S, Butzal M, Otten J, Schweizer M, Fischer U, Bokemeyer C, Hossfeld DK, Schuch G, Fiedler W.** Cilengitide inhibits proliferation and differentiation of human endothelial progenitor cells in vitro. *Biochem Biophys Res Commun*. 2007; 357: 1016-20.
174. **Nisato RE, Tille JC, Jonczyk A, Goodman SL, Pepper MS.** alphav beta 3 and alphav beta 5 integrin antagonists inhibit angiogenesis in vitro. *Angiogenesis*. 2003; 6: 105-19.
175. **Buerkle MA, Pahernik SA, Sutter A, Jonczyk A, Messmer K, Dellian M.** Inhibition of the alpha-nu integrins with a cyclic RGD peptide impairs angiogenesis, growth and metastasis of solid tumours in vivo. *Br J Cancer*. 2002; 86: 788-95.
176. **Yamada S, Bu XY, Khankaldyyan V, Gonzales-Gomez I, McComb JG, Laug WE.** Effect of the angiogenesis inhibitor Cilengitide (EMD 121974) on glioblastoma growth in nude mice. *Neurosurgery*. 2006; 59: 1304-12; discussion 12.
177. **Stupp R, Ruegg C.** Integrin inhibitors reaching the clinic. *J Clin Oncol*. 2007; 25: 1637-8.
178. Merck: Phase III Trial of Cilengitide Did Not Meet Primary Endpoint in Patients With Newly Diagnosed Glioblastoma. 2013: http://www.merckgroup.com/en/media/extNewsDetail.html?newsId=BE2FE07AD630830EC1257B1D001F007B&newsType=1.
179. **Reardon DA, Fink KL, Mikkelsen T, Cloughesy TF, O'Neill A, Plotkin S, Glantz M, Ravin P, Raizer JJ, Rich KM, Schiff D, Shapiro WR, Burdette-Radoux S, Dropcho EJ, Wittemer SM, Nippgen J, Picard M, Nabors LB.** Randomized phase II study of cilengitide, an integrin-targeting arginine-glycine-aspartic acid peptide, in recurrent glioblastoma multiforme. *J Clin Oncol*. 2008; 26: 5610-7.
180. **Robinson SD, Hodivala-Dilke KM.** The role of beta3-integrins in tumor angiogenesis: context is everything. *Curr Opin Cell Biol*. 2011; 23: 630-7.
181. **Brooks PC, Montgomery AM, Rosenfeld M, Reisfeld RA, Hu T, Klier G, Cheresh DA.** Integrin alpha v beta 3 antagonists promote tumor regression by inducing apoptosis of angiogenic blood vessels. *Cell*. 1994; 79: 1157-64.
182. **Oliveira-Ferrer L, Hauschild J, Fiedler W, Bokemeyer C, Nippgen J, Celik I, Schuch G.** Cilengitide induces cellular detachment and apoptosis in endothelial and glioma cells mediated by inhibition of FAK/src/AKT pathway. *J Exp Clin Cancer Res*. 2008; 27: 86.
183. **Stromblad S, Becker JC, Yebra M, Brooks PC, Cheresh DA.** Suppression of p53 activity and p21WAF1/CIP1 expression by vascular cell integrin alphaVbeta3 during angiogenesis. *J Clin Invest*. 1996; 98: 426-33.
184. **Taga T, Suzuki A, Gonzalez-Gomez I, Gilles FH, Stins M, Shimada H, Barsky L, Weinberg KI, Laug WE.** alpha v-Integrin antagonist EMD 121974 induces apoptosis in brain tumor cells growing on vitronectin and tenascin. *Int J Cancer*. 2002; 98: 690-7.
185. **Mahabeleshwar GH, Chen J, Feng W, Somanath PR, Razorenova OV, Byzova TV.** Integrin affinity modulation in angiogenesis. *Cell Cycle*. 2008; 7: 335-47.
186. **Mahabeleshwar GH, Feng W, Phillips DR, Byzova TV.** Integrin signaling is critical for pathological angiogenesis. *J Exp Med*. 2006; 203: 2495-507.
187. **Mahabeleshwar GH, Feng W, Reddy K, Plow EF, Byzova TV.** Mechanisms of integrin-vascular endothelial growth factor receptor cross-activation in angiogenesis. *Circ Res*. 2007; 101: 570-80.
188. **Masson-Gadais B, Houle F, Laferriere J, Huot J.** Integrin alphavbeta3, requirement for VEGFR2-mediated activation of SAPK2/p38 and for Hsp90-dependent phosphorylation of focal adhesion kinase in endothelial cells activated by VEGF. *Cell Stress Chaperones*. 2003; 8: 37-52.
189. **Soldi R, Mitola S, Strasly M, Defilippi P, Tarone G, Bussolino F.** Role of alphavbeta3 integrin in the activation of vascular endothelial growth factor receptor-2. *EMBO J*. 1999; 18: 882-92.
190. **Somanath PR, Ciocea A, Byzova TV.** Integrin and growth factor receptor alliance in angiogenesis. *Cell Biochem Biophys*. 2009; 53: 53-64.
191. **West XZ, Meller N, Malinin NL, Deshmukh L, Meller J, Mahabeleshwar GH, Weber ME, Kerr BA, Vinogradova O, Byzova TV.** Integrin beta3 crosstalk with VEGFR accommodating tyrosine phosphorylation as a regulatory switch. *PLoS One*. 2012; 7: e31071.
192. **Gong Y, Yang X, He Q, Gower L, Prudovsky I, Vary CP, Brooks PC, Friesel RE.** Sprouty4 regulates endothelial cell migration via modulating integrin beta3 stability through c-Src. *Angiogenesis*. 2013; 16: 861-75.
193. **Ravelli C, Mitola S, Corsini M, Presta M.** Involvement of alphavbeta3 integrin in gremlin-induced angiogenesis. *Angiogenesis*. 2013; 16: 235-43.

194. **Strieth S, Eichhorn ME, Sutter A, Jonczyk A, Berghaus A, Dellian M.** Antiangiogenic combination tumor therapy blocking alpha(v)-integrins and VEGF-receptor-2 increases therapeutic effects in vivo. *Int J Cancer*. 2006; 119: 423-31.
195. **Papo N, Silverman AP, Lahti JL, Cochran JR.** Antagonistic VEGF variants engineered to simultaneously bind to and inhibit VEGFR2 and alphavbeta3 integrin. *Proc Natl Acad Sci U S A*. 2011; 108: 14067-72.
196. **Hodivala-Dilke KM, McHugh KP, Tsakiris DA, Rayburn H, Crowley D, Ullman-Cullere M, Ross FP, Coller BS, Teitelbaum S, Hynes RO.** Beta3-integrin-deficient mice are a model for Glanzmann thrombasthenia showing placental defects and reduced survival. *J Clin Invest*. 1999; 103: 229-38.
197. **Reynolds LE, Wyder L, Lively JC, Taverna D, Robinson SD, Huang X, Sheppard D, Hynes RO, Hodivala-Dilke KM.** Enhanced pathological angiogenesis in mice lacking beta3 integrin or beta3 and beta5 integrins. *Nat Med*. 2002; 8: 27-34.
198. **Robinson SD, Reynolds LE, Wyder L, Hicklin DJ, Hodivala-Dilke KM.** Beta3-integrin regulates vascular endothelial growth factor-A-dependent permeability. *Arterioscler Thromb Vasc Biol*. 2004; 24: 2108-14.
199. **D'Amico G, Robinson SD, Germain M, Reynolds LE, Thomas GJ, Elia G, Saunders G, Fruttiger M, Tybulewicz V, Mavria G, Hodivala-Dilke KM.** Endothelial-Rac1 is not required for tumor angiogenesis unless alphavbeta3-integrin is absent. *PLoS One*. 2010; 5: e9766.
200. **Reynolds AR, Hart IR, Watson AR, Welti JC, Silva RG, Robinson SD, Da Violante G, Gourlaouen M, Salih M, Jones MC, Jones DT, Saunders G, Kostourou V, Perron-Sierra F, Norman JC, Tucker GC, Hodivala-Dilke KM.** Stimulation of tumor growth and angiogenesis by low concentrations of RGD-mimetic integrin inhibitors. *Nat Med*. 2009; 15: 392-400.
201. **Alghisi GC, Ponsonnet L, Ruegg C.** The integrin antagonist cilengitide activates alphaVbeta3, disrupts VE-cadherin localization at cell junctions and enhances permeability in endothelial cells. *PLoS One*. 2009; 4: e4449.
202. **Robinson SD, Reynolds LE, Kostourou V, Reynolds AR, da Silva RG, Tavora B, Baker M, Marshall JF, Hodivala-Dilke KM.** Alphav beta3 integrin limits the contribution of neuropilin-1 to vascular endothelial growth factor-induced angiogenesis. *J Biol Chem*. 2009; 284: 33966-81.
203. **Hodivala-Dilke K.** alphavbeta3 integrin and angiogenesis: a moody integrin in a changing environment. *Curr Opin Cell Biol*. 2008; 20: 514-9.
204. **Maubant S, Saint-Dizier D, Boutillon M, Perron-Sierra F, Casara PJ, Hickman JA, Tucker GC, Van Obberghen-Schilling E.** Blockade of alpha v beta3 and alpha v beta5 integrins by RGD mimetics induces anoikis and not integrin-mediated death in human endothelial cells. *Blood*. 2006; 108: 3035-44.
205. **Hamano Y, Zeisberg M, Sugimoto H, Lively JC, Maeshima Y, Yang C, Hynes RO, Werb Z, Sudhakar A, Kalluri R.** Physiological levels of tumstatin, a fragment of collagen IV alpha3 chain, are generated by MMP-9 proteolysis and suppress angiogenesis via alphaV beta3 integrin. *Cancer Cell*. 2003; 3: 589-601.
206. **Banerjee D, Harfouche R, Sengupta S.** Nanotechnology-mediated targeting of tumor angiogenesis. *Vasc Cell*. 2011; 3: 3.
207. **Taverna D, Moher H, Crowley D, Borsig L, Varki A, Hynes RO.** Increased primary tumor growth in mice null for beta3- or beta3/beta5-integrins or selectins. *Proc Natl Acad Sci U S A*. 2004; 101: 763-8.
208. **Watson AR, Pitchford SC, Reynolds LE, Direkze N, Brittan M, Alison MR, Rankin S, Wright NA, Hodivala-Dilke KM.** Deficiency of bone marrow beta3-integrin enhances non-functional neovascularization. *J Pathol*. 2010; 220: 435-45.
209. **Feng W, McCabe NP, Mahabeleshwar GH, Somanath PR, Phillips DR, Byzova TV.** The angiogenic response is dictated by beta3 integrin on bone marrow-derived cells. *J Cell Biol*. 2008; 183: 1145-57.
210. **Morgan EA, Schneider JG, Baroni TE, Uluckan O, Heller E, Hurchla MA, Deng H, Floyd D, Berdy A, Prior JL, Piwnica-Worms D, Teitelbaum SL, Ross FP, Weilbaecher KN.** Dissection of platelet and myeloid cell defects by conditional targeting of the beta3-integrin subunit. *FASEB J*. 2010; 24: 1117-27.
211. **Steri V, Ellison TS, Gontarczyk AM, Weilbaecher K, Schneider JG, Edwards D, Fruttiger M, Hodivala-Dilke KM, Robinson SD.** Acute depletion of endothelial beta3-integrin transiently inhibits tumor growth and angiogenesis in mice. *Circ Res*. 2014; 114: 79-91.
212. **Kostourou V, Lechertier T, Reynolds LE, Lees DM, Baker M, Jones DT, Tavora B, Ramjaun AR, Birdsey GM, Robinson SD, Parsons M, Randi AM, Hart IR, Hodivala-Dilke**

K. FAK-heterozygous mice display enhanced tumour angiogenesis. *Nat Commun*. 2013; 4: 2020.
213. **Atkinson SJ, Ellison TS, Steri V, Gould E, Robinson SD.** Redefining the role(s) of endothelial alphavbeta3-integrin in angiogenesis. *Biochem Soc Trans*. 2014; 42: 1590-5.
214. **Cheresh DA, Stupack DG.** Tumor angiogenesis: putting a value on plastic GEMMs. *Circ Res*. 2014; 114: 9-11.
215. **Lorger M, Krueger JS, O'Neal M, Staflin K, Felding-Habermann B.** Activation of tumor cell integrin alphavbeta3 controls angiogenesis and metastatic growth in the brain. *Proc Natl Acad Sci U S A*. 2009; 106: 10666-71.
216. **Kaur S, Kenny HA, Jagadeeswaran S, Zillhardt MR, Montag AG, Kistner E, Yamada SD, Mitra AK, Lengyel E.** {beta}3-integrin expression on tumor cells inhibits tumor progression, reduces metastasis, and is associated with a favorable prognosis in patients with ovarian cancer. *Am J Pathol*. 2009; 175: 2184-96.
217. **De S, Razorenova O, McCabe NP, O'Toole T, Qin J, Byzova TV.** VEGF-integrin interplay controls tumor growth and vascularization. *Proc Natl Acad Sci U S A*. 2005; 102: 7589-94.
218. **Kuo JC, Han X, Hsiao CT, Yates JR, 3rd, Waterman CM.** Analysis of the myosin-II-responsive focal adhesion proteome reveals a role for beta-Pix in negative regulation of focal adhesion maturation. *Nat Cell Biol*. 2011; 13: 383-93.
219. **Schiller HB, Friedel CC, Boulegue C, Fassler R.** Quantitative proteomics of the integrin adhesome show a myosin II-dependent recruitment of LIM domain proteins. *EMBO Rep*. 2011; 12: 259-66.
220. **Schiller HB, Hermann MR, Polleux J, Vignaud T, Zanivan S, Friedel CC, Sun Z, Raducanu A, Gottschalk KE, Thery M, Mann M, Fassler R.** beta1- and alphav-class integrins cooperate to regulate myosin II during rigidity sensing of fibronectin-based microenvironments. *Nat Cell Biol*. 2013; 15: 625-36.
221. **Ajeian JN, Horton ER, Astudillo P, Byron A, Askari JA, Millon-Fremillon A, Knight D, Kimber SJ, Humphries MJ, Humphries JD.** Proteomic analysis of integrin-associated complexes from mesenchymal stem cells. *Proteomics Clin Appl*. 2015.
222. **Byron A, Humphries JD, Craig SE, Knight D, Humphries MJ.** Proteomic analysis of alpha4beta1 integrin adhesion complexes reveals alpha-subunit-dependent protein recruitment. *Proteomics*. 2012; 12: 2107-14.
223. **Humphries JD, Byron A, Bass MD, Craig SE, Pinney JW, Knight D, Humphries MJ.** Proteomic analysis of integrin-associated complexes identifies RCC2 as a dual regulator of Rac1 and Arf6. *Sci Signal*. 2009; 2: ra51.
224. **Zamir E, Katz M, Posen Y, Erez N, Yamada KM, Katz BZ, Lin S, Lin DC, Bershadsky A, Kam Z, Geiger B.** Dynamics and segregation of cell-matrix adhesions in cultured fibroblasts. *Nat Cell Biol*. 2000; 2: 191-6.
225. **Rossier O, Octeau V, Sibarita JB, Leduc C, Tessier B, Nair D, Gatterdam V, Destaing O, Albiges-Rizo C, Tampe R, Cognet L, Choquet D, Lounis B, Giannone G.** Integrins beta1 and beta3 exhibit distinct dynamic nanoscale organizations inside focal adhesions. *Nat Cell Biol*. 2012; 14: 1057-67.
226. **Roca-Cusachs P, Gauthier NC, Del Rio A, Sheetz MP.** Clustering of alpha(5)beta(1) integrins determines adhesion strength whereas alpha(v)beta(3) and talin enable mechanotransduction. *Proc Natl Acad Sci U S A*. 2009; 106: 16245-50.
227. **Geiger T, Zaidel-Bar R.** Opening the floodgates: proteomics and the integrin adhesome. *Curr Opin Cell Biol*. 2012; 24: 562-8.
228. **Zaidel-Bar R, Geiger B.** The switchable integrin adhesome. *J Cell Sci*. 2010; 123: 1385-8.
229. **Robertson J, Jacquemet G, Byron A, Jones MC, Warwood S, Selley JN, Knight D, Humphries JD, Humphries MJ.** Defining the phospho-adhesome through the phosphoproteomic analysis of integrin signalling. *Nat Commun*. 2015; 6: 6265.
230. **Manes T, Zheng DQ, Tognin S, Woodard AS, Marchisio PC, Languino LR.** Alpha(v)beta3 integrin expression up-regulates cdc2, which modulates cell migration. *J Cell Biol*. 2003; 161: 817-26.
231. **Miyamoto Y, Yamauchi J, Chan JR, Okada A, Tomooka Y, Hisanaga S, Tanoue A.** Cdk5 regulates differentiation of oligodendrocyte precursor cells through the direct phosphorylation of paxillin. *J Cell Sci*. 2007; 120: 4355-66.
232. **Zhong Z, Yeow WS, Zou C, Wassell R, Wang C, Pestell RG, Quong JN, Quong AA.** Cyclin D1/cyclin-dependent kinase 4 interacts with filamin A and affects the migration and invasion potential of breast cancer cells. *Cancer Res*. 2010; 70: 2105-14.
233. **Kuo JC.** Mechanotransduction at focal adhesions: integrating cytoskeletal mechanics in migrating cells. *J Cell Mol Med*. 2013; 17: 704-12.
234. **Wehrle-Haller B.** Assembly and disassembly of cell matrix adhesions. *Curr Opin Cell Biol*. 2012; 24: 569-81.

235. **Kim H, McCulloch CA.** Filamin A mediates interactions between cytoskeletal proteins that control cell adhesion. *FEBS Lett*. 2011; 585: 18-22.
236. **Razinia Z, Makela T, Ylanne J, Calderwood DA.** Filamins in mechanosensing and signaling. *Annu Rev Biophys*. 2012; 41: 227-46.
237. **Baldassarre M, Razinia Z, Burande CF, Lamsoul I, Lutz PG, Calderwood DA.** Filamins regulate cell spreading and initiation of cell migration. *PLoS One*. 2009; 4: e7830.
238. **Glogauer M, Arora P, Chou D, Janmey PA, Downey GP, McCulloch CA.** The role of actin-binding protein 280 in integrin-dependent mechanoprotection. *J Biol Chem*. 1998; 273: 1689-98.
239. **Das M, Ithychanda SS, Qin J, Plow EF.** Migfilin and filamin as regulators of integrin activation in endothelial cells and neutrophils. *PLoS One*. 2011; 6: e26355.
240. **Ehrlicher AJ, Nakamura F, Hartwig JH, Weitz DA, Stossel TP.** Mechanical strain in actin networks regulates FilGAP and integrin binding to filamin A. *Nature*. 2011; 478: 260-3.
241. **Rognoni L, Stigler J, Pelz B, Ylanne J, Rief M.** Dynamic force sensing of filamin revealed in single-molecule experiments. *Proc Natl Acad Sci U S A*. 2012; 109: 19679-84.
242. **Shifrin Y, Arora PD, Ohta Y, Calderwood DA, McCulloch CA.** The role of FilGAP-filamin A interactions in mechanoprotection. *Mol Biol Cell*. 2009; 20: 1269-79.
243. **Jacquemet G, Morgan MR, Byron A, Humphries JD, Choi CK, Chen CS, Caswell PT, Humphries MJ.** Rac1 is deactivated at integrin activation sites through an IQGAP1-filamin-A-RacGAP1 pathway. *J Cell Sci*. 2013; 126: 4121-35.
244. **Heissler SM, Manstein DJ.** Nonmuscle myosin-2: mix and match. *Cell Mol Life Sci*. 2013; 70: 1-21.
245. **Betapudi V.** Myosin II motor proteins with different functions determine the fate of lamellipodia extension during cell spreading. *PLoS One*. 2010; 5: e8560.
246. **Harburger DS, Calderwood DA.** Integrin signalling at a glance. *J Cell Sci*. 2009; 122: 159-63.
247. **Deakin NO, Pignatelli J, Turner CE.** Diverse roles for the paxillin family of proteins in cancer. *Genes Cancer*. 2012; 3: 362-70.
248. **Deakin NO, Turner CE.** Paxillin comes of age. *J Cell Sci*. 2008; 121: 2435-44.
249. **Choi CK, Zareno J, Digman MA, Gratton E, Horwitz AR.** Cross-correlated fluctuation analysis reveals phosphorylation-regulated paxillin-FAK complexes in nascent adhesions. *Biophys J*. 2011; 100: 583-92.
250. **Huttenlocher A, Horwitz AR.** Integrins in cell migration. *Cold Spring Harb Perspect Biol*. 2011; 3: a005074.
251. **Webb DJ, Donais K, Whitmore LA, Thomas SM, Turner CE, Parsons JT, Horwitz AF.** FAK-Src signalling through paxillin, ERK and MLCK regulates adhesion disassembly. *Nat Cell Biol*. 2004; 6: 154-61.
252. **German AE, Mammoto T, Jiang E, Ingber DE, Mammoto A.** Paxillin controls endothelial cell migration and tumor angiogenesis by altering neuropilin 2 expression. *J Cell Sci*. 2014; 127: 1672-83.
253. **Yang WJ, Yang YN, Cao J, Man ZH, Li Y, Xing YQ.** Paxillin regulates vascular endothelial growth factor A-induced in vitro angiogenesis of human umbilical vein endothelial cells. *Mol Med Rep*. 2015; 11: 1784-92.
254. **Takagi S, Kasuya Y, Shimizu M, Matsuura T, Tsuboi M, Kawakami A, Fujisawa H.** Expression of a cell adhesion molecule, neuropilin, in the developing chick nervous system. *Dev Biol*. 1995; 170: 207-22.
255. **Pellet-Many C, Frankel P, Jia H, Zachary I.** Neuropilins: structure, function and role in disease. *Biochem J*. 2008; 411: 211-26.
256. **Raimondi C, Ruhrberg C.** Neuropilin signalling in vessels, neurons and tumours. *Semin Cell Dev Biol*. 2013; 24: 172-8.
257. **Fujisawa H.** Discovery of semaphorin receptors, neuropilin and plexin, and their functions in neural development. *J Neurobiol*. 2004; 59: 24-33.
258. **Gu C, Rodriguez ER, Reimert DV, Shu T, Fritzsch B, Richards LJ, Kolodkin AL, Ginty DD.** Neuropilin-1 conveys semaphorin and VEGF signaling during neural and cardiovascular development. *Dev Cell*. 2003; 5: 45-57.
259. **Kitsukawa T, Shimizu M, Sanbo M, Hirata T, Taniguchi M, Bekku Y, Yagi T, Fujisawa H.** Neuropilin-semaphorin III/D-mediated chemorepulsive signals play a crucial role in peripheral nerve projection in mice. *Neuron*. 1997; 19: 995-1005.
260. **Schwarz Q, Ruhrberg C.** Neuropilin, you gotta let me know: should I stay or should I go? *Cell Adh Migr*. 2010; 4: 61-6.
261. **Cai H, Reed RR.** Cloning and characterization of neuropilin-1-interacting protein: a PSD-95/Dlg/ZO-1 domain-containing protein that interacts with the cytoplasmic domain of neuropilin-1. *J Neurosci*. 1999; 19: 6519-27.

262. **Shintani Y, Takashima S, Asano Y, Kato H, Liao Y, Yamazaki S, Tsukamoto O, Seguchi O, Yamamoto H, Fukushima T, Sugahara K, Kitakaze M, Hori M.** Glycosaminoglycan modification of neuropilin-1 modulates VEGFR2 signaling. *EMBO J*. 2006; 25: 3045-55.
263. **Kawasaki T, Kitsukawa T, Bekku Y, Matsuda Y, Sanbo M, Yagi T, Fujisawa H.** A requirement for neuropilin-1 in embryonic vessel formation. *Development*. 1999; 126: 4895-902.
264. **Kitsukawa T, Shimono A, Kawakami A, Kondoh H, Fujisawa H.** Overexpression of a membrane protein, neuropilin, in chimeric mice causes anomalies in the cardiovascular system, nervous system and limbs. *Development*. 1995; 121: 4309-18.
265. **Fantin A, Vieira JM, Plein A, Denti L, Fruttiger M, Pollard JW, Ruhrberg C.** NRP1 acts cell autonomously in endothelium to promote tip cell function during sprouting angiogenesis. *Blood*. 2013; 121: 2352-62.
266. **Gerhardt H, Ruhrberg C, Abramsson A, Fujisawa H, Shima D, Betsholtz C.** Neuropilin-1 is required for endothelial tip cell guidance in the developing central nervous system. *Dev Dyn*. 2004; 231: 503-9.
267. **Fantin A, Schwarz Q, Davidson K, Normando EM, Denti L, Ruhrberg C.** The cytoplasmic domain of neuropilin 1 is dispensable for angiogenesis, but promotes the spatial separation of retinal arteries and veins. *Development*. 2011; 138: 4185-91.
268. **Lanahan A, Zhang X, Fantin A, Zhuang Z, Rivera-Molina F, Speichinger K, Prahst C, Zhang J, Wang Y, Davis G, Toomre D, Ruhrberg C, Simons M.** The neuropilin 1 cytoplasmic domain is required for VEGF-A-dependent arteriogenesis. *Dev Cell*. 2013; 25: 156-68.
269. **Fantin A, Herzog B, Mahmoud M, Yamaji M, Plein A, Denti L, Ruhrberg C, Zachary I.** Neuropilin 1 (NRP1) hypomorphism combined with defective VEGF-A binding reveals novel roles for NRP1 in developmental and pathological angiogenesis. *Development*. 2014; 141: 556-62.
270. **Gelfand MV, Hagan N, Tata A, Oh WJ, Lacoste B, Kang KT, Kopycinska J, Bischoff J, Wang JH, Gu C.** Neuropilin-1 functions as a VEGFR2 co-receptor to guide developmental angiogenesis independent of ligand binding. *Elife*. 2014; 3: e03720.
271. **Raimondi C, Fantin A, Lampropoulou A, Denti L, Chikh A, Ruhrberg C.** Imatinib inhibits VEGF-independent angiogenesis by targeting neuropilin 1-dependent ABL1 activation in endothelial cells. *J Exp Med*. 2014; 211: 1167-83.
272. **Evans IM, Yamaji M, Britton G, Pellet-Many C, Lockie C, Zachary IC, Frankel P.** Neuropilin-1 signaling through p130Cas tyrosine phosphorylation is essential for growth factor-dependent migration of glioma and endothelial cells. *Mol Cell Biol*. 2011; 31: 1174-85.
273. **Herzog B, Pellet-Many C, Britton G, Hartzoulakis B, Zachary IC.** VEGF binding to NRP1 is essential for VEGF stimulation of endothelial cell migration, complex formation between NRP1 and VEGFR2, and signaling via FAK Tyr407 phosphorylation. *Mol Biol Cell*. 2011; 22: 2766-76.
274. **Jia H, Bagherzadeh A, Hartzoulakis B, Jarvis A, Lohr M, Shaikh S, Aqil R, Cheng L, Tickner M, Esposito D, Harris R, Driscoll PC, Selwood DL, Zachary IC.** Characterization of a bicyclic peptide neuropilin-1 (NP-1) antagonist (EG3287) reveals importance of vascular endothelial growth factor exon 8 for NP-1 binding and role of NP-1 in KDR signaling. *J Biol Chem*. 2006; 281: 13493-502.
275. **Kawamura H, Li X, Goishi K, van Meeteren LA, Jakobsson L, Cebe-Suarez S, Shimizu A, Edholm D, Ballmer-Hofer K, Kjellen L, Klagsbrun M, Claesson-Welsh L.** Neuropilin-1 in regulation of VEGF-induced activation of p38MAPK and endothelial cell organization. *Blood*. 2008; 112: 3638-49.
276. **Koch S, Tugues S, Li X, Gualandi L, Claesson-Welsh L.** Signal transduction by vascular endothelial growth factor receptors. *Biochem J*. 2011; 437: 169-83.
277. **Soker S, Miao HQ, Nomi M, Takashima S, Klagsbrun M.** VEGF165 mediates formation of complexes containing VEGFR-2 and neuropilin-1 that enhance VEGF165-receptor binding. *J Cell Biochem*. 2002; 85: 357-68.
278. **Wang L, Zeng H, Wang P, Soker S, Mukhopadhyay D.** Neuropilin-1-mediated vascular permeability factor/vascular endothelial growth factor-dependent endothelial cell migration. *J Biol Chem*. 2003; 278: 48848-60.
279. **Zachary IC.** How neuropilin-1 regulates receptor tyrosine kinase signalling: the knowns and known unknowns. *Biochem Soc Trans*. 2011; 39: 1583-91.
280. **Prahst C, Heroult M, Lanahan AA, Uziel N, Kessler O, Shraga-Heled N, Simons M, Neufeld G, Augustin HG.** Neuropilin-1-VEGFR-2 complexing requires the PDZ-binding domain of neuropilin-1. *J Biol Chem*. 2008; 283: 25110-4.
281. **Le Boeuf F, Houle F, Sussman M, Huot J.** Phosphorylation of focal adhesion kinase (FAK) on Ser732 is induced by rho-dependent kinase and is essential for proline-rich tyrosine

kinase-2-mediated phosphorylation of FAK on Tyr407 in response to vascular endothelial growth factor. *Mol Biol Cell*. 2006; 17: 3508-20.
282. **Murga M, Fernandez-Capetillo O, Tosato G.** Neuropilin-1 regulates attachment in human endothelial cells independently of vascular endothelial growth factor receptor-2. *Blood*. 2005; 105: 1992-9.
283. **Becker PM, Waltenberger J, Yachechko R, Mirzapoiazova T, Sham JS, Lee CG, Elias JA, Verin AD.** Neuropilin-1 regulates vascular endothelial growth factor-mediated endothelial permeability. *Circ Res*. 2005; 96: 1257-65.
284. **Salikhova A, Wang L, Lanahan AA, Liu M, Simons M, Leenders WP, Mukhopadhyay D, Horowitz A.** Vascular endothelial growth factor and semaphorin induce neuropilin-1 endocytosis via separate pathways. *Circ Res*. 2008; 103: e71-9.
285. **Naccache SN, Hasson T, Horowitz A.** Binding of internalized receptors to the PDZ domain of GIPC/synectin recruits myosin VI to endocytic vesicles. *Proc Natl Acad Sci U S A*. 2006; 103: 12735-40.
286. **Koch S, van Meeteren LA, Morin E, Testini C, Westrom S, Bjorkelund H, Le Jan S, Adler J, Berger P, Claesson-Welsh L.** NRP1 presented in trans to the endothelium arrests VEGFR2 endocytosis, preventing angiogenic signaling and tumor initiation. *Dev Cell*. 2014; 28: 633-46.
287. **Kofler NM, Simons M.** Angiogenesis versus arteriogenesis: neuropilin 1 modulation of VEGF signaling. *F1000Prime Rep*. 2015; 7: 26.
288. **Valdembri D, Caswell PT, Anderson KI, Schwarz JP, Konig I, Astanina E, Caccavari F, Norman JC, Humphries MJ, Bussolino F, Serini G.** Neuropilin-1/GIPC1 signaling regulates alpha5beta1 integrin traffic and function in endothelial cells. *PLoS Biol*. 2009; 7: e25.
289. **Seerapu HR, Borthakur S, Kong N, Agrawal S, Drazba J, Vasanji A, Fantin A, Ruhrberg C, Buck M, Horowitz A.** The cytoplasmic domain of neuropilin-1 regulates focal adhesion turnover. *FEBS Lett*. 2013; 587: 3392-9.
290. **Fantin A, Lampropoulou A, Gestri G, Raimondi C, Senatore V, Zachary I, Ruhrberg C.** NRP1 Regulates CDC42 Activation to Promote Filopodia Formation in Endothelial Tip Cells. *Cell Rep*. 2015; 11: 1577-90.
291. **Wang L, Dutta SK, Kojima T, Xu X, Khosravi-Far R, Ekker SC, Mukhopadhyay D.** Neuropilin-1 modulates p53/caspases axis to promote endothelial cell survival. *PLoS One*. 2007; 2: e1161.
292. **Fuh G, Garcia KC, de Vos AM.** The interaction of neuropilin-1 with vascular endothelial growth factor and its receptor flt-1. *J Biol Chem*. 2000; 275: 26690-5.
293. **Pellet-Many C, Frankel P, Evans IM, Herzog B, Junemann-Ramirez M, Zachary IC.** Neuropilin-1 mediates PDGF stimulation of vascular smooth muscle cell migration and signalling via p130Cas. *Biochem J*. 2011; 435: 609-18.
294. **Barr MP, Byrne AM, Duffy AM, Condron CM, Devocelle M, Harriott P, Bouchier-Hayes DJ, Harmey JH.** A peptide corresponding to the neuropilin-1-binding site on VEGF(165) induces apoptosis of neuropilin-1-expressing breast tumour cells. *Br J Cancer*. 2005; 92: 328-33.
295. **Bartsch G, Jr., Eggert K, Soker S, Bokemeyer C, Hautmann R, Schuch G.** Combined antiangiogenic therapy is superior to single inhibitors in a model of renal cell carcinoma. *J Urol*. 2008; 179: 326-32.
296. **Berge M, Allanic D, Bonnin P, de Montrion C, Richard J, Suc M, Boivin JF, Contreres JO, Lockhart BP, Pocard M, Levy BI, Tucker GC, Tobelem G, Merkulova-Rainon T.** Neuropilin-1 is upregulated in hepatocellular carcinoma and contributes to tumour growth and vascular remodelling. *J Hepatol*. 2011; 55: 866-75.
297. **Gagnon ML, Bielenberg DR, Gechtman Z, Miao HQ, Takashima S, Soker S, Klagsbrun M.** Identification of a natural soluble neuropilin-1 that binds vascular endothelial growth factor: In vivo expression and antitumor activity. *Proc Natl Acad Sci U S A*. 2000; 97: 2573-8.
298. **Hong TM, Chen YL, Wu YY, Yuan A, Chao YC, Chung YC, Wu MH, Yang SC, Pan SH, Shih JY, Chan WK, Yang PC.** Targeting neuropilin 1 as an antitumor strategy in lung cancer. *Clin Cancer Res*. 2007; 13: 4759-68.
299. **Jarvis A, Allerston CK, Jia H, Herzog B, Garza-Garcia A, Winfield N, Ellard K, Aqil R, Lynch R, Chapman C, Hartzoulakis B, Nally J, Stewart M, Cheng L, Menon M, Tickner M, Djordjevic S, Driscoll PC, Zachary I, Selwood DL.** Small molecule inhibitors of the neuropilin-1 vascular endothelial growth factor A (VEGF-A) interaction. *J Med Chem*. 2010; 53: 2215-26.
300. **Jia H, Cheng L, Tickner M, Bagherzadeh A, Selwood D, Zachary I.** Neuropilin-1 antagonism in human carcinoma cells inhibits migration and enhances chemosensitivity. *Br J Cancer*. 2010; 102: 541-52.

301. **Karjalainen K, Jaalouk DE, Bueso-Ramos CE, Zurita AJ, Kuniyasu A, Eckhardt BL, Marini FC, Lichtiger B, O'Brien S, Kantarjian HM, Cortes JE, Koivunen E, Arap W, Pasqualini R.** Targeting neuropilin-1 in human leukemia and lymphoma. *Blood*. 2011; 117: 920-7.
302. **Nasarre C, Roth M, Jacob L, Roth L, Koncina E, Thien A, Labourdette G, Poulet P, Hubert P, Cremel G, Roussel G, Aunis D, Bagnard D.** Peptide-based interference of the transmembrane domain of neuropilin-1 inhibits glioma growth in vivo. *Oncogene*. 2010; 29: 2381-92.
303. **Schuch G, Machluf M, Bartsch G, Jr., Nomi M, Richard H, Atala A, Soker S.** In vivo administration of vascular endothelial growth factor (VEGF) and its antagonist, soluble neuropilin-1, predicts a role of VEGF in the progression of acute myeloid leukemia in vivo. *Blood*. 2002; 100: 4622-8.
304. **Starzec A, Vassy R, Martin A, Lecouvey M, Di Benedetto M, Crepin M, Perret GY.** Antiangiogenic and antitumor activities of peptide inhibiting the vascular endothelial growth factor binding to neuropilin-1. *Life Sci*. 2006; 79: 2370-81.
305. **Xu L, Duda DG, di Tomaso E, Ancukiewicz M, Chung DC, Lauwers GY, Samuel R, Shellito P, Czito BG, Lin PC, Poleski M, Bentley R, Clark JW, Willett CG, Jain RK.** Direct evidence that bevacizumab, an anti-VEGF antibody, up-regulates SDF1alpha, CXCR4, CXCL6, and neuropilin 1 in tumors from patients with rectal cancer. *Cancer Res*. 2009; 69: 7905-10.
306. **Ruffini F, D'Atri S, Lacal PM.** Neuropilin-1 expression promotes invasiveness of melanoma cells through vascular endothelial growth factor receptor-2-dependent and -independent mechanisms. *Int J Oncol*. 2013; 43: 297-306.
307. **Fukasawa M, Matsushita A, Korc M.** Neuropilin-1 interacts with integrin beta1 and modulates pancreatic cancer cell growth, survival and invasion. *Cancer Biol Ther*. 2007; 6: 1173-80.
308. **Yaqoob U, Cao S, Shergill U, Jagavelu K, Geng Z, Yin M, de Assuncao TM, Cao Y, Szabolcs A, Thorgeirsson S, Schwartz M, Yang JD, Ehman R, Roberts L, Mukhopadhyay D, Shah VH.** Neuropilin-1 stimulates tumor growth by increasing fibronectin fibril assembly in the tumor microenvironment. *Cancer Res*. 2012; 72: 4047-59.
309. **Krilleke D, DeErkenez A, Schubert W, Giri I, Robinson GS, Ng YS, Shima DT.** Molecular mapping and functional characterization of the VEGF164 heparin-binding domain. *J Biol Chem*. 2007; 282: 28045-56.
310. **Claxton S, Kostourou V, Jadeja S, Chambon P, Hodivala-Dilke K, Fruttiger M.** Efficient, inducible Cre-recombinase activation in vascular endothelium. *Genesis*. 2008; 46: 74-80.
311. **Tomayko MM, Reynolds CP.** Determination of subcutaneous tumor size in athymic (nude) mice. *Cancer Chemother Pharmacol*. 1989; 24: 148-54.
312. **Baker M, Robinson SD, Lechertier T, Barber PR, Tavora B, D'Amico G, Jones DT, Vojnovic B, Hodivala-Dilke K.** Use of the mouse aortic ring assay to study angiogenesis. *Nat Protoc*. 2012; 7: 89-104.
313. **Reynolds LE, Hodivala-Dilke KM.** Primary mouse endothelial cell culture for assays of angiogenesis. *Methods Mol Med*. 2006; 120: 503-9.
314. **Tavora B, Reynolds LE, Batista S, Demircioglu F, Fernandez I, Lechertier T, Lees DM, Wong PP, Alexopoulou A, Elia G, Clear A, Ledoux A, Hunter J, Perkins N, Gribben JG, Hodivala-Dilke KM.** Endothelial-cell FAK targeting sensitizes tumours to DNA-damaging therapy. *Nature*. 2014; 514: 112-6.
315. **Ewan LC, Jopling HM, Jia H, Mittar S, Bagherzadeh A, Howell GJ, Walker JH, Zachary IC, Ponnambalam S.** Intrinsic tyrosine kinase activity is required for vascular endothelial growth factor receptor 2 ubiquitination, sorting and degradation in endothelial cells. *Traffic*. 2006; 7: 1270-82.
316. **Remacle A, Murphy G, Roghi C.** Membrane type I-matrix metalloproteinase (MT1-MMP) is internalised by two different pathways and is recycled to the cell surface. *J Cell Sci*. 2003; 116: 3905-16.
317. **Clark RA, Mason RJ, Folkvord JM, McDonald JA.** Fibronectin mediates adherence of rat alveolar type II epithelial cells via the fibroblastic cell-attachment domain. *J Clin Invest*. 1986; 77: 1831-40.
318. **Sottile J, Hocking DC, Swiatek PJ.** Fibronectin matrix assembly enhances adhesion-dependent cell growth. *J Cell Sci*. 1998; 111 (Pt 19): 2933-43.
319. **Tvorogov D, Wang XJ, Zent R, Carpenter G.** Integrin-dependent PLC-gamma1 phosphorylation mediates fibronectin-dependent adhesion. *J Cell Sci*. 2005; 118: 601-10.
320. **Phillips DR, Nannizzi-Alaimo L, Prasad KS.** Beta3 tyrosine phosphorylation in alphaIIbbeta3 (platelet membrane GP IIb-IIIa) outside-in integrin signaling. *Thromb Haemost*. 2001; 86: 246-58.

321. **Goel HL, Pursell B, Standley C, Fogarty K, Mercurio AM.** Neuropilin-2 regulates alpha6beta1 integrin in the formation of focal adhesions and signaling. *J Cell Sci*. 2012; 125: 497-506.